Neoproterozoic to Lower Paleozoic Evolution of the Pre-Caledonian Magma-Rich Margin of Baltica

Hans Jørgen Kjøll

Dissertation submitted for the degree of Philosophiae Doctor

The Centre for Earth Evolution and Dynamics
Department of Geosciences
The Faculty of Mathematics and Natural Sciences
University of Oslo

April, 2019

Series of dissertations submitted to the
Faculty of Mathematics and Natural Sciences, University of Oslo
No. 2157

ISSN 1501-7710

Cover: Hanne Baadsgaard Utigard.
Print production: Reprosentralen, University of Oslo.

Principal supervisor

Torgeir B. Andersen

Centre for Earth Evolution and Dynamics, University of Oslo

Subsidiary supervisors

Fernando Corfu

Trond Torsvik

Centre for Earth Evolution and Dynamics, University of Oslo

Eric Tohver

University of Western Australia

Funding

This work was funded by the Research Council of Norway through the Centre of Excellence funding scheme to CEED, project Number 223272 and the NFR-FRINAT project 250327 “Hyperextension in magma-poor and magma-rich domains along the pre-Caledonian passive margin of Baltica”.

A three month research stay at the University of Western Australia was partially funded by a grant from the Norwegian research school for Dynamics and Evolution of Earth and Planets (DEEP; 249040/F60).

"Geologists have a saying - rocks remember"

-Neil Armstrong

Preface – Do rocks remember?

Yes, rocks do remember. They may not remember things like humans do, selective and usually with an agenda. No, rocks remember in absolute terms. They remember in the form of growth of new minerals – metamorphic mineral assemblages, and they remember in the form of structures – development of fabrics. Although rocks can have a good memory, their memory can easily be disturbed and if something new and exciting happens they may completely forget their previous memories. But if we are lucky, vague or partial memories can survive even the harshest of conditions.

When rocks undergo metamorphism, a change in temperature, pressure or fluid activity, new mineral assemblages may be stabilized. These new minerals react from the previous mineral assemblages and this will, either completely or partially, reset the memory of the rocks. Fluids can also cause rock amnesia and completely wipe clean their memory by promoting chemical reactions and metasomatism. But if treated with care and by using the right methods, a geologist can find the faintest memories of times past and piece them together like a jigsaw puzzle to tell their story.

For the past four years I have had the pleasure of asking 600 million year old rocks what they remember from their turbulent lives. Some did not remember anything, whereas most others only remembered partially. But, by asking the right questions to the right minerals it has been possible to piece together a portion of their story. This includes the astonishing tale of how volcanoes ripped a continent apart forming an ocean that later closed and made a Himalaya-sized mountain chain in Norway and Sweden.

One of the many spectacular mountains in Sarek with a good memory

To my parents Tone and Øivind, for sharing their love of nature with me

Acknowledgements

Although the writing of the Ph.D. is something I have done by myself, it would not have been possible without the help, guidance and support from many people and on many different levels.

I would like to thank my supervisors and first and foremost **Torgeir**. You have guided me through this endeavor and shared your extensive knowledge about every aspect of geology and science in general. You have also given me freedom to pursuit what I found most interesting, which has been challenging and rewarding. I would also like to thank **Eric** for welcoming me to three wonderful months in Perth and an epic trip to Svalbard as well as numerous skype chats. **Fernando**, thanks for always being so helpful and thoughtful and sharing your knowledge and skepticism, as well as your time. **Trond**, you are an inspiration and it has been great to learn from your endless expertise and mindset towards science.

I have had a lot of collaborators as well and I would especially like to thank **Olivier**, your enthusiasm and involvement in the dyke emplacement paper has been crucial. But most of all thank you for being such a great and caring guy! **Loic**, you stepped in when needed and helped me out in the field and kept me safe on the glaciers! I really enjoyed all our conversations in the field and numerous “fjellpanne” and French wine. **Sverre**, thanks for always having a ton of ideas and sharing them. Your enthusiasm is contagious. **Christian**, it was great to work with you and learning about geochemistry. **Mansour**, thanks for providing your expertise on rifted margins. **Geoffroy**, thanks for taking Johannes and I on a fantastic trip to the Swiss Alps and thanks for the many discussions about rifted margins.

A significant piece of lab work has been conducted for this thesis and it would not have been possible without the help and support from **Dan**, **Muriel**, **Marius**, **Gunnborg**, **Siri** and **Tulio**.

Coming in to work every day has been a pleasure due to all my wonderful colleagues at CEED. Even when times were tough there were always someone to talk to that could make me smile or find a solution to a problem, so thanks and cheers to all the wonderful people at CEED! I especially would like to mention the Italians, **Valentina** and **Sara** for always being open-hearted and so non-Norwegian! Also, I would like to say thanks to **Joost** for so many wonderful runs, cycle- and ski trips as well as triceps pumping in the gym before the cross-country season. **Eivind and Krister**, CEED would not have been the same without your dry, awful humor! **Johannes**, you have been a mentor and role model for me. Your extensive knowledge of the Caledonides has been invaluable. Also, organizing and leading the WGR field trip with you was a great experience that I will always remember. **Thea**, you truly drove me nuts sometimes, but I would not been without our numerous conversations about everything and anything. I really appreciate our friendship.

Another person who has meant a lot to me during these four years is **Espen**. Every time we have talked my motivation has skyrocketed. You really have the ability to make other people feel great.

Although an enormous amount of time has been spent in the field and in the office these last four years, there has also been some memorable moments together with friends and family outside of work. The G4 gang (Geologistuderendes Gutte Grotte Gruppe), **Martin**, **Eero** og **Ivar** have meant a lot to me. Planning and going on trips, both long and short, as well as discussing current affaires has been great and I really look forward to new adventures with you guys! I would also like to mention some of my friends from back home: **Andreas**, **Sindre**, **Erlend** and **Bjørn André**. Hanging out with you guys playing COD and eating junk food is something I really enjoy and has helped me to free my mind. **Atle**, drinking beer and indulge in reminisce about our round-the-world adventure is always a blast and thanks for always asking about my Ph.D.

I would like to thank my **family** for always being there for me and providing a safe haven to relax and let the mind wander. And also, for providing and letting me drive big and heavy farm equipment and cut down trees using the chainsaw, it really is the best therapy!

Finally, I would like to thank **Julie** for always being there for me no matter if I am up surfing a cloud or down in the dumps. You have always been supportive and given me the freedom to pursuit the Ph.D. even if that has meant prioritizing travelling and work. For that I am very grateful. Now I look forward to new adventures with you!

Summary

In the Late Neoproterozoic the supercontinent Rodinia started to disintegrate, and the continents Baltica and Laurentia began to rift apart to form the Iapetus Ocean. Early stages of subsidence caused by ductile stretching of the middle crust led to deposition of a clastic sedimentary succession, which transitioned into shallow marine carbonates. Locally evaporite deposits and stromatolites are present and indicate deposition in an arid environment at low latitudes. This unit was directly overlain by a glaciogenic diamictite, correlated with the 635 Ma Marinoan glaciation, showing the turbulent climatic situation in the Neoproterozoic. Onset of rifting is presumably marked by a sudden change in sedimentary detritus and the deposition of a > 2 km thick formation of shallow marine sandstone.

This entire sedimentary succession is cut by mafic dykes that were emplaced around 606 Ma. The sedimentary succession had then been buried to *c.* 8-14 kilometers depth, as constrained by geothermobarometry. The geochemical signature of the dyke swarm suggests that the magma formed above a zoned mantle with temperatures at the Lithosphere-Asthenosphere Boundary (LAB) *c.* 75 to 250°C higher than normal. During the dyke emplacement event the thermal structure of the crust changed dramatically because of the heat brought by the mafic magma. The ambient temperatures in the host rock reached 650-700°C, enough to cause partial, contact metamorphic melting of the host rock. Field observations indicate that whereas some early dykes show brittle features, the emplacement of others was accommodated by significant ductile mechanisms as well. Crustal anatexis of some areas, however, occurred already 5 million years prior to dyke emplacement and lasted until the dykes were emplaced. This suggests that a high geothermal gradient was established before the dyke swarm intruded, possibly because of a blanketing effect caused by the platform sedimentary succession and/or incipient lower crustal magma underplating. During the dyking event the magma influx rate was larger than the tectonic stretching rate, which caused the influx of magma to inflate the crust and locally led to a 27% vertical thickening as well as 94% horizontal extension. This shows that the magma was not passively filling a gap provided by the tectonics, but rather forced its way through the crust. It is still uncertain if this would have translated into surface uplift.

The final architecture of the pre-Caledonian margin of Baltica when the Iapetus Ocean was formed was relatively complex. It was a wide margin that had strong lateral geometric and compositional variations, both along and across strike, such as a microcontinent and magma-poor and magma-rich domains separated by a 200 kilometer wide transition zone. These complexities partly controlled the build-up of the Scandinavian Caledonides when Baltica and Laurentia collided in the Silurian, through reactivation of rift-inherited structures. Today it can be shown that variations in nappes at the same tectonostratigraphic position reflect lateral changes along the pre-Caledonian margin of Baltica.

Sammendrag

Da superkontinentet Rodinia begynte å bryte opp mot slutten av Neoproterozoikum, drev også de tektoniske platene Baltika og Laurentia fra hverandre og dannet havet Iapetus mellom seg. Tidlig bassengutvikling skyldtes duktil strekking i midtre skorpe hvilket dannet et bredt innsynkningsbasseng som ble fylt av klastiske sedimenter. Gradvis forandret avsetningsmiljøet seg og karbonatavsetninger med lokale evaporittavsetninger og stromatolitter ble avsatt, hvilket indikerer at det var tørt og varmt klima. Denne enheten ble dekket over av en glasiogen diamiktitt, som har sammenheng med den 635 millioner år gamle verdensomspennende glasiale «Marinoan-hendelsen» og viser hvor turbulente de klimatiske forholdene var i Neoproterozoikum. Selve oppsprekkingen startet rett etter den glasiale hendelsen og kan sees i form av en tykk grunnmarin sandsteinformasjon, mulig som en konsekvens av erosjon av oppløftede riftflanker.

Hele den sedimentære lagrekken er kuttet av mafiske ganger som intruderte for *c.* 606 millioner år siden. Da hadde de sedimentære bergartene blitt begravet til c. 8-14 kilometer. Gangene har en geokjemisk signatur som tyder på at magmaen ble dannet på grunn av en varmesøyle med temperaturer opptil 75-250°C høyere enn det som er vanlig på mantel-litosfære grensen. Da gangene intruderte, forandret temperaturstrukturen i skorpen seg dramatisk på grunn av varmen fra den mafiske magmaen. Temperaturen i vertsbergartene nådde 650-700°C og forårsaket delvis kontaktmetamorf smelting. Feltobservasjoner har vist at intrusjonen av tidlige mafiske ganger stort sett var styrt av sprø prosesser, mens senere ble duktile mekanismer viktigere. Enkelte steder finnes bevis for at smelting av vertsbergartene fant sted så tidlig som 5 millioner år før de mafiske gangene intruderte, hvilket viser at en høy geotermal gradient var etablert tidlig. Dette kan ha skjedd som en konsekvens av en varmeteppeeffekt p.g.a tidlige plattformsedimentene og/eller på grunn av mafiske magmareservoarer i nedre skorpe. Da gangene intruderte var innstrømningen av magma høyere enn den tektoniske ekstensjonen og dette førte til at gangene «blåste opp» skorpen slik at skorpen ble 27% tykkere, og 94% lengre. Dette viser at intrusjon av magma i enkelte tilfeller bør regnes som en aktiv prosess som kan deformere vertsbergartene. Det er uvisst om dette vil føre til oppløft av topografien på overflaten.

Oppbygningen av den pre-Kaledonske marginen til Baltika da havet Iapetus oppstod var relativt kompleks. Den var en bred margin som hadde viktige laterale geometriske variasjoner, slik som et mikrokontinent og en magmafattig og magmarik del, skilt av en 200 km bred overgangssone. Disse kompleksitetene var med på å kontrollere hvordan de Skandinaviske Kaledonidene ble bygget opp gjennom reaktivering av strukturer arvet fra oppsprekkingen som fant sted 200 millioner år tidligere. I dag ser vi at enkelte skyvedekker i samme tektonostratigrafiske posisjon reflekterer laterale forandringer langs den pre-Kaledonske marginen.

Table of Content

PART I

1. Aim and scope of the thesis

Continental rifts are scars in the crust that form when a continent is broken apart by large plate tectonic forces. The extension is generally accommodated along weak, brittle normal faults in the upper crust and by ductile shear zones in the middle and perhaps the lower crust. When the lithosphere is thinned, the underlying mantle is lifted and can undergo decompression melting, and the hot and buoyant melt can then either migrate through the crust and erupt on the surface or freeze as layer-parallel sills or layer-discordant dykes within the crust. If a self-sustaining, steady-state seafloor spreading is reached, magmatism and volcanism will accommodate the extension and the stress field changes from a vertical σ_1 to a horizontal σ_1, as the spreading center pushes on the adjacent continents.

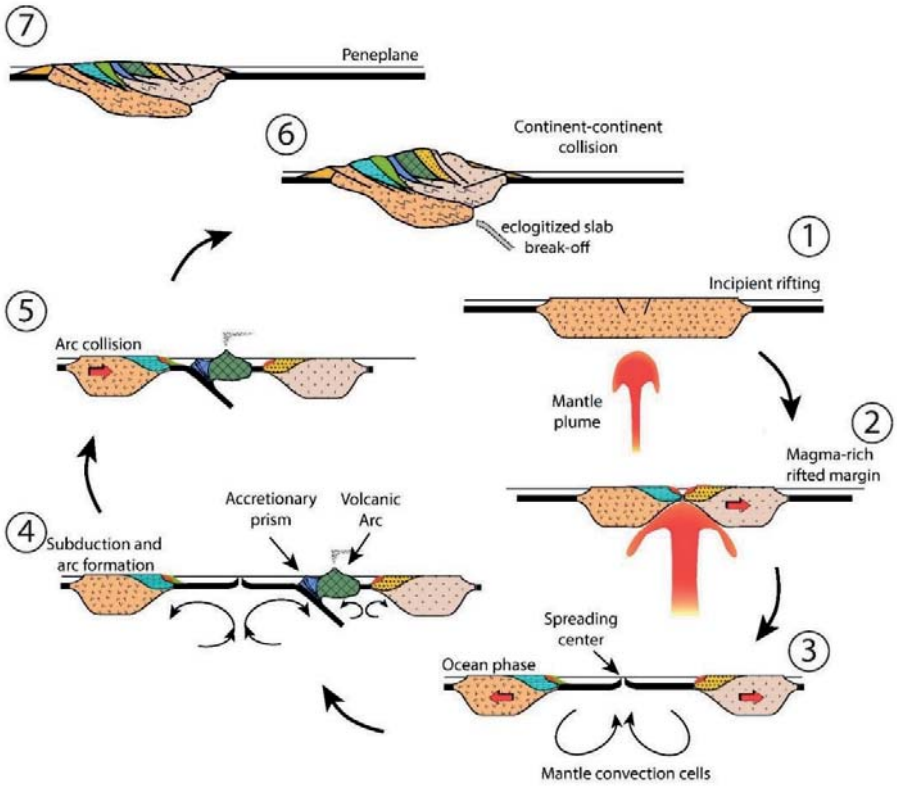

Figure 0-1: Schematic view of a plume induced Wilson cycle modified after the original artwork by Fichter (1999). 1) Incipient rifting of a stable craton. 2) Plume impingement and continental break-up. 3) Steady-state seafloor spreading. 4) Convergence as the ocean subducts and an Arc with an accompanying back-arc basin. 5) Arc-continent collision. 6) Continent-continent collision. Rifted margins and arcs are preserved in the mountain. 7) Erosion and ready for next round.

No significant tectonic strain will be localized in the rifted margin at this stage, which then has become a passive continental margin. Incipient continental rifts therefore represent the conception of an ocean, and the eventual break-up is the actual birth of the ocean (Fig. 0-1). After millions of years, oceans retire in subduction zones where they sink down into the mantle, causing the ocean to close and send the continents on a collision course (Fig. 0-1). As the entire ocean is consumed at the subduction zone, the continents may collide (Fig. 0-1). Then, the once passive margins become active as their weak faults can be reactivated as thrusts and reverse faults, accommodating the contraction and thickening of the crust caused by the sinking of the heavy oceanic lithosphere. This process, which describes the life of an ocean, has been coined "the Wilson Cycle", named after James Tuzo Wilson by e.g. Dewey and Burke (1974). Wilson was the first to describe the entire cycle in his landmark paper entitled: "Did the Atlantic close and then re-open?" (Wilson, 1966; Figure 0-2), describing the same tectonic cycle which is the focus for this thesis.

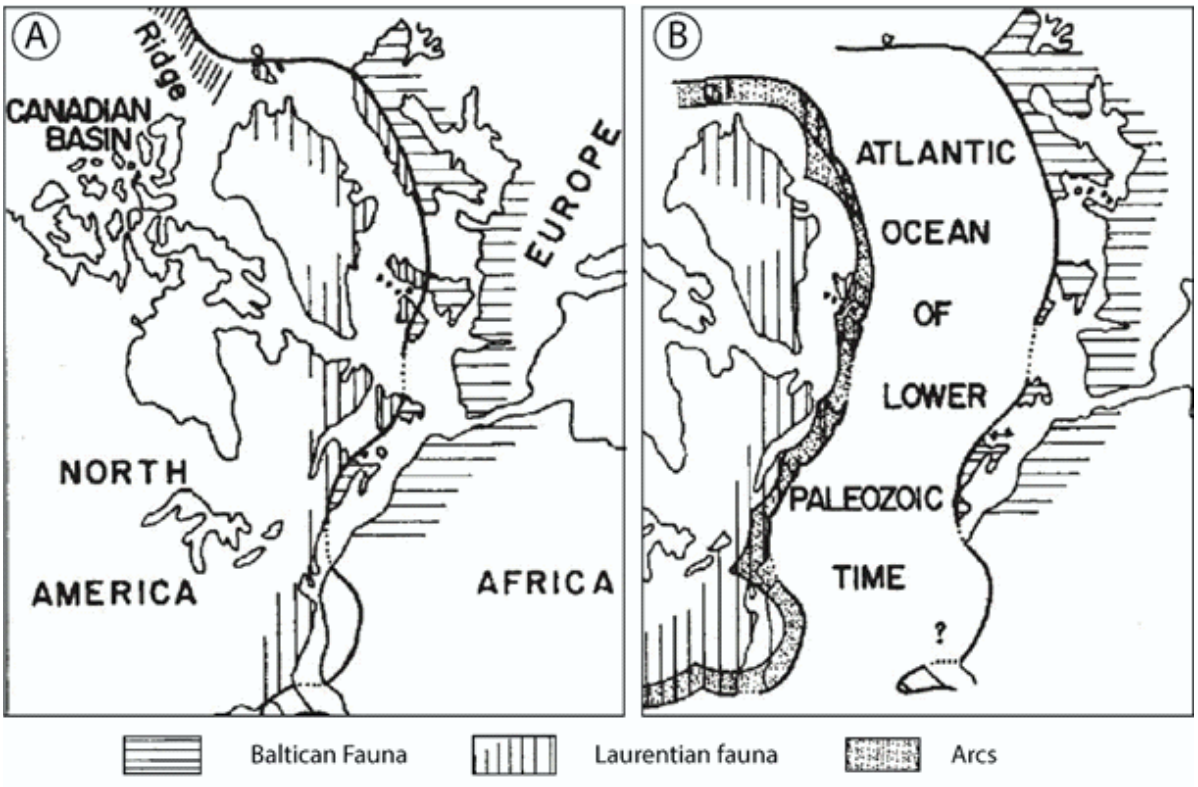

Figure 0-2: How Wilson envisaged the Paleogeography in his landmark 1966 paper. A) Figure depicting North America, Europe and Africa prior to the opening of the current Atlantic Ocean. B) Paleogeography of the Iapetus Ocean in the Lower Paleozoic. Vertical and horizontal lines represent North American and European/African fauna provincialities, respectively. The dotted rim of N. America represents arcs. Note the missing "eastern" margin of Baltica, today we envisage this to have been a wide margin.

Since then, an extensive amount of work has been conducted to understand the individual stages of the Wilson Cycle, from continental break-up and sea-floor spreading to subduction and orogeny. And while orogeny often is referred to as the "destruction of a margin", a better term could be the not so glorious: "partial preservation of a margin", because over the past decades it has been shown that rifted margins can partly be preserved within nappes in orogens (e.g. Dietrich, 1970; Manatschal and Nievergelt, 1997; Lagabrielle et al., 2010). This has been an advent in the understanding of rifted margins as they are generally submerged under the ocean and buried beneath kilometers of sediments. Fortunately, their high economic potential, primarily in the form of hydrocarbons, has led to an extensive mapping and acquisition and interpretation of 2D and 3D reflection and wide-angle seismic data. This has provided insights into the architecture of rifted margins world-wide and has revealed an exceptional variety of different rift types (e.g. Levell et al., 2010). Despite recent technological advances in the acquisition and processing, the resolution at depth is still limited and the interpretation of the seismic data can be challenging and lead to non-unique interpretations (e.g. McDermott and Reston, 2015). Although scientific and industrial drilling programs have provided ground truthing of some models, these pin-point observations cannot provide a full understanding of the complexities observed at rifted margins, such as the relation between crustal stretching, magmatism and break-up. At so-called magma-rich rifted margins (see section 2.3.2. below), the challenges become even greater due to difficulties in sub-basalt seismic imaging, causing poor resolution with depth. The need for fossil analogues exposing all levels of rifted margins is therefore essential to verify models proposed from interpretations of seismic sections as well as modelling studies. Such analogues, however, are rarely preserved in the geological record.

This thesis reports field observations from perhaps the only preserved fossil analogue of a deep crustal section of the distal domain of a Neoproterozoic magma-rich rifted margin, which is preserved in the Scandinavian Caledonides. The detailed observations presented in this thesis are of a mafic dyke swarm called the Scandinavian Dyke Complex (SDC), also known as the Baltoscandian Dyke Swarm (BDS), emplaced into pre- and syn-rift sediments. The area has allowed detailed first-hand observations constraining the temporal evolution of the thermal structure of the fossil margin, as well as putting high-precision geochronological constraints on the timing of major events such as onset of rifting relative to the onset- and peak magmatism. The deeply incised glacial valleys and cirques provide exceptional large-scale overview of the mafic dyke swarm, allowing to deduce the dynamics of the plumbing system of a Large Igneous Province (LIP), leading to continental break-up and the formation of a magma-rich rifted margin. These unique observations provide the basis to better understand the deep levels of magma-rich rifted margins.

2. Scientific background

2.1. Why and how continents rift apart

Plate boundary stresses such as slab-pull, slab roll-back, ridge push and mantle drag at the base of the Lithosphere, are generally suggested to be the primary forces causing continental rifting (e.g. Forsyth and Uyeda, 1975; Ziegler, 1992). Constructive interference between several forces are often necessary to split a continent (Ziegler and Cloetingh, 2004), as several studies suggest that plate tectonic forces are not enough to rupture normal continental lithosphere (Buck and Karner, 2004; Brune, 2016). A number of mechanisms and factors have been proposed to explain this conundrum, *e.g.* the role of inheritance, such as relatively weak orogenic sutures. This was first proposed by Wilson (1966) and have later been shown using numerical modelling (Salazar-Mora et al., 2018). A prerequisite for the reactivation of orogenic structures in a rifting phase is, among other things, that faults remain weak (Op. cit.). Thick-skinned orogenic thrusts generally form at shallow angles and have distinct fabrics. They are generally defined by relative weak minerals with anisotropic shape, such as mica and amphiboles, making them ideal for tectonic reactivation during *e.g.* gravitational collapse of orogens (e.g. White et al., 1986). Such reactivation of inherited orogenic fabrics has been inferred for the first rifting events in *e.g.* the North Sea (Fossen et al., 2017).

Another important factor controlling continental rifting is thermal weakening by mantle plumes and mantle convection leading to elevated temperature at the Lithosphere-Asthenosphere Boundary (LAB; e.g. White and McKenzie, 1989; Courtillot et al., 1999; Buiter and Torsvik, 2014; Geoffroy et al., 2015; Kjøll et al., 2019a; Kjøll et al., 2019b; Tegner et al., 2019; Chapters 1, 2 and 3, this thesis). Such elevated LAB temperatures may lead to dramatic melting of the lithospheric mantle and the emplacement of large quantities of mafic magma below, within and on top of the continental crust (Menzies et al., 2002; see section 2.3.2. below). The temporal link between tectonic extension and magmatism, however, is not always entirely clear as it appears that it can vary from margin to margin. Some argue, for plume-related magmatism, that early arrivals of the plume can cause active rifting (e.g. Geoffroy et al., 2015), whereas others argue for late arrival of the plume after substantial tectonic extension (e.g. Armitage et al., 2009). The latter has been proposed for the opening of the Norwegian-Greenland Sea, where the Møre and Vøring margins underwent several episodes of extension (Fig. 0-3A). It started with late to post-orogenic collapse and transtension in the Devonian followed by Late Jurassic to Early Cretaceous rifting. This led to extreme crustal thinning and possibly even local mantle exhumation (Osmundsen et al., 2016). These early phases of extension were then followed by a period of quiescence (Gernigon et al., 2019) without evidence of magmatism until the impingement of the Iceland plume, leading to a magma-rich break-up in the Eocene. This occurred after 280 million years characterized by distinct rifting episodes (Skogseid, 1994; Ren et al.,

1998; Ziegler and Cloetingh, 2004; Gernigon et al., 2006; Péron-Pinvidic et al., 2013). In the Central Atlantic, by contrast, rifting started at 224 Ma and flood volcanism took place at 201 Ma during emplacement of the Central Atlantic Magmatic Province (CAMP; e.g. Marzoli et al., 1999; Heimdal et al., 2018). Steady state sea floor spreading did, however, not commence until the Early Jurassic (e.g. Labails et al., 2010; Biari et al., 2017; Fig. 0-3B), leaving a gap of possibly 25 million years from the peak magmatic event to actual seafloor spreading. The question whether rifts focuses plumes or if plumes focuses rifting remains ambiguous.

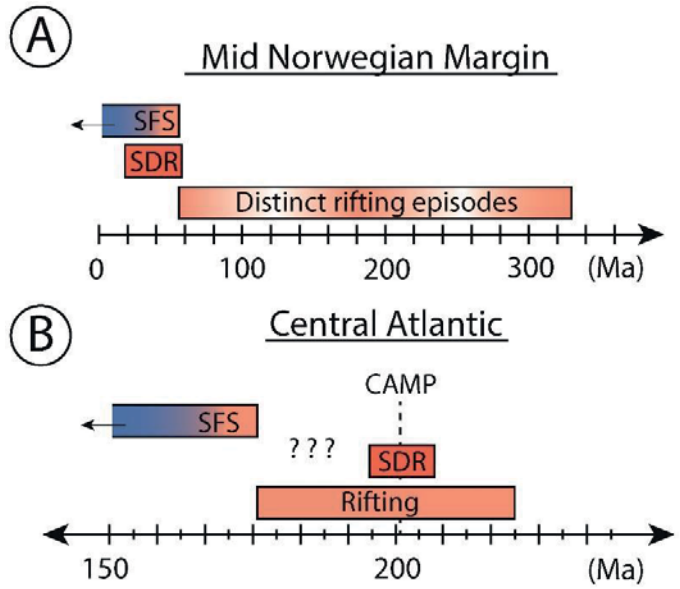

Figure 0-3: Timeline showing a proposed temporal evolution of the Mid Norwegian Margin and the Central Atlantic. A) The Mid Norwegian Margin shows several distinct phases of rifting before massive magmatic activity related to the impingement of the Iceland plume. B) Magmatism in the Central Atlantic is related to the emplacement of the CAMP, but there is a time gap between the intrusion of CAMP rocks and the actual opening represented by steady-state seafloor spreading. CAMP: Central Atlantic Magmatic Province, SDR: Seaward Dipping Reflectors, SFS: SeaFloor Spreading.

2.2. Rifted margin architecture

High resolution, deep seismic imaging has provided a good overview of the first order architecture of rifted margins and show that individual margins have very distinct, but variable characteristics including mode of extension, magmatic budget, structural and thermal inheritance (e.g. Levell et al., 2010; Clerc et al., 2018; Tugend et al., 2018). In general, most rifts display a network of half-graben basins delineated by normal faults and a progressively thinning crust towards the ocean, as deformation localizes oceanward. Rifted margins are generally divided in to a proximal and a distal domain (see e.g. Péron-Pinvidic et al., 2013). The proximal domain is often associated with a low β-factor and is separated from the distal domain by a necking zone where the crustal thickness is dramatically reduced (Mohn et al., 2012). The architecture of the distal domain varies greatly depending on the magmatic budget. In magma-poor systems the distal domain often has a hyperextended crust thinned to less than 10 km thickness, and occasionally a zone of exhumed continental mantle can be found oceanward of the hyperextended domain. The extent of magmatism, even at magma-poor margins, increases towards the ocean (Tugend et al., 2018). In contrast

to magma-poor margins, the distal domain of the magma-rich endmember is generally characterized by a higher abundance of magmatic products such as lava flows, and intrusive sill and dyke complexes fed from lower crustal magma reservoirs (e.g. Geoffroy, 2005; Geoffroy et al., 2015; Tugend et al., 2018). Magma-rich margins and their distal domain are dealt with in more detail below.

The extensional deformation is accommodated by large normal faults, which may become shallow towards the brittle-ductile transition and turn into a sub-horizontal decoupling zone (Mohn et al., 2012). Although these faults are generally thought to dip towards the ocean, the polarity may vary, such as in the magma-rich Uruguayan margin, where they dip towards the continent (Clerc et al., 2018; Tugend et al., 2018). Such continentward dipping normal faults have been envisaged to play an important role, especially in magma-rich margins where they are interpreted to be responsible for providing accommodation space for the characteristic Seaward Dipping Reflectors (SDRs; see section 2.3.2.1. below). Clerc et al. (2018) propose three methods of their formation: 1) Reactivation of inherited faults, 2) Relative motion between asthenosphere and lithosphere, and 3) gravity-collapse above a plume head impinging on the base of the lithosphere.

While the study of seismic sections can provide an overview of the architecture of the margin, the controlling parameters can be assessed by carefully set-up numerical models. Such studies have investigated parameters like strain-rate and the thermal structure as well as the rheological structure of the crust to investigate how these parameters control the evolution and final architecture of rifted margins (Huismans and Beaumont, 2011; Brune et al., 2014; Huismans and Beaumont, 2014; Naliboff and Buiter, 2015; Petri et al., 2019). It is important to note, however, that these models are set up for magma-poor margins as models are not yet able to take magmatism and melt production into account. Numerical and analogue modelling has shown that for magma-poor systems, the final rift architecture is greatly dependent on the rheological structure of the entire lithosphere and the coupling between the different levels. For example in the case of a dry mafic lower crust overlain by weak, quartzofeldspathic middle crust, a decoupling will occur between the brittle upper crust and the lower crust (Type I rift in Manatschal, 2004; Péron-Pinvidic et al., 2007; Huismans and Beaumont, 2011; Mohn et al., 2012), allowing for a sharp necking domain with concave-down fault systems that can exhume the underlying mantle to the sea-floor in a rolling-hinge system (e.g. Lavier and Manatschal, 2006). In the case of weak middle and lower crust located between a strong upper crust and the upper mantle (Type II rifts in Huismans and Beaumont, 2011; Clerc et al., 2018), there is a strong decoupling and ductile thinning of the weak layer leading to distributed thinning of the upper crust, but no mantle exhumation. These layer-cake models consider average and continuous rheological properties of the lithosphere. Field observations from the magma-poor fossil margin, *e.g.* in the Alps, has revealed that the crust has inherited heterogeneities, such as gabbroic bodies, and is

thus more complex than layer-cake models. Modelling of such complex systems has shown the importance of structural softening caused by necking of strong layers and strain localization along the weak layers (Duretz et al., 2016; Petri et al., 2019).

A Type II rheological configuration has been proposed where the lower crust is thermally weakened either by high heat flow or by ingress of large quantities of mafic melts (Clerc et al., 2015) making the lower crust hot and weak, which in turn allows distributed deep intra-basement deformation and a lower taper angle of the entire margin (Clerc et al., 2018). High-resolution reflection seismic profiles indicate the presence of an anastomosing network of ductile shear zones at depth below margins such as the Barents Sea and Uruguay margin, which was caused by high heat-flow related to a continuous sedimentary cover (e.g. Allen and Allen, 2013) or the impingement of a mantle plume to the base of the lithosphere (Clerc et al., 2018). Kjøll et al. (2019a and Chapter 1 of this thesis) describe abnormally hot conditions during continental rifting of the pre-Caledonian margin of Baltica with ambient temperatures in excess of 650°C and locally pervasive migmatization at 8-14 km depth. Some of the shallow migmatization is related to the contact metamorphic melting at dyke-host rock contacts. A thick, early syn-rift sedimentary cover sequence may have acted as a thermal blanket contributing to elevated thermal gradients in the rift. Another likely possibility, which does not exclude the previous one, is that the excessive heat was introduced by the massive emplacement of the SDC (Kjøll et al., 2019a; Kjøll et al., 2019b; Tegner et al., 2019; Chapters 1-3, this thesis). The thermal weakening effect of such magmatism on the crust has been shown to cause an upward migration of the brittle ductile transition (Kjøll et al., 2019b; Chapter 2, this thesis) and thereby a thickening of the ductile crust relative to the brittle crust. Such thermal weakening leads to a modification of the rheological structure of the lithosphere (Bialas et al., 2010; Daniels et al., 2014; Kjøll et al., 2019b; Chapter 2, this thesis) and therefore has large implications on the dynamics of continental rifting as described above (*e.g.* Huismans and Beaumont, 2011; Huismans and Beaumont, 2014). In the Main Ethiopia Rift, thermal weakening caused by mafic dykes led to a final tectonic stretching event and adiabatic decompression melting which caused the final break-up to take place (Bastow and Keir, 2011).

2.3. Two archetypes of rifted margins

Despite the above mentioned complexities, two archetype margins are generally recognized (e.g. Mutter et al., 1988; White and McKenzie, 1989): 1) magma-poor rifted margins (Fig. 0-4A; also known as non-volcanic or sedimentary margins e.g. Whitmarsh et al., 2001; Schaltegger et al., 2002; Contrucci et al., 2004; Péron-Pinvidic and Manatschal, 2009) and 2) magma-rich rifted margins (Fig. 0-4B; also known as volcanic rifted margins; e.g. Geoffroy, 2001; Menzies et al., 2002; Geoffroy, 2005; Franke, 2013; Kjøll et al., 2019a; Chapter 1, this thesis). The latter are commonly associated with excessive magmatism often

caused by mantle plumes (e.g. Iceland and Tristan plumes; White and McKenzie, 1989; Storey, 1995; White et al., 2008). The former connotation of volcanic and non-volcanic has been abandoned due to the realization that non-volcanic margins also may show some magmatism (e.g. Tugend et al., 2018). The distribution of magma-rich vs. magma-poor margins is *circa* equal, but for the Atlantic margins the magma-rich dominate by up to 75% (Menzies et al., 2002), perhaps because of their favorable location above the African Large Low Shearwave Velocity Province (LLSVP; Burke et al., 2008) and the association with a Plume Generation Zone (PGZ; Steinberger and Torsvik, 2012; Torsvik and Cocks, 2013). The two endmembers are often found within the same ocean basin, like in the south Atlantic, where the South Atlantic central segment is classified as magma-poor, and the southern South Atlantic segment is classified as magma-rich (e.g. Blaich et al., 2011). Transition zones between magma-rich and magma-poor are, however, little explored, but pre-existing lithospheric structures together with the degree of mantle melting may play an important role in controlling where the transition occurs (Gouiza and Paton, 2019; Jakob et al., 2019; Chapter 5, this thesis). In the following sections there will be a description of the two archetypes. Since this thesis mainly deals with magma-rich systems, there will only be a short description of the magma-poor margins. A more extensive description is provided about the magma-rich margins and its characteristic features.

2.3.1. Magma-poor margins

Magma-poor margins are generally characterized by tectonic stretching of the lithosphere due to far field stresses like plate tectonic movement or body forces related to over-thickened crust (Dewey, 1988). In general, such margins are relatively wide, for example the Iberia-Newfoundland margins, which are more than 300 km wide (Fig. 0-5 Contrucci et al., 2004; Manatschal and Müntener, 2009). Analogue and numerical simulations have shown that rheological strength of the crust and mantle, as well as crustal extension rates are factors that govern the margin architecture (Brun and Beslier, 1996; Huismans and Beaumont, 2014; Tetreault and Buiter, 2018). Magma-poor rifted margins become hyperextended when the crustal thickness is reduced to < 10 km. As in the case of Iberia-Newfoundland conjugate margins, crustal thinning may be extreme and crustal scale, concave down shear zones may cause exhumation of sub-continental lithospheric mantle in their footwall (Boillot et al., 1980; Manatschal et al., 2001; Tucholke et al., 2007; Péron-Pinvidic and Manatschal, 2009; Péron-Pinvidic et al., 2013). Within this domain, magmatism becomes progressively more important oceanward as an oceanic crust develops (Whitmarsh et al., 2001; Gillard et al., 2017; Tugend et al., 2018).

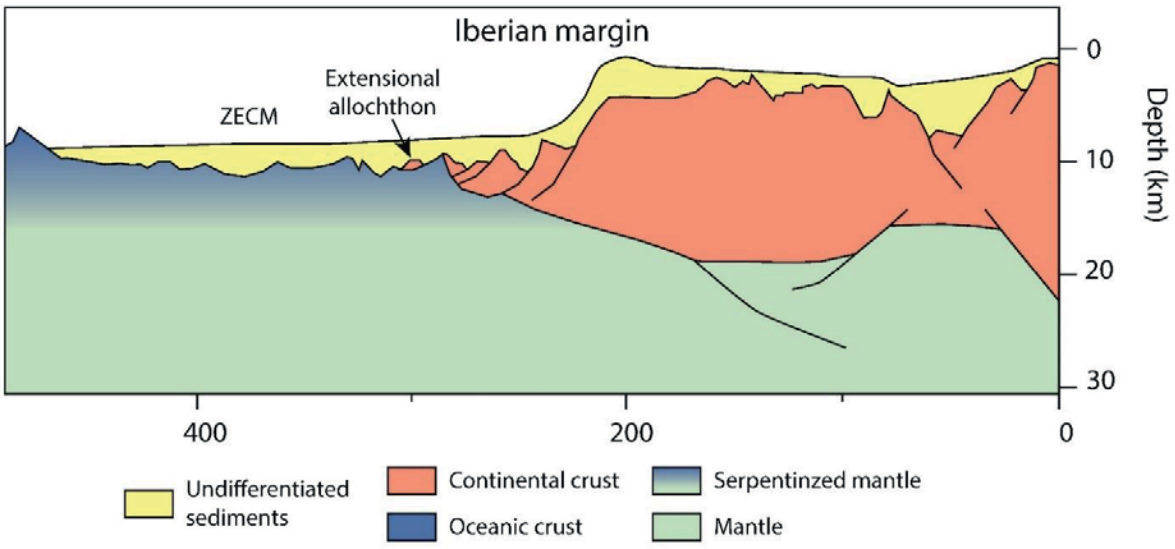

Figure 0-5: Sketch of a magma-poor margin after (Péron-Pinvidic and Manatschal, 2009). ZECM: Zone of Exhumed Continental Mantle.

2.3.2. Magma-rich rifted margins

Magma-rich rifted margins are generally characterized by voluminous syn-rift magmatism. They often show a higher taper angle, *i.e.* sharp necking. Due to the magmatism, they have several characteristic features that can be observed on 2D seismic reflection lines (Fig. 0-6):

- One or several domains of seaward dipping reflectors (SDR) that have been the target of several ODP cruises and shown to be mostly comprised of mafic lava flows interbedded with volcanogenic sediments.
- Sill complexes in the associated sedimentary basins, important for hydrocarbon maturation as well as gas release tied to environmental changes.
- A high P-wave velocity (> 7.2 km/s) lower crust often dubbed the “Lower Crustal Body” (LCB) of an unknown composition.

In addition, feeder-dyke systems are inferred to feed the sub-aerial volcanic edifice. The seismic imaging of the deeper features is, however, challenging due to for example large impedance contrast between basalts and sediments, leading to a loss in seismic signal with depth. The abovementioned features are all associated with significant igneous activity along the margin and are caused either by decompressional melting or elevated LAB temperatures. Estimation of the mantle potential temperatures can be done using Rare Earth Elements (REE) and major elements using the phase transitions of garnet and spinel (Tegner et al., 1998a; Brown and Lesher, 2016; Tegner et al., 2019; Chapter 3 this thesis). Both deep seated mantle plumes (e.g.

Steinberger et al., 2019) and relatively shallow small-scale convection (Geoffroy, 2005) can explain the elevated LAB temperatures. The degree of partial mantle melting depends on the difference between mantle potential temperatures and how refractory the affected mantle is (e.g. Brown and Lesher, 2016; Tegner et al., 2019; Chapter 3 this thesis). Magma-rich margins are associated with large volumes of mafic magma and volume estimation of the extrusive SDRs along the East coast of the United States suggest a total volume of the "thick igneous crust" of *c.* 2.7×10^6 km^3 (Kelemen and Holbrook, 1995). A minimum igneous volume for the South Atlantic and North Atlantic Igneous Province has been estimated to 3.62×10^6 km^3, which include a minimum of 2.13×10^6 km^3 extrusive components for the south (Gladczenko et al., 1998) and 1.8×10^6 km^3 flood basalts for the North Atlantic magma-rich margins (Eldholm and Grue, 1994). These estimated volumes are predicted from seismic sections and have large uncertainties because they account for the total volume of rock with a certain P-wave velocity, representing an average of the rock volume. The field observations presented below (Kjøll et al., 2019a; Chapter 1 this thesis) provides the means to better constrain the magmatic volumetric estimates for distal rifted margins, by providing a better understanding of the distribution of continental crust with respect to magmatic crust.

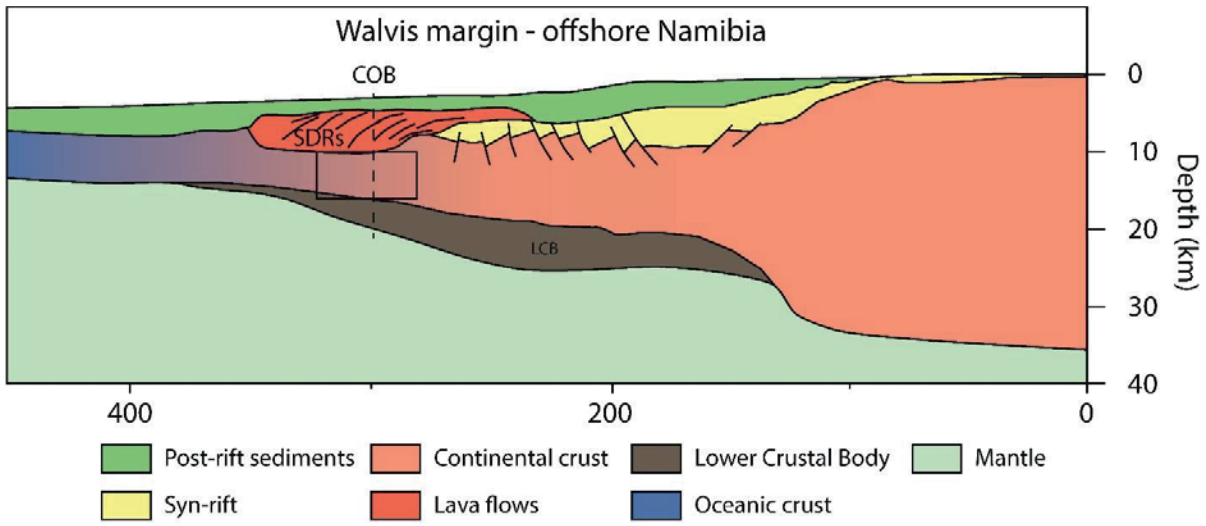

Figure 0-6: Magma-rich margin after Blaich et al. (**2011**). Black square indicates a possible location of the field area studied in this thesis. COB: Continent-Ocean Transition, SDRs: Seaward Dipping Reflectors, LCB: Lower Crustal Body

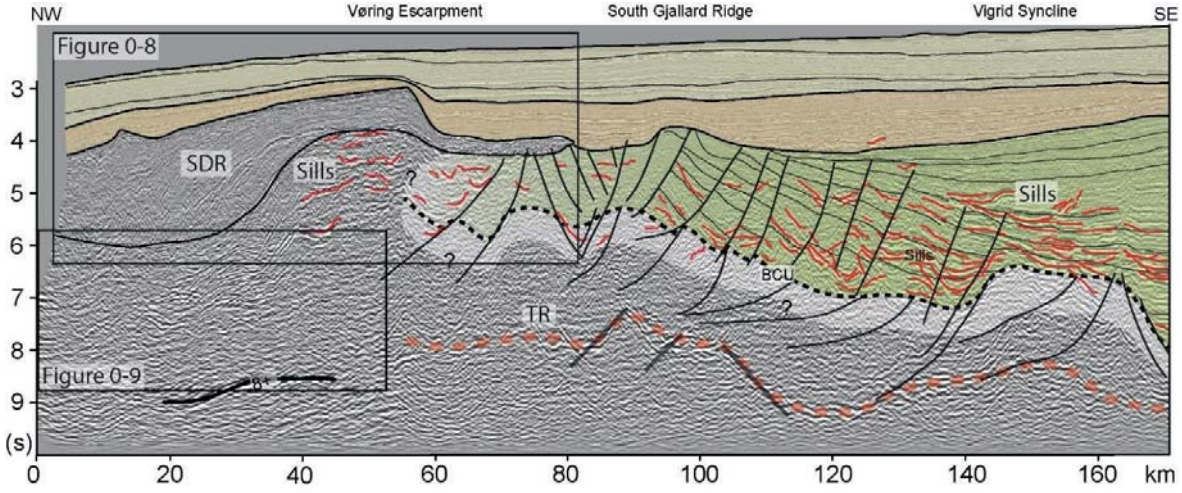

Figure 0-7: Seismic line across the distal part of the Vøring magma-rich rifted margin offshore central Norway. Modified after Abdelmalak et al. (2017). SDR: Seaward Dipping Reflectors, TR: T-reflection, after Gernigon et al. (2004). BCU: Base Cretaceous Unconformity. Red lines are sills. Black line show where seismic speeds exceed 8 km/s. Black squares show location of figure **0-8** and **0-9**.

2.3.2.1. Extrusive complex

Seismic sections of the distal part of magma-rich rifted margins display one or several wedge shaped domains with strong seaward dipping reflections, so called Seaward Dipping Reflector sequences (SDRs; e.g. Planke and Eldholm, 1994; Fig. 0-7 and 0-8). These features are omnipresent in magma-rich rifted margins and are considered as a diagnostic feature. Commonly, inner SDRs develop on top of continental crust at the Continent-Ocean Boundary (COB) and outer SDRs develop on top oceanic crust. The SDRs have been drilled on the Vøring margin, offshore central Norway, and shown to comprise a thick sequence (from 3 to 6 seconds; Fig. 0-8A) of subaerial lava flows interlayered with volcanogenic and terrestrial sediments (e.g. Mutter et al., 1982). There are several models which describes the formation of SDRs although the internal architecture may vary even within the same wedge (Tugend et al., 2018). McDermott et al. (2018) found two types of SDRs (Fig. 0-8B), one controlled by syn-magmatic faulting (Geoffroy, 2005; Clerc et al., 2018) and the other by crustal flexure caused by solidification of the feeder dykes. Furthermore, where the magma gets in contact with water the lava is quenched and fragments into hyaloclastites, which often, such as the Vøring escarpment, form Gilbert-type deltas (Fig. 0-8A; Abdelmalak et al., 2016). Outer SDRs are interpreted to form as deep marine flows and pillows (Planke and Alvestad, 1999).

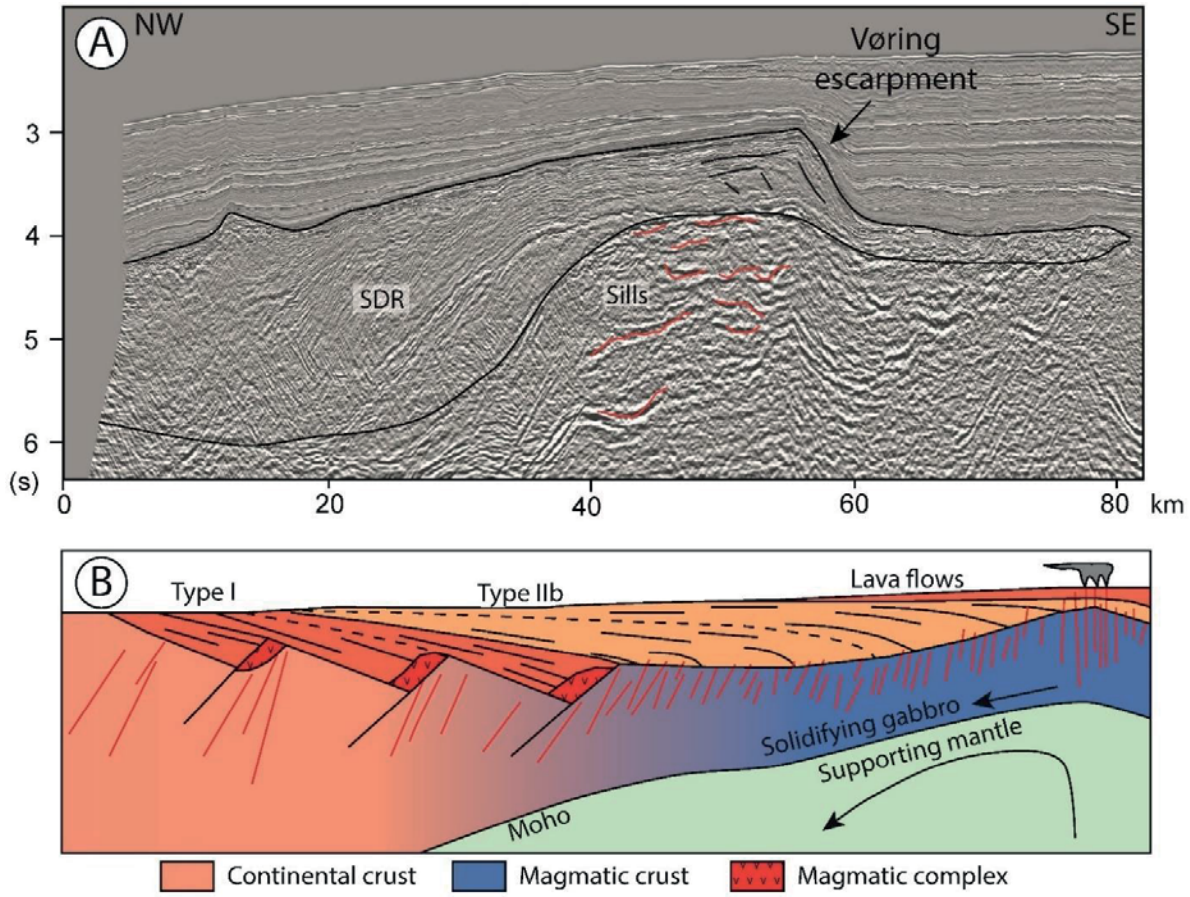

Figure 0-8: Extrusive features at magma-rich rifted margins. A) Reflection seismic image showing what has been interpreted to represent the extrusive domain of the Vøring margin, with a thick package of SDR (Seaward dipping reflectors) and a Gilbert type delta, where the lava quenched in water to form hyaloclastites in a prograding delta (Abdelmalak et al., 2016). Interpretation is from Abdelmalak et al. (2017). B) Model drawing showing two different types of SDRs after McDermott et al. (2018). Type I form due to syn-magmatic faulting and Type IIb form due to isostatic loading due to crystallizing gabbro and decreasing support from mantle away from spreading center. Note that the spreading center is to the left in A and right in B.

2.3.2.2. Sills and dikes in the sediments

Another important aspect of magma-rich rifted margins is the emplacement of large sill and dike complexes in the proximal basin (Fig. 0-7; Svensen et al., 2012). Such sill complexes are spectacularly exposed in *e.g.* the Karoo basin, which display kilometer scale, saucer-shaped sills still surrounded by the contact metamorphic host rocks (Svensen et al., 2006; Galerne et al., 2008; Galerne et al., 2011). Both degassing from the magma as well as degassing from the contact metamorphic aureole surrounding the sills have shown to have great climatic implications possibly leading to mass extinctions if the sills are emplaced in organic rich shales or evaporite deposits (e.g. Svensen et al., 2004; Heimdal et al., 2019). The produced

gasses are released through vent-structures often propagating to the surface from the tip of saucer shaped sills (e.g. Jamtveit et al., 2004; Svensen et al., 2006). Such relatively shallow magmatic complexes into sedimentary basins can potentially have important economic implications for *e.g.* hydrocarbon maturation (e.g. Iyer et al., 2017) and sediment-hosted deposits such as Mississippi Valley Type (MVT) Pb-Zn deposits (e.g. Cawood and Hawkesworth, 2015).

2.3.2.3. Basement dike complex

Below the extrusive lava flows are the lower part of the magmatic plumbing system, which is represented by a highly intruded crust, that acted as feeders to the subaerial lava flows (Fig. **0-9**). This domain of the magma-rich rifted margin is poorly known, mainly due to the difficulties of sub-basalt seismic imaging, as well as imaging of sub-vertical structures. Some vertical and inclined structures have, however, been imaged on seismic profiles and these are interpreted to be dykes (Abdelmalak et al., 2015; Fig. 0-9). This area is particularly important as this is where the continental crust transitions into oceanic crust by increasing the density of dykes.

There are two field analogues of this domain. One is the uplifted parts of the central east Greenland margin where a mafic dyke complex intrudes into Paleoproterozoic orthogneisses and can be shown to feed lava flows on top (Klausen and Larsen, 2002), and the second is the dyke swarm described in detail in this thesis (Kjøll et al., 2019a; Kjøll et al., 2019b; Tegner et al., 2019; Chapters 1-3). The dyke complex in East Greenland, not a fossil analogue, but rather an uplifted rift flank, is interpreted to be related to the flexure of the continental crust at the innermost part of the inner lava flows (Karson and Brooks, 1999). The flows rest directly on the Proterozoic basement and are locally separated by an erosional surface. Some dykes can be followed from the basement and into the lava pile as well (Klausen and Larsen, 2002).

The dyke swarm studied in this thesis differs from the Greenland swarm in that it intrudes a pre- or early syn-rift, platform sedimentary succession and a syn-rift sedimentary succession (Nystuen et al., 2008; Chapter 5) rather than cratonic basement. Also, no subaerial lava flows have been recognized so far in the Scandinavian Caledonides. The preserved section is deeper and presumably more distal due to the locally denser network of mafic dykes and the brittle-ductile emplacement mechanisms (Kjøll et al., 2019b; Chapter 2 this thesis), as shown by the geothermobarometry presented in Chapter 1 and Kjøll et al. (2019a). More details on the dyke swarm and the host rock can be found in Chapters 1, 2, 3 and 5.

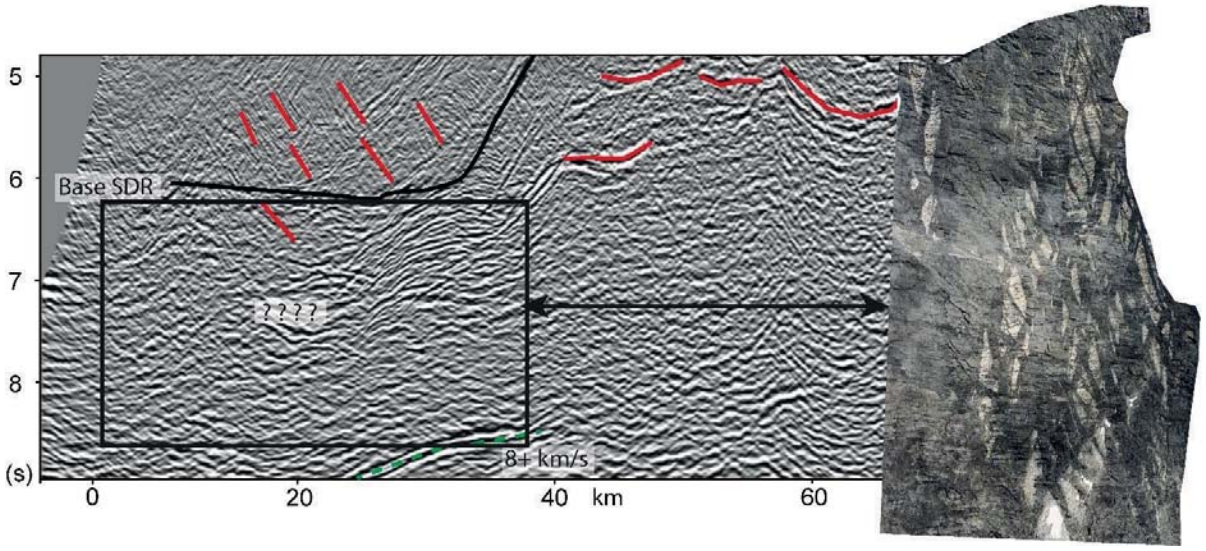

Figure 0-9: Seismic reflection line from the sub-SDR part of the Vøring margin, offshore central Norway. Interpreted seismic line after Abdelmalak et al. (2017). Black line indicates base of SDRs. Red lines from 40-60 km represent sill intrusions whereas red lines from 10-35 km represent dykes. Green dashed line shows the "T-reflection" of Gernigon et al. (2004). Insert to the right is the cliff in Sarek, rotated to right-way-up. Black rectangle indicates a possible analogue area. The width of view for the insert is approximately 200 meters.

2.3.2.4. High seismic-velocity lower crust

Another characteristic feature of magma-rich rifted margins is a high compressional wave (P-wave) velocity lower crust, referred to as a Lower Crustal Body (LCB) or High Velocity Lower Crust (HVLC). These bodies generally have P-wave velocities (V_P) higher than 7.0 km/s and a P- and S-wave ratio, V_P/V_S of *c.* 1.8 (Mjelde et al., 2003). They have never been properly described in the field and due to overlapping geophysical properties of the possible rock types, no consensus on the composition has been reached. Several different models have been proposed to explain the composition of the LCBs. The four most common ones are shown in Figure 0-10 and listed here: 1) Massive mafic underplating, 2) Serpentinized mantle, 3) Inherited high grade metamorphic lower crust and 4) Highly intruded lower crust. The occurrence of massive mafic to ultramafic magmatic underplates was suggested early. It was based on major element chemistry, specifically on the northeast Atlantic margin which opened during impingement of the Iceland plume (*e.g.* White and Mckenzie, 1989). These data showed that the extrusive lavas had undergone magmatic fractionation, leaving behind a high Mg# mafic to ultramafic fractionation product (Op. cit). The second alternative model proposes that seawater can flow along faults at a hyperextended margin segment and percolate into the mantle promoting serpentinization reactions of the mantle peridotites and dunites (Lundin and Doré, 2011). The third alternative is slivers of high grade metamorphic continental crust, such as eclogites, preserved below the sedimentary basins. This model does not necessarily distinguish between

magma-rich and magma-poor margins, since it is mostly dependent on the rock type of the continental basement. This is the preferred model for the relatively proximal LCBs found in the northern North Sea (Hord platform) where there is a natural offshore continuation of the high grade onshore Western Gneiss Region (WGR; Christiansson et al., 2000; Labrousse et al., 2010). The last alternative model combines models 1 and 3 and consists of a highly sill intruded, inherited lower crust. This model is typically used where seismic reflections are present within the LCB (*e.g.* Abdelmalak et al., 2017; Blaich et al., 2011). Seismic wave speed modelling from active rifts (Main Ethiopia Rift; Bastow et al., 2011) and failed rifts (Baikal rift, Thybo and Nielsen, 2009; Oslo rift, Stratford and Thybo, 2011) suggest that LCBs develop relatively early during continental rifting and at least before break-up. This suggests a magmatic origin.

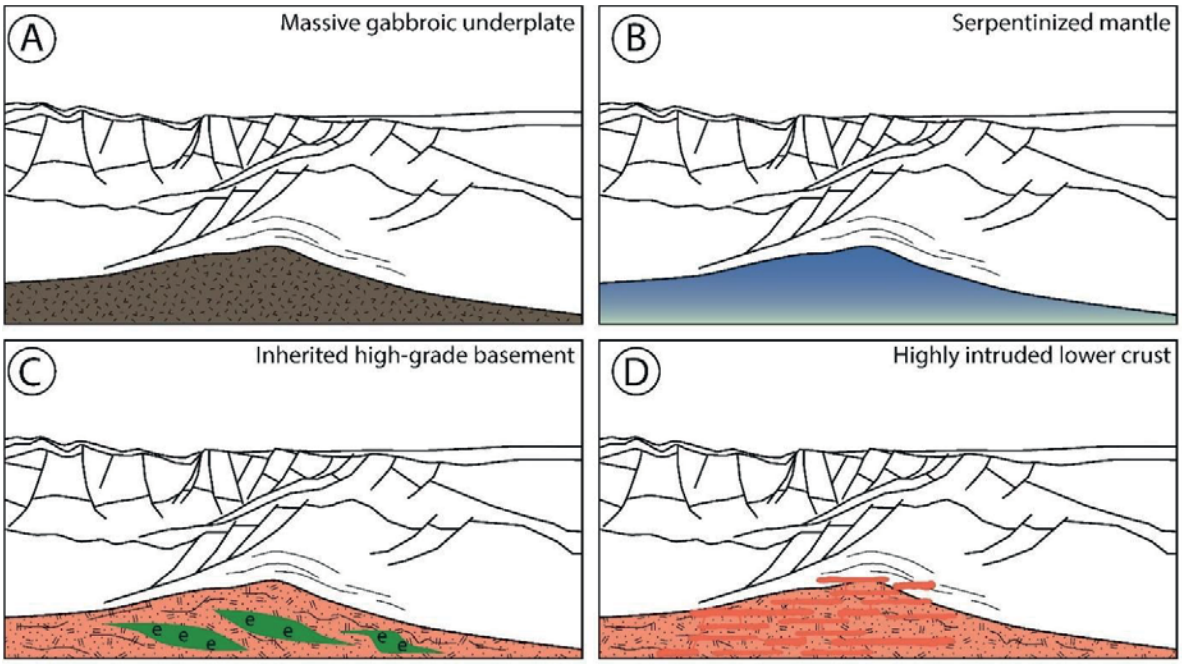

Figure 0-10: Possible scenarios for the composition of an LCB below the Vøring margin. Modified after Gernigon et al. (2004). A) Massive gabbroic underplate B) Serpentinized mantle, C) Inherited high-grade gneiss with eclogite boudins (e, green). For the Vøring and Møre margin, this would be an extension of the Western Gneiss Region. D) Highly intruded lower crust containing large sill complexes. See text for further explanations.

The LCBs represent a large and primary feature which is developed at magma-rich rifted margins and is therefore potentially an important element in our understanding of how continents can break apart. For example, if they represent massive ultramafic to mafic underplates, they would presumably influence the thermal structure of the rifting crust, facilitating rifting by promoting ductile deformation and causing a higher heat-flow in the basin, possibly affecting hydrocarbon maturation. If they represent a highly intruded lower crust they may also influence the thermal structure of the crust. But perhaps more

importantly the lower crust, which is generally thought to be dry and strong. Introducing melts and fluids will presumably promote deformation and ductile flow as well, at least locally in the lower crust. A similar scenario can be envisaged for serpentinization of the mantle, which at only 15% serpentinization will reduce the strength of the upper mantle significantly (Escartín et al., 2001). This process may also be important for the preservation of the rifted margin during subsequent inversion. A thorough understanding of these structures is therefore pivotal to understand the formation and evolutionary processes of these first order lower crustal structures.

2.4. Inversion of rifted margins and rift inheritance

Studies of mountain belts have shown that rifted margins play a crucial role in controlling the architecture of orogens *e.g.* the Pyrenees (Lagabrielle et al., 2010; Roca et al., 2011; Clerc and Lagabrielle, 2014), Alps (Dietrich, 1970; Manatschal and Nievergelt, 1997; Manatschal, 2004; Mohn et al., 2014; Beltrando et al., 2015), and in the Caledonides (Andersen et al., 2012; Jakob et al., 2017; Jakob et al., 2019; Chapter 5 this thesis). Crustal thinning at rifted margins is accommodated by crustal-scale detachment faults and steeper normal faults. These faults remain weak and in favorable orientation when the stress regime changes to horizontal compression and thereby enables the reactivation of the faults during late stages of the Wilson cycle (Fig. 0-1). The reactivation of rift-faults in a horizontal compressional stress field is one of the main processes that controls rift inheritance during orogenic convergence (Epin et al., 2017). This process, partially and locally, preserves the association of rift-related domains in the nappe stack. Thus, if thrusting is in-sequence it will preserve the proximal domain at the base with the distal domain thrusted on top (e.g. Jakob et al., 2019; Chapter 4, this thesis). If the thrusting is out-of-sequence, however, the structural architecture will be more complex and thereby recognizing rift inheritance more challenging.

The understanding of magma-poor margins greatly benefitted from the recognition of rift inheritance in orogens such as the Alps or Pyrenees, as it allowed research to be conducted on the out-crop scale rather than in seismic sections and drill cores. Fossil analogues to magma-rich margins, on the other hand, have until now never been properly recognized as fossilized within mountain belts. This is presumably due to their dense nature and thereby also low preservation potential during the continental collision. The papers presented in this thesis show that certain levels of the Scandinavian Caledonides may represent a fossil analogue of a magma-rich margin. Although the rocks were thoroughly described in the 90’s (Kathol, 1989; Andréasson et al., 1992; Stølen, 1994; Svenningsen, 1994a, 2001), their geodynamic significance was not much elaborated. Therefore, one of the aims of this thesis has been to put the observations into the framework of the current knowledge of rifted margins.

3. Regional geological framework for this thesis

The fossil magma-rich rifted margin presented herein formed during the Late Neoproterozoic, when the continents Baltica and Laurentia rifted apart. In order to understand the complexities of this margin it is necessary to build a proper geological and paleogeographic framework to put the observations presented in Chapter 1-5 in context. The following section will deal with the paleogeography of the pre-Caledonian margin as well as the evolution and composition of the Seve Nappe Complex (Seve NC).

3.1. Global and local paleogeography in the Neoproterozoic

There are some significant uncertainties related to global Neoproterozoic paleogeographic reconstructions, but most models agree that the continents were arranged in some sort of a supercontinent configuration, named Rodinia (e.g. Li et al., 2008; Cawood et al., 2016; Merdith et al., 2017; Fig. 0-11 A and B). Most models also agree that Baltica and Laurentia were close together at least during the late Neoproterozoic. This correlation is primarily based on similar aged paleomagnetic poles, similarities in sedimentary stratigraphy and the relatively limited fossil record (Nystuen et al., 2008; Pease et al., 2008), as well as similarities in age between the Grenville and Sveconorwegian orogenies, although this has recently been disputed (Slagstad et al., 2017). Two of the most reliable paleomagnetic poles come from mafic dyke swarms of similar age intruded into autochthonous rocks (Fig. 0-11C): the 616 ± 3 Ma Egersund dykes (Bingen et al., 1998; Walderhaug et al., 2007), and the 615 ± 2 Ma Long Range dykes (Kamo et al., 1989; Murthy et al., 1992; Kamo and Gower, 1994). These two paleomagnetic poles places Baltica and Laurentia at low latitudes in the Ediacaran, possibly on the southern hemisphere (Fig. 0-11), which is also corroborated by the sedimentary depositional environment of carbonates with local evaporite deposits (e.g. Kumpulainen, 1980; Svenningsen, 1994b; Chapter 5, this thesis). For paleomagnetism older than 210 Ma (oldest seafloor), the proximity between continental blocks cannot be constrained because paleomagnetism does not constrain longitude. Longitude can, nevertheless, be constrained if one assumes that the LLSVPs have been stable since the Ediacaran and that LIPs derive at the PGZ (Torsvik et al., 2014). Then the continents can be reconstructed back to a position where all the magmatic centers, such as the kimberlites and carbonatites belonging to the Central Iapetus Magmatic Province (CIMP; Ernst and Bell, 2010), fit the outline of a PGZ (Fig. 0-11C; Tegner et al., 2019; Chapter 3, this thesis). Relative longitudinal constraints can also be found in the geological record by assessing the microbiotic record. Microfossils (acritarches and cyanobacteria) preserved in the sedimentary succession of the shelves of Baltica and Laurentia suggest a close proximity and that there must have been a continuous platform between the continents as these

microorganisms could not swim across deep ocean basins (e.g. Pease et al., 2008and references therein; Chapter 5, this thesis).

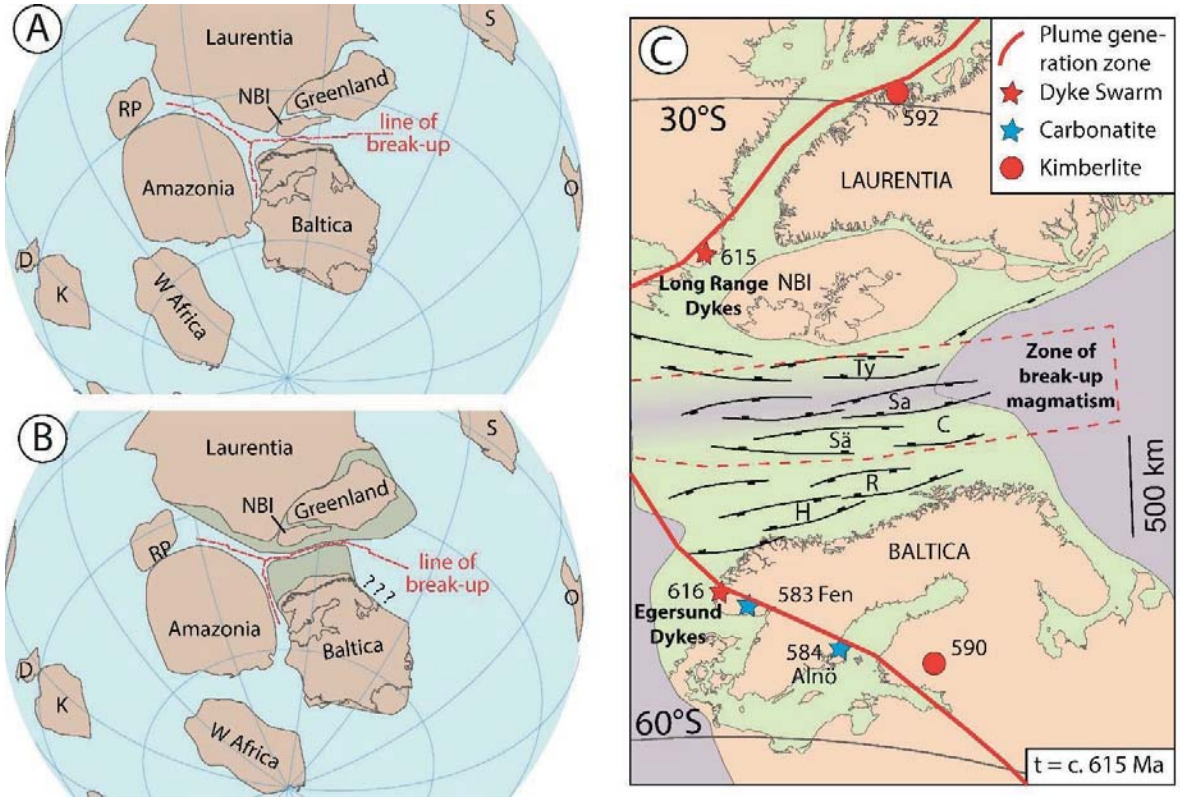

Figure 0-11: Paleogeographic reconstructions at *c.* 615 Ma. A) and B) Possible paleogeographic reconstructions of Rodinia, constructed using data presented in Merdith et al. (2017). In A the extent of the current margin is used. In B an inferred wide Baltica margin is proposed. D: Dronning Maud Land, K: Kalahari, O: Ordoc, R: Rockall RP: Rio de Plata, S: Siberia. C) Detailed reconstruction based on Tegner et al. (2019), where longitude is constrained assuming the stability of the LLSVPs. Numbers next to symbol are ages in million years. H: Hedmark R: Risbäck, Sä: Särv, Sa: Sarek, C: Corrovarre are areas investigated for this thesis. Ty: Tyvallich comprise similar types of rocks as in the Seve NC and is presently found on the NBI: North British Isles (Chew and van Staal, 2014).

There are not only uncertainties about the global paleogeographic reconstructions, but also about the paleogeography and architecture of the pre-Caledonian margin of Baltica. Traditionally, the margin was assumed to have a cylindrical and simple geometry with a rapidly thinning crust that transitioned into oceanic crust and with little lateral variability (e.g. Stephens and Gee, 1989). Recent studies have shown

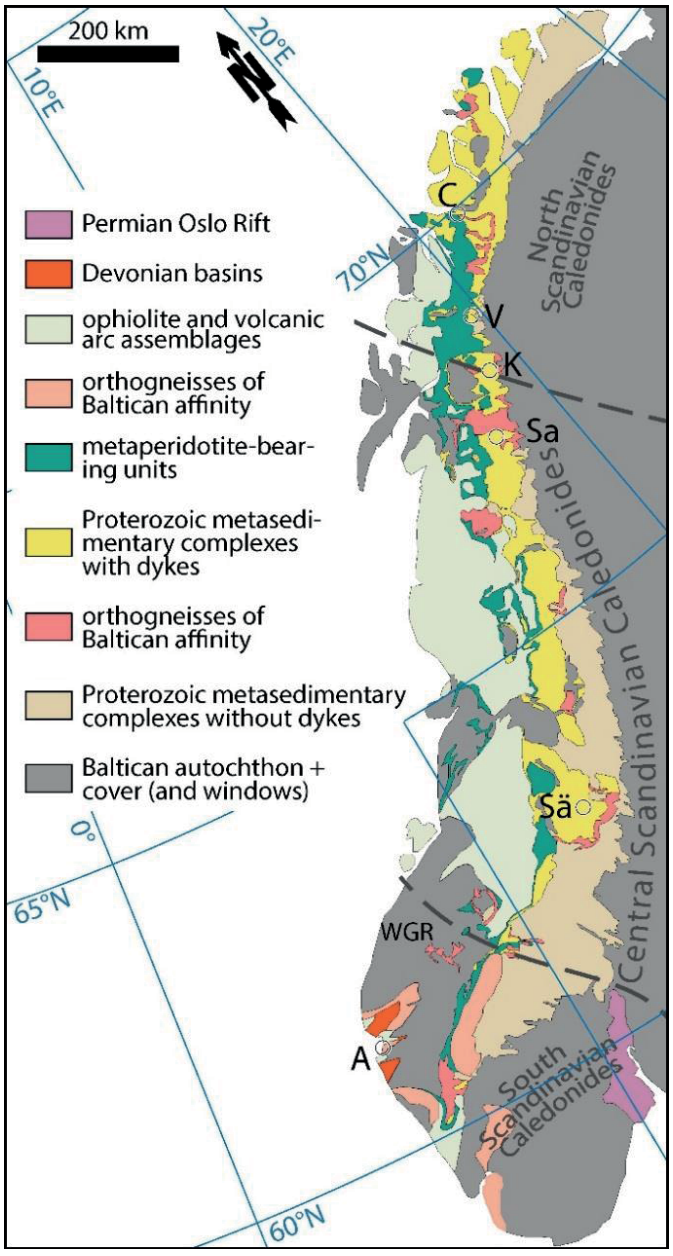

Figure 0-12: Tectonostratigraphic map of the Scandinavian Caledonides, divided into a south, central and northern part. Circles denote the field areas for this thesis Sä: Särv, S: Sarek, K: Kebnekaise, V: Váivvancohkka, C: Corrovarre, A: Atløy, WGR: Western Gneiss Region

that the pre-Caledonian margin of Baltica was more complex and had significant lateral variability along and across strike, such as: 1) magma-poor and a magma-rich domain with an intervening *c.* 200 km wide transition zone (Jakob et al., 2019; Kjøll et al., 2019a; Tegner et al., 2019; Chapter 1-5 this thesis), 2) the Jotun microcontinent (Fig. 0-12), which is underlain by a meta-peridotite bearing mélange unit, referred to as an OCT assemblage; (Fig. 0-12; Andersen et al., 1990b; Andersen et al., 2012; Jakob et al., 2017; Jakob et al., 2019; Chapter 4 this thesis), and 3) a hyperextended domain, although the age of the hyperextension is unclear. Further complexities are introduced in the northern part of the Scandinavian Caledonides (Fig. 0-12), represented by the Kalak Nappe Complex. Wherein their affinity (Baltica or not) is still debated due to a complex Early to Late Neoproterozoic deformation and metamorphic history which is rarely recognized elsewhere on Baltica (e.g. Corfu et al., 2007; Kirkland et al., 2007; Corfu et al., 2011; Gasser et al., 2015; Gee et al., 2016). With the aforementioned complexities together with the more comprehensive knowledge of rifted margins that has been gained over the last decades it is reasonable to think that the pre-Caledonian margin of Baltica was more complex than previously assumed and therefore that the previous models may have been too simplistic to explain some of the major features preserved in the mountain belt (Corfu et al., 2014).

3.2. The Scandinavian Caledonides

The Scandinavian Caledonides is a Silurian to early Devonian aged mountain belt. It is part of the Caledonian-Appalachian orogen that developed when the Iapetus Ocean was subducted and closed, causing the paleocontinents Baltica and Avalonia and Laurentia to collide. The field work for this thesis has mainly been focused in the central and northern Scandinavian Caledonides and therefore the following introduction will mainly focus on these areas (Fig. 0-12).

The Scandinavian Caledonides stretches from the North Sea, south of Egersund in southern Norway, through Norway and Sweden and the onshore exposure terminates on the Varanger Peninsula in northern Norway, where it continues northeast into the Barents Sea (Fig. 0-12; Corfu et al., 2014). It is traditionally subdivided into Allochthons that were further subdivided into Lower, Middle, Upper and Uppermost Allochthons (Roberts and Gee, 1985), which now rest on the Baltican Autochthon. Initially this subdivision was purely descriptive and did not have any assigned paleogeographic interpretation. Stephens and Gee (1989) argued that the Lower, Middle and partly Upper allochthon represent Baltican basement and cover, whereas the upper part of the Upper and Uppermost Allochthon are inferred to be of oceanic and Laurentian affinity, respectively. This has been a useful subdivision but has, with the present knowledge of complexities of rifted margins, proven to be insufficient and in part confusing in explaining the observed geology (Andersen et al., 2012; Corfu et al., 2014; Jakob et al., 2019; Chapter 4, this thesis).

In the central part of the Scandinavian Caledonides (Fig. 0-12), which has been the primary target for fieldwork related to this thesis, a sedimentary cover called the Dividalen Group rests parautochthonously above the Paleoproterozoic to Mesoproterozoic Baltican basement. This unit was deposited in the Early Cambrian to Ordovician. The unit can be traced below most of the Caledonian nappes in Scandinavia and in the younger Permo-Carboniferous Oslo rift (Fig. 0-12). There are no mafic dykes described from the Dividalen Group. An extensive Meso- to Paleoproterozoic basement unit, called the Akkajaure NC in the north, is thrust on top of the Dividalen Gr (Rehnström et al., 2002; Chapter 5, this thesis). Locally this allochthonous basement unit is imbricated and preserves a Paleoproterozoic cover sequence (Kirkland et al., 2011; Chapter 5, this thesis). This entire unit is cut by variously metamorphosed, undated mafic dykes (Rehnström and Corfu, 2004; Chapter 5, this thesis). On top of the basement units, like the Akkajaure NC, rest several allochthonous supracrustal units, such as the Särv Nappe and the Seve NC. Traditionally the Särv Nappe was ascribed to the lower allochthon due to its low metamorphic overprint, but is now generally interpreted to belong to the middle allochthon due to its lithological similarities to the Seve NC (Andréasson et al., 1998; Gee et al., 2013). An interpretation which is corroborated by the correlation between basins presented in Chapter 5 of this thesis. The Särv Nappe consists of a little deformed, Neoproterozoic

sedimentary succession and contain abundant mafic dolerite dykes. Several correlatives of the Särv, such as the Risbäck Basins, do not contain dykes and are therefore generally given a more proximal location on the pre-Caledonian margin of Baltica (Fig. 0-11C; Nystuen et al., 2008). The Seve NC contains primarily supracrustal rocks, such as psammites and mica schists with minor amphibolites, eclogite boudins and peridotites. Locally, large lenses have escaped most penetrative Caledonian strain and metamorphism, and these lenses have been the field targets for this thesis (detailed descriptions can be found in Chapters 1-5 below). Above and below these mega-boudins the rocks are deformed and metamorphosed, locally reaching eclogite facies mineral assemblages (Kullerud et al., 1990). Thrusted on top of the Seve NC is the Köli NC of the Upper Allochthon, traditionally interpreted to represent Iapetus derived rocks. The Köli NC is primarily comprised of greenschist to amphibolite facies metasedimentary successions with interlayered volcanogenic products. Also associated with this allochthon are ophiolites and island arc type rocks (e.g. Andresen and Steltenpohl, 1994). The Uppermost Allochthon consists of units with affinities foreign to Baltica, presumably with a peri-Laurentian affinity. These rocks are comprised mainly of metasediments and Proterozoic orthogneisses and large magmatic arc-complexes of mostly Ordovician age in the Helgeland Nappe (Fig. 0-12).

This short description provides a quick overview of the idealized Caledonian nappe stack. There has, however, been a significant post-orogenic extensional phase, which has caused basement windows to be exposed in the footwall of large normal faults (Fig. 0-12). This is especially pronounced in the southern Scandinavian Caledonides where for example the Norfjord-Sogn detachment system can be followed for several hundred kilometers along strike of the orogen (Andersen, 1998). It can also be observed in the central part of the Caledonides, west of this thesis study area (e.g. Cashman, 1989; Eide et al., 2002).

3.3. Age, composition and structure of the Seve Nappe Complex

In the central Scandinavian Caledonides, the Seve NC shows a significant lateral variability in its composition. Despite this, the Seve NC, especially in the south-central parts, has traditionally been subdivided in three units: an upper, middle and lower unit. In the northern parts, the upper and lower Seve units contain eclogites or retro-eclogites, whereas the middle is largely undeformed and unmetamorphosed. All three units contain supracrustal rocks intruded by mafic intrusions, but there is some uncertainty regarding the timing of deposition as an interbedded felsic rhyolite was deposited at 945 Ma (Albrecht, 2000). This age suggests an Early Neoproterozoic rather than a Late Neoproterozoic depositional age, as has been constrained for the lower and middle Seve unit (Kirkland et al., 2011; Chapter 5, this thesis). Furthermore, in the Kebnekaise area Paulsson and Andreasson (2002) dated a bimodal magmatic complex to 845 Ma, also suggesting that the Seve NC comprise a significant old “basement” component relative to the sedimentary succession studied in this thesis. This “basement” unit is also intruded by mafic dykes. The

upper part of the Seve NC consists of a sedimentary succession of unknown age, which is occasionally dyked. Locally preserved pillow lavas were metamorphosed at eclogite facies (Fig. 0-13 A and B) and have REE patterns largely overlapping the REE pattern of the mafic dykes of the underlying Sarektjåhkka nappe, suggesting at least a source with similar chemistry and/or degree of melting (Fig. 0-13C).

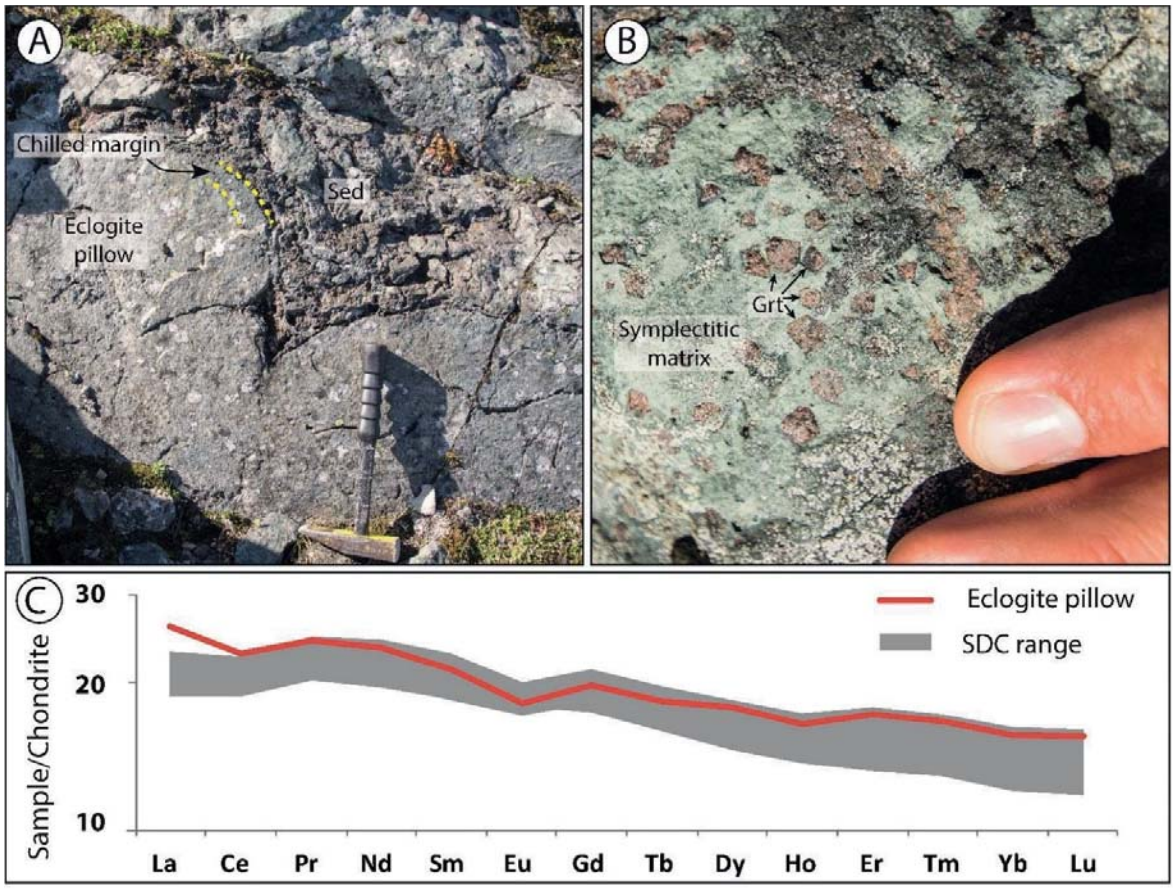

Figure 0-13: Photographs of eclogite facies lavas from Sarek and their geochemistry. A) The eclogitization process was static and primary features such as pillow shapes with chilled margins (!), marked with a yellow dashed line, can still be distinguished. B) Close up photograph of the texture in the center of a pillow. Large, idiomorphic garnet porphyroblast are set in a fine grained, greenish, presumably symplectitic matrix with some omphacite locally preserved. C) REE plot displaying the range from the Sarek dykes in grey. Red line shows the REE pattern from one of the eclogite pillows (presented in Tegner et al., 2019 and Chapter 3 this thesis). This is not a diagnostic feature tying them together, but it is an indication that the magma source could have been similar.

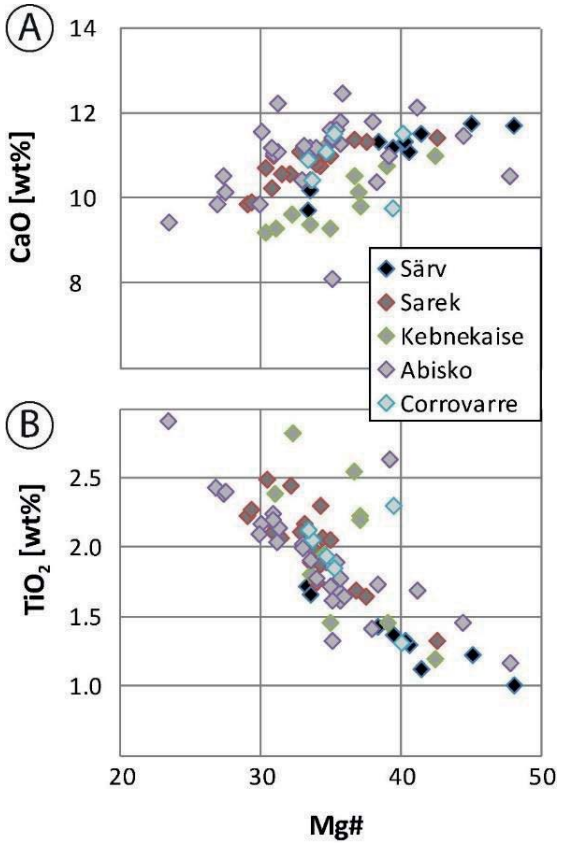

Figure 0-14: Plots showing fractionation trends from data presented in Tegner et al. (2019) and Chapter 3, this thesis. A) Mg# vs CaO in wt% show decreasing CaO content with decreasing Mg#. B) Mg# vs TiO_2 shows increasing TiO_2 content with decreasing Mg#.

The Seve NC and its correlative Blåhø NC in Norway has been interpreted to represent the distal margin of Baltica (Andréasson, 1994; Svenningsen, 1995; Andréasson et al., 1998; Svenningsen, 2001; Kjøll et al., 2019a; Chapters 1 and 5 of this thesis). This interpretation mainly comes from the middle Seve unit, where the protoliths still can be discerned. Here it has been shown that the preserved sedimentary succession is cut by an extensive mafic dyke swarm (Svenningsen, 1994a; Kjøll et al., 2019a; Chapter 1, this thesis). The sedimentary succession represents a transition from an early, slowly subsiding basin with little sedimentary input to a later, rapidly subsiding basin with a large input of siliciclastic sediments, presumably marking the onset of rifting (Chapter 5, this thesis). Locally this dyke swarm comprises 70-95% of the area and can occur as sheeted dyke complexes interpreted to represent the OCT (Svenningsen, 2001). The dyke swarm is called the Scandinavian Dyke Complex (SDC) and is also known as the Baltoscandian Dyke Swarm (BDS; Andréasson et al., 1992) and was emplaced during a relatively short and intense magmatic event at around 608 - 596 Ma (*e.g.* Svenningsen, 2001; Tegner et al., 2019; Kjøll et al., 2019a). The SDC comprises tholeiitic ferrobasalts with a relatively low Mg#, suggesting that the magma underwent significant fractional crystallization before it was emplaced (Tegner et al., 2019; Chapter 3, this thesis; Fig. 0-14). The dyking event has been interpreted to mark the final break-up after at least 30 M.yr. of extension (Svenningsen, 2001; Chapter 5, this thesis).

The depth of emplacement for the SDC has been constrained to be at *c.* 2.5 - 4.5 kbar, which equates to *c.* 8 - 14 km depth without considering any type of over- or under-pressure. This depth range corresponds to the depth directly below the SDRs on modern day rifted margins (Fig. 0-6 and 0-8), where seismic sections indeed have been interpreted to show dyke networks on *e.g.* the Vøring margin, offshore central Norway (Abdelmalak et al., 2015). In modern volcanic rifts, such as the Main Ethiopia Rift (MER), a zone directly below the central rift axis shows abnormally high P-wave velocities that decrease laterally away

from the rift axis (Fig. 0-15). This is interpreted to represent a highly dyke-intruded area (Keir et al., 2011), The highly intruded nature of the Seve NC studied for this thesis would presumably show a similar signature in a velocity inverted seismic refraction line and it is therefore possible that the SDC is an exposed analogue to the domain just below the rift axis of the MER. It is worth noting, however, that the East Africa rift zone is located above a hotspot and that the magmatic influx likely is much less than what was associated with the emplacement of the SDC, which has been proposed to represent a LIP (Tegner et al., 2019; Kjøll et al., 2019b; Chapters 2 and 3 this thesis).

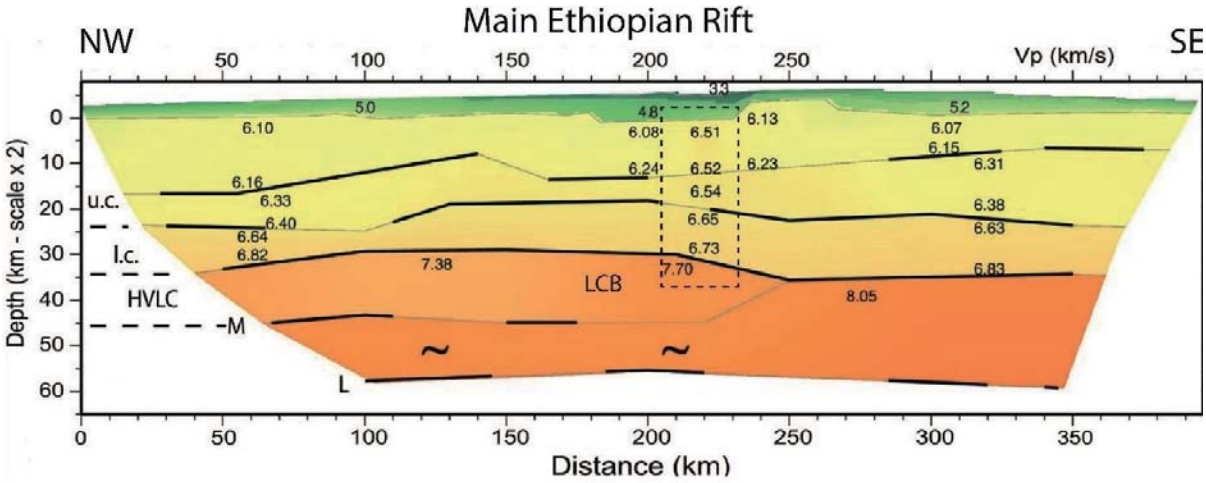

Figure 0-15: A velocity inverted seismic line across the Main Ethiopian Rift. Values, written on the section indicate P-wave velocities. Note the high velocities directly below the rift axis at *c.* 220 km, highlighted with a rectangle with dashed line, and how the values rapidly decrease to the side. This has been interpreted to represent a localization of dyking, such that there is a higher density of mafic dykes directly below the rift axis (Bastow et al., 2011). u.c.: Upper crust, l.c.: lower crust; HVLC: High Velocity Lower Crust, M: Moho, L: Lithosphere. After Bastow et al. (2011)

After the emplacement of the SDC, the rifted margin was presumably passive until early convergent stages of the Caledonian orogeny. The central Seve NC (at *c.* 67°N) was deformed and metamorphosed in the Early Ordovician at *c.* 480 Ma, locally reaching eclogite facies metamorphism (Kullerud et al., 1990; Root and Corfu, 2012; Barnes et al., 2018; Fig. 0-12). Rocks from further south in Seve (*c.* 64.5°N) and at Atløy (*c.* 61.3°N, southern Scandinavian Caledonides; Fig. 0-12) reached (U)HP conditions in the Middle Ordovician at around 450 Ma (Andersen and Jamtveit, 1990; Janák et al., 2013; Majka et al., 2014; Klonowska et al., 2017). These early ages of eclogitization, compared to *e.g.* the Western Gneiss Region (WGR), indicate that the Seve rocks may have been far outboard of Baltica, *i.e.* the WGR, when Baltica and Laurentia or a non-preserved arc collided with the Seve rocks (Jakob et al., 2019; Chapter 4, this thesis). $^{40}Ar/^{39}Ar$ cooling ages from Sarek suggest that they went through the hornblende closing temperature at *c.*

470-460 Ma (Dallmeyer et al., 1991). Muscovite and biotite on the other hand, show ages of *c*. 432 and 428 Ma, either indicating resetting or that they remained above their respective $^{40}Ar/^{39}Ar$ closing temperatures until that time (Svenningsen, 2000). During the final nappe emplacement event, the Seve NC, at least at Sarek, underwent asymmetric folding around a ESE-WNW trending axis with a steep southern limb (Fig. 0-16). The northern part of Sarek, the Sarektjåhkka area (Kjøll et al., 2019a; Chapters 1 and 5 in this thesis), is in the hinge zone of such a kilometer-scale fold and the structures here are exceptionally well preserved.

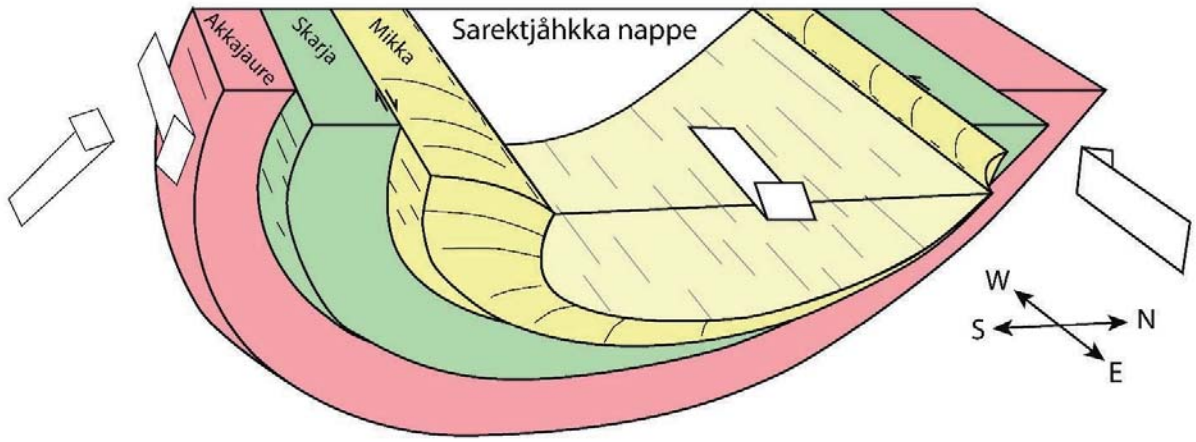

Figure 0-16: Sketch of the fold at Sarektjåhkka. Mihka is here interpreted to be the deformed variety of the Sarektjåhkka nappe rather than a nappe on its own, as it is traditionally interpreted to be. The Skárjá "nappe" is the Paleoproterozoic sedimentary cover of Akkajaure (Kirkland et al., 2011; Chapter 5, this thesis). The exceptionally well preserved dyke swarm is found in the core of the fold in the Sarektjåhkka nappe.

Although the Seve NC preserves a thick crustal section, a complete cross-section through the magma-rich margin has not been recognized so far as both the extrusive domain, as well as the lower crustal domain appear to be missing or not yet recognized. From the large number of dykes it could be expected that a large volcanic edifice at the paleosurface was present. Only minor lavas are, however, preserved in the Scandinavian Caledonides. These are the undated pillow basalts that are geographically limited to a small area in the Tsäkkok lens in the upper Seve unit (Fig. 0-13; Kullerud et al., 1990) and within the Høyvik Gr. at Atløy (Andersen et al., **1990**). Basaltic lavas may also be present in the magma-rich to magma-poor transition zone in the Sjongsæter Gr. (Jakob et al., 2019; Chapter 4, this thesis). Lastly, a highly intruded lower crust has not been recognized within the Seve NC yet. There are however, some geochemical indications of the presence of lower crustal magma reservoirs and more extensive field work is needed to document any occurrence of such rock assemblages properly.

4. Organization of the study

This article-based thesis contains three first-authored manuscript, two of which have been published in the international journals *Tectonics* and *Earth and Planetary Science Letters*. The latter, single-authored manuscript is currently (April 30th, 2019) under review in *Journal of the Geological Society*. Two co-authored manuscripts are important parts of this thesis and derives from the same project. These have been published in *Geochemistry, Geophysics and Geosystems – G*^{3} and *Earth Science Reviews* (Tegner et al., 2019 and Jakob et al., 2019, respectively). Each manuscript is presented with its own chapter in the following text.

Chapter 1 is published in the AGU journal *Tectonics* and presents detailed field observations from a large area in north Norway and Sweden. It also presents a new high precision age of the dyke swarm in Corrovarre, northern Norway, as well as an age for the migmatization of the host rock. Crystallization pressure and temperature data from dykes along the entire 900 km long Scandinavian dyke complex. These results are corroborated by other pressure and temperature estimates of the ambient temperature at a specific crustal level from the contact metamorphic mineral assemblages. Together these new data provide insight into the temporal evolution as well as an interpretation of crustal level. Furthermore, the high precision crystallization age for the dyke reveal that the dyke swarm should be correlated with the Seve NC dyke swarm to the south, rather than the previously correlation with the younger Seiland Igneous Province to the north.

Chapter 2 has been published in the prestigious journal *Earth and Planetary Science Letters*. This paper investigates the emplacement mechanisms of mafic dykes at magma-rich rifted margins and show how the increasing ambient temperature caused by crystallizing mafic magma results in a progressively more ductile behavior of the crust and how ductile mechanisms thereby becomes progressively more important. The paper also shows that the forceful emplacement of the mafic magma can deform its host rock and even in a tectonic rift cause vertical thickening of the crust. This is possible because the dykes are inclined with respect to what is inferred to be paleo-horizontal. This shows that during the dyke emplacement the magma influx rate was greater than the tectonic stretching rate.

Chapter 3 is published in the AGU journal *G*^{3} (Geochemistry, Geophysics and Geosystems) and deals with geochemistry of the dyke swarm and paleogeographical reconstructions. It presents a comprehensive set of geochemical data sampled for this project as well as compiled from the literature. Geochemical modelling conducted on this extensive dataset suggests that the magma formed because of elevated LAB temperatures of 75 to 250°C. These elevated temperatures are interpreted to have been caused by a mantle plume. A rudimentary calculation of the volume of magma suggests that the magmatism was

related to a LIP. Furthermore, by assuming the stability of the LLSVPs and their associationas PGZ, longitude could be constrained and a paleogeographic reconstruction of Baltica and Laurentia in the Late Neoproterozoic was proposed.

Chapter 4 was published in the prestigious journal *Earth Science Reviews*. It reinterprets some key units of the tectonostratigraphy of the Scandinavian Caledonides based on the current understanding of a more complex architecture of the paleogeography of the Baltican margin. Furthermore, the contribution also assesses the influence of rift inheritance in the telescoping of the pre-Caledonian margin of Baltica during the main phase of the Caledonian orogeny and proposes that the current configuration of the nappe stack can be explained by reactivation of rift inherited faults.

Chapter 5 is currently under review in *Journal of the Geological Society, London*. This paper shows that by using some key sedimentary units and their detrital zircon age record, it is possible to correlate at least the central parts of the highly intruded Late Neoproterozoic basins. Age constraints have been put on the deposition of the sedimentary succession. A lower age constraint is provided by the age of the mafic dykes, whereas an upper constraint is proposed by the discovery of a glaciogenic diamictite and the youngest detrital zircon, suggesting that the diamictite can be correlated with the Marinoan glaciation and thus deposited at c. 635 Ma. This is further supported by direct dating of a ductile top-west fabric in an underlying gneiss unit with an age of 637 Ma.

5. Perspectives and future work

5.1. Synthetic seismic

The exceptional degree of exposure in areas such as Sarek, provides the opportunity to map out large cliffs using tools such as Unmanned Aerial Vehicle (UAV) and helicopters equipped with cameras (Fig. 0-17). The acquired georeferenced photographs have been used to generate 3D models with an exceptional level of detail. Such 3D models can, together with the petrophysical properties of the different rock types, be used to generate synthetic seismic sections through the OCT domain. These models can further be used to compare with actual seismic reflection lines from magma-rich rifts and passive margins today and thereby enhance our knowledge on the relatively poorly known architecture and composition of the OCT and COB domains on magma-rich rifted margins.

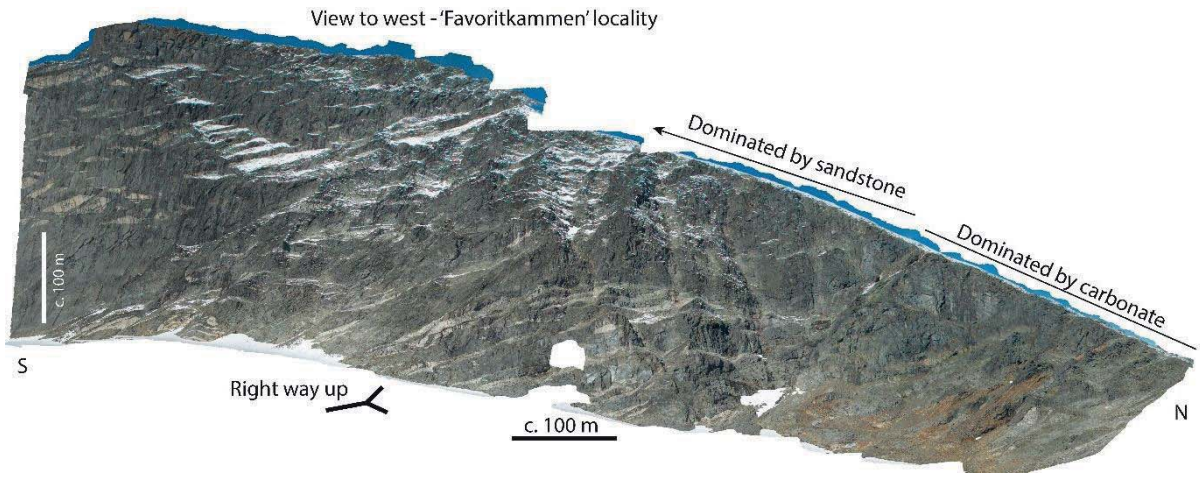

Figure 0-17: Continuous exposure of a c. 1.5 kilometer long and 300 meter high glacial cirque which has been mapped in detail using a helicopter. Petrophysical properties of the different rock types can be measured and the high resolution photogrammetric model used to generate a synthetic seismic section.

5.2. A lower crustal body?

In most magma-rich rifted margins and rifts, the lower crust shows exceptionally high P-wave velocities in domains dubbed "Lower Crustal Bodies" (LCB; see section 2.3.2.4. above). Such domains, originating at the distal margin of a fully developed, Atlantic-type ocean, have never been observed directly in the field. An area in the Seve NC, however, has the potential to represent a large sliver of a remnant, highly intruded, lower crust (Fig. 0-18). This domain has been mapped and sampled for this thesis, but more work is needed to constrain the timing of the different stages of metamorphism as well as the conditions during metamorphism. Preliminary studies have revealed at least two phases of metamorphism, 1) Low pressure, high temperature and 2) high pressure, high temperature within the same rock (Fig. 0-18). If a temporal link between the different metamorphic events can be drawn, this would be the largest and possibly best preserved example of an LCB related to a large ocean basin ever discovered. Such a discovery would have large implications for how the thermal structure of the pre-Caledonian margin of Baltica is envisaged and could further help to constrain the tectonothermal conditions at break-up. This would also have transferable implications to modern margins and help constrain thermal models of modern day magma-rich margins, which again have implications for hydrocarbon maturity and thus the prospectivity of magma-rich margins.

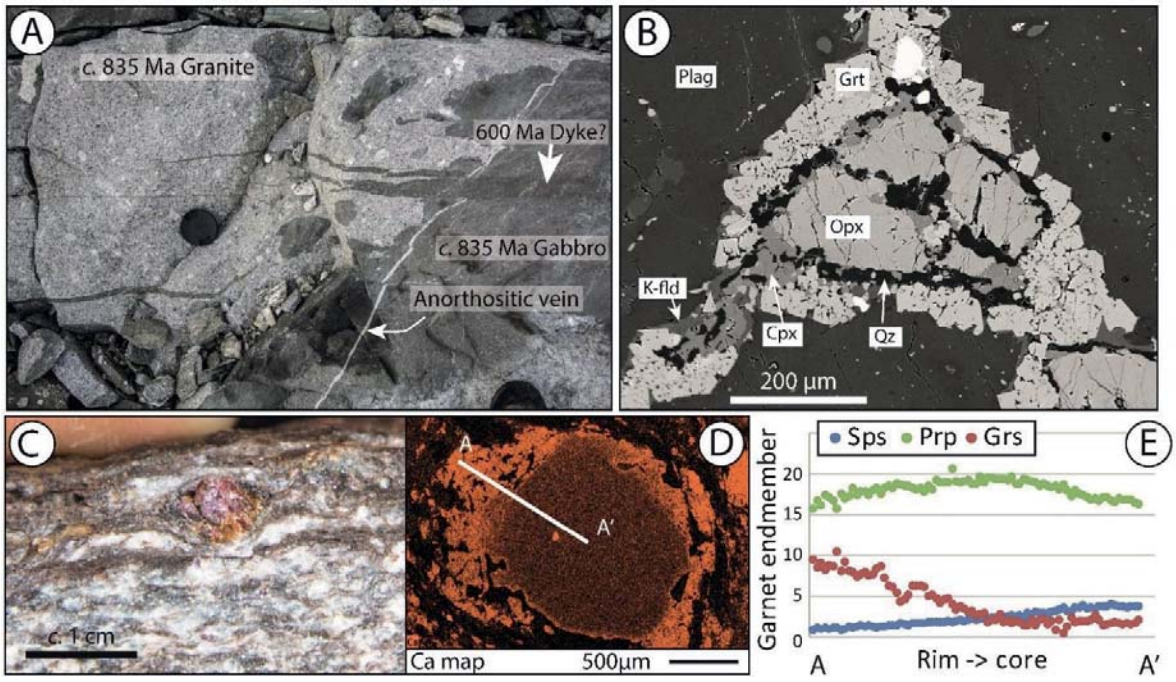

Figure 0-18: A possible analogue to a Lower Crustal Body in the Seve nappe. A) Bimodal magmatic complex with anorthositic veins. The entire magmatic complex is cut by mafic dykes. B) Gabbronorite show high temperature metamorphic reactions: orthopyroxene + plagioclase -> garnet + clinopyroxene + quartz ± K-feldspar. C) Host rock contains two generations of garnet, pink core and orange rim. D) EDS Ca-map indicate two growth stages, where the first was low in Ca compared to the second (E) significant differences in chemical composition along the profile in D. Note the apparent plateau in grossular (Ca) composition in the core of the garnet.

5.3. A reinterpretation of the Seve NC

This study could also lead to a reinterpretation of the Seve NC, which traditionally is interpreted to only consist of supracrustal rocks with variable amount of mafic sheet intrusions. The fieldwork conducted during this study, however, indicates that a significant part of the Seve NC has an older component, such that it may rather represent “basement” rocks to the Neoporterozoic cover. This is for example shown for the lower part of the Seve NC where the aforementioned 835 Ma magmatic complex was emplaced into a strongly deformed metasedimentary unit. Such a study would require detailed studies of the metamorphic mineral assemblages and dating of the mineral reactions and fabric (petrochronology), to unravel the presumably complex metamorphic and deformation history of these rocks.

5.4. Early deformation and boudinage

Furthermore, the base of the well preserved Sarektjåhkka nappe preserves dykes which have been dramatically thinned in a pinch-and-swell geometry from several meters thick to only a few centimeters (Fig. 0-19A). This hyper-thinned domain of the dyke can continue for several meters before it abruptly returns to its original thickness. Subsequently, after an unknown time, the pinch-and-swell structures are

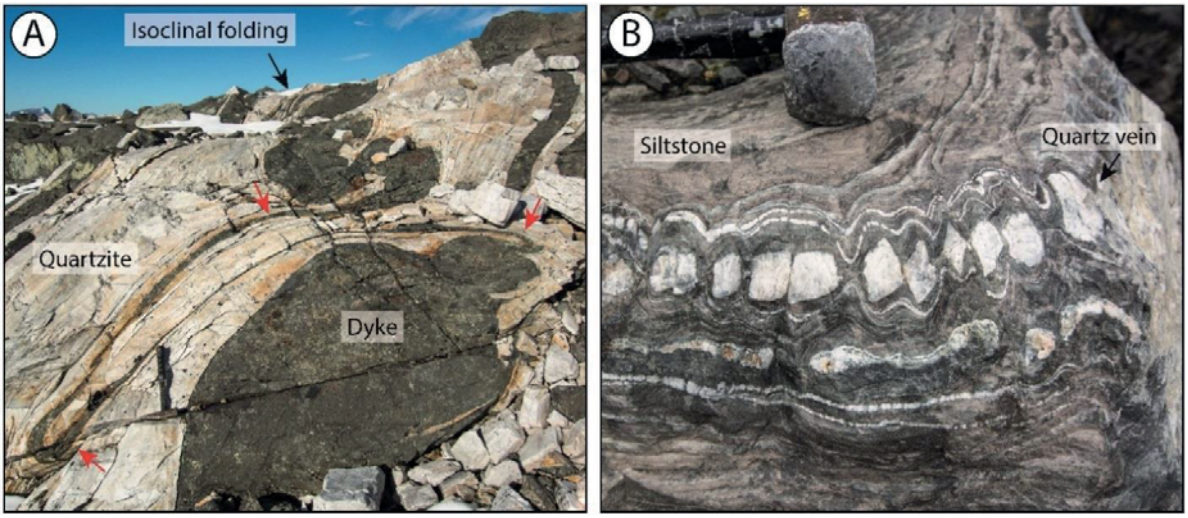

Figure 0-19 Folded boudinage. A) A dramatically thinned dyke is subsequently being folded. Red arrows highlight the hyper-thinned domain. The folding at the top is isoclinal. The host rock is a quartzite with detrital zircons and other datable minerals. B) “Dental boudinage”. A quartz vein intruded into a siltstone has been boudinaged into equant boudins and subsequently shortened, giving rise to the peculiar structure.

folded (Fig. 0-19A). This can also be observed for other lithologies, although then the boudinage is often complete (Fig. 0-19B). Such extreme thinning (without breaking) is presumably a high temperature phenomenon with little competence contrast. By constraining the timing of the two deformation events and tie them to a geodynamic setting it could provide insights into the deformation and formation of the Seve NC as these features are progressively superimposed on the undeformed Sarektjåhkka nappe.

5.5. Rift inheritance in the north-central Caledonides

A second important aspect would be to expand the study of Jakob et al. (2019) presented in Chapter 4 below, and asses the role of rift inheritance further north, in the magma-rich domain. Field observations conducted for this contribution have revealed unclear relations between different units in northern Sweden such as the different Seve units and the Köli. These relations include normal metamorphic zonation with low grade metamorphic rocks structurally overlying high-grade metamorphic rocks. These observations

may be explained by different models: 1) out-of-sequence thrusting during imbrication, or 2) displacement of the two units along normal faults either pre-, syn- or post-orogenic.

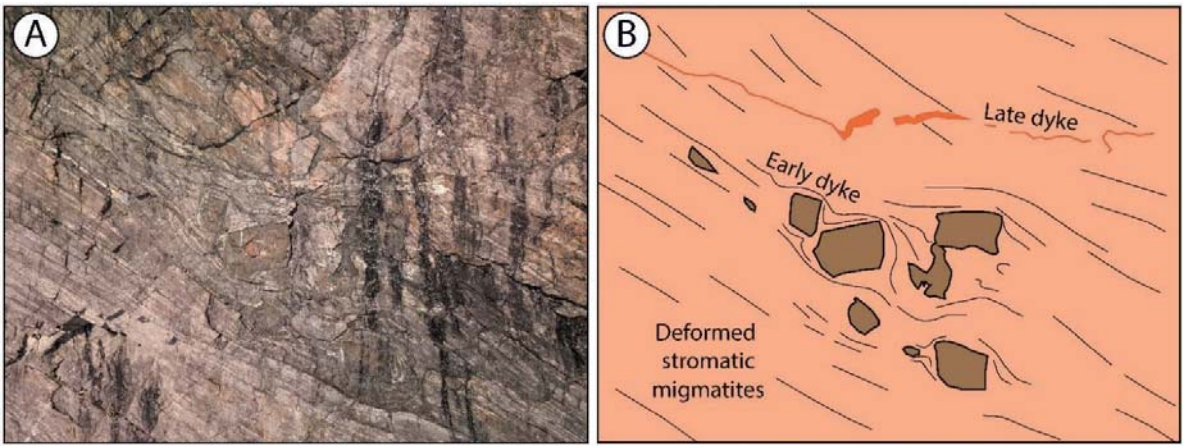

Figure 0-20: Photograph acquired using UAV in the Kebnekaise area of a deformed migmatitic basement intruded by one pre-foliation mafic sheet (brown), subsequently boudinaged and now parallel to the locally stromatic foliation and one post-foliation mafic dyke (orange). Width of view is approximately 15 meters.

These questions may be addressed by using *e.g.* petrochronology of the shear zones (e.g. Engi et al., 2017; Oriolo et al., 2018). One example is the shear zone below Váivvancohkka that contains two generations of garnet. Here, the earliest garnet has undergone frictional deformation in the otherwise ductile shear zone, indicating that the first garnet generation is either pre- or syn kinematic. Whereas the last generation, which is idiomorphic, grows in the ductile fabric in the shear zone, indicating that it is syn- or late syn-kinematic. Furthermore, other datable minerals are fine-grained (< 50 μm) biotite in the foliation and muscovite porphyroblast fishes after sillimanite, which locally have finer grained recrystallized tails. These minerals and textures suggest a poly-tectonometamorphic evolution and may therefore provide time constraints on the different tectonic episodes. By analyzing the mineral chemistry and isotopic ratios, pressure and temperature data may provide a full PTt path (Airaghi et al., 2017). These new data would investigate the hypothesis of out-of-sequence thrusting in the Caledonides as recently proposed by Bender et al. (2018).

PART II

Chapter 1

Timing of break-up and thermal evolution of a pre-Caledonian Neoproterozoic exhumed magma-rich rifted margin

Hans Jørgen Kjøll, Torgeir B. Andersen, Fernando Corfu, Loic Labrousse, Christian Tegner, Mohamed Mansour Abdelmalak, Sverre Planke

This manuscript has been published in *Tectonics*

Supplementary material is available online at: https://doi.org/10.1029/2018TC005375 and in Appendix 1

Abstract: During the terminal stages of Wilson cycles, remnants of magma-poor margins may be incorporated into the orogens, whereas the magma-rich margins often are lost in subduction due to low buoyancy. The understanding of magma-rich margins is therefore mostly based on drill holes and geophysical observations. In this contribution, we explore the temporal evolution and the ambient conditions of a magma-rich rifted margin preserved within the Scandinavian Caledonides. The Scandinavian Dike Complex was emplaced into a sedimentary basin during the initial break-up and opening of the Iapetus Ocean 615 to 590 million years ago. The dike complex constitutes 70-90% of the magma-rich, syn-rift basins and is locally well preserved despite the complex Caledonian history. This contribution provides new observations about the geometry, relative timing, and development of the margin. Jadeite-in-clinopyroxene geothermobarometry, titanium-in-biotite geothermometry, and garnet isopleth modeling show that the ambient pressure and temperature conditions were similar for the entire dike complex at 0.25

to 0.45 GPa, with contact metamorphic temperatures up to c. 700°C. In the northernmost part of the study area U-Pb dating of magmatic zircon shows that partial melting of the sedimentary host-rock, at relatively shallow levels, occurred at 612 Ma. This shows that the crust was molten already 6 million years before the northernmost dike swarm was emplaced at 605.7 ± 1.8 Ma. We propose that the locally pervasive partial melting occurred due to high geothermal gradients and introduction of mafic melt in the lower crust. These processes significantly reduced the strength of the crust, eventually facilitating continental break-up.

Plain text summary: This project investigates how the crust looks like and how it behaves when continents are rifting and finally break apart to form a new ocean. Sometimes the break-up is associated with magmatism. When this is the case the structure and behavior of the crust change dramatically from their state when no magma is involved. One important implication is that the heat brought by the magma presumably makes the crust very hot and weak, and thus easier to break. Direct observations of magma-rich rifted margins are sparse, but in an area of Scandinavia the deep parts of a rift in the Earth's crust has been preserved and exposed through complex geological processes. The study of these rocks reveals the processes that were active at depth when the continents broke apart. We have used mineral chemistry and age dating to show that the studied areas formed at c. 9-16 km depth more than 600 million years ago. Our observations indicate that the stretching started when the crust was relatively cold, possibly causing earthquakes. Later, the crust was heated by magma intrusions to such a degree that it started to melt and became very weak, which made it easier to stretch and break the continent apart.

1 Introduction

Understanding the formation and evolution of passive margins is important because they provide clues as to how continents break apart and to constrain the transition from rifting to drifting in the divergent stages of the Wilson cycles (e.g. Brune, 2016; Buiter and Torsvik, 2014). Present day rifted margins are generally submerged and buried like the northeast-Atlantic (e.g. Gernigon et al., 2004; Faleide et al., 2008; Clerc et al., 2018) and only rarely exposed, like in the Afar rift (e.g. Bastow and Keir, 2011; Stab et al., 2016) or in the Gulf of California (e.g. van Wijk et al., 2018). Some fossil rifted margin analogues can be found in Phanerozoic mountain belts around the world like in the southern Scandinavian Caledonides (Andersen et al., 2012; Jakob et al., 2017), Appalachians (Chew and van Staal, 2014), Alps (e.g. Manatschal, 2004; Manatschal and Müntener, 2009; Mohn et al., 2014) and Pyrenees (Lagabrielle et al., 2010), but these are generally classified as magma-poor rifted margins. Their magma-rich counterparts, on the other hand, are often lost by subduction due to metamorphic densification. Exposed crustal sections of the magma-rich end-member are therefore much less known and what we do know about their architecture

mainly comes from geophysical methods and drill hole data (e.g. Direen and Crawford, 2003; Gernigon et al., 2004; Theissen-Krah et al., 2017; Zastrozhnov et al., 2018). In general, these magma-rich rifted margins show an anomalously thick ocean - continent transition (~20 km thickness), commonly referred to as the outer high (Fig. 1-1). This area is generally characterized by three levels, which, from top to bottom are: 1) major extrusive complexes represented by wedges of basaltic flows and tuffs, which are seismically imaged as Seaward Dipping Reflectors (SDRs in Fig. 1-1; Eldholm, 1991; Planke et al., 2000; Menzies et al., 2002); 2) dike and sill complexes within the upper and middle continental crust (Abdelmalak et al., 2015; Geoffroy et al., 2007; Klausen and Larsen, 2002) and 3) a lower crust of unknown composition, characterized by high seismic velocity (LCB in Fig. 1-1; White et al., 1987; Kelemen and Holbrook, 1995; Holbrook et al., 2001; White et al., 2008).

Although tectonic rifting generally precedes magmatism at rifted margins, anomalous magmatic productivity resulting from elevated mantle temperatures, will significantly weaken the lithosphere and promote strain-localization (Buiter and Torsvik, 2014). However, magma emplacement is commonly a very rapid process. Its effect on the crustal rheology may be dual depending upon the duration of the magmatism: (1) thermal weakening, when newly-formed hot intrusions are emplaced and heat their surroundings, and (2) rheological hardening when mafic intrusions solidify and cool and thereby becoming more competent. Consequently, the localization of the deformation depends on the emplacement rate, volume and spatial organization of the mafic system (Bialas et al., 2010; Daniels et al., 2014).

Understanding the relationship between rifting and magmatism in magma-rich margins requires additional constraints on melting conditions such as pressure, temperature and melt fraction. Unraveling the age sequence of magmatic products is therefore essential to constrain magmatic productivity in time and space. These parameters are important to test and validate geodynamic scenarios and to improve input parameters for numerical models of magma-rich margins. Most of the present-day magma-rich margins are submerged offshore and are therefore difficult to study by direct observation.

The Scandinavian Dike Complex (SDC) in northern Scandinavia offers a unique chance to study an exhumed and thrusted ancient analogue of a magma-rich margin, permitting direct observation and sampling and thereby providing an improved understanding, particularly of the deeper crustal levels. In this contribution we report field observations from a section representing deep levels of the ocean-continent transition of a magma-rich rifted margin. The field areas are generally constituted by more than 70% mafic dikes, which intrude syn-rift sediments (Fig. 1-1b). We use field observations coupled with U-Pb geochronology to investigate the temporal and spatial development of the rifted margin. Geothermobarometry of magmatic clinopyroxenes and contact metamorphic mineral assemblages that escaped metamorphism related to Caledonian burial and nappe stacking, are used to estimate pressure and

temperature at the time of dike crystallization and how these parameters have changed through time. These data suggest that the arrival of a heat pulse led to local widespread anatexis during continental stretching.

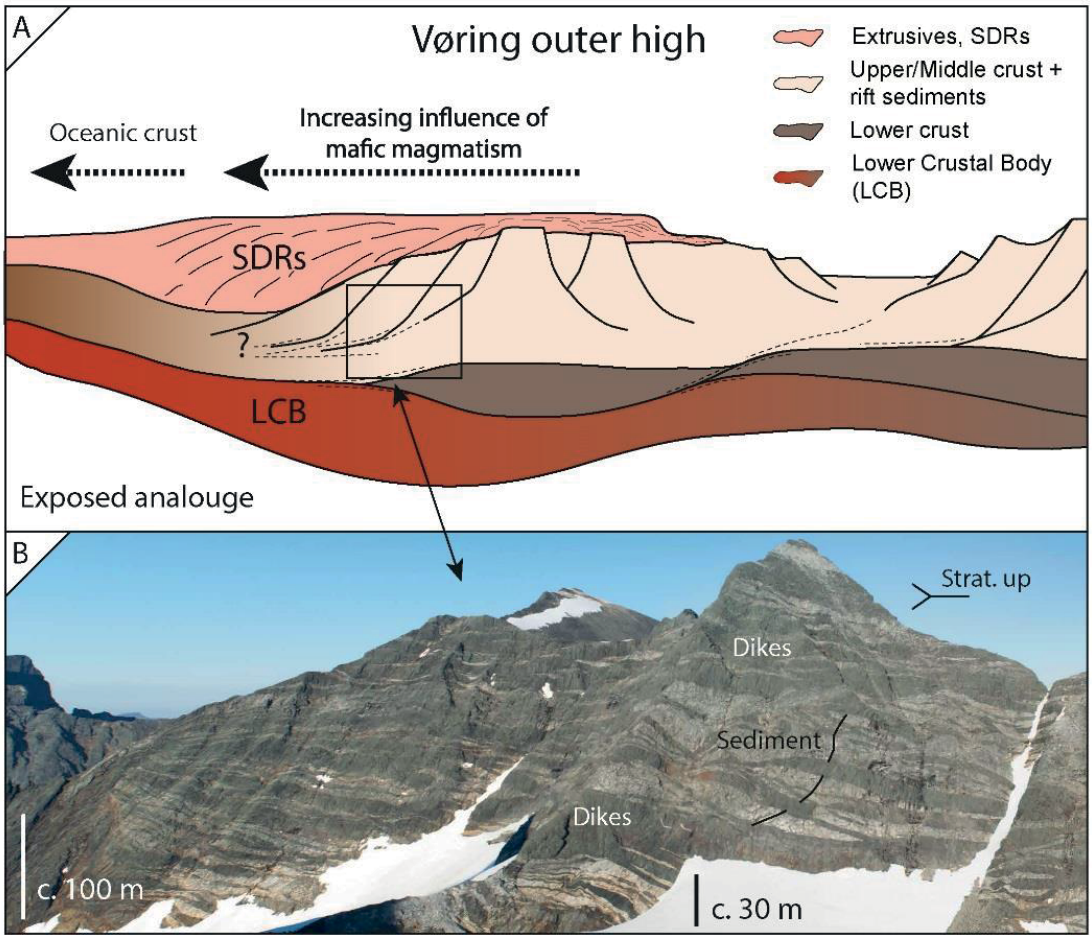

Figure 1-1: A) Schematic illustration of a magma-rich margin, modified from Abdelmalak et al. (2017). Fossil analogue indicated by black rectangle. The fossil analogue is in an area with syn-rift sediments and originally vertical dikes. SDR: Seaward Dipping Reflector sequence. LCB: Lower Crustal Body. Dashed lines indicate ductile shear zones. B) Oblique photograph of a cliff section in the southern segment showing the exposed analogue. Light colored rocks are sediments (black lines indicate bedding), dark colored rocks are doleritic dikes. Bedding is sub vertical and indicated by black lines. Dikes are sub-horizontal. The entire area was tilted during the Caledonian orogeny and stratigraphic up is towards the right in the picture. The exposed cliff section is approximately 1 km long and c. 250 m high.

2 Geological setting

The first evidence for an attempted opening of the Iapetus Ocean is represented by local magmatic events that occurred c. 835 to 850 Ma (Walderhaug et al., 1999; Paulsson and Andreasson, 2002; Fig. 1-2), but it was not until 200 million years later, in the Late Neoproterozoic that Baltica and Laurentia finally rifted apart and the Iapetus Ocean opened. Before the opening, however, rift basins developed, and syn-rift

sediments were deposited. These sediments consisted primarily of Neoproterozoic sandstone and shale overlain by a sequence of carbonate, which locally show evidence for evaporite deposits (Svenningsen, 1994b). Locally, the carbonate sequence is overlain by a diamictite unit, which again is overlain by thick clastic packages, locally up to several kilometers of shallow marine sandstone (Nystuen et al., 2008; Stølen, 1994; Svenningsen, 1994b; Zwaan and van Roermund, 1990).

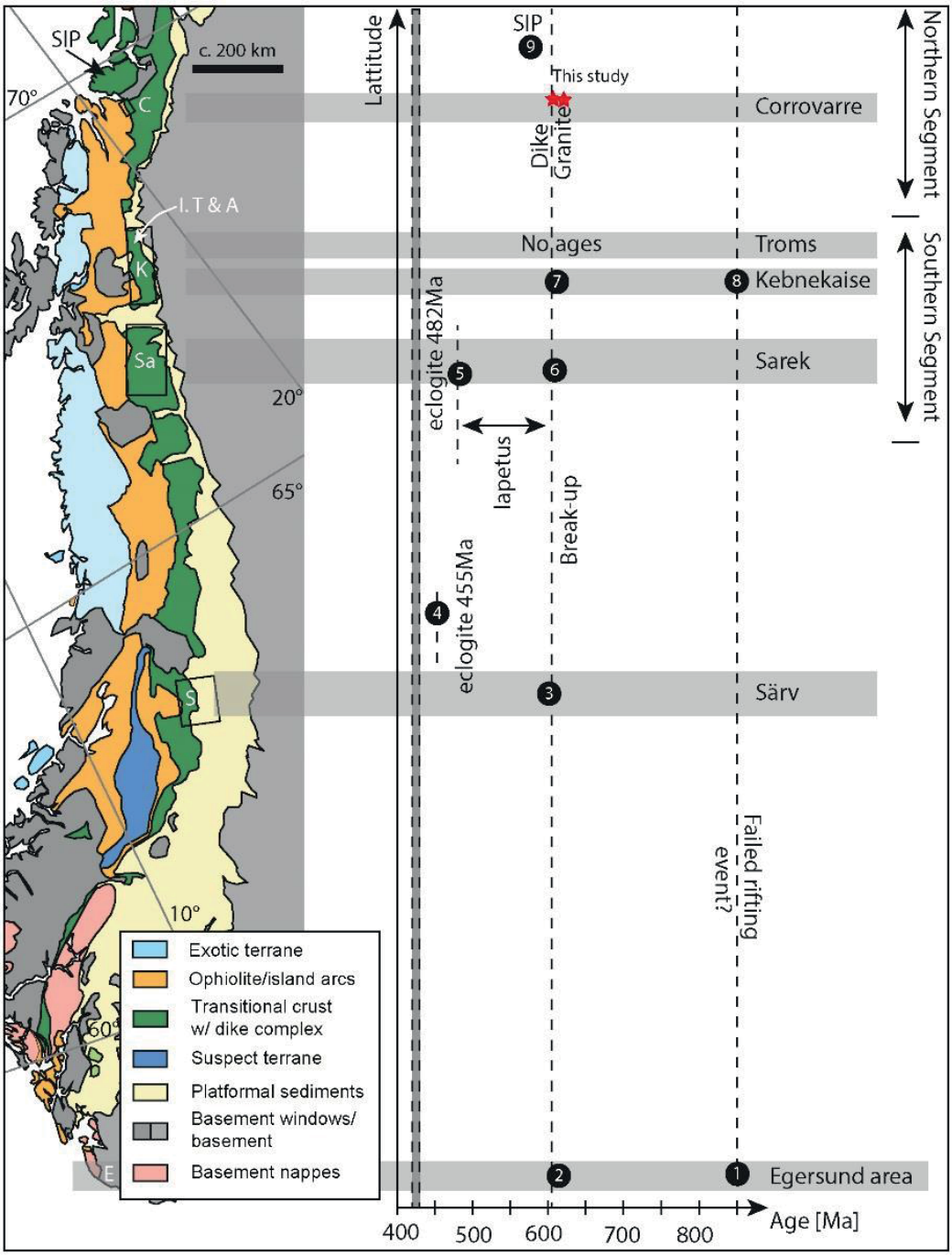

Figure 1-2 (previous page): Simplified tectonic map of the Scandinavian Caledonides and timeline of the initial Caledonian Wilson Cycle. A) The map is schematic with field areas indicated by black rectangles. E = Egersund, S = Särv, Sa = Sarek, K = Kebnekaise, I.T = Indre Troms, A = Abisko, C = Corrovarre, SIP = Seiland Igneous Province. B) Latitude vs. age diagram displaying all major events from the proposed 850 Ma failed rifting event, through the successful rifting event at 600 Ma and finally closure of the Iapetus Ocean during Scandian collision. 1 = Hunnedalen dikes (Walderhaug et al., 1999), 2 = Egersund dikes (Bingen et al., 1998), 3 = Särv dikes (Kumpulainen et al., 2016), 4 = Jamtland eclogites (Majka et al., 2012), 5 = Tsäkkok eclogites (Root and Corfu, 2012), 6 = Sarek dikes (Svenningsen, 2001), 7 = Kebnekaise dikes (Baird et al., 2014), 8 = Vistas granite (Paulsson and Andréasson, 2002), 9 = Seiland Igneous Province (Roberts et al., 2010).

During the break-up event, the SDC was emplaced along c. 1600 km of Baltican continental margin (e.g. Andréasson et al., 1992; Andréasson et al., 2018; Tegner et al., 2019). During this event the sediments were metamorphosed (for convenience the prefix “meta-” is omitted from the rest of the text). Precise U-Pb zircon and baddeleyite ages of mafic dikes from various sites along the original margins of Iapetus vary from 616 to 595 Ma (e.g. Kamo et al., 1989; Bingen et al., 1998; Svenningsen, 2001; Ernst and Bell, 2010; Baird et al., 2014; Gee et al., 2016; Kumpulainen et al., 2016; this study, see section 3.1.3). The best-preserved remnants of the allochthonous SDC crop out over an area covering roughly 6000 km^2 and stretching for almost 900 km from 62.8°S in central Sweden to ca 70°N in northern Norway (Fig. 1-2). The southernmost exposure of the SDC, however, is the 616 ± 3 Ma Egersund dikes, which were emplaced in the autochthonous Baltican basement (Fig. 1-2; Bingen et al., 1998). A recent compilation of the geochemistry of the SDC reveals a systematic zonation in trace element compositions with a geographically progressive δ-Nb and La/Sm enrichment (E-MORB) relative to mid-ocean-ridge-basalt, implying that the formation of the magma was associated with elevated temperatures at the lithosphere-asthenosphere boundary (Tegner et al., 2019).

The distal, magma-rich rift segment was affected by convergent plate motions both during early and late stages of the Caledonian-Appalachian mountain-building, as interlayered metasedimentary rocks (marble, pelites and thin-bedded quartzites) and pillow basalts and sills/dikes in the Seve nappe of northern Sweden were affected by Early Ordovician eclogite facies metamorphism at c. 480 Ma (Kullerud et al., 1990; Root and Corfu, 2012; Fig. 1-2). Final closure of Iapetus and continental collision took place in the Middle Silurian (Fig. 1-2; 430-425 Ma) and peaked at 410 ± 10 Ma during Caledonian ‘Scandian’ continental collision (e.g. Corfu et al., 2014) when outer parts of the Baltican basement reached ultra-high pressure conditions (e.g. Smith, 1984; Hacker et al., 2010). The magma-rich rifted margin was stacked in nappe complexes and transported more than 600 km onto Baltica and is now called the Seve Nappe Complex (e.g. Gee, 1975; Jakob et al., 2019). Most of the rocks underwent intense deformation and metamorphism, but there are km-sized tectonic lenses of the SDC and their wall rocks that are little deformed and preserve the pre-Caledonian mineral assemblages. These lenses are presently found as km-

sized tectonic lenses with gradational boundaries to intensely-deformed counterparts and constitute the field area for this study.

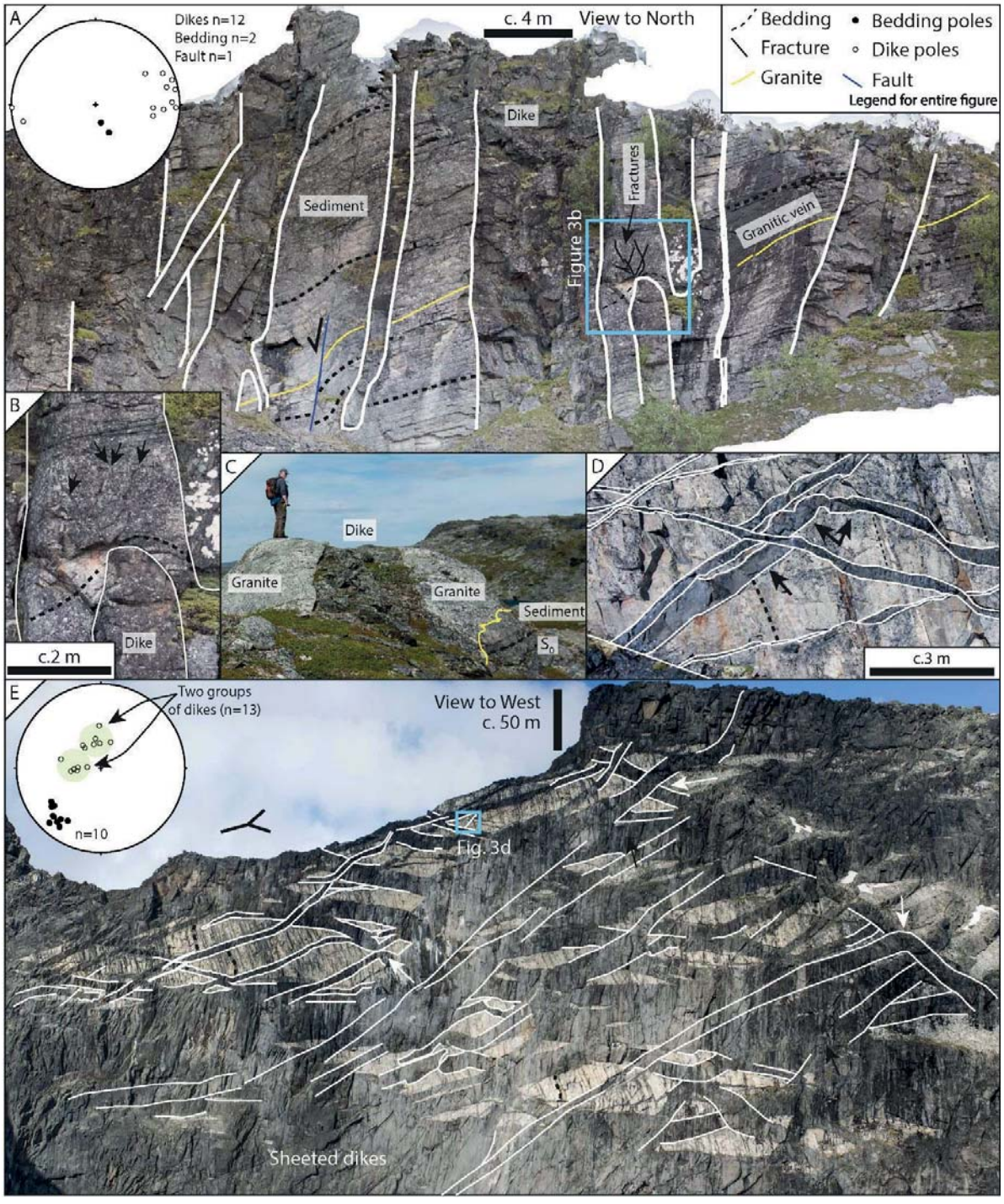

Figure 1-3 (previous page): Overview figure showing dike geometries in large cliff walls. A) 12 m tall cliff in Corrovarre with mafic dikes cutting already metamorphosed sediments and pre-dike granite veins (yellow line) of unknown age. Stereonet shows poles of dikes (open circles) and bedding (closed circles).

Locally, there are steep normal faults sub-parallel to the dikes. They also cut bedding and the thin granitic veins. B) Close-up of a dike tip (black rectangle in Fig. 1-3A); the termination is blunt, and the bedding is folded around the tip (dashed line), with fractures propagating into the arkosic host sandstone. C) A mafic dike truncates a granite sheet in Corrovarre. The yellow line indicats the discordant contact between granite and host sandstone (See section 4.2 for geochronology of this granite). D) Detail of figure 3E from Sarek shows the complexities of the dike emplacement, where a dike, indicated with black arrows, display an abrupt change in orientation. Dashed line indicate bedding E) Part of a 300 meter high, vertical cliff from Sarek, which is composed of more than 80% mafic dikes (dark rocks, highlighted locally with white lines to indicate cross-cutting relationships). Some dikes show abrupt changes in orientation (white arrows). The dikes intrude arkosic sandstone (light colored rocks) with preserved, but locally folded bedding (black dashed lines; see also supplementary material). Stereonet show poles of dikes (open circles) and bedding (closed circles Note grouping of dike orientations, separated by a 30-degree angle. The entire sequence has been tilted and stratigraphic up is now towards left in the figure.

3 Field Observations

This paper mainly focusses on the allochthonous dike complex from ca 69.8°N in Corrovarre to ca 67°N in Sarek, but also presents paleo pressure data from ca 63°N in Särv (Fig. 1-2). The field areas have been subdivided in a northern and a southern segment and show well-exposed and well-preserved sections of densely dike-intruded sediments and basement (Figs. 1-1 and 1-2). As all the areas reside in nappes, absolute orientations of dikes and bedding are secondary and will not be discussed further. Relative angles i.e. angle between dike and bedding will be reported and discussed. Internal shear zones within the nappes further complicate correlations, therefore we are focusing on observations from large and well-exposed outcrops and avoid zones with obvious overprint of Scandian deformation and regional metamorphism.

3.1 Northern segment

The least deformed parts of the northern segment cover an area of ca 24 km^2 and consist largely of highly intruded sediments. The best preserved lens near Corrovarre (Fig. 1-2) was mapped in detail by Zwaan and van Roermund (1990) and Lindahl et al. (2005).

3.1.1 Mafic dike complex and contact relationships

The mafic dike swarm at Corrovarre intrudes quartzite, marble and arkose, with mica-rich horizons displaying the sedimentary layering in the clastic rocks (Fig. 1-3a). The bedding is typically disrupted by shear bands indicating bedding parallel stretching (Fig. 1-4a). The mafic dikes form anastomosing networks with en-echelon geometries covering approximately 50-70% of the area. Chilled margins are preserved. Locally, some dikes are vesicular where emplaced in carbonates. The geometry of the dikes is strongly controlled by the rheology of the sediments in which they intrude, e.g. where they intrude carbonates they

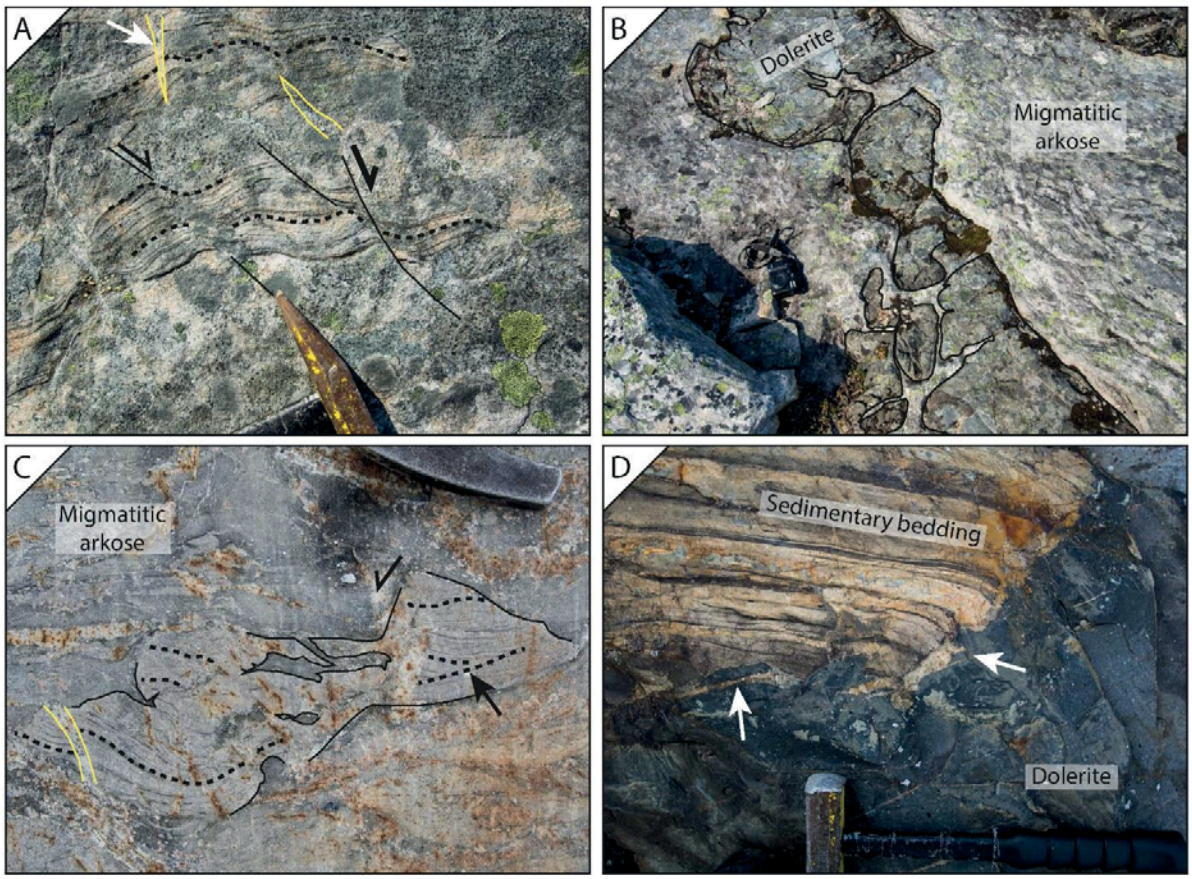

Figure 1-4: Overview plate showing evidence for migmatization of the host rock in the dike complex. A) Deformed migmatitic arkosic sandstone in Corrovarre. Shear bands are highlighted by black lines and are locally filled with leucosomes (yellow lines) indicating contemporaneous melting and deformation. Black dashed lines indicate bedding. B) Dolerite intruded into partially molten arkose forms highly irregular and lobate boundaries to the host rock indicating that dike emplacement was contemporaneous with migmatization. Digital camera for scale C) Deformed and migmatitic arkosic sandstone from Indre Troms developed bedding parallel stretching during anatexis. Bedding is highlighted with black dashed lines. Black arrow shows cross-bedding. The preserved sandstone is highlighted by black solid lines. Leucosome has segregated and coalesced in shear bands. Locally a thin granitic dike (highlighted by yellow lines) cut the bedding. D) Mingling between dolerite and granite. The accumulation of leucosome at the contact with a sedimentary raft (white arrows), together with the back-veining in the dolerite and irregular contacts of the raft suggest contact metamorphic melting of the sediment during dike emplacement.

commonly have a short and stubby shape and apparent boudinage (Kjøll et al., 2019b). Their tips, where visible, are blunt with sediments draping over the tip indicating that the dikes were emplaced in a forceful manner (Kjøll et al., 2019b; Fig. 1-3a-b).

3.1.2 Migmatization and deformation

The sediments at Corrovarre show variable degrees of partial melting and are in general more affected by migmatization than in the southern segment, locally reaching diatexite textures. In some areas, pristine sediments can only be found in rafts floating in leucosome (Fig. 1-4c). Asymmetric shear bands that record bedding parallel stretching are common and show that the sediments were at supra-solidus conditions during the stretching stage (Fig. 1-4a). Partial melting appears to have been contemporaneous with the stretching as leucosomes coalesce in the developing shear bands and, locally, granites intrude the stretched sediments (Fig. 1-4c-d). Mafic dikes cut both the sediments and the granites (Fig. 1-3a and c), although locally the granites and the mafic dikes also show evidence of mingling, suggesting that there are both pre- and syn-dolerite granites. Furthermore, mafic dikes with highly irregular and lobate boundaries to the host migmatite / sediment indicate that the migmatite was partially molten during mafic dike emplacement (Fig. 1-4b). Locally, the leucosomes coalesce and form granite sheets (Fig. 1-3c). These are cut and locally drag-folded along margins of dolerites.

3.2 Southern segment

The southern segment includes the areas of Sarek, Kebnekaise, Abisko and Indre Troms, and covers an area of ca 1660 km^2 (Fig. 1-2). The dike complex in Sarek and Kebnekaise has yielded U-Pb zircon ages ranging from 608 to 578 Ma (Svenningsen, 2001; Baird et al., 2014; Kirsch and Svenningsen, 2015) and intrudes presumed late Neoproterozoic syn-rift sediments and basement (Kumpulainen and Nystuen, 1985; Nystuen et al., 2008). In the lower part of the stratigraphy the sedimentary rocks also comprise a carbonate unit with local evaporite deposits (Spika Fm) overlain by thick bedded sandstones, locally with more micaceous domains (cf. Favoritkammen Group, Svenningsen, 1994b; Fig. 1-3d-e). In the upper part of the carbonates at Sarek, we recently discovered columnar stromatolites directly below a diamictite horizon that separates the carbonates and the sandstones. This may be a key horizon for correlation between the different basins in the SNC as well as other basins in the circum-Iapetus.

3.2.1 Dike complex and contact metamorphism

Approximately 70% of the area consists of mafic dikes that intrude the more than 2.5 kilometer thick sedimentary pile (Svenningsen, 1994a). Dikes mainly form two groups separated by an angle of c. 30° (Fig. 1-3e), but bent geometries are also common (Fig. 1-3d). Mutually cross-cutting relationships between these two orientations suggest contemporaneous emplacement (Kjøll et al., 2019b; Fig. 1-3d-e). At a larger scale (100's of meters) the dikes form an anastomosing network as seen for example in a 1.5 km long continuous cliff exposure of the dike complex (Kjøll et al., 2019b; Fig. 1-3e and supplementary material). Features such as chilled margins, dike apophyses and bridges are common.

Most of the host sediments have been metamorphosed into hornfels without cleavage. Locally contact metamorphic mineral assemblages are preserved in the more micaceous domains, where dendritic to hopper-type garnets have grown together with andalusite (chiastolite), which has been pseudomorphosed into sillimanite (see section 5.3). At lower levels in the stratigraphy, chlorine-rich scapolite (Me_{45-50}) is commonly present along margins and as veins along fractures in the dolerites and in the matrix of the sediments. It is derived from metasomatic alteration sourced from the evaporitic horizons (Svenningsen, 1994b). Locally, both sediments and thin mafic dikes are completely metasomatized into calc-silicates with grt + scp + di (the contact metamorphism is quantified in section 5, below; mineral abbreviations are from Whitney and Evans, 2010).

3.2.2 Partial melting and deformation

Variable partial melting textures are observed throughout the southern segment. In Indre Troms melting was locally pervasive forming metatexites with up to 10% leucosome (Fig. 1-4c). Locally the melt back-veined the dolerites, especially where partial melting of the host sediments was pervasive (Fig. 4d). In the south, the migmatization was less pervasive with leucosome pockets only found at contacts between dikes and sediments (Fig. 1-4d). Leucosome pockets derived from the sediments are observed especially close to dike terminations where the dikes are organized in an en-echelon configuration with bridges both intact and broken (Fig. 1-4d). Domains with no partial melting are also common, especially in the southernmost part of the segment.

The earliest deformation recorded in the southern segment is a progressive bedding-parallel stretching of the sediments. Where partial melting of the host sediments associated with dike emplacement was pervasive, the bedding-parallel stretching is recorded in the migmatites as asymmetric boudinage with outcrop-scale shear bands (Fig. 1-4c). Where the migmatization was less pervasive and concentrated at the dike contacts, leucosomes are intrusive into the dolerites (Fig. 1-4d). Early phases of bedding parallel stretching have been preserved in the sediments as >50 m displacements along low angle normal faults locally decorated by extremely fine-grained material forming injection veins into the undisturbed host sandstones (Fig. 1-5a). In the weaker carbonate layers the bedding parallel stretching is accommodated by outcrop-scale shear bands deforming thin, early mafic dikes along asymmetric shear bands (Fig. 1-5b). At one location in the sandstone dominated areas, a dike cutting a normal fault is bent and stretched in the upper part, parallel to the normal fault, but is shortened (folded) where the dike lies at a higher angle to the normal fault (Fig. 1-5c). On a larger scale, in the same area, thicker dikes have been boudinaged. In the boudin necks the dikes are partially amphibolitized, but in the undeformed parts, they retain primary magmatic mineral assemblages (Fig. 1-5d).

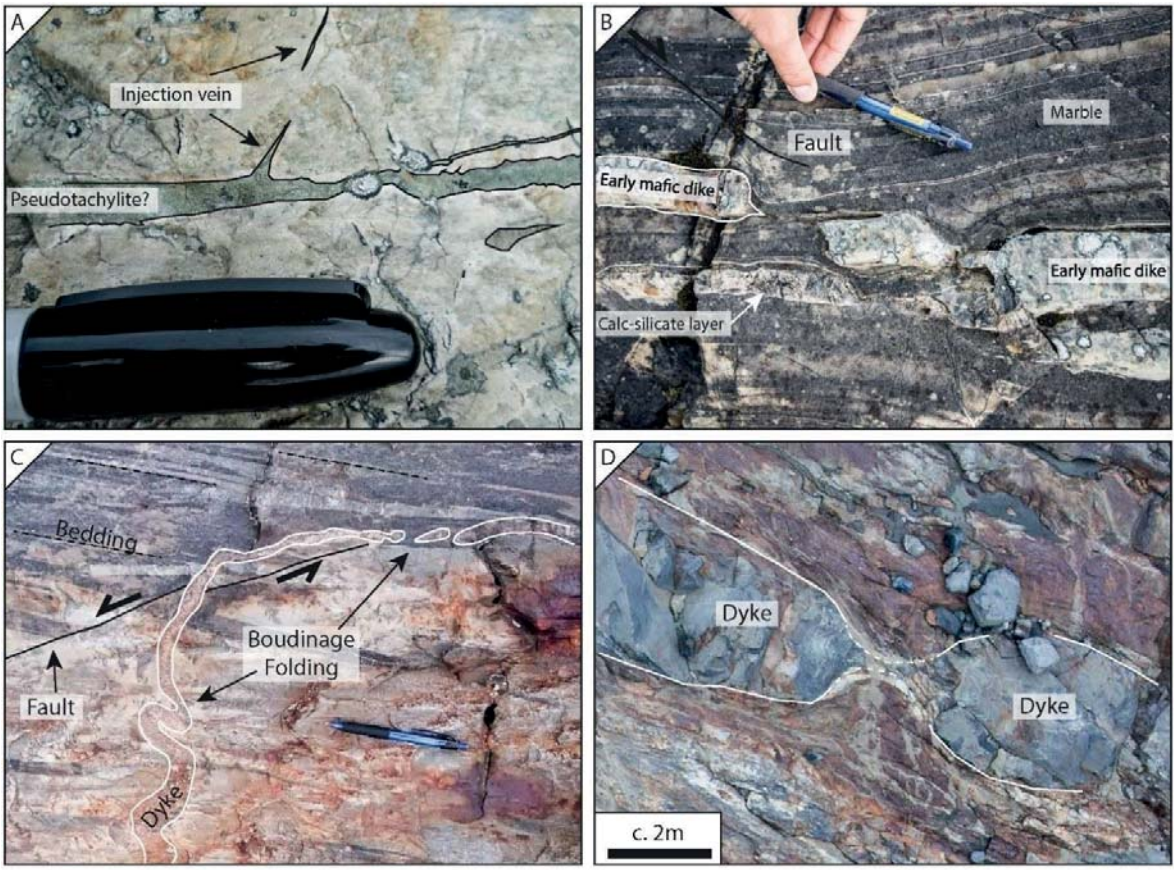

Figure 1-5: Overview figure showing bedding parallel stretching in the same area, but by different mechanisms. A) injection veins of very fine-grained material, presumably recrystallized pseudotachylite or ultra-cataclasite, into homogenous sandstone. B) Early mafic dike (early with respect to the main dike emplacement) and calc-silicate layers defining bedding in a marble, being cut asymmetrically by shear bands (black line). The color of the dike is caused by surface oxidation. C) Thin dike cutting a low angle normal fault (black line; inclined with respect to the bedding) in a sandstone. The dike is bent above the normal fault and the upper part parallel to the fault is boudinaged, whereas the lower part, at an apparent angle of c. 60° to the normal fault, is folded. All three deformational features are compatible with bedding-parallel stretching and bedding-normal shortening. D) Symmetric boudinage of a c. 2 m thick dike (highlighted by white lines.

3.3 Särv

The Ottfjället mafic dike swarm intrudes a >4.5 km thick sequence of late Neoproterozoic syn-rift siliciclastic sediments, comprising well-bedded quartzitic to arkosic sandstone verlain by calcareous deposits and a tillite/diamictite unit. These sediments are again overlain by clastic rocks and conglomerates (e.g. Gee, 1975; Kumpulainen, 1980; Hollocher et al., 2007).

Generally, the dikes and the bedding are near orthogonal. One direction dominates the dike-orientation, but cross-cutting dikes also appear. The dikes are locally rotated by Caledonian ramp-structures (Gilotti and Kumpulainen, 1986). The geometry of the dikes suggests en-echelon formation with straight and sharp margins without cataclastic contacts to the host rock. The sandstone has a hard hornfels texture at the contacts changing to a primary sedimentary clastic texture further away. There is no evidence for either regional or local partial melting of the host sediment. The mafic dikes are generally well preserved and commonly contain fresh olivine together with clinopyroxene and plagioclase. The matrix has clinopyroxene and plagioclase as the main minerals and Fe-Ti oxides as accessory minerals. Although allochthonous, no penetrative Scandian deformation has been observed. Recent U-Pb dating of baddeleyite gives an age of 596 Ma for the dike complex (Kumpulainen et al., 2016).

4. Geochronology from the northern segment

Dolerites from the Corrovarre lens have previously been dated by Rb-Sr and Sm-Nd on minerals and whole-rocks at 578 ± 64 Ma and 582 ± 30 Ma, respectively (Zwaan and van Roermund, 1990). Granite from the same lens was dated with U-Pb in zircon at 610.2 ± 1.1 Ma (Gee et al., 2016). In this study we have obtained new U-Pb ages for granite and dolerite using the Sensitive High-Resolution Ion Micro Probe (SHRIMP) at Curtin University (see online supplementary material and Appendix 1) and Chemical Abrasion Isotope Dilution Thermal Ionization Mass Spectrometer (CA-ID-TIMS) at the University of Oslo. The latter follows the analytical procedures described in (Corfu, 2004) with additional information given in the online supplementary material and in Appendix 1.

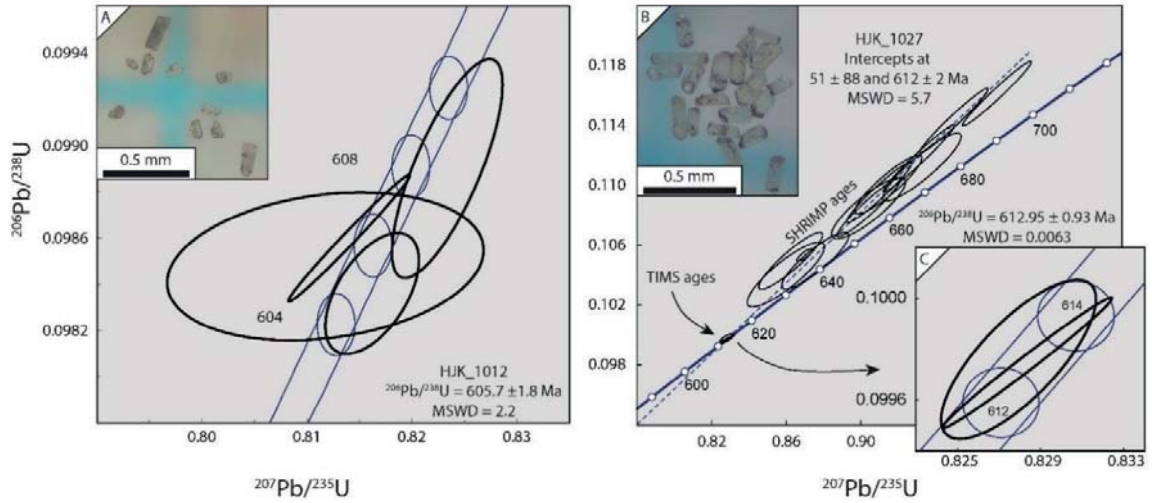

Figure 1-6 (previous page): Geochronological data of zircon in a dolerite dike and a granite from Corrovarre. A) Concordia diagram with data for four zircons from a medium-grained mafic dike. B) Zircon data for a granitic sheet. The SHRIMP analyses yield reversely discordant data, presumably due to a matrix effect related to the high uranium content. A line fitted through the SHRIMP data intercepts the Concordia at 612 ± 2 Ma. C) Two zircon grains from the same sample, dated using CA-ID-TIMS, yield concordant data with a $^{206}Pb/^{238}U$ average at 612.95 ± 0.93 Ma.

4.1. Dolerite dike

A medium-grained dike with sub-ophitic texture has plagioclase and clinopyroxene preserving magmatic zonation. The ten zircons found in the crushed sample were equidimensional fragments with diameters > 50 μm (Fig. 1-6a). The fragments were clear with some yellow-brown patches and often some crystal faces preserved, testifying to a euhedral growth of the zircon. Some euhedral grains were also found. These can be divided in two categories: 1) high aspect ratio (> 2) and dark, brown color. 2) low aspect ratio (< 2) clear, double terminated crystals (Fig. 1-6a).

Four zircon fragments were selected based on clarity, lack of inclusions and crystal shape and dated by CA-ID-TIMS, yielding an average $^{206}Pb/^{238}U$ age of 605.7 ± 1.8 Ma (Table 1-1; Fig. 1-6a).

Table 1-1: Analytical ID-TIMS data from two Corrovarre samples. [A] Model value calculated using $^{208}Pb/^{206}Pb$ ratio and the age of zircon. [B] Total common lead including blank and initial. [C] Corrected for spike contribution and fractionation. [D] Corrected for fractionation, spike and common lead, both blank and initial. [E] Corrected for fractionation, spike and common lead, both initial and blank. [F] Degree of discordance using $^{206}Pb/^{238}U$ and $^{207}Pb/^{206}Pb$ ratios.

					Isotopic ratios					Calculated ages					
Sample #	Weight [µg]	U [ppm]	Th/U[A]	Pb_c [pg][B]	$^{206}Pb_c/^{204}Pb$[C]	$^{207}Pb/^{235}U$[D]	2σ (%)	$^{206}Pb/^{238}U$[D]	2σ (%)	ρ	$^{207}Pb/^{206}Pb$[E]	2σ (abs)	$^{207}Pb/^{235}U$[E]	2σ (abs)	$^{206}Pb/^{238}U$[E]	2σ (abs)	D[F]
HJK_1012	<1	300	1.8	1.2	1515.7	0.816	0.4458	0.098	0.2166	0.55	607.6	8.1	603.6	2.0	604.8	1.3	0.5
HJK_1012	1	255	2.5	0.9	1810.4	0.823	0.5255	0.099	0.3905	0.76	614.8	7.3	609.9	2.4	607.9	2.3	1.1
HJK_1012	<1	141	2.2	0.8	1093.6	0.814	0.5802	0.099	0.2307	0.99	596.6	11.2	604.7	2.6	606.2	1.3	-1.6
HJK_1012	<1	100	2.4	1.6	390.6	0.812	1.5167	0.098	0.2646	0.22	593.2	32.1	603.4	6.9	605.5	1.5	-2.1
HJK_1027	<1	964	0.1	2.1	2801.4	0.828	0.3673	0.100	0.2565	0.76	608.0	5.2	612.5	1.7	613.0	1.5	-0.8
HJK_1027	<1	479	0.1	0.4	6689.4	0.828	0.4019	0.100	0.2106	0.99	609.4	7.2	612.7	1.8	612.9	1.2	-0.6

Coordinates for sample HJK_1012: 21° 38' 38.17"E, 69° 50' 0.698"N
Coordinates for sample HJK_1027: 21° 40' 6.174"E, 69° 49' 38.708"N

4.2. Granites

A granite consisting of Qz + Plag + Kfs + Bt + Ms forms a sheet sub-parallel to the bedding, truncated by dolerites of the SDC, i.e. a pre-dike emplacement granite (Fig. 1-3c). The sample contained abundant zircon grains that in general are clear and euhedral (Fig. 1-6b). The zircons are often flat and plate-like with an aspect ratio of the zircons varying from very high, > 3 to < 2. Growth zonation can be discerned even under the binocular microscope. The SHRIMP analyses plot reversely discordant (Fig. 1-6b), probably due to a matrix effect caused by high levels of uranium (up to 11.800 ppm; White and Ireland, 2012), but may also have been affected by U-Pb perturbations. Therefore, an attempt was made to date the zircon grains using CA-ID-TIMS. After chemical abrasion, however, only two zircon fragments were left. They yielded two overlapping concordant analyses with an average $^{206}Pb/^{238}U$ age of 612.95 ± 0.93 Ma (Fig. 6b). This age is identical within error to the average $^{207}Pb/^{206}Pb$ age of the SHRIMP data.

5. Mineral chemistry and geothermobarometry

Pressure and temperature are important factors that affect the geometries of a dike swarm as they control fracture mechanisms (Weinberg and Regenauer-Lieb, 2010). The Scandian thrusting of the SDC has caused rotations and in most sections the sedimentary bedding is now steeply dipping to vertical (Fig. 1-3e). In addition, the structural tops and bases, and even some internal domains of the observed sections, have secondary shear zone boundaries. Therefore, the depth of intrusion must be estimated by other methods than direct thickness

measurements. We have already described the wall rocks as contact metamorphic with variable degree of partial melting and variably overprinted by regional Caledonian metamorphism. Here, we distinguish the various generations of metamorphic mineral assemblages and apply several geobarometers to the contact metamorphic paragenesis in the best-preserved areas of the dike swarm to determine PT-conditions during emplacement.

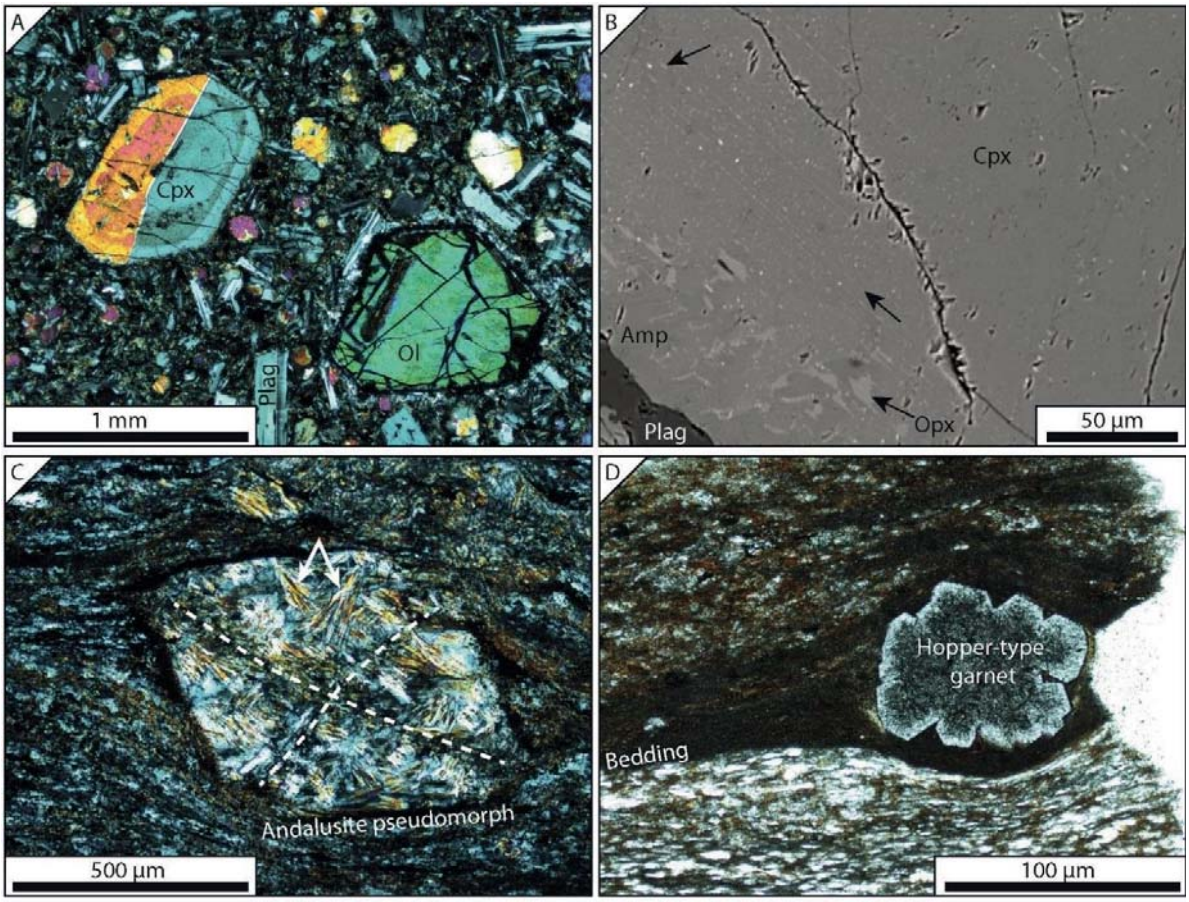

Figure 1-7: Overview of characteristic petrography. A) Photomicrograph of a porphyric dolerite with phenocrysts of cpx, ol and plag in a groundmass of cpx, plag and opaques, mainly Fe-Ti oxides. B) Back-scatter electron image of a cpx crystal with c. 1-5 µm thick exsolutions of Fe-Ti oxides (arrow) and exsolved opx (lighter phase) in the rim (bottom-left). C) Photomicrograph of a chiastolite pseudomorph in a contact metamorphic fine-grained argillaceous sediment. The andalusite is completely replaced by fibrous sillimanite. D) A hopper-type garnet, indicating rapid growth (Jamtveit and Andersen, 1992), in a biotite-rich horizon of an argillaceous sediment. The garnet has a thin (<10 µm) rim with less abundant inclusions of quartz and biotite.

5.1. Dike petrography

Texturally the dolerites vary from porphyritic, with cpx ± plag ± ol as phenocrysts, to aphanitic with a matrix of cpx + opx + plag + opaques (Fig. 1-7a). The most pristine mineral compositions are plagioclase (average: $Ab_{43} – An_{57}$ - Or_{0-1}), pyroxene (average: $Wo_{39} – En_{46} – Fs_{13}$), ± olivine (average: Fo_{82}) + Fe-Ti oxides ± scapolite (average: $Me_{43} – Mi_{50} – Si_7$) ± Qz ± Amp ± Bt. Plagioclase is zoned with An-rich cores. Within some of the clinopyroxenes a pervasive exsolution presumably of Fe-Ti oxides is present as thin (ø = ~1 µm) needles following crystallographic planes (Fig. 1-7b). Most samples also show exsolution between clinopyroxene and orthopyroxene to varying degrees (Fig. 1-7b). Electron Microprobe Analysis (EMPA) of the cpx crystals suitable for the pressure estimate (see below) display relatively homogeneous Al_2O_3 and CaO content (Fig. 1-8a and b). The Sarek analyses show a weak trend with Al_2O_3 increasing and CaO decreasing with Mg#. For Na_2O most analyses are < 0.35 wt%, except for Kebnekaise and five analyses from Sarek, which plot around 0.5 wt%. Kebnekaise analyses are clearly distinct from those from other localities (Fig. 1-8b).

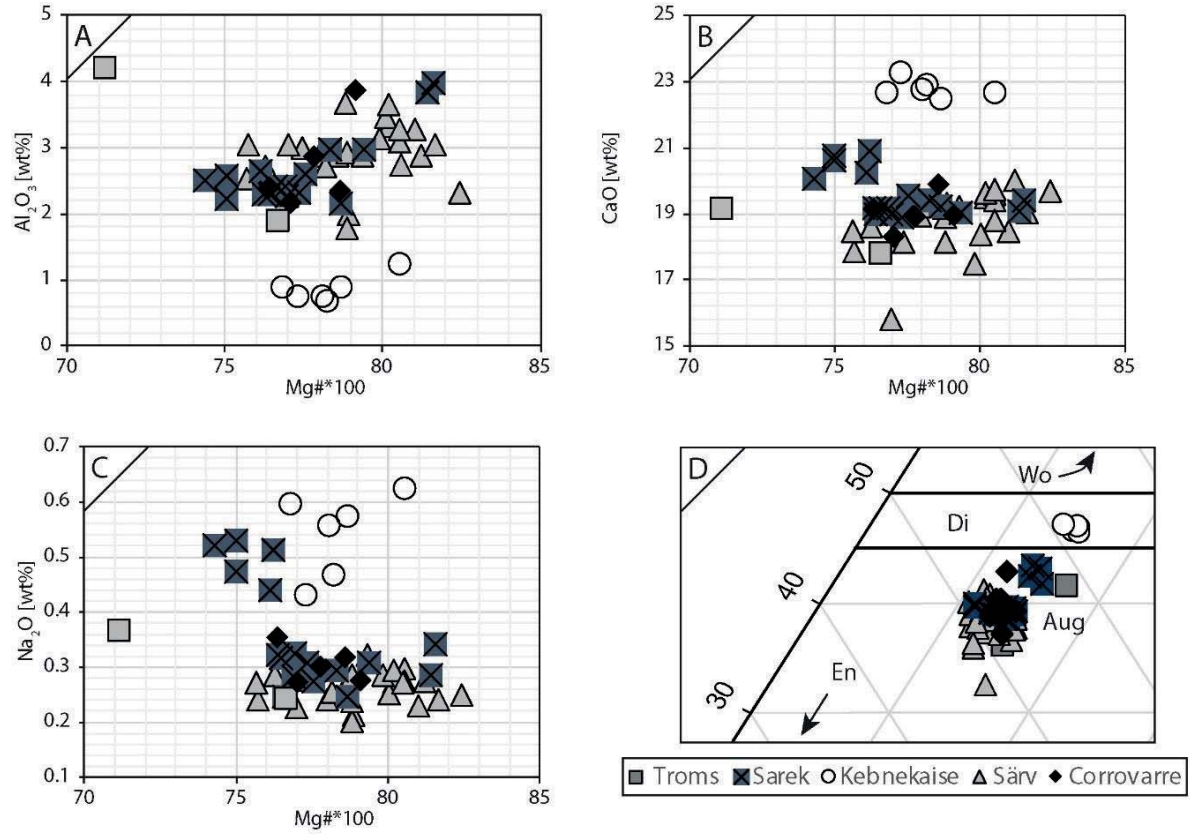

Figure 1-8: Clinopyroxene geochemistry A-C) Major element chemical compositions of clinopyroxene plotted against Mg# of the clinopyroxenes. D) Zoom-in of the pyroxene triangular diagram. Note that the Kebnekaise samples all have magmatic diopside, rather than augite and thus plot away from the other analyses.

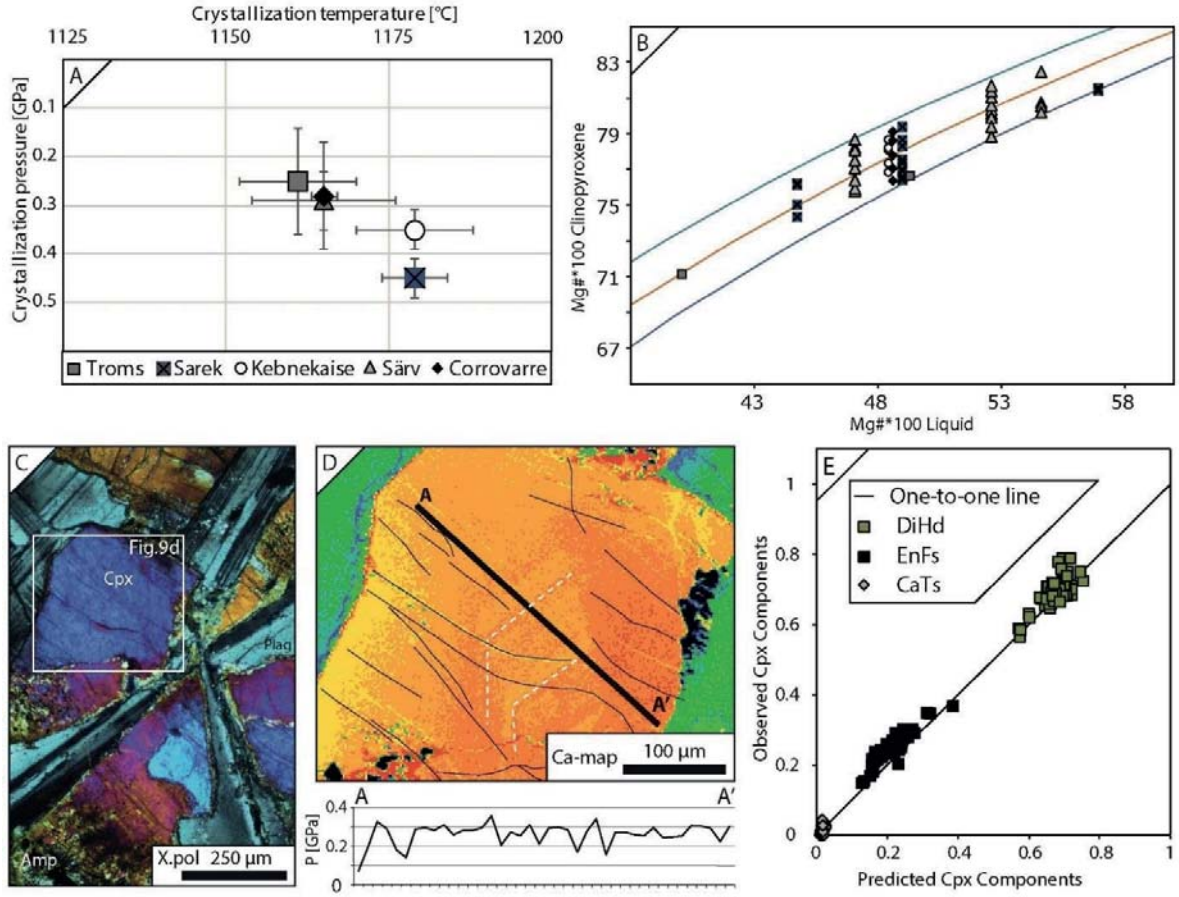

Figure 1-9: Overview of the crystallization pressure and temperature estimates. A) Average crystallization temperature vs. average crystallization pressure of the clinopyroxene. B) Rhodes diagram checking equilibrium between cpx composition and 'liquid', which in this case is assumed to be the whole-rock composition of the chilled margin of the dike (Putirka, 2008). Plot shows a selected K_D value of 0.27 (orange line) ± 0.03 for Fe-Mg in Cpx-liquid pairs. C) Photomicrograph (crossed polarizers) of an analyzed magmatic cpx crystal from Corrovarre. D) CaO, EMPA map of the cpx crystal in C shows magmatic zonation (white dashed lines) in the crystal. Thin black lines outline cracks seen on BSE image. Graph at the bottom shows P-estimates along profile A-A'. E) Observed and predicted cpx components used to calculate the crystallization PT conditions of the cpx.

5.2. Magmatic clinopyroxene geobarometry

Crystallization pressures (Fig. 1-9a) were estimated using the jadeite-in-clinopyroxene-liquid (jd-in-cpx-liq) geobarometer from Neave and Putirka (2017) and crystallization temperatures (Fig. 1-9a) were estimated using equation 33 in Putirka (2008) as suggested in (Neave and Putirka, 2017). The jd-in-cpx-liq geobarometer is based on the pressure dependent incorporation of jadeite, the Na-component in clinopyroxene crystallized in equilibrium with basaltic liquid. The EMPA data were filtered and checked for equilibrium with the whole-rock composition (Fig. 1-9b and e) of the chilled margins as a proxy for the

liquid composition. The strict filtering parameters suggested by Neave and Putirka (2017) reduced the number of cpx analyses from a total of 325 to the 56 suitable for the crystallization pressure and temperature determination (Fig. 1-9; online supplementary material). Similar results are also obtained when using more lenient filtering methods, substantiating the validity of the method. More details of the procedure and the filtering criteria can be found in the online supplementary material and Appendix 1.

The crystallization pressure calculations are summarized in figure 1-9a. Results show some variation between different field areas. The southern segment is inhomogeneous with Sarek at 0.45 ± 0.04 GPa, Kebnekaise at 0.35 ± 0.04 GPa and Troms at 0.25 ± 0.11 GPa. It should be noted that for Troms only two cpx analyses (out of 28) fulfilled the criteria of the geothermobarometer as given in Neave and Putirka (2017). Corrovarre, in the northern segment, yields 0.28 ± 0.11 GPa and Särv in the south 0.29 ± 0.06 GPa.

Calculations of the crystallization temperatures were based on the same filtered analyses as for the geobarometer and yield similar temperatures for all the field areas (Table 1-2). The temperature estimates are relatively homogenous and agree within 18°C, with 1161 and 1179 as the extreme values, for the four different field areas. A positive correlation is observed between T and P estimates (Fig. 1-9a).

Table 1-2: Results from P/T estimates using jd-in-cpx-liq geothermobarometry from Neave and Putirka (2017) and the geothermometer Ti-in-Bt from Henry et al. (2005).

	Crystallization pressure		**Crystallization temperature**		**Avg. T from Ti-in-Bt**		**#samples / #analysis**
Area	**P[GPa]**	**1σ [GPa]**	**T [°C]**	**1σ**	**T [°C]**	**1σ**	
Särv	0.29	0.06	1165	11	-	-	-
Sarek	0.45	0.04	1179	5	693	14	6/50
Kebnekaise	0.35	0.04	1179	9	713	3	1/7
Troms	0.25	0.11	1161	9	696	19	2/15
Corrovarre	0.28	0.11	1165	2	-	-	-

5.3. Host rock petrography

The most common clastic sediments (quartzite, arkose and greywacke) hosting the dike complex contain varying amounts of mica in mineral assemblages of Qz + Fsp + Grt +Bt + Sil ± Ms ± Scp ±Ttn ± Ap ± Tur ± Zr. Carbonates, with bedding defined by calc-silicate layers, are generally found in the lower parts of the stratigraphy. In the least deformed parts, the sediments have a hornfels texture, generally without cleavage. Locally, mm-sized pseudomorphs of andalusite are statically recrystallized into fibrous sillimanite, without preferred orientation and the characteristic chiastolite habitus preserved (Fig. 1-7c). Where the host rock consists of arkose and greywacke the more mica-rich domains often contain hopper- to dendritic shaped garnets rich in inclusions as well as fibrous sillimanite (Fig. 1-7d). Biotite has commonly overgrown the bedding in random directions.

5.4. P-T estimates from pseudosection modeling

Where the dikes intrude argillaceous sediments several pressure and temperature sensitive minerals have grown and can be used to deduce the metamorphic history of the rock. The garnets are generally unzoned and poikilitic and grew in the mm-thick mica-rich horizons that define the bedding in the sediment (e.g. Fig. 1-7d). In general, the garnets are almandine-rich (Alm_{70}), except for one sample, which is more grossular-rich (Alm_{40}, Grs_{25}). The spessartine and pyrope contents are similar for all samples ($Prp_{10\ to\ 19}$). Most of the samples have sillimanite as very fine-grained fibrolite and, as previously mentioned, andalusite pseudomorphed by static growth of sillimanite, suggesting a prograde pressure and/or temperature path from the earliest to late stages of static growth (Fig. 1-7c). Both biotite and muscovite also occur as neoblasts.

Calculation of almandine, grossular, pyrope and spessartine garnet endmember isopleths (Theriak-Domino; de Capitani and Petrakakis, 2010) on a sample from Indre Troms (Fig. 1-2) was used to estimate the ambient conditions during contact metamorphism. The sample is a mica-rich arkose sampled c. 3 m from a fresh, c. 5 m thick dolerite dike. The pressures range from 0.25 to 0.35 GPa and temperatures are 675-725°C.

5.5. Ti-in-biotite geothermometry

Titanium in biotite geothermometry (Engel and Engel, 1960; Henry et al., 2005) has been applied on sediments containing biotite from Sarek and Indre Troms (Fig. 1-2). The samples used for these analyses were collected ca 1-5 meters away from the dikes. The biotite used for the geothermometry shows subhedral to euhedral crystal shapes. To avoid complications due to multiple metamorphic events and secondary alteration processes, only analyses of biotite with random orientations (i.e. static growth) were used to calculate the contact metamorphic temperatures. Furthermore, analyses that indicate incipient alteration of

biotite to chlorite were disregarded. Biotite has an average Mg# of 43 and average TiO_2 of 3.1 wt% (see online supplementary material).

This geothermometer yields crystallization temperature of 693 ± 14°C at Sarek, 713 ± 3°C for Kebnekaise, 696 ± 19°C and for Indre Troms 634 ± 6°C (errors are 1σ).

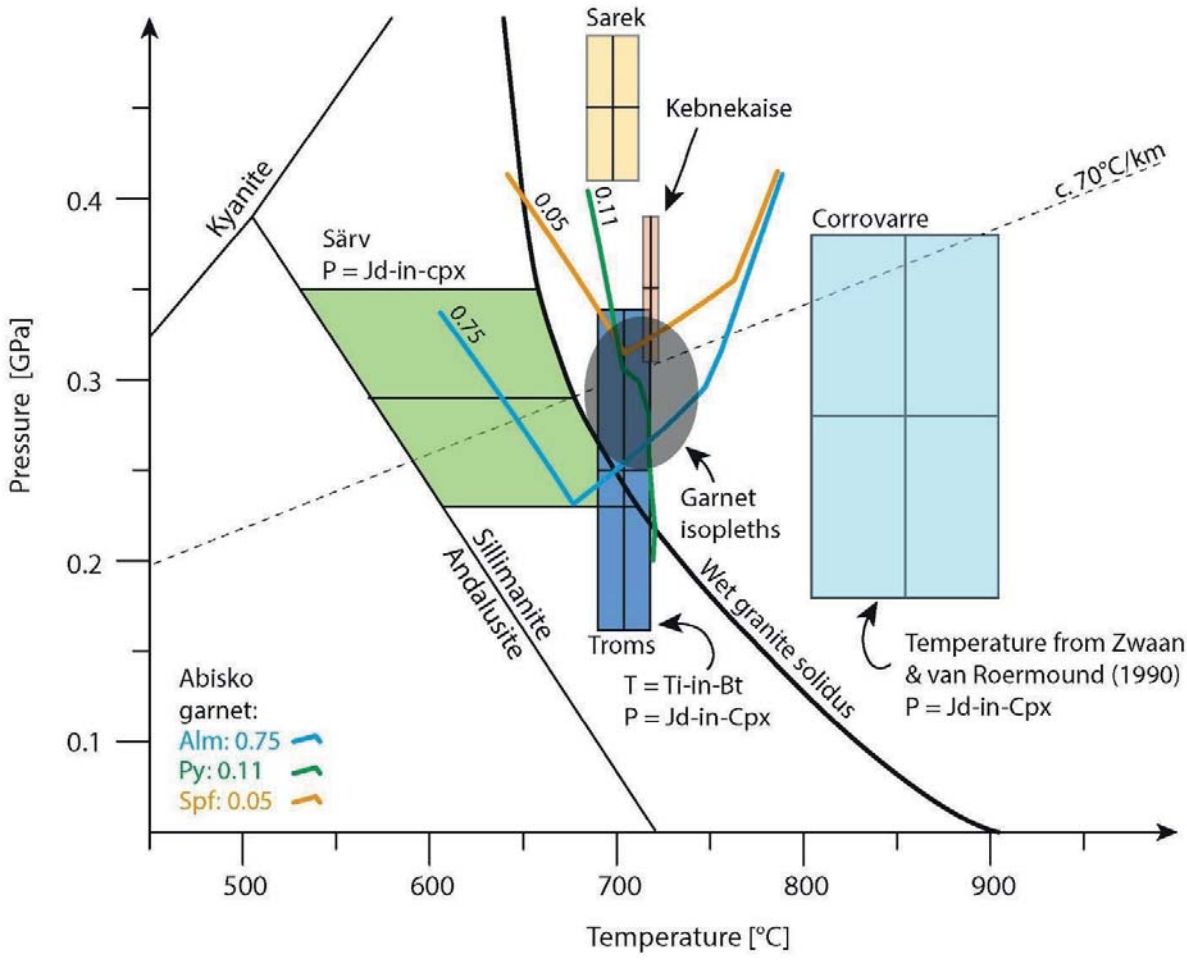

Figure 1-10: Summary of PT data from various geobarometers and geothermometers as well as garnet isopleths. Wet granite solidus is from Huang and Wyllie (1981), while the temperature estimate for Corrovarre is from Zwaan and van Roermund (1990).

6. Discussion

The rocks investigated in this study have undergone multiple metamorphic events. The first event, considered in this contribution, reflects the contact metamorphic heating by mafic intrusions emplaced at the distal margin of the Iapetus. The second event, i.e. the orogenic event, is more frequently studied in the literature but also more complex and reflect the changing pressures and thermal imprint of the burial and subsequent nappe emplacement of the distal margin. Locally, this event reached eclogite facies conditions, although (garnet) amphibolite facies is more common. Shear zones cross-cutting all emplacement-related structures have amphibolite facies mineral assemblages. In summary, the first contact metamorphism was a high temperature, low pressure event, whereas the second, Caledonian event reached a diversity of metamorphic conditions (not discussed in detail here), but in general producing higher pressure mineral assemblages.

6.1. Ambient conditions during dike emplacement

In the studied areas, the crystallization pressure estimates from the jd-in-cpx-liq geothermobarometer vary from 0.25 to 0.45 GPa indicating a depth ranging from 9 and 16 km. Contact metamorphic temperatures estimated using Ti-in-biotite (Henry et al., 2005; Fig. 1-10) are as high as 693 to 713°C. This is also in agreement with contact metamorphic garnet isopleth calculations from Theriak-Domino modeling, which suggest temperatures ranging from 700 to 750°C. The sediments sampled for geothermometry were collected 1 to 5 meters from the dike contacts at different sites. They were originally sampled for detrital zircon geochronology; therefore, no profiles away from a dike have been sampled. The temperature estimates are therefore limited to one specific spot at varying distances to the dikes. All sample sites are highly intruded (> 70% by volume) by dikes. As such we believe that the calculated temperature is a good estimate of the ambient thermal conditions of the area. We cannot assess how much magma flowed through the conduit and for how long. Such parameters would increase the temperature effect on the host rocks as the temperature at a specific distance from the dike will be closer to the temperature of the magma the more magma has been flowing through the dike. This factor may have caused the higher degrees of partial melting that we observe in Indre Troms, Corrovarre and to a certain degree Sarek. The field observations presented above, show that the pressure-temperature conditions for the contact metamorphism estimated here are above the solidus for partial melting of water-rich arkoses with a granitic mineralogy at ~660°C at 0.3 GPa (e.g. Johannes, 1984; Clemens and Holness, 2000). No samples suitable for Ti-in biotite were collected from Corrovarre, but Zwaan and van Roermund (1990) using a leucosome containing two pyroxenes obtained a temperature of 850 ± 50°C, significantly higher than what has been shown for the other areas to the south.

Field observations from the southern segment of the SDC show a progressive evolution of the strain accommodation mechanisms (brittle to ductile) as the temperature increased. In the southern segment, some early faults are decorated by recrystallized pseudotachylite veins (Fig. 1-5a). These faults are cut by mafic dikes, which are themselves deformed by ductile mechanisms. The orientation and kinematics of these structures can be explained by a single stress system, resulting in stretching in the long limb and shortening in the short limb of the bent dike. Furthermore, the normal fault truncated by the dike is also favorably oriented within such a stress field (Fig. 1-5c). It is also noticeable that in the same area where the sediments have undergone brittle faulting, contact metamorphic melting of the sediments mostly took place at dike/sediment contacts; whereas in the northern segment the anatexis of host rocks was more pervasive and is also found away from dike contacts. These observations, together with the prograde transformation of andalusite to sillimanite, suggest a significant increase in ambient temperatures from conditions where the deformation was brittle during the early non-magmatic faulting stage to above 600°C during the emplacement of the mafic dikes, contemporaneous with late stages of the stretching.

Three models can explain the temperature increase described above: 1) Burial under the typical thickness of extrusive and intrusive volcanic rocks generally found at magma-rich rifted margins (seaward dipping reflector sequences of 3-7 km; Skogseid et al., 1992; Menzies et al., 2002), which, with a moderate geothermal gradient of 35°C/km would give a temperature increase of 105 to 245°C. 2) Related to volcanism at the margin there is also an increased heat influx from the accumulation of lower crustal magma reservoirs and the introduction of dikes. 3) Condensation of geotherms during rift-related thinning of the continental crust. A combination of all or several of these factors is presumably the most likely scenario. Further studies to quantify the individual impact of these processes would be interesting but they are beyond the scope of this study.

The pressure data from the dike complex are intriguing as some samples suggest relatively high pressure (i.e. 0.5 GPa for one Sarek sample), which indicates that the clinopyroxene crystals started crystallizing at greater depths than the others, possibly in a deeper magma reservoir. Crystallization in such a reservoir is likely also due to the evolved nature of the mafic dikes, which have an average Mg# of 49.5 (See online supplementary material), and thereby suggest that significant fractional crystallization of the mafic magma occurred prior to dike emplacement. Although such magma reservoirs have not been described from the Caledonides, they likely have a relatively small preservation potential during continental collision, due to their mafic composition and thereby dense nature. Furthermore, the distinctly older age of the granite than the dolerite at Corrovarre, and its implication of pervasive pre-dike emplacement anatexis of the host sediments, suggests that an elevated geothermal gradient was established already before the main stage of mafic diking. Such excess heat at relatively shallow crustal levels is difficult to envisage

without the effect of magmatism. The observations, radiometric ages and P-T analyses presented here may imply that magma was emplaced and stored within the lower crust prior to the main dike emplacement, and thereby developed early in the rifting history. The existence of such early lower crustal magma reservoirs is also corroborated from modern examples of rifts and failed rifts, such as the main Ethiopia and Baikal rifts (Thybo et al., 2000; Nielsen and Thybo, 2009; Bastow et al., 2011).

6.2. Timing of magmatism and continental break-up

In the North Atlantic Large Igneous Province (NALIP), continental break-up resulted in voluminous igneous activity generating both extrusives and intrusives into the sedimentary basin and underlying stretched continental crust. The magmatism was short-lived and intense, with a peak lasting c. 3 Myr (e.g. Menzies et al., 2002; Storey et al., 2007), consistent with other modern magma-rich rifted margins (Menzies et al., 2002).

By contrast, in the Scandinavian Caledonides there is evidence for at least 20 Myr of rift related magmatism preserved. The predominantly mafic magmatism with its paucity of magmatic zircon and other datable minerals, and the variably strong Caledonian overprint, complicate the documentation and precise dating of the evolution of the SDC. Ages of mafic magmatism obtained by CA-ID-TIMS generally fall within the time interval 608 to 596 Ma (Fig. 1-2; Svenningsen, 2001; Baird et al., 2014; Kirsch and Svenningsen, 2015; Kumpulainen et al., 2016) suggesting that most of the SDC was emplaced during a short time period similar to the duration of the break-up of the NALIP. A younger SIMS age of 578 Ma has, however, also been found at Kebnekaise (Kirsch and Svenningsen, 2015).

The new zircon age for the crystallization of the Corrovarre dike swarm at 605.7 ± 1.8 Ma, presented above (Fig. 1- 6) is similar to those in Kebnekaise and Sarek, but older than the 570 and 560 Ma timing of the Seiland Igneous Complex (See Fig. 1-2; Roberts et al., 2006; Roberts et al., 2010) with which it was previously correlated (Zwaan and van Roermund, 1990). The new age for the Corrovarre dolerites as well as similarities in geochemistry (Roberts, 1990) documents that they are part of the SDC and can be correlated with the rest of the SDC in the southern segment. Tegner et al. (2019) have shown that, like the NALIP, the SDC was triggered by elevated upper mantle temperatures.

Opening of the Iapetus Ocean occurred in stages between about 620 and 550 Ma, beginning with rifting of rocks now found mainly in Caledonian nappes on Baltica and ending with break-up of southern Iapetus between Laurentia and Gondwana (Cawood et al., 2001). Rifting and opening of the portions of the Iapetus between Laurentia and Baltica is constrained by dating of mafic as well as felsic rift-related magmatic rocks in sedimentary basins and basement from both the Laurentian side (e.g. Halliday et al.,

1989; Kamo et al., 1989; Dempster et al., 2002) and the Baltican side (Svenningsen, 2001; Bingen et al., 1998; Root and Corfu, 2012; Baird et al., 2014; Kirsch and Svenningsen, 2015; Kumpulainen et al., 2016; this study; Fig. 1-11a). The oldest rift-related age on the Baltican side is that of the Egersund dikes, 616 ± 3 Ma (Bingen et al., 1998), whereas the youngest dikes at around 578 ± 9 has been found in the Kebnekaise area (Kirsch and Svenningsen, 2015). However, many ages of both mafic and felsic magmatism fall between 608 and 596 Ma (Fig. 1-11b), suggesting that although the magmatic record shows prolonged activity, the final break-up of Baltica and Laurentia was punctuated by a major dike emplacement event between 608 and 596 Ma.

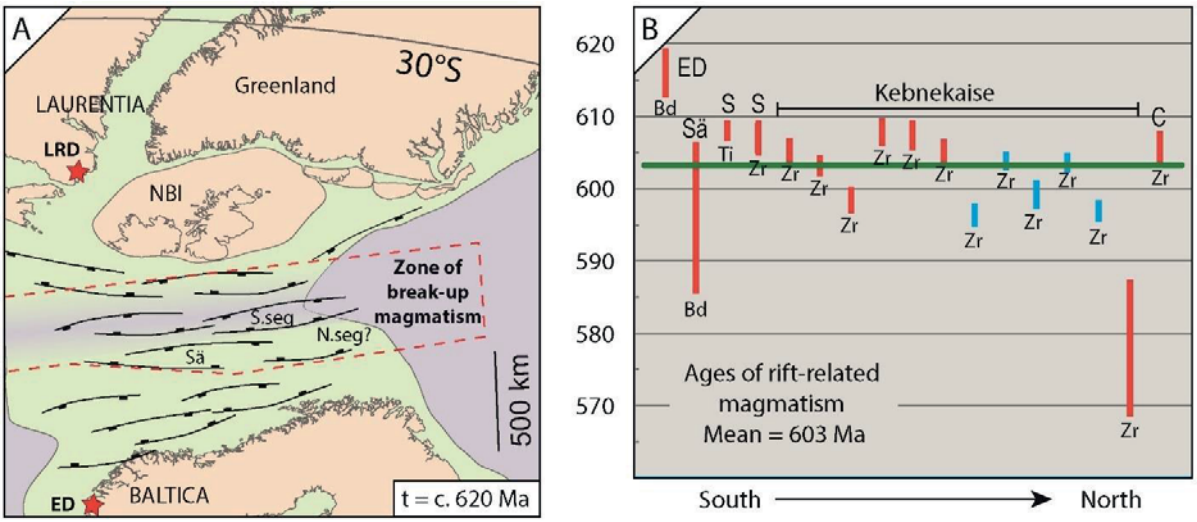

Figure1- 11: A) Suggested paleogeographic reconstruction of Baltica and Laurentia at c. 620 Ma, based on Tegner et al., 2019. Red stars show the locations of LRD: Long range dikes and ED: Egersund dikes, Sä: Särv, S.seg: South segment, N.seg: Northern segment, NBI: North British Isles. B) Overview of the age data from rift-related magmatism now preserved in the Scandinavian Caledonides. Ages of mafic dikes are colored red, whereas ages of granitoids are colored blue. ED: Egersund dikes, Sä: Särv, S: Sarek, C: Corrovarre, Bd: Baddeleyite, Zr: Zircon.

6.3. Geodynamic implication

The data presented above show that the intrusion of the 605.7 ± 1.8 Ma dolerites at Corrovarre, was preceded by a widespread regional metamorphism coupled with a bedding parallel stretching and anatexis of the host sediments (Fig. 1-4a and b). Partial-melt migration and coalescence into granitoid veins, sills and minor intrusive bodies occurred contemporaneously with the deformation (Lindahl et al., 2005; Zwaan and van Roermund, 1990; this study). The new granite age of 612.94 ± 0.93 Ma is similar to the age presented by Gee et al. (2016) of 610 ± 1 Ma from the Corrovarri granite but somewhat older than the 602

± 5 Ma U-Pb zircon age presented by Corfu et al. (2007) for the nearby Rappesvarre granite. These ages coupled with field observations show that the host rock sediments were partially molten already prior to the main phase of dike emplacement (Fig. 1-6d). In order to melt water-bearing sedimentary rocks at temperatures between 650 and 750°C, an elevated pressure is required (Fig. 1-10), which agrees with the calculated crystallization pressure of 0.3 GPa presented here, suggesting that a high geotherm was established already prior to the emplacement of the SDC. Similar observations of S-type granites derived from water-present crustal anatexis have also been made in relatively shallow boreholes from the Vøring margin, offshore central Norway (Meyer et al., 2009), testifying to the high geothermal gradient at magma-rich rifted margins. Such partial melting has been proposed to constitute an important weakening process promoting continental break-up (Buiter and Torsvik, 2014). The new documentation presented here clearly shows that partial melting of host rocks prior to dike emplacement may have constituted the first step in a sequence of events with positive feedback leading to continental break-up.

From the data presented herein and elsewhere in the literature we conclude that the structural and tectono-thermal evolution of the Iapetus rifted margin in the Neoproterozoic can be summed up in 4 major events (See figure 1-2 for timeline): 1) Incipient stretching after c. 850 Ma (Nystuen et al., 2008) and local magmatic activity (Walderhaug et al., 1999; Paulsson and Andreasson, 2002); 2) Continuous or localized extension evolved through the Neoproterozoic with deposition of carbonates, sandstones and eventually thick syn-rift clastic wedges (e.g. Kumpulainen and Nystuen, 1985). This period also included a few episodes of deposition of glaciogenic sediments; 3) As stretching continued, the crust thinned significantly and adiabatic melting of the upper mantle, associated with elevated lithosphere-asthenosphere temperatures, caused partial melting, LIP-magmatism and build-up of large mafic magma reservoirs at the base of the lithosphere. The stretching and the increased heat flux from incipient mafic intrusions in the crust and the lower crustal reservoirs caused local pervasive melting of the host rock at c. 610-612 Ma; 4) The plume related LIP-magmatism peaked at 608-596 Ma. This event produced large amounts of mafic dikes constituting ≥ 70 - 100 % of the crustal volume. This event has been interpreted to represent the rift to drift transition and thus marks the opening of the Iapetus Ocean. This intense dike event and LIP-magmatism probably also led to the rapid accumulation of thick (3-7 km) sequences of volcanics similar to present-day SDR, which presently are only sparsely preserved in the Scandinavian Caledonides.

7. Conclusions and summary

It is demonstrated here that the mafic dikes at Corrovarre crystallized at 605.7 ± 1.8 Ma and thus have a similar crystallization age to the rest of the SDC further south. The SDC magmatism spans a relatively long period of time, but the peak mafic magmatism occurred between 608 and 596 Ma. This age span is interpreted to represent the opening of the Iapetus Ocean along the pre-Caledonian margin of Baltica.

Geothermobarometry from contact metamorphic host sediments (thermodynamic modeling and Ti-in-bt) and the cross-cutting mafic dikes (jd-in-cpx-liq) suggests that the studied parts of the SDC were emplaced at 0.25 to 0.45 GPa and at temperatures of c. 700°C in the wall rocks, in areas where the dike-density was most intense.

There was a significant increase in the geotherm during the crustal extension; from early, possibly co-seismic brittle faulting during the non-magmatic rifting stage, to the thermal weakening and break-up triggered by the introduction of large volumes of plume generated LIP magmas.

In the northern segment, crustal anatexis commenced already at 612-610 Ma, prior to dike emplacement. We interpret this temporal relation as being due to the formation of the pre-Caledonian LIP associated with the Central Iapetus Magmatic Province (Ernst and Bell, 2010). Accumulations of a lower crustal magma reservoir may have significantly heated parts of the extending crust.

Based on the new data presented and discussed here we suggest that the SDC represents the intermediate to lower levels of a distal magma-rich rifted margin invaded by LIP-magmatism. More specifically the dike swarms were probably feeding major volcanic systems, which are only locally preserved. The volcanic edifice was most likely a major component of the overburden. The abrupt increase in the geotherm and the prograde static metamorphic transformation (andalusite to sillimanite) of the initial contact metamorphic assemblages was associated with the LIP-magmatism, which probably also was important for the lithospheric weakening that eventually resulted in continental break-up and sea-floor spreading.

Acknowledgments

All the data that led to the conclusions of this article are presented in the figures, tables and supplementary files linked to the electronic version of this paper. This project was funded with the support from the Research Council of Norway through the Centre of Excellence funding scheme to CEED, project

Number 223272 and the NFR-FRINAT project 250327 “Hyperextension in magma-poor and magma-rich domains along the pre-Caledonian passive margin of Baltica”. This research was also funded by the Danish National Research Foundation Niels Bohr Professorship grant 26-123/8 to CT. We are indebted to Alex Zagorevski and David Chew for providing constructive reviews. The manuscript has improved significantly from their comments. Lars Augland is thanked for support in the TIMS lab; Sara Callegaro and David Neave are thanked for support with the PT estimates and Eric Tohver for support with SHRIMP analyses. National Park authorities in Norway and Sweden are acknowledged for the permissions to use helicopter to access remote areas in the parks.

Chapter 2

Emplacement mechanisms of a dyke swarm across the Brittle-Ductile transition and the geodynamic implications for magma-rich margins

Hans Jørgen Kjøll, Olivier Galland, Loic Labrousse, Torgeir B. Andersen

This manuscript has been published in *Earth and Planetary Science Letters*

Supplementary material is available online at: https://doi.org/10.1016j.epsl.2009.04.16

Abstract: Igneous dykes are the main magma transport pathways through the Earth's crust and, in volcanic rifts, they are considered to be the main mechanism to accommodate for tectonic extension. Dykes are typically considered to result from brittle fracturing, even in the ductile crust. A common assumption is that dyke orientation is controlled by tectonic stresses, such that dykes in rifts are expected to be vertical and perpendicular to extension. Here we report on detailed field observations of a spectacularly well-exposed dyke swarm to show that dykes were not systematically emplaced by purely brittle processes and that dyke orientation may differ from the dominant tectonic stress orientations. The dyke complex formed near the brittle-ductile transition during opening of the Iapetus Ocean and is now exposed in the Scandinavian Caledonides. Distinct dyke morphologies related to different emplacement mechanisms has been recognized: 1) Brittle dykes that exhibit straight contacts with the host rock, sharp tips, en-echelon segments with bridges exhibiting angular fragments; 2) Brittle-ductile dykes that exhibit undulating contacts, rounded tips, ductile folding in the host rock and contemporaneous brittle and ductile features; 3)

Ductile “dykes” that exhibit rounded shapes and mingling between the soft ductile host rock and the intruding mafic magma. The brittle dykes exhibit two distinct orientations separated by c. 30° that are mutually cross-cutting, suggesting that the dyke swam did not consist of only vertical sheets perpendicular to regional extension, as expected in rifts. We were able to use the well-exposed host rock layers as markers to perform a kinematic restoration to quantify the average strain accommodating the emplacement of the dyke complex: it accommodated for >100% extension, but counter-intuitively it also accommodated for 27% crustal thickening. We infer that the magma influx rate was higher than the tectonic stretching rate, implying that magma was emplaced forcefully, as supported by field observations. Finally, our observations suggest that the fast emplacement of the dyke swarm triggered a rapid shallowing of the brittle-ductile transition, and lead to a considerable weakening of the crust. The interpretations presented here could potentially have large implications for surface topography and seismicity in active rifts and volcanic areas around the world.

1. Introduction

Dykes, and igneous sheet intrusions in general, are fundamental magma pathways through the Earth’s crust. Their emplacement is controlled by a complex set of factors, such as crustal stress, crustal heterogeneities, topographic loading and magma viscosity (e.g. Halls and Fahrig, 1987; Magee et al., 2016; Spacapan et al., 2017; Kavanagh, 2018). Most models consider dykes as hydrofractures propagating as tensile cracks (mode I) in a brittle fashion with opening perpendicular to the least principal stress, implying that dykes emplaced in rifts are expected to be vertical and accommodate crustal extension (Keir et al., 2011). Because the rates for dyke emplacement are much higher than the tectonic strain rates, dyke emplacement is assumed to be a brittle process even in the ductile crust (Sassier et al., 2009; White et al., 2011; e.g. Rivalta et al., 2015). The low seismicity in the lower crust in active volcanic rifts, however, questions the purely brittle propagation of dykes in deep crustal levels (e.g. Legrand et al., 2002; Ágústsdóttir et al., 2016; White and McCausland, 2016) and suggest that ductile mechanisms may play a pivotal role in dyke emplacement. In addition, field observations (Spacapan et al., 2017), numerical modelling (Weinberg and Regenauer-Lieb, 2010), laboratory experiments (Bertelsen et al., 2018) and theory (Rubin, 1993) show that dykes and sheet intrusions can be emplaced by a combination of brittle and ductile deformation of the host rock, namely viscoelastic fingering or ductile fracturing. To what extent ductile deformation accommodates the emplacement of dykes in the ductile crust is still poorly known.

Andersonian theory predicts that the emplacement of dykes is controlled at a first order by far-field crustal stresses (Anderson, 1936; Nakamura, 1977), implying that tectonic stresses dominate over stresses

induced by magmatism. Such a scenario is likely when the magma influx rate is lower than the tectonic stretching rate. However, field evidence shows that magma influx rates at central volcanoes in rifts can be large enough to produce local magmatic stresses that overcome tectonic stresses, leading to the emplacement of cone sheet swarms (Pasquare and Tibaldi, 2007; e.g. Burchardt et al., 2013). In Large Igneous Provinces, magmatic rates can be extreme at lithospheric scale (e.g. up to 0.78 km^3/yr for the Karoo Basin; Svensen et al., 2012), but the effects of such high influx rate on magma emplacement mechanisms and crustal deformation have not been investigated. Furthermore, the thermal footprint of magmatism related to such major events has been shown to potentially significantly weaken the crust (Daniels et al., 2014; Kjøll et al., 2019a). Such weakening strongly depends on the balance between the tectonic stretching rate and the magma influx rate (Daniels et al., 2014). However, geodynamic models of continental breakup associated with Large Igneous Provinces do not account for the thermo-mechanical impact of the magmatism (e.g. Allken et al., 2012). This suggests that the effects of magmatism on the rheological structure of the crust and the tectonic evolution of magma-rich rifted margins need to be addressed and better documented in order to understand the active processes that can be inferred from remote sensing and geophysics, deep within rifts (e.g. Bastow et al., 2011).

In this paper, we report on detailed field observations of a spectacularly exposed dyke swarm emplaced at mid-crustal levels in the magma-rich rifted margin related to a large igneous province that developed during the breakup of the palaeocontinents Baltica and Laurentia, ~605 Ma ago. Our observations allow us to reveal (1) the complex brittle/ductile emplacement of dykes in deep crustal levels, (2) magma emplacement mechanism and related crustal deformation associated with high magma influx rates, and (3) upward migration of the brittle-ductile transition (BDT) because of magmatism.

2. Geological setting

The geological observations presented here are from two distinct regions in northern Norway and Sweden, referred to as Corrovarre and Sarek, respectively (Fig. 2-1). In Corrovarre, the studied outcrops are from a 0.5 x 6 km lens in a mountainous area. In Sarek, the field area consists of high mountains deeply dissected by glaciers, where high cliffs expose exceptionally well preserved and large outcrops. Among these we investigated two localities informally named ‘Favoritkammen’ and ’Favorithelleren’ by Svenningsen (1995), using a helicopter to get overview pictures (Fig. 2-1A and C).

The studied dyke complex can be observed along a string of outcrops spreading 900 km from south to north along the Caledonian mountain belt in Scandinavia (Fig. 2-1B). The dykes are mostly of basaltic composition and show little chemical variability (Tegner et al., 2019 and references therein). Radiometric

dating shows that the dyke complex developed between 616 and 596 Ma (Kjøll et al., 2019a and references therein). Specifically, in Sarek and Corrovarre, new U-Pb dating indicates that the swarms were emplaced at 608 ± 1 and 605.7 ± 1.8 Ma, respectively (Svenningsen, 2001; Kjøll et al., 2019a). The dyke complex was part of a magma-rich rifted margin (Abdelmalak et al., 2015; Kjøll et al., 2019a) associated with the interaction between a mantle plume (Tegner et al., 2019) and an active rift system that marked the opening of the Iapetus Ocean (Andréasson et al., 1992; Andréasson et al., 1998), separating the tectonic plates Baltica and Laurentia (Cawood et al., 2001). The dykes were emplaced in thick packages of Late Neoproterozoic sedimentary rocks (Svenningsen, 1994a). In Sarek, the dykes' host rock consists of evaporitic deposits and carbonates (100-500 m) overlain by a >2500 m-thick succession of arkosic sandstone with thin micaceous layers (Svenningsen, 1994a). At Corrovarre, most of the host rock consist of sandstone, with local discontinuous carbonate layers (Zwaan and van Roermund, 1990; Lindahl et al., 2005). At both Sarek and Corrovarre, geothermobarometry indicate that the dykes crystallized at a pressure of c. 0.3 - 0.45 GPa, suggesting an emplacement depth of ~10 km (Kjøll et al., 2019a), *i.e.* close to the BDT for a geotherm of 30°C/km. At Corrovarre, geothermobarometry suggests granulite facies metamorphic conditions at the time of dyke emplacement (Zwaan and van Roermund, 1990; Kjøll et al., 2019a), suggesting that the geotherm increased significantly during dyke emplacement.

In the Late Silurian to Early Devonian, the most distal parts of the Baltican margin, which contained the studied dyke complex, was subducted and subsequently exhumed during the Caledonian orogeny (Andréasson et al., 1998). Locally, the dyke complex escaped penetrative Caledonian strain and metamorphism, and remained preserved in large tectonic lenses (Svenningsen, 1994a). The studied outcrops are at the core of these undeformed lenses (Fig. 2-1). A more comprehensive description of the geological setting can be found in the supplementary material, part 1.

3. Geological observations

Given the large size of the studied outcrops, we performed photogrammetric surveys using an Unmanned Aerial Vehicle (DJI Phantom 4) and pictures taken using a SLR camera with GPS sensor from a helicopter. The georeferenced images were processed using Adobe Lightroom to enhance contrasts and colours, and subsequently used to compute 3D photogrammetric models, Digital Elevation Models, 3D textured meshes and orthomosaics with the Agisoft PhotoScan Professional software.

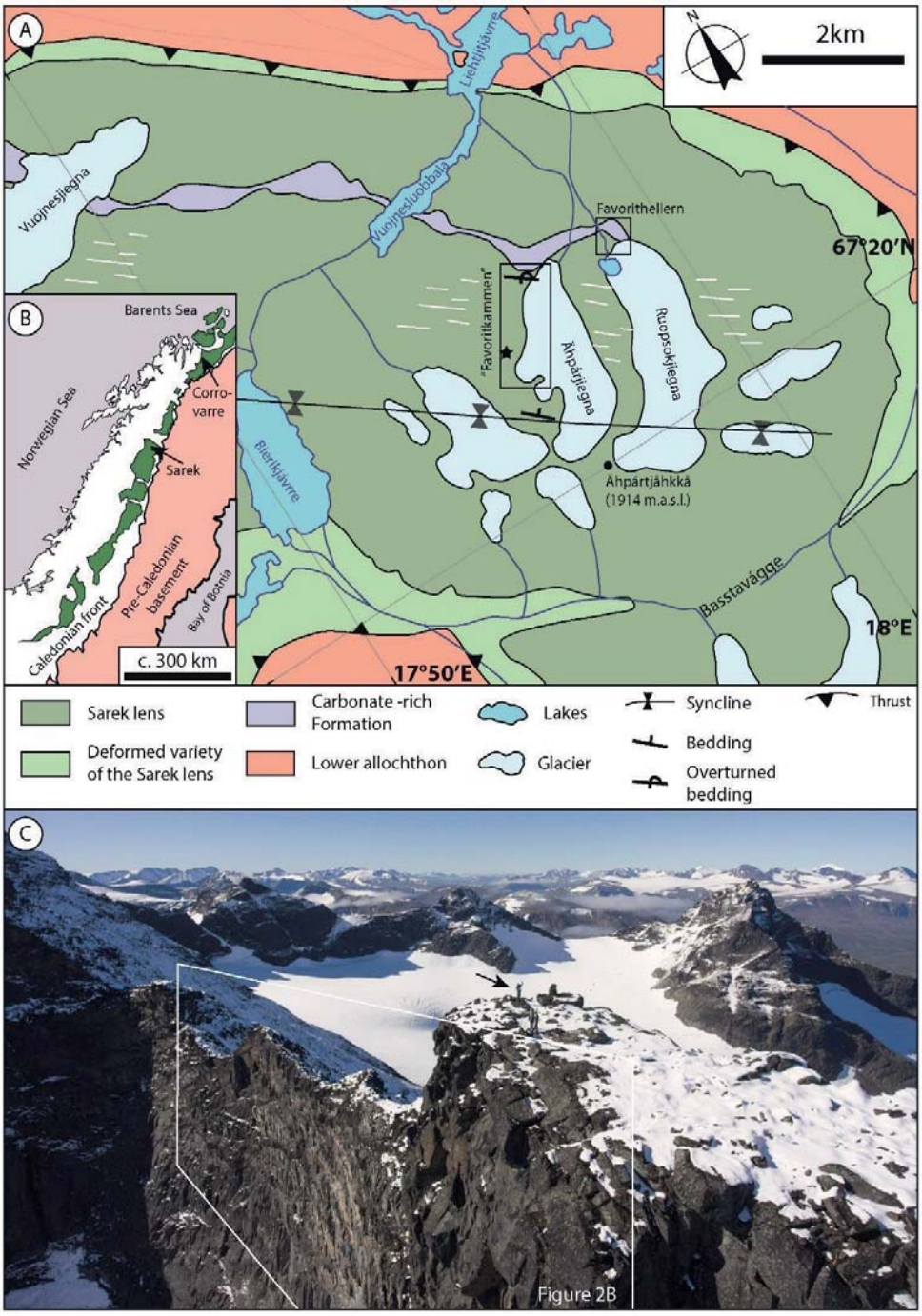

Figure 2-1: A) Generalized geological map of Sarek after Svenningsen (1995). Field areas are indicated by black rectangles. Note that bedding is locally overturned on the north limb of the syncline. White lines indicate orientation of dykes. B) Simplified geological map of the central and northern Scandes. White (and green) areas are rocks affected by Caledonian deformation. Green areas indicate the extent of the variably metamorphosed pre-Caledonian margin of Baltica. Pink is basement unaffected by Caledonian deformation and metamorphism. C. Photograph of the summit of the Favoritkammen cliff (geologists for scale highlighted by arrow), in Sarek. The only access was with a helicopter. This picture shows the remoteness and inaccessibility of many of the key field localities in Sarek National Park, north of the polar circle in Sweden.

The 3D mesh generated in PhotoScan was imported in the open source software LIME, developed by the Virtual Outcrop Geology Group, Uni Research CIPR at the University of Bergen, which allows structural measurements of geological planes, by picking three points on the measured surface (Buckley et al., 2019). When outcrops were accessible, direct outcrop observations, measurements and descriptions were conducted.

3.1. Observations in Sarek area

The sedimentary layering of the host rock is sub-vertical, showing large rotation of the exposed crustal block with unknown finite rotations. Nevertheless, the relative orientations of the dykes with respect to each other, and with respect to the sedimentary layering of their host rock, are mostly preserved and primary, given that there is no significant internal tectonic deformation in the studied sub-areas. Cross-bedding, upwards fining sequences and erosional surfaces, all indicate right-way-up toward the south both at the Favoritkammen and Favorithelleren localities (Fig. 2-2; Svenningsen, 1994b), showing that the current sub-horizontal cross-section represents a vertical profile through the crust. This implies that the Favorithelleren outcrop was deeper than the Favoritkammen outcrop (Fig. 2-1) since no major shear zone was detected between them. These exceptional exposures allow detailed descriptions of dyke shapes and strain recorded in the host rock in a continuous vertical section for almost 2 km. Structural mapping along the entire profile highlights the presence of brittle, ductile and brittle-ductile structures related to dykes and their emplacement. The following sections report on these respective structures.

3.1.1. Brittle structures

The dykes at the Favoritkammen cliff appear as relatively straight segments (Fig. 2-2 and Fig. 2-3). The contacts are very sharp and regular. Locally, gentle undulations of the contacts are visible (Fig. 2-3A). Only a few dyke tips have been identified in the area. They appear as very sharp tips terminating wedge-shaped dykes that are significantly thinner than the other dykes (Fig. 2-3C). These thinner dykes also exhibit regular and straight contacts with the host rock. Local jogs/deflections are common along the strike of the dykes where the dykes cross-cut thin micaceous layers between quartzite beds (Fig. 2-3C, inset). It is noticeable that even if the host rock is strongly layered, no sill, i.e. layer-parallel intrusion, is observed. Where dyke segments are arranged in en-echelon pattern, bridges develop between segments. Generally, these bridges are broken with irregularly shaped pieces of host rock floating in the dyke where it steps (Fig. 2-3D).

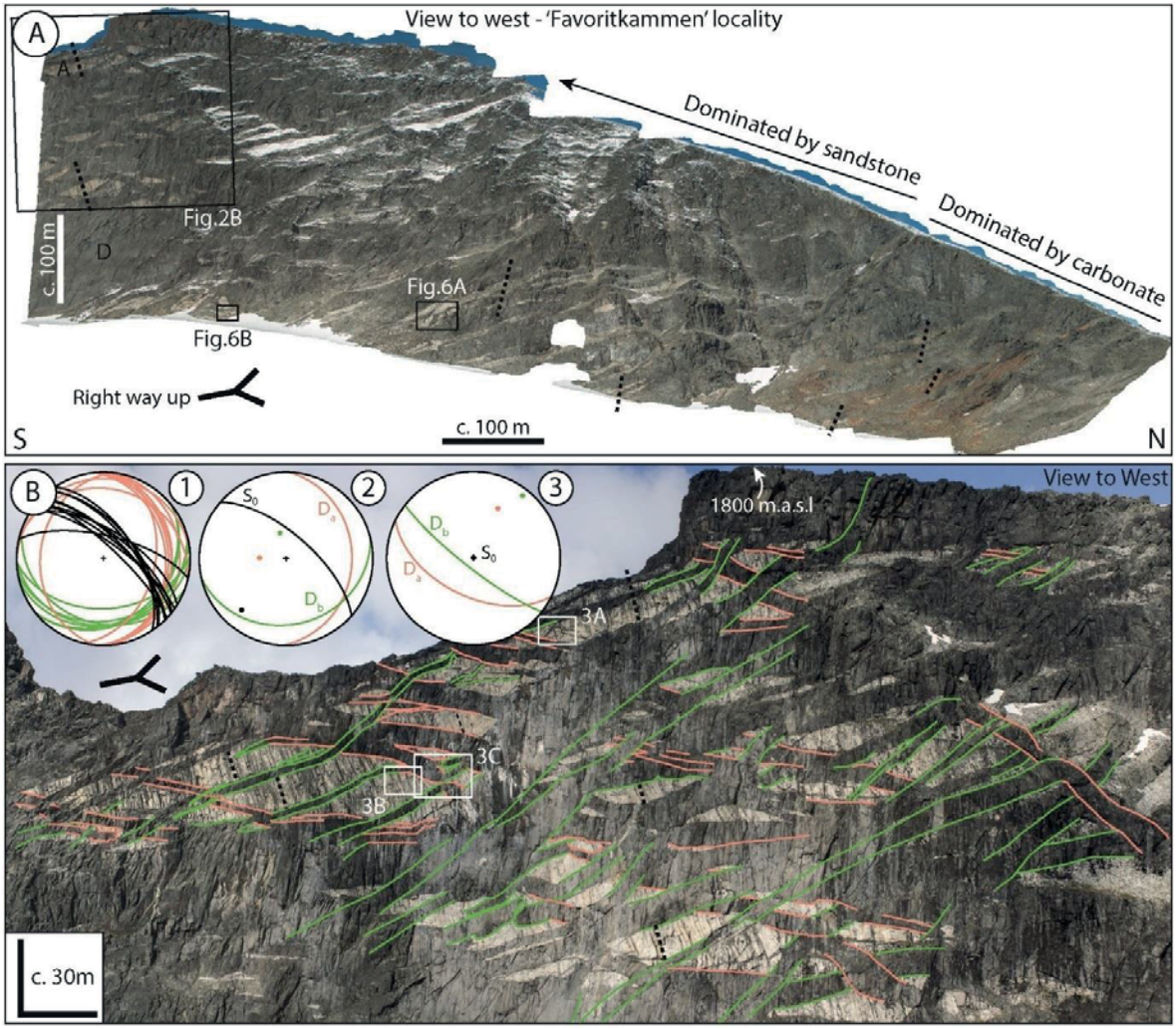

Figure 2-2: Overviewphotographs of the "Favoritkammen" locality, a 200 m tall, vertical cliff wall in Sarek National park, northern Sweden. Sedimentary layering is indicated by black dashed lines. A) Overviewof the entire "Favoritkammen", c. 1.5 km long, continuous outcrop that show both brittle, ductile and brittle-ductile structures related to the dyke emplacement. Some topography causes some distortion of the composite orthomosaic. Black rectangles show location of respective figures. D: Dolerite, A: Arkose B) Detailed composite photograph of a small part of Favoritkammen, where dykes are colour coded according to orientation. Note that the dykes with the different orientations are mutually cross-cutting i.e. D_a (orange) cuts D_b (green) and vice versa. In addition, at several localities the dykes bend and change direction (*e.g.* Fig 2-3A and D). Stereonet #1 shows raw data acquired from 3D outcrop model. Note that the dykes form two groups, one E-dipping and one SSE-dipping. Stereonet #2 shows the present average dyke orientation for the two dyke groups and the bedding, denoted D_a, D_b and S_0, respectively. Stereonet #3 shows average dyke orientations for the two dyke groups when bedding is rotated to horizontal. Where cross-cutting relationships can be discerned they are colour coded according to the stereonets.

Outcrop-scale observations at Favorithelleren show that most dykes exhibit chilled margins (Fig. 2-3B. When both dyke walls are in contact with the sedimentary host rock, dykes display double-sided chilled margins. Stacked dykes and sheeted dykes (Fig. 2-2 and Fig. 2-3), with a more complex chilled margin distribution, have also been observed.

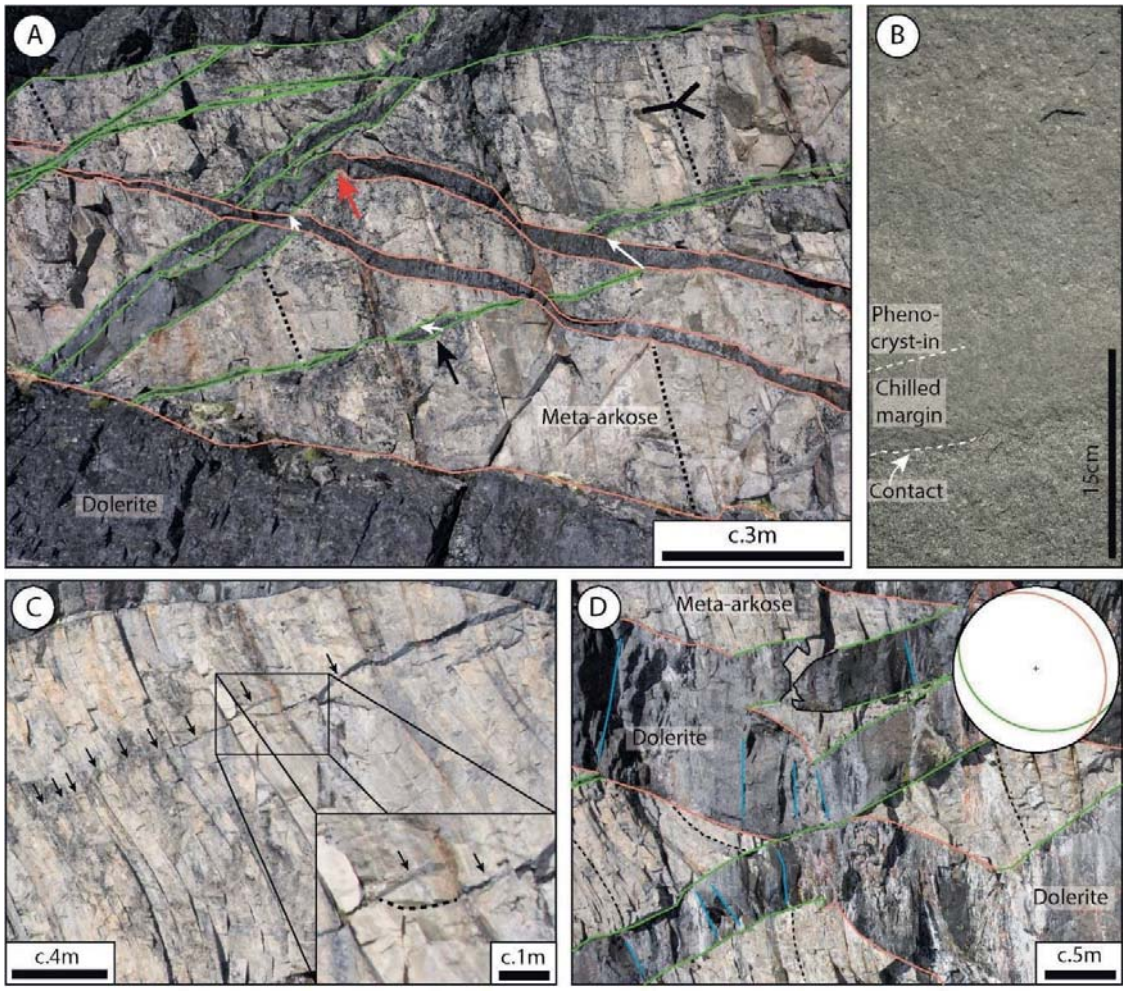

Figure 2-3: Overview figure of areas where the dyke emplacement primarily is controlled by brittle mechanisms. A) Complex cross-cutting relationships between the two orientations of dykes displayed in Figure 2a. The central dyke, highlighted with a red arrow, displays a dramatic bend of c. 80° from D_a to D_b. Black arrow indicate transtensional opening of a dyke. Opening vectors are drawn as white arrows. The opening is constrained to the sandstone layers with minimal opening in the argillaceous domains between the pure sandstone layers. Black dashed lines indicate bedding in meta-arkose. B) Chilled margin at contact between two dykes. White dashed line indicates chilled margin. C) Thin, dyke tip propagated orthogonal to bedding. Somewhat affected by heterogeneities in the host rock as seen in the insert. Here the dyke made an abrupt shift in direction at the end of the sandstone bed, but the fracture propagated straight before bending in (dashed line in zoom) D) Two dykes with sharp and dramatic bends. Orientation are measured directly in 3D model and plotted in stereonet. Joints, orthogonal to the dyke margin can be observed in both dykes marked by blue lines. Black dashed lines indicate bedding in meta-arkose. Note partially broken bridge with angular edges.

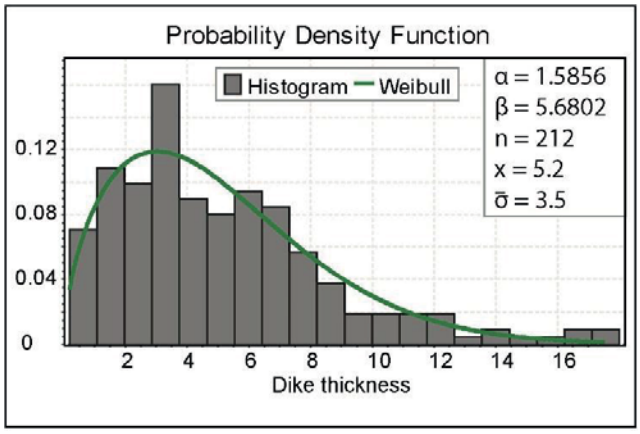

Figure 2-4: The probability density function of the dykes follows a Weibull distribution. α is the shape parameter and β is the scale parameter of the distribution. n denotes the number of measured dykes. $\bar{x}$ and σ denote the mean and standard deviation, respectively. Measurements have been done directly on the 3D model where the exposed dyke segment appears to display an average thickness.

The complete exposure at Favoritkammen and Favorithelleren allowed a reconstruction of the entire outcrop on virtual 3D models, which were used for systematic measurements of 212 dyke thicknesses as well as the orientation of some of the dykes and the strike/dip of the bedding in the host rock (Fig. 2-2 and Fig. 2-3). Note that the dyke thicknesses are measured on the 3D models, such that they are estimates of the true thicknesses, not the apparent thickness on the cliff. The measurement was taken away from tips and where the dyke segments were assumed to display an average thickness. The measured dyke thicknesses range from 0.2 m to 18 m, the mean value being 5.2 m and the median being 4.5 m (Fig. 2-4). Figure 2-4 displays the histogram of the dyke thickness, which exhibits a significantly right-skewed distribution. Following Krumbholz et al. (2014), we fitted our dataset with a Weibull probability function, the fitting parameters being listed in Figure 2-4. Note that all measured dykes presented here intrude arkose and not the underlying carbonate, meaning that the thickness distribution is not affected by distinct host rock lithologies.

The spectacular outcrop at Favoritkammen shows that the dykes are not all parallel. The methodical measurements of the dyke orientations show two dominant trends, one dipping to the ENE (orientation D_a, orange on Figure 2-2 and Figure 2-3) and one dipping to the south (orientation D_b, green on Figure 2-2 and Figure 2-3). These two main orientations are separated by an average acute angle of ca. 30°. D_a is sub-orthogonal to bedding (83° precisely) while D_b shows an acute angle of 53° (Fig. 2-2A). We observe mutual cross-cutting relation between the D_a and D_b dyke populations, meaning that the two populations are contemporaneous (Fig. 2-2 and Fig. 2-3A). In addition, we locally observe sharp bends between long dyke segments of distinct orientations, highlighting that a single dyke can have segments with orientation D_a and other segments with orientation D_b (Fig. 2-2 and Fig. 2-3A and D).

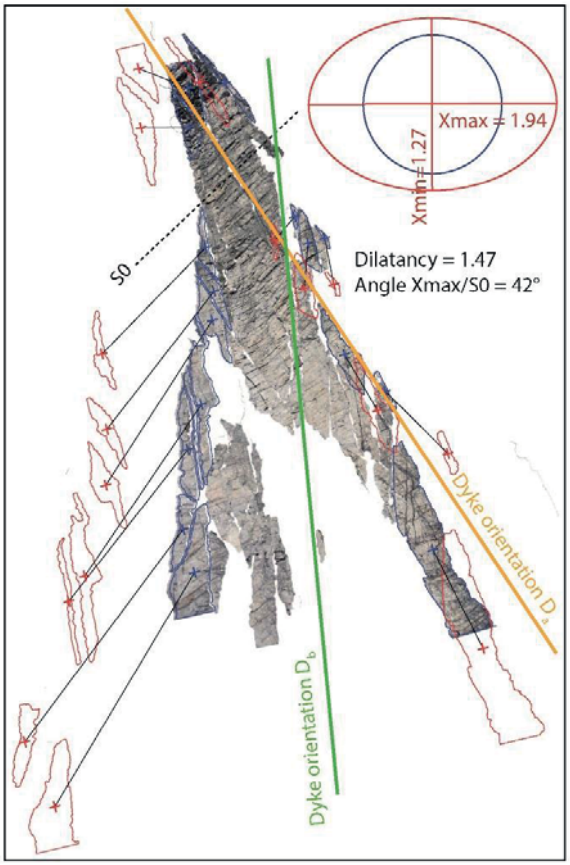

Figure 2-5: Diagram showing estimates of inverse strain ellipse related to dyke emplacement in two dimensions. Pre-intrusion geometry was reconstructed by correlating host-rock markers in the orthorectified image of Fig. 3A. These markers were used to restore back the host-rock polygon centroids to estimate homogeneous strain ellipse. This method does not account for any out of plane motion.

On the cliff of Favoritkammen, the host rock of the dykes is remarkably well exposed and well preserved from the Caledonian deformation and regional metamorphism. The sedimentary layering is visible throughout, forming massive beds that range in thickness from a few tens of centimetres to several metres (Fig. 2-2 and Fig. 2-3). Remarkably, the sedimentary layers exhibit very little deformation, except gentle bending (Fig. 2-3C and D). We correlated the layer sequences on both sides of the dykes by utilizing characteristic markers in the meta-sediments, such that it was possible to reconstruct the kinematics associated with the emplacement of each dyke. Such reconstruction shows that the mode of opening of most dykes is oblique to the dyke walls, implying mixed mode I and mode II fracturing (Fig. 2-3A). Furthermore, this leads to an apparent offset of early dykes cross-cut by later dykes (Fig. 2-3A).

Based on these observations, we performed a 2D strain restoration of the Favoritkammen outcrop, in order to quantify the strain induced by the emplacement of the dyke complex (Fig. 2-5). The restoration method is described in supplementary material, part 2. The calculated strain ellipse deduced from eigenvectors of the 2D strain field tensor indicates that the intrusion of the dykes is responsible for an overall 2D dilatancy of 147%, which is consistent with volume addition due to magma injection (Fig. 2-5). However, this measured dilatancy is not isotropic, as illustrated by the non-equidimensional calculated strain ellipse (Fig. 2-5): the maximum stretching (X_{max}) is 194%, while the minimum stretching (X_{min}) is 127%. We observe that the axis of maximum stretching is sub-perpendicular to the direction of the dyke family D_b, and oblique to the direction of the dyke family D_a. We note as well that the maximum stretching direction is also oblique to the bedding.

3.1.2. Brittle-Ductile structures

At the base of the Favoritkammen cliff (Fig. 2-2B), the shapes and structures of the dykes are different than those observed in the upper parts of the cliff (Fig. 2-2B). Contacts between the dolerite and the host rock are still sharp, but they are not planar, and they often display wavy boundaries and complex morphologies such as pinch-and-swell structures (Fig. 2-6A). The intrusions also exhibit significant thickness variations (Fig. 2-6A). The host rock layers appear much more deformed (Fig. 2-6A). The outcrop of Figure 2-6B provides very precise relationships between successive dykes and the host rock. There, an early large dyke was emplaced (Dolerite #1 in Fig. 2-6B), with a thin wedge-shaped offshoot sheet characteristic of brittle fracturing (highlighted by white arrows in Fig. 2-6B). The thin offshoot is cross-cut by a later thicker dyke (Dolerite #2 in Fig. 2-6B), which has an en-echelon configuration with two branches, separated by a broken bridge with both sharp angular and rounded contacts with the host rock. The host rock layering as well as the thin offshoot from dolerite #1, below the lower branch of dolerite #2 is planar, whereas the thin offshoot dyke above dolerite #2, as well as the host rock layering, are folded. Note that the outcrops of Figure 2-6A and B are at a very similar stratigraphic level as those of Figure 2-3 (see locations on Fig. 2-2), with the same host rock lithology (arkosic sandstone).

Outcrop observations at the Favorithelleren locality shows that the carbonate layers of the host rock exhibit folds near a dyke, with axial plane parallel to the dyke contact (Fig. 2-6C). Centimetre-scale reverse shear zones affect calc-silicate layers of the host rock a few centimetres away from the dyke wall. Both folds and reverse shear zones accommodate ductile and brittle shortening perpendicular to the dyke wall. Fig. 2-6D displays another intrusive contact at Favorithelleren, which displays a very irregular, “blobby” shape showing local melting of the host rock. The sedimentary layering is bended at the intrusion contact. Note that the outcrop of Fig. 2-6D is located in a higher stratigraphic position than the outcrop of Fig. 2-6C.

3.2. Observations from the Corrovarre lens

The topography at Corrovarre is much smoother and lower than at Sarek, such that the studied outcrops are discontinuous because of vegetation and local slope deposits. Detailed outcrop observations highlight the presence of brittle-ductile and ductile structures related to the dykes and their emplacement. Purely brittle structures have not been observed.

3.2.1. Brittle-ductile structures

A cliff in the southern part of the Corrovarre lens displays several mafic dykes emplaced in similar arkosic sandstone as those of the Favoritkammen outcrop described above (Fig. 2-7A). The intrusive

contacts are sharp. Some contacts are relatively straight, whilst others exhibit more irregular curved shapes. A few dyke tips are visible at the outcrop, and they are all blunt and rounded, which is markedly different from the dyke tips observed in Sarek. The sedimentary layers are draped around the dyke tip and cut by a swarm of fractures that radiate from the tip of the dyke (Fig. 2-7B), showing that the host rock behaved in a brittle and ductile manner in response to the imposed stress associated with the propagating dyke tip.

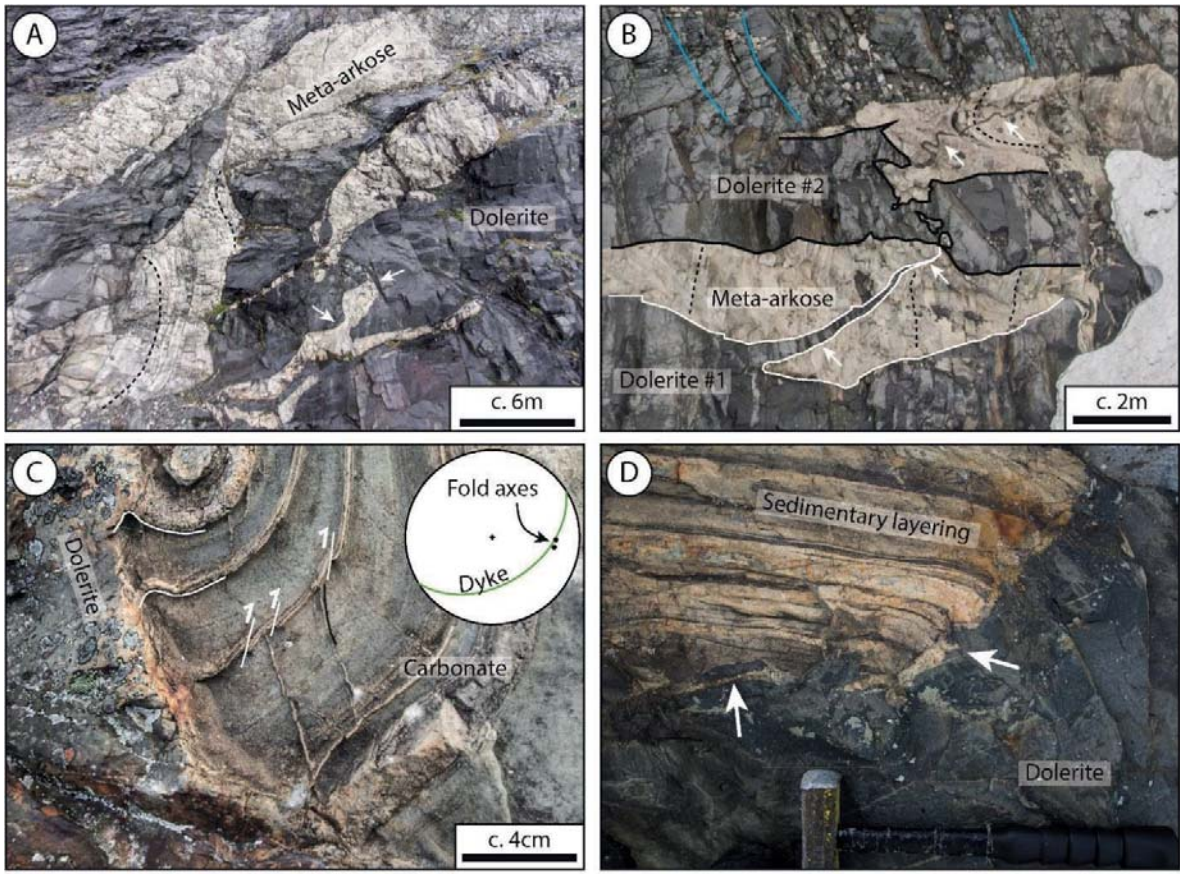

Figure 2-6: Overview plate showing evidence for brittle-ductile deformation related to the emplacement of mafic dykes in Sarek. A) Complex geometric relations between dykes and bridges in the Favoritkammen locality. Dashed black lines indicate bedding in the arkose. White arrow points to rounded bridge in the host rock. B) Shows the temporal evolution of the BDT as dolerite #1 shows a thin, tapered dyke offshoot which intruded meta-arkose, highlighted by white line and arrows. This thin offshoot is subsequently folded as dolerite #2 is emplaced. Black dashed line indicate bedding in the meta-arkose. Blue lines indicate preserved columnar jointing in a later dyke. C) Carbonate with stronger calc-silicate layers show small scale thrust faults duplicating the calc-silicate layers as well as folds with axial planes parallel to dyke contact. D) Leucosomes (white arrows) forming at the contact between a sedimentary rock and a dolerite.

3.2.2. Ductile structures

Throughout Corrovarre, we found numerous outcrops of mafic intrusions exhibiting highly irregular shapes. Figure 2-8A displays a string of dolerite pillows within a migmatitic arkose, where migmatization is regional, but there is no evidence for Caledonian deformation. Extensional Crenulation Cleavage (Fig. 2-8B) structures within the migmatites are cross-cut by the dyke swarm, implying that regional shearing and stretching was accommodated prior to intrusion. We also found other irregular doleritic intrusions emplaced within marbles. Figure 2-8C displays a lens-shape dolerite draped by the foliation in the marble, resembling a tectonic boudin. The dolerite-marble contact is sharp, with local angular apophyses. The dolerite exhibits a chilled margin at the contact, the magmatic texture is preserved, and it does not display any evidence of tectonic deformation. The dolerite also has regular columnar jointing perpendicular to the lens contacts (blue lines in Fig. 2-8C). The right tip of this dolerite body is highly irregular, with complex lobes resembling mingling structures that are in angular contact with the foliation of the host marble (Fig. 2-8D). All these observations evidence that the shape of the dolerite body is primary, *i.e.* of intrusive origin.

4. Interpretation

4.1. Emplacement mechanisms of individual intrusions

Most of the dyke segments in Sarek exhibit regular and straight contacts with the host rock and sharp and thin tips (Fig. 2-3A and D). The thin dykes exhibit a clear wedge shape. In addition, angular broken bridges separate dyke segments, where angular clasts of the host rock are often observed surrounded by crystallised mafic dyke (Fig. 2-3C). From these observations we infer that the emplacement of most of the dykes was primarily controlled by brittle fracturing of the host rock, in good agreement with established models of dyke emplacement (e.g. Rivalta et al., 2015). This conclusion is corroborated by the measured Weibull distribution of the dyke thicknesses, in agreement with the field measurements of Krumbholz et al. (2014), who interpreted such a thickness distribution by brittle failure of the crust with distributed weaknesses of different sizes.

Conversely, other dykes exhibit distinct shapes and associated structures related to other emplacement mechanisms. The intrusions of Figure 2-6A and B at Favoritkammen exhibit irregular and wavy contacts, and their host rock exhibit significant ductile folding. In addition, observed broken bridges along these intrusions exhibit highly irregular, rounded shapes (Fig. 2-6A and B). The detailed observations at Favorithelleren (Fig. 2-6C) highlight coeval ductile folding and brittle faulting of the host rock layers

near a dyke wall. Finally, the dyke of Figure 2-7 at Corrovarre exhibits parallel walls and a blunt tip, and both ductile doming and brittle fracturing of the host rock ahead of the tip. It is important to note that the observed ductile deformation is not related to Caledonian regional tectonics, as (1) the brittle/ductile features of Figure 2-6C and Figure 2-7B are restricted to the vicinity of the intrusions, and (2) the ductile deformation visible in Figure 2-6B only affects the early dykes but not the later ones. We infer from these observations that these intrusions were emplaced by viscoelastic fracturing or viscoelastic fingering (Bertelsen et al., 2018).

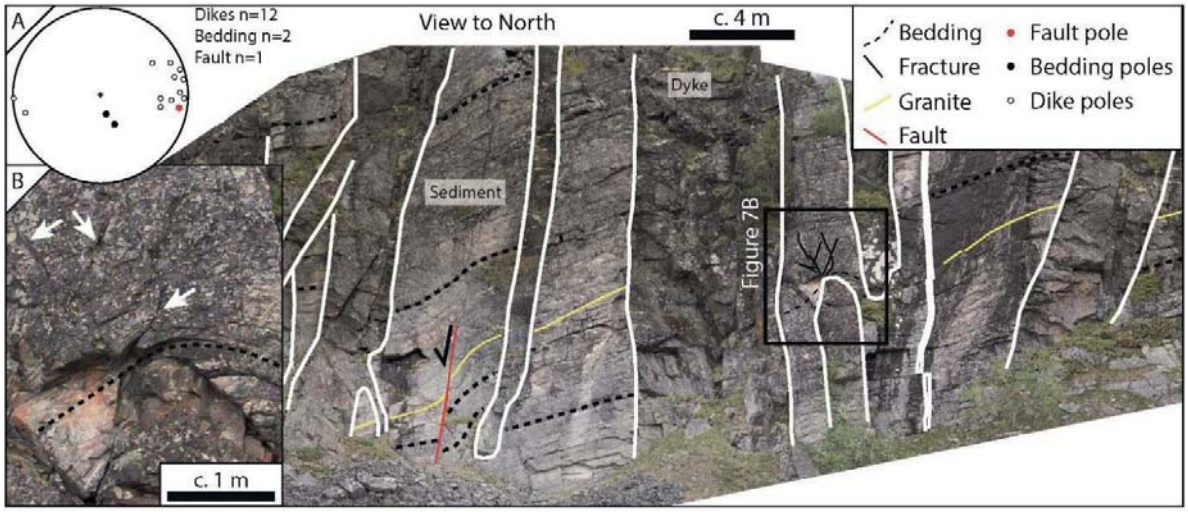

Figure 2-7: Figure showing details from a cliff in southern Corrovarre. A) Overview of the cliff. Stereonet show structural data of the dykes and host rock. White lines outline dykes. Note a granitic vein, cut by mafic dykes. Note also the shape of the dykes, which exhibit equal thickness of the dykes, which abruptly terminate in a blunt tip. B) Detail of a dyke tip shows bedding wrapps the tip and fractures cutting the folded bedding ahead of the tip.

The local brittle/ductile deformation on Figure 2-6C is related to shortening perpendicular to the dyke wall. In addition, the ductile bending, and associated fracturing, ahead of the tip of the dyke on Figure 2-7B suggest that the dyke tip was pushing its host rock ahead. These observations show that the emplacement of the magma in the ductile-brittle crust is a forceful process, such that the overpressured magma deforms its host rock to create its own space, even in a rifting setting. To accommodate the increasing magma volume, the host rock deforms either by brittle failure, ductile flow, or both at the same time.

Numerous intrusions in the Corrovarre area exhibit complex shapes, such as lenses (Fig. 2-8) and pillow-like shape (Fig. 2-8A). In addition, the host rock exhibits significant ductile foliation draping around the intrusions. These structures could casually be interpreted as post-emplacement tectonic boudins,

however, chilled margins observed at the contacts of the igneous bodies show that they are primary emplacement features. The close-up photographs of Figure 2-8A and D show that the intrusion contacts are highly irregular with complex lobes. Note that on Figure 2-8A, the host rock was partially molten when the dolerite was emplaced. Such morphology strongly resembles a Saffman-Taylor instability (Saffman and Taylor, 1958), which develops during the inflow of a viscous fluid into another fluid of higher viscosity.

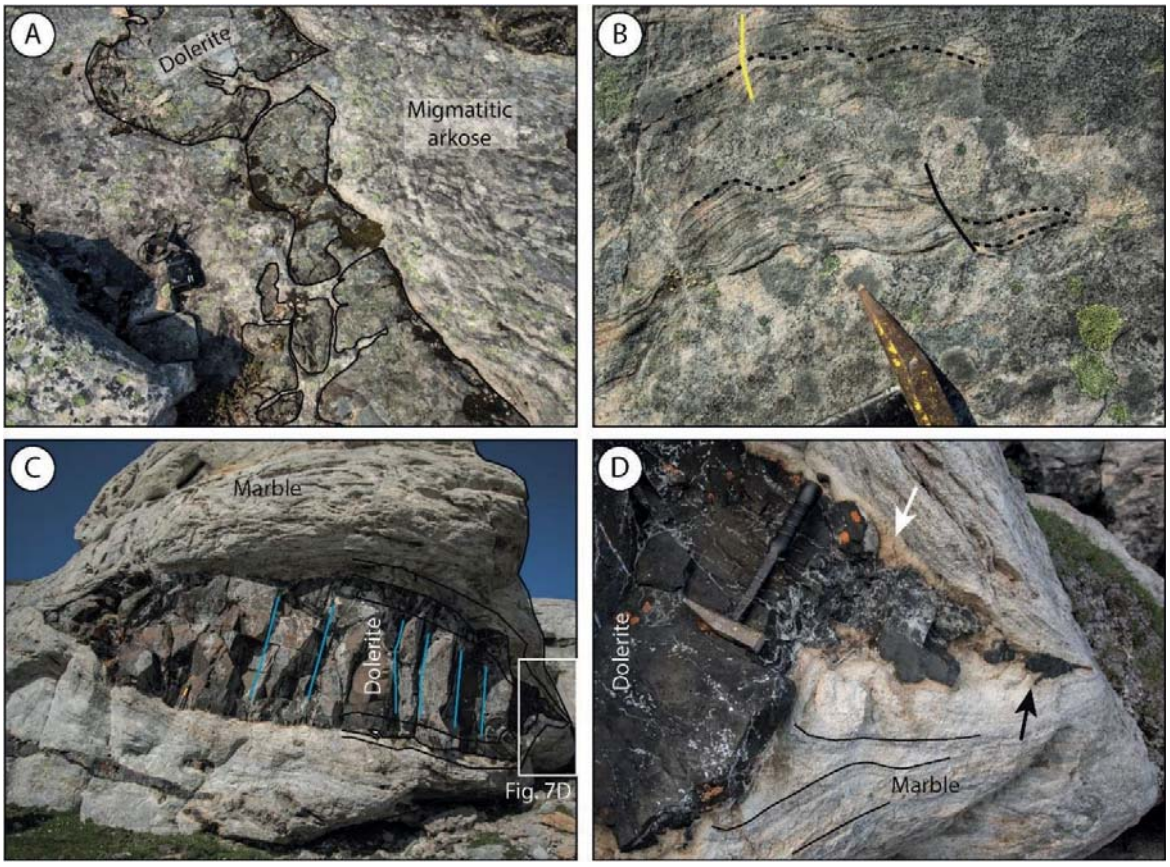

Figure 2-8: Overview plate of the northern segment. A) Mafic magma which intruded a soft migmatitic arkosic sandstone formed tortuous contacts and complex lobes. Digital camera for scale B) ECC fabric in the migmatitic arkose shows layer-parallel stretching and intrusion local leucosomes (yellow line). C) Dolerite magmatic "boudin" in marble. Dolerite show cooling joints (blue lines), c. 10-15 cm thick chilled margin, and a contact metamorphic aureole seen as a discolouration of the marble at the contact between dyke and marble. Note hammer for scale in the central left of the image. White rectangle shows location of picture but note that the photograph in D is taken at a different angle than C. D) Magmatic "boudin" neck. White arrow indicates contact metamorphic aureole as a yellow-ish discolouration. Black arrow shows the complex lobes at the "boudin" neck, resembling Saffman-Taylor structures (Saffman and Taylor, 1958), suggesting a magmatic origin.

These structures are also very similar to intrusions emplaced in low-viscosity salt diapirs (Schofield et al., 2014). These observations show that the emplacement of these intrusions was dominantly controlled by ductile deformation of the host rock, which behaved as a relatively low viscosity fluid.

Our observations at Sarek show that magma emplacement was dominantly accommodated by brittle deformation and mixed ductile/brittle deformation in the meta-arkose sandstone and the slightly deeper carbonates, respectively (compare Figure 2-3 and Figure 2-6C). Locally, Figure 2-6C shows that ductile folding affects carbonate layers, whereas brittle faulting offset calc-silicate layers. Finally, our observations at Corrovarre show that magma emplacement was dominantly accommodated by mixed ductile/brittle to entirely ductile deformation in the meta-arkoses and the carbonate sediments, respectively (compare Figure 2-7 with Figure 2-8). Such systematic differences show how the host rock and their associated rheologies are critical factors controlling magma emplacement and the morphologies of the intrusive bodies.

4.2. Emplacement of the whole dyke swarm

The spectacular Favoritkammen outcrop allows the identification of two groups of dykes with distinct orientations, separated by an acute angle of ca. 30°. Their mutual cross-cutting relationships, and the sudden shift from one direction to another along a single dyke (Fig. 2-2 and Fig. 2-3) show that these two dyke groups were contemporaneous and not the result from two successive intrusive episodes. This implies that the studied dyke swarm is not a simple stack of parallel dykes perpendicular to the least principal stress (here extensional stresses related to rifting), as expected from the Anderson's theory (Anderson, 1905). We therefore infer that many of the studied dykes were not vertical at the time of emplacement but had a dip of 70° or less.

The restoration shown in Figure2- 5 displays that the dyke swarm accommodated for large crustal stretching (94%), as expected in rifts. However, counter-intuitively, the restoration also indicates that the positive dilation associated with the dyke swarm also accommodated for 27% of crustal thickening (Fig. 2-5). This shows that the emplacement of a dyke swarm also can contribute to significant crustal thickening, even in a rift setting. Such a mechanism is only possible if the emplacement of the dyke swarm is a forceful process, as corroborated by local-scale structural observations (see section 4.1). We infer that the magma influx rate was larger than the tectonic stretching rate, such that the tectonic extension was not fast enough to accommodate for the input of magma. This is corroborated by high-precision radiometric (U-Pb zircon) dating of the dykes, which suggests that the whole dyke swarm was emplaced in a period of ~4 Ma or less (Kjøll et al., 2019a), which is significantly shorter than characteristic time scale of continental rifting (e.g. Courtillot et al., 1999; Menzies et al., 2002).

In both the Sarek and Corrovarre areas, we observed brittle as well as ductile deformation accommodating the emplacement of the studied intrusions. Based on this study and the previous estimates of pressure-temperature conditions for the magma emplacement (650-700°C and 3-4 kb from the contact

metamoprhic aureole; Kjøll et al., 2019a), we infer that the studied intrusive complex was initially emplaced near the BDT. In addition, Figure 2-6B shows that an early thin, sharp-tipped dyke, the emplacement of which was likely controlled by brittle deformation, has been folded in ductile fashion to accommodate the emplacement of later dykes. This suggests that earlier dykes were emplaced in a brittle crust, whereas later dykes at the same stratigraphic level were emplaced in a more ductile crust. This strongly suggests that the BDT moved upward with time during the emplacement of the dyke swarm. Such an upward migration of the BDT is likely a response to the heating of the crust resulting from the fast influx of mafic magma (Daniels et al., 2014).

5. Discussion

5.1. Regional constraints

In this study, we integrate field observations from two localities, Sarek and Corrovarre, which are separated by ~300 km in the Seve and Kalak nappe complexes of the Caledonides and has been transported over large distances (e.g. Jakob et al., 2019). The similarities in exposed crustal depth, in intrusion age and host rock lithologies strongly suggest that these areas can be correlated, and that the studied intrusions represent the same magmatic event. The Caledonian deformation rotated the crustal block exposed at Sarek, such that it is challenging to reconstruct the palaeo-horizontal at the time of emplacement of the dykes. Our observations, however, allow us to propose three scenarios to discuss the palaeo-horizontal at the time of dyke emplacement (Fig. 2-9). In scenario 1, the host rock layering S_0 is sub-horizontal and the dykes with orientation D_a are sub-vertical (Fig. 2-9A). In this case, the dykes with orientation D_b and the finite maximal stretching direction calculated in Figure 2-5 are inclined. We would interpret the inclined finite maximal stretching direction, as a result of a syn-intrusion tectonic shear. In scenario 2, the main stretching direction of Figure 2-5 is horizontal, and the dykes with orientation D_b are sub-vertical (Fig. 2-9B). In this case, the host rock layering is already tilted and the dykes with orientation D_a are inclined. Finally, in scenario 3, the two dyke orientations are a conjugate fracture set related to syn-magma emplacement, and the bisector line of the obtuse angle marks the palaeo-horizontal (Fig. 2-9C). In this case, the host rock layering is tilted and both dyke orientations D_a and D_b are inclined. Our observations do not allow us to distinguish between these three scenarios. Nevertheless, in all three cases, at least one dyke orientation is inclined, and we interpret that the opening of these dykes accommodated for the observed crustal thickening. Hence these three scenarios are compatible with crustal thickening induced by the emplacement of the dyke swarm.

5.2. Tectonic and geodynamic implications for magma-rich margins

The geodynamic interpretation of crustal thickening resulting from the emplacement of the dyke swarm strongly relies on the robustness of the kinematic restoration of Figure 2-5. This kinematic restoration was computed from a 2D cliff section, whereas the restored objects are 3D. The dykes are, however, almost perpendicular to the cliff, and so the exposed outcrop is very close to display the section perpendicular to the dyke segments and therefore we infer that the kinematic restoration in the plane of the cliff is reliable. We cannot rule out some out-of-plane displacements, which are not reachable with our method. However, the geodynamic setting at the time of dyke emplacement was inferred to have a limited, if not negligible, trans-tensional component implying that out-of-plane kinematics is likely limited (Svenningsen, 1995).

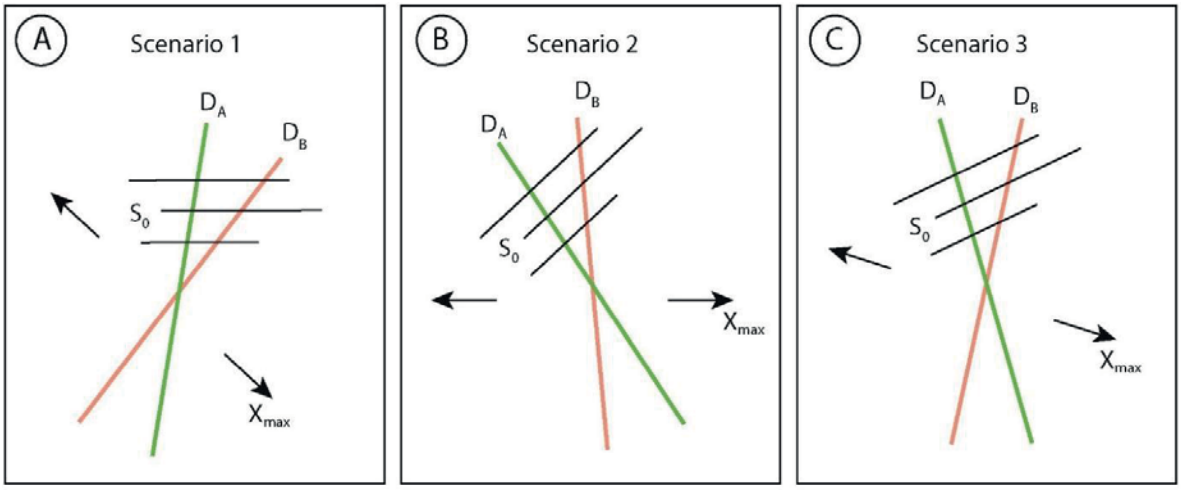

Figure 2-9: Configuration of dykes (D_A and D_B), bedding (S_0) and direction of maximal stretching (X_{max}). Three indistinguishable scenarios are proposed. Note that all three scenarios result in at least one dyke orientation being inclined. A) Bedding was horizontal at time of emplacement. B) The maximum stretching direction was horizontal at the time of emplacement. C) The bisector line of the obtuse angle between the two dyke sets marks the horizontal.

The emplacement of the studied dyke swarm accommodates for almost 100% stretching (β-factor = 1.94; Fig. 2-5), as expected in a rift setting. However, more surprisingly the restoration indicates that the emplacement of the dyke swarm accommodated 27% of crustal thickening. Such thickening was possible because the dyke swarm consisted of at least one dyke population that was not vertical and not oriented perpendicular to the rifting direction (Fig. 2-9). Furthermore, we show that some dyke segments are emplaced as mixed mode I and II, which increases the amount of thickening relative to an inclined dyke opening as a mode I fracture (Figure 2-3A). Their opening vector therefore had a vertical component resulting in crustal thickening. We infer that the tectonic stretching rate did not balance the rate of magma

injected in the crust, hence the magma input dominated over the tectonic extension. This is supported by the high-precision radiometric dating, which shows that the peak magmatic event occurred within a short period of time (~4 Ma; Kjøll et al., 2019a) and is in good agreement with estimated short durations of magmatism related to Large Igneous Provinces (e.g. Svensen et al., 2012; Tegner et al., 2019). The observations presented here suggest that voluminous and fast emplacement of large dyke swarms at depths of 10 to 14 km can contribute to significant crustal thickening, even in rifting settings, if the magma influx rate is larger than the tectonic stretching rate. Our observations differ from common observations in "normal" volcanic rifts and rift zones of hot spot volcanism, where dyke emplacement is often accompanied by normal faulting (e.g. Rubin, 1992). In these settings, magma influx rates are significantly lower than those in LIPs, and we suggest that the magma influx rate did not fully balance the tectonic stretching rate.

The thickening accommodated by the emplacement of the dyke swarm is estimated to ~27% (Fig. 2-5). If this thickening is applied to a normal 15-km thick brittle crust, this can lead to ~4 km of crustal thickening. Unless accommodated for by dyke induced normal faults in the upper crust, such thickening would result in substantial surface uplift (Figure 2-10). In Large Igneous Provinces, uplift is observed and systematically interpreted as dynamic topography resulting from the interactions between a rising viscous plume and the overlying lithosphere (e.g. Pik et al., 2008). Our observations suggest instead that at least parts of this uplift may be caused by the emplacement of a dyke swarm in the crust. Such thickening can explain the presence of thick distal crustal segments (so-called outer highs) along magma-rich margins (e.g. Mjelde et al., 2001). This is supported by recent geophysical observations that an outer high in the mid-Norwegian margin likely hosts a dense dyke swarm (Abdelmalak et al., 2015).

The field observations from Sarek suggest that the BDT may have moved upward during the ~4 Ma-long period of emplacement of the dyke swarm (Fig. 2-3 and Fig. 2-6). We propose that the fast emplacement and cooling of large volumes of mafic magma advected heat into the crust (e.g. Daniels et al., 2014; Kjøll et al., 2019a), which lead to shallowing of the BDT, thinning of the brittle crust and a viscosity decrease of the ductile crust (Figure 2-10). This process has the potential to considerably weaken the crust (Fig. 2-6D). Such an interpretation is in agreement with the model of Bastow and Keir (2011) which suggests that the intrusion of dykes in the East Africa Rift system and the Danakil depression induced weakening of the crust. Such a mechanism can promote stretching and thereby thinning of the ductile crust and lithosphere, as well as brittle failure of the upper crust, leading to enhanced decompression melting and eventually the final break-up (Keir et al., 2013; Bastow et al., 2018). Our interpretation implies that fast, voluminous injection of magma can deeply and quickly modify the rheological structure of the lithosphere, which is proven to be a first-order parameter on tectonic deformation style (e.g. Clerc et al., 2015; Labrousse et al., 2016). However, models of continental rifting usually only account for the tectonic time-scale thermal

evolution of the lithosphere, but not for the thermal impact of a short, voluminous magmatic event (e.g. Keller et al., 2013). Our study shows that implementing magma input is essential for revealing the tectonic evolution of magma-rich rifted margins.

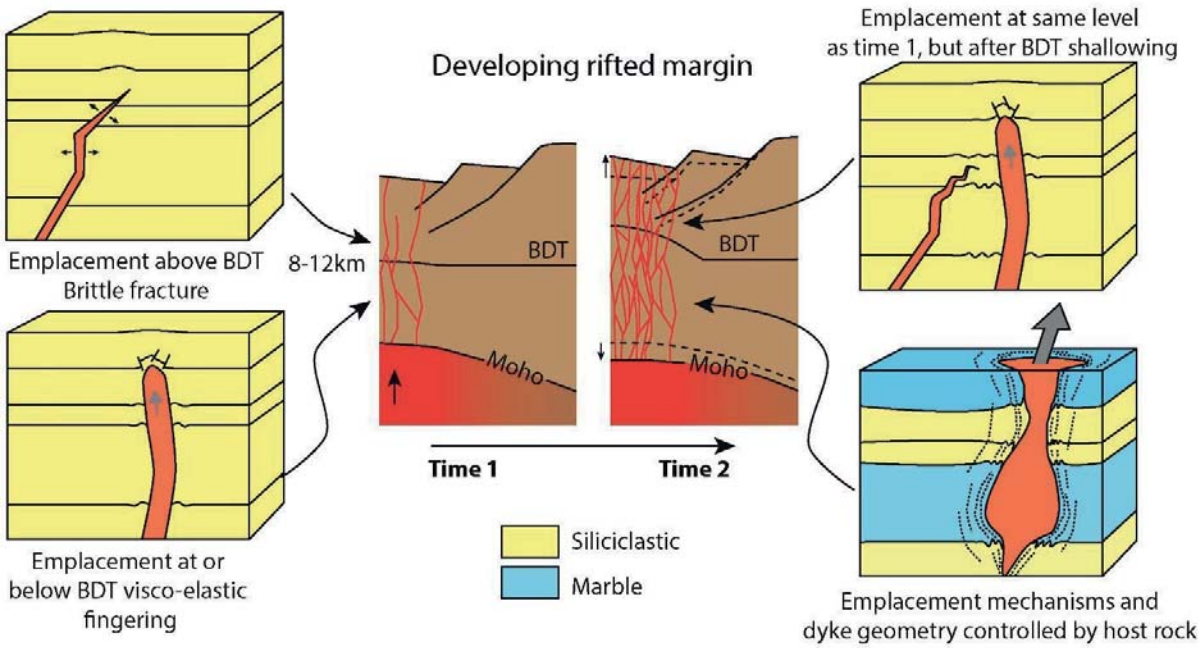

Figure 2-10: Conceptual model showing evolution of the Brittle-Ductile Transition (BDT) during rifting and what type of dyke geometries can be expected at different levels in the rift. At Time 1, the BDT is slightly elevated due to rise of the underlying asthenosphere. Brittle fractures will govern the dyke emplacement above the BDT and visco-elastic fingering govern the emplacement at and below the BDT. This is also the case for Time 2, but the rise of the BDT causes ductile conditions where the dyke emplacement first was controlled by brittle mechanisms. Where the host rock is weak, like where carbonates dominate, the dyke morphology can become complex.

5.3. Mechanical implications

A key observation from the studied outcrop is the two inclined dyke segment orientations. Several factors have been identified to control inclined dyke emplacement. First, the two dyke segment orientations are clearly contemporaneous and therefore conjugate, but with acute angles of about 30° rather than 60°, as would be expected under the Mohr-Coulomb brittle regime. Given that the dyke swarm was emplaced in a tectonic rift setting, the inclined dykes could be interpreted to be controlled by pre-existing conjugate extensional shear fractures. However, this hypothesis implies that we would expect an acute angle of ~60° between the dyke orientations, in disagreement with the observed 30° acute angle. Second, topographic loading can deviate dyke trajectories (Maccaferri et al., 2014). However, the deviation is expected to be

gently gradual over the whole length of the dykes, which is incompatible with the observed abrupt orientation changes of the studied dykes (Figure 2-3). Third, the interference between dykes intruding simultaneously can also lead to deviation of their trajectory (Kühn and Dahm, 2008). This mechanism, however, cannot explain the systematic grouping of the measured dyke orientations in two sets.

Other key observations necessary to explain the inclined conjugate orientations of the studied dykes are that (1) the opening of the dykes exhibit a shearing component (Fig. 2-3 and Fig. 2-4), and (2) the emplacement of the dyke swarm lead to crustal thickening (Fig. 2-5). These observations are in good agreement with the 2D experiments of Abdelmalak et al. (2012) and Bertelsen et al. (2018), which show that the forceful propagation of a dyke tip into a cohesive brittle crust is accommodated by a local conjugate set of small-scale shear structures that can control the subsequent oblique propagation of the tip. In these experiments, where there no tectonic extension, the resulting dykes consisted of steeply-dipping segments of alternating dip-directions. In addition, the emplacement of the dykes in these experiments also triggered surface uplift and thickening of the models. The similarity between these experiments and the observations presented here suggests that the oblique segments of the dykes are markers of a forceful dyke emplacement mechanism, i.e. the emplacing dykes generated their own stress field that overcame both the vertical load of the overburden and the tectonic stresses.

This mechanism is supported by seismological data, which show that the propagation of dykes in active volcanoes triggers significant shear failure of the host, where the fault planes exhibit small acute angle between groups of fault planes (White et al., 2011; Ágústsdóttir et al., 2016). Another mechanism has been proposed by Weinberg and Regenauer-Lieb (2010), who argue that conjugate micro-scale shear damage is triggered by ductile fracturing, which subsequently controls the orientation of the emplacing magma. These elements strongly suggest that hybrid mode I-II failure of the host rock plays a major role in the emplacement of the studied dyke swarm. This is in contradiction to the established theory assuming pure mode I dyke propagation along a tensile fracture perpendicular to σ_3.

Our field observations show distinct modes of emplacement of the intrusions highlighted by contrasting deformation mechanisms of the host rock. Rubin (1993) and Galland et al. (2014) show that magma emplacement is controlled not only by the mechanical behaviour of the host rock, but also by the magma properties and emplacement rate. In our study area, all intrusions are of very similar mafic composition (Tegner et al., 2019) and have a similar magma crystallization temperature (~1150°C) over the 900 km long exposure of the dyke complex (Kjøll et al., 2019a). We infer that the magma properties along the whole dyke complex were relatively homogeneous, which strongly suggests that the observed emplacement mechanisms dominantly resulted from distinct brittle/ductile rheology of the host rock (Figure 2-10).

The time scale of emplacement of mafic sheet intrusions (days to years) is orders of magnitude shorter than the rates of ductile tectonic deformation (10-13 to 10-15 s-1; e.g. Sassier et al., 2009). This has been used to argue that at such short time scales, the ductile crust can rupture in a brittle fashion to accommodate the emplacement of dykes. However, our observations show that ductile deformation also plays a major role in accommodating the emplacement of magma in the study areas. This implies that the emplacement of dykes in the ductile crust is not necessarily controlled by brittle fracturing. This is corroborated by our field observations at Corrovarre and Sarek, which show that significant volumes of magma can be transported along sheets that are not purely brittle structures. The laboratory experiments of Bertelsen et al. (2018) show that sheet-like intrusions can form by viscoelastic fingering. In these experiments, the visco-elastic fingers exhibit straight, parallel walls and blunt tips that push their host rock ahead, exactly like the intrusions shown in Figure 2-7. We infer that dykes in the ductile crust can be emplaced by viscoelastic fingering, so that their systematic interpretation as brittle structures should be done with caution. The observations presented here also imply that ductile deformation of the Earth's crust can take place at rates that are several orders of magnitude faster than tectonic strain rates.

6. Conclusions

This paper presents detailed field observations of a spectacularly exposed dyke swarm emplaced at 10 to 15 km depth at a magma-rich rifted margin related to the breakup of the palaeocontinents Baltica and Laurentia at ~606 M.yr. ago. Such level of a magma-rich rifted margin is rarely exposed at the surface and these observations are relatively unique in this setting. This study, based on field examples from northern Sweden and Norway, allows us to reveal fundamental features related to (1) dyke emplacement mechanisms near the brittle-ductile transition, and (2) to discuss the geodynamic implications of the fast emplacement of a dyke swarm in a magma-rich rifted continental margin.

Our conclusions on dyke emplacement mechanisms are:

- The emplacement of numerous dykes was accommodated by brittle failure, whereas the emplacement of some dykes was accommodated by significant ductile deformation of the host rock.
- The brittle dykes form a conjugate set, separated by an average acute angle of 30° Hybrid mode I-II fracture propagation accommodated the emplacement of this conjugate dyke system, in disagreement with the commonly established models assuming a pure mode I propagation.
- The dyke-tip shapes and the associated brittle-ductile structures suggest that dykes can also be emplaced as 'visco-elastic fingers' near the brittle-ductile transition.

- In ductile host rock, magma conduits may exhibit strongly lobate shapes suggesting that magma transport can be accommodated dominantly by ductile flow of the host rock along finger-like channels.

The geodynamic implications of this study are the following:

- Dykes emplaced contemporaneously may exhibit two main orientations and demonstrate that dykes are not always systematically perpendicular to the rifting direction.
- The studied dyke swarm accommodated for both crustal stretching (94%) and crustal thickening (~27%), indicating that when magma emplacement rate is greater than tectonic stretching rate, the magma pressure can lift the overburden and thicken the crust.
- Even in an active rift setting, the dykes were emplaced in a forceful manner and did not accommodate passively for the tectonic stretching.
- The emplacement of the dyke swarm lead to a shallowing of the brittle-ductile transition.

Our study highlights that the thermal impact of a dyke swarm can considerably weaken the crust and potentially affect the geodynamic evolutions of magma-rich rifted margins and be a major factor controlling ocean-continent break-up.

Acknowledgments

HJK, L.L. and TBA acknowledges support from the Research Council of Norway through its Centres of excellence funding scheme, to CEED, Project Number 223272. The field work and analyses conducted for this paper was funded by NFR Fri-Nat project number: 250327. We also acknowledge National Park authorities in Norway and Sweden for authorizing the use of helicopters to access the remote areas described in this study. The manuscript greatly benefitted from two thorough and constructive reviews by Janine Kavanagh and Craig Magee. Tamsin Mather is thanked for comments and editorial handling of the manuscript.

Chapter 3

A Mantle Plume Origin for the Scandinavian Dyke Complex: A "Piercing Point" for 615 Ma Plate Reconstruction of Baltica?

Christian Tegner, Torgeir B. Andersen, Hans Jørgen Kjøll, Eric Brown, Graham Hagen-Peter, Fernando Corfu, Sverre Planke, Trond Torsvik

This manuscript has been published in *Geochemistry, Geophysics, Geosystems*

Supplementary material is available online at: https://doi.org/10.1029/2018GC007941

Abstract: The origin of Large Igneous Provinces (LIPs) associated with continental breakup and the reconstruction of continents older than ca. 320 million years (pre-Pangea) are contentious research problems. Here we study the petrology of a 615-590 Ma dolerite dyke complex that intruded rift basins of the magma-rich margin of Baltica and now is exposed in the Scandinavian Caledonides. These dykes are part of the Central Iapetus Magmatic Province (CIMP), a LIP emplaced in Baltica and Laurentia during opening of the Caledonian Wilson Cycle. The >1,000 km long dyke complex displays lateral geochemical zonation from enriched to depleted basaltic compositions from south to north. Geochemical modelling of major and trace elements shows these compositions are best explained by melting hot mantle 75–250 °C above ambient mantle. Although the trace element modelling solutions are nonunique, the best explanation involves melting a laterally zoned mantle plume with enriched and depleted peridotite lithologies, similar to present-day Iceland and to the North Atlantic Igneous Province. The origin of CIMP appears to have

involved several mantle plumes. This is best explained if rifting and breakup magmatism coincided with plume generation zones at the margins of a Large Low Shear-wave Velocity Province (LLSVP) at the core mantle boundary. If the LLSVPs are quasi-stationary back in time as suggested in recent geodynamic models, the CIMP provides a guide for reconstructing the paleogeography of Baltica and Laurentia 615 million years ago to the LLSVP now positioned under the Pacific Ocean. Our results provide a stimulus for using LIPs as piercing points for plate reconstructions.

1. Introduction

The opening and closure of ocean basins is known as the plate tectonic Wilson Cycle (Dewey and Burke, 1974) and was first suggested to explain the North-Atlantic Appalachian-Caledonian mountain belt (Wilson, 1966). Here the first known opening took place 615 to 590 million years ago and led to the inception of the Iapetus Ocean and was associated with the Central Iapetus Magmatic Province (CIMP), a large igneous province (LIP) exposed today as giant dyke complexes and other intrusive complexes and volcanics in northeast America and northwest Europe (Ernst and Bell, 2010). The second opening took place ca. 54 million years ago and led to the inception of the North Atlantic Ocean in the Norwegian-Greenland Sea. Again, the opening was associated with the emplacement of a LIP known as the North Atlantic Igneous Province (NAIP) exposed today in the borderlands of the North-Atlantic and the Norwegian-Greenland Seas (Á Horni et al., 2017). Volcanic activity within the NAIP commenced at around 62 Ma, more than 300 million years after initiation of post-Caledonian rifting and basin formation but shortly (ca. 8 Myrs) before continental breakup (Torsvik et al., 2014). Following Morgan (1971), Hill (1991), Campbell (2007), and others, Buiter and Torsvik (2014) therefore argued that rifting was initiated and sustained by tectonic forces, but upwelling of mantle plume material (Iceland plume) into the rifted and thinned lithosphere was the trigger for LIP volcanism, final continental breakup, and the beginning of the new Wilson Cycle. A deep, lower mantle plume origin for present-day Iceland volcanism is supported by seismic tomography (e.g. French and Romanowicz, 2015) and from geochemistry (e.g. Moreira et al., 2001). This has been linked to the plume generation zone (PGZ) at the edge of a Large Low Shear-wave Velocity Province (LLSVP) at the core-mantle boundary (Torsvik et al., 2006). Asserting the origin of the older NAIP and CIMP is more challenging. For NAIP, however, anomalously thick oceanic crust of the Greenland-Iceland-Faroes ridge (Holbrook et al., 2001) and geochemical enrichment (e.g. Fitton et al., 1997; Brown and Lesher, 2014) point to a mantle plume origin. Moreover, Torsvik et al. (2006) showed that NAIP coincided with a mantle PGZ at around 62 Ma. For CIMP, the records of magmatic crustal thickness and potential mantle plume tracks have been obliterated by the Caledonian Wilson Cycle, and inference about its origin therefore must rely on geology and geochemistry of the magmatic complexes

(Seymour and Stephen Kumarapeli, 1995; Andréasson et al., 1998; Puffer, 2002; Hollocher et al., 2007). To further constrain the origin, plate tectonic setting, and deep mantle dynamics of CIMP, we (i) present new geochemical bulk rock data, and Sr isotope data for plagioclase, for the Scandinavian Dyke Complex (also referred to as the "Baltoscandian Dyke Complex"). The dyke swarms are exposed in Caledonian nappes interpreted to have constituted the distal pre-Caledonian continental margin of Baltica (Ottfjället, Sarek, Kebnekaise, Tornetrask, Indre Troms, and Corrovarre); (ii) compiled published compositional data and examined geochemical variations along the more than 1,000-km length of the Scandinavian Dyke Complex; and (iii) modeled mantle melting dynamics. We also compare the geochemistry of CIMP, NAIP, and Iceland and discuss the origin of LIPs associated with the opening phases of the Wilson Cycle. Finally, we produce a new 615 Ma plate reconstruction of Baltica and Laurentia and discuss the potential usage of LIPs as piercing points for plate reconstructions.

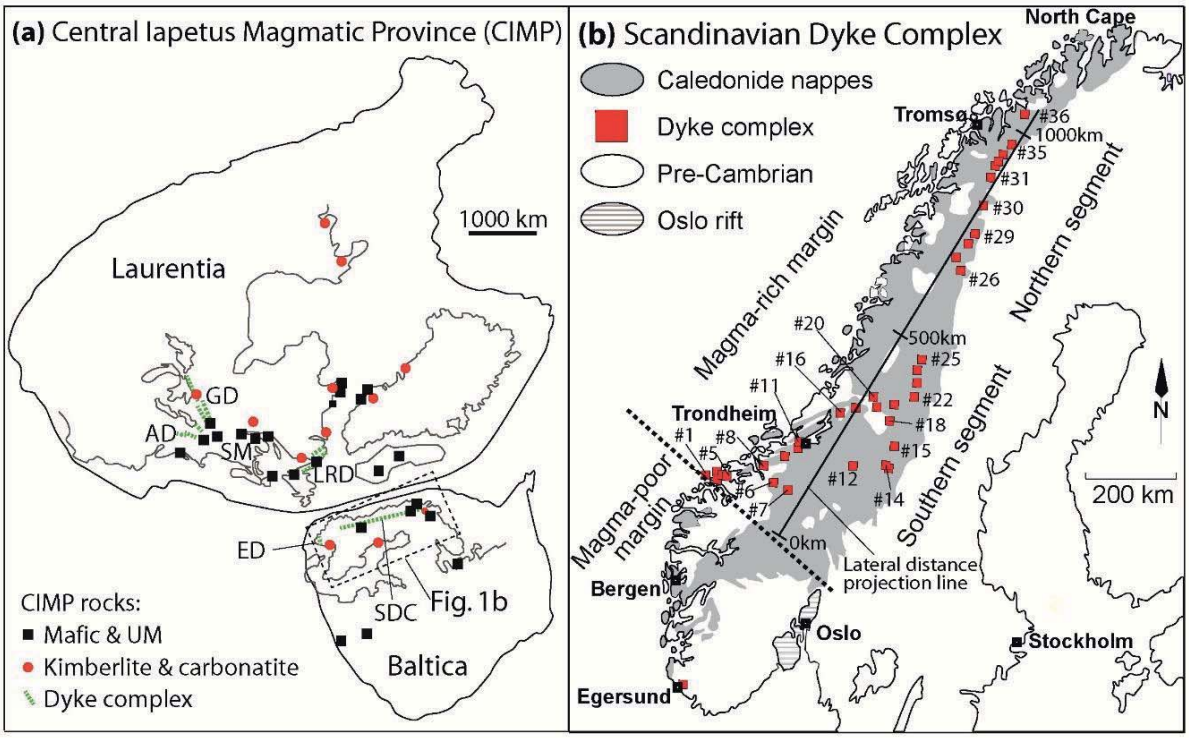

Figure 3-1 (previous page): A) Locations of magmatic rocks of the Central Iapetus Magmatic Province (CIMP) shown in a reconstruction of the Rodinia supercontinent (Li et al., 2008). Slightly modified from Ernst and Bell (2010) and Torsvik et al. (2010). GD = Grenville Dyke Complex; AD = Adirondack Dyke Complex; LRD = Long Range Dyke Complex; ED = Egersund Dyke Complex; SDC = Scandinavian Dyke Complex; SM = Sutton Mountain triple junction. B) Map showing the Caledonian nappes of Scandinavia and the subdivision of the pre-Caledonian rifted margin of Baltica into a more than 1000 km long magma-rich margin in the north and a hyperextended magma-poor margin in the south (present frame of reference) (Andersen et al., 2012; Abdelmalak et al., 2015). The locations of the 36 areas with outcrops of the Scandinavian Dyke Complex discussed in this contribution and for which we have compiled new and published geochemical data are shown and numbered in accordance with Table 3-1. Also shown is a distance line used to estimate the lateral position of the dyke areas from SW to NE. The mid-point of each area is projected orthogonally to the distance line.

2. The CIMP: Chronology and Background

The Central Iapetus Magmatic Province (CIMP) was emplaced over a huge area (>9 million square kilometers; Figure 3-1) and encompasses magmatic rocks exposed today in NW Europe, Greenland, and NE America that originally formed in the borderlands of the Iapetus Ocean (Ernst and Bell, 2010). Carbonatites and kimberlites were also emplaced throughout the CIMP (615–550 Ma) and have been identified across most of the area covered

by CIMP (Ernst and Bell, 2010; Torsvik et al., 2010; Fig. 3-1). Here we focus on the main basaltic events. In Laurentia, the oldest CIMP magmatism (group 1) includes the Long Range (615 ± 2 Ma; Kamo et al., 1989), the >700 km long Grenville (590 ± 2 Ma; Kamo et al., 1995), and the Adirondack dyke swarms (Fig. 3-1). They have compositions similar to continental flood basalts (Puffer, 2002). The Grenville and Adirondack dyke swarms have been interpreted as failed arms of a triple junction centered on the Sutton

mountains (Fig. 3-1) and associated with rifting above a CIMP mantle plume (Burke and Dewey, 1973; Seymour and Stephen Kumarapeli, 1995; Hodych and Cox, 2007). Younger magmatism (group 2; 565–550 Ma) is also dominated by basaltic dyke swarms that are most intense in the Sutton mountains but also includes mafic and granite plutons and lavas (Cawood et al., 2001; Hodych and Cox, 2007; Chew and van Staal, 2014). The Sutton mountain dykes have affinities to ocean island basalt (OIB) and have been interpreted as deep melts of a mantle plume (Puffer, 2002); whereas other young basalt flows and dykes are more akin to mid-ocean ridge basalt (MORB) and have been explained as the result of a second stage of rifting and breakup (Cawood et al., 2001).

In NW Europe, the timing of CIMP magmatism is very similar. The oldest and most extensive magmatism is composed of basaltic dyke swarms at Egersund, Norway (616 ± 3 Ma; Bingen et al., 1998), the Tayvallich lavas and intrusive rocks in the Dalradian of Scotland (601 ± 4 Ma; Dempster et al., 2002; Fettes et al., 2011), and the Scandinavian Dyke Complex exposed in the Caledonian nappes (610–596 Ma;

Baird et al., 2014; Gee et al., 2016; Root and Corfu, 2012; Svenningsen, 2001; Fig. 3-1). The dyke complexes are postdated by ultramafic, mafic, and felsic plutons of the Seiland Igneous Province (580–560 Ma; Roberts et al., 2006), the Volyn LIP in eastern Europe (ca. 570 Ma; Shumlyanskyy et al., 2016), and several carbonatite and kimberlite complexes (590–520 Ma; Ernst and Bell, 2010, Torsvik et al., 2010). The parental magmas to the Seiland Igneous Province include picrites similar to OIB and are often explained as deep, hot mantle plume melts (e.g. Larsen et al., 2018b), whereas the origin of the dominantly tholeiitic basalts of the dyke complexes is debated (Andréasson et al., 1998; Hollocher et al., 2007; Baird et al., 2014; Kirsch and Svenningsen, 2015).

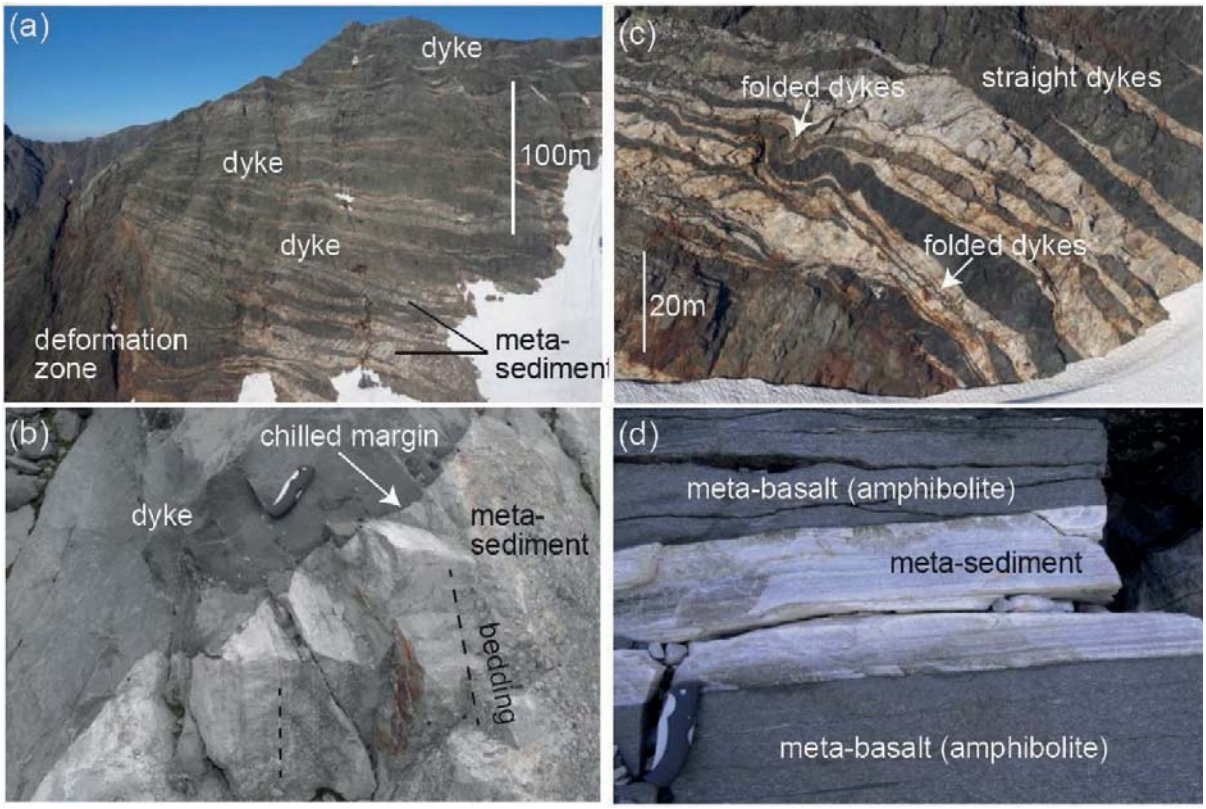

Figure 2 A) Dyke swarm in the Sarek mountains showing undeformed dykes in the central and upper part of the cliff, and a deformation zone the lower, left part of the outcrop. B) chilled margin of dyke cutting metasediments at a high angle to the original sedimentary bedding. C) Gently folded and deformed dykes underlying straight and undeformed dykes. D) Banded gneiss composed of amphibolite (metamorphosed dyke) and metasediment.

3. Scandinavain Dyke Complex

3.1. Nomenclature and Paleogeographic Origin

Dolerite dyke complexes are prominently outcropping in the Seve, Särv, and Corrovarre nappes of the Scandinavia Caledonides (Fig. 3-1). They have been referred to as the Ottfjället dolerites (or Ottfjället dyke swarm) in the central part of Scandinavia (Hollocher et al., 2007) and the Sarek Dyke Swarm (Svenningsen, 2001) and the Kebne Dyke Complex (Baird et al., 2014) in northern Sweden. The same dyke complex continues into northern Norway at Indre Troms and Corrovarre (Zwaan and van Roermund, 1990; Stølen, 1994). Andréasson et al. (1998) described the dykes as a coherent intrusive complex into sedimentary basins at the rifted margin of Baltica exceeding 1,000 km in length, and they used the term Baltoscandian Dyke Swarm. In this contribution we refer to these as the Scandinavian Dyke Complex.

The pre-Caledonian continental margin of Baltica formed during the Ediacaran and was closely associated with ~616-590 Ma breakup magmatism. Breakup and magmatism followed a long period (~200 Ma) of crustal extension and rifting of Rodinia in the Late Proterozoic (Nystuen et al., 2008). The margin constituted a more than 1,000-km-long magma-rich portion in the north which is the focus of this paper and further divided into southern and northern segments (see below) and a hyperextended magma-poor portion further to the south and not dealt with in this paper (present frame of reference, Fig. 3-1; Abdelmalak et al., 2015; Andersen et al., 2012; Jakob et al., 2017). The origin of the dyke swarms either in the magma-rich rifted margin of Baltica or including outboard “exotic” terrains has been discussed. Kirkland et al. (2007) and Corfu et al. (2007) argued for the latter based on the geochronology of Neoproterozoic paragneisses and granitoids (610–980 Ma) that are cut by the dyke complexes and now part of the nappes of Finnmark in northernmost Scandinavia (Fig. 3-1). Such basement ages are not found in situ in northernmost Scandinavia, and the nappes were therefore suggested to have an outboard origin. Other studies suggested that Middle Proterozoic Grenvillian and Sveconorwegian orogens continued north (present frame of reference) to East Greenland and as far as the Caledonides of Svalbard (e.g., Gee et al., 2016). This study and our recent work in the Ottfjället, Sarek, Kebnekaise, Indre Troms, and Corrovarre areas (Fig. 3-1) support the traditional interpretation that these terranes and their dyke swarms are correlative, continuous, and of Baltican origin.

3.2. Field relations

Many places such as Ottfjället, Sarek, Kebnekaise, Torneträsk, and Indre Troms (Fig. 3-1) show spectacular outcrops of pristine magmatic dykes intruded into metasediments with cross-cutting relations and chilled margins (Fig. 3-2 and Movie S1 of the supporting information). These outcrops constitute

large (kilometer-size) low-strain lenses that have avoided Caledonian deformation and grade from essentially undeformed dykes and wall-rock metasedimentary hornfelses to strongly deformed and banded gneisses composed of amphibolite with or without garnet (i.e., metamorphosed mafic intrusions) and metasediments (Fig. 3-2). The metamorphism ranges from well-preserved dykes with contact metamorphic wall-rock hornfelses to foliated amphibolite and locally eclogite facies tectonites (< 750°C and 7–14 kbar) formed during the Caledonian orogeny (Andréasson et al., 1998; Hollocher et al., 2007; Kullerud et al., 1990).

3.3. Is the Scandinavian Dyke Complex a LIP?

The dyke complex extends over 1,000 km in the Caledonian nappes (Fig. 3-1), and the abundance of dykes ranges from 20 to > 90% in well-exposed areas (Fig. 3-2; e.g. Roberts, 1990; Stølen, 1994; Svenningsen, 1994a; Klausen, 2006; Baird et al., 2014). Although the original volume of magmatism is impossible to constrain due to the Caledonian overprint and later erosion, a minimum volume may be estimated from present-day exposures. Klausen (2006) estimated the thickness and width of the Seve and Särv nappes to 4.5–6 and 80 km, respectively. If a minimum abundance of dykes is assumed to be 30% by volume and the minimum volume of the nappes is 1,000 km long, 80 km wide, and 5.3 km thick, the volume of dykes exceeds 0.13 Mkm3. This minimum estimate, alone, fulfills the criteria for the size of a LIP (Bryan and Ernst, 2008). The short duration for the dyke emplacement discussed above also is similar to other LIPs (Bryan and Ernst, 2008).

4. Samples

To examine the lateral geochemical variations of the Scandinavian Dyke Complex, we have collected new dyke samples (n = 80) over four field seasons (2014–2017) along the length of the Scandinavian Caledonides (online supporting information S1). In addition, we compiled all published geochemical data (n = 550; Tab. 3-1; online supporting information S5). To ease the overview, the dyke outcrops were grouped into 36 geographical areas (typically one mountain area each) as shown in Figure 3-1 and listed in Table 3-1. The lateral distance measured from SW was estimated by projection of the mid-position of each mountain area to a SW-NE line (Tab. 3-1 and Fig. 3-1). We will also collectively refer to the mountain areas #26 to #36 as the northern segment and areas #1 to #25 as the southern segment (Fig. 3-1). The nature of the sampled rocks ranges from intrusive dykes with magmatic textures to garnet-bearing amphibolite gneiss and in one case eclogite (location #27, Tab. 3-1). The magmatic textures range from fine-grained basalt over dolerite to microgabbros that sometimes carry plagioclase and rare pyroxene phenocrysts.

5. Methods

The whole rock compositions of 80 samples were measured at Bureau Veritas Commodities Canada Ltd. By X-ray fluorescence (major elements) and by inductively coupled plasma-mass spectrometry (trace elements) and are reported in supporting information S2. Analyses of certified reference materials show that the relative deviation from the reference values are less than 1% for the major elements, less than 4% for P_2O_5, and less than 7% for the trace elements discussed in this paper (supporting information S3). Repeat analyses of samples demonstrate reproducibility within 1.4% for the major elements, within 8% for MnO and P_2O_5, and within 14% for the trace elements discussed in this paper, with one exception at 40% (Th) in one sample with low concentrations (online supporting information S4).

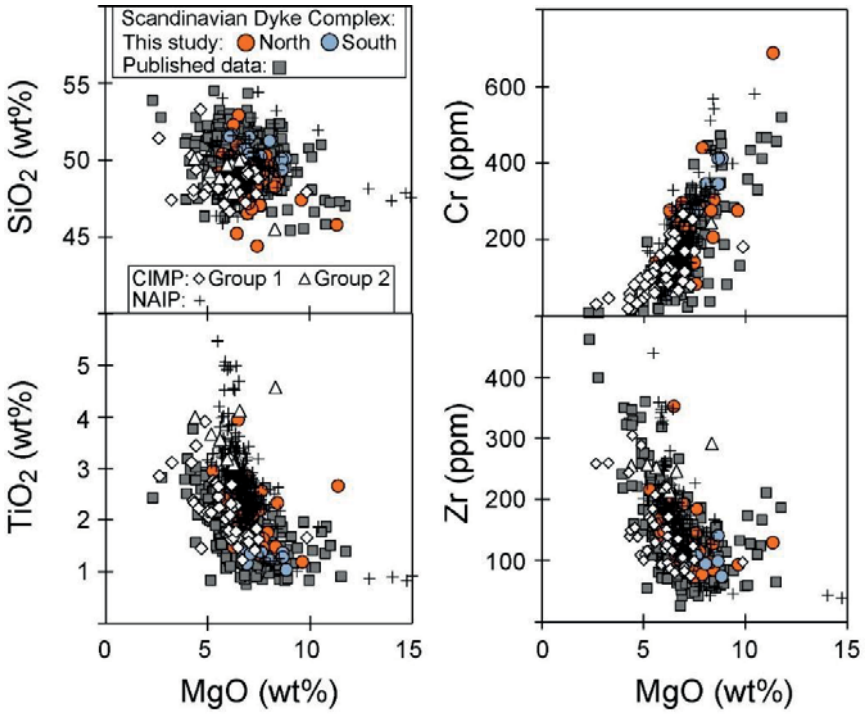

Figure 3-3: Compositions of the Scandinavian Dyke Complex for the compiled dataset screened for crustal contamination (36 samples with Th/Nb > 0.15 are excluded) totalling 606 analyses. New data (n = 80) in Supplementary file 2 and published data (n = 550) in Supplementary file 5. Also shown are: (i) flood basalts of the Northeast Atlantic Igneous Province (NAIP) from the 6 km thick volcanic pile in East Greenland (Tegner et al., 1998); (ii) Group 1 tholeiitic dykes of the Central Atlantic Magmatic Province (CIMP) in northeast America (Seymur and Kumarapeli, 1995; Ernst and Buchan, 2010; Volkert et al., 2015); and (iii) Group 2 CIMP dykes in the Sutton mountains of northeast America referred to as Laurentian OIB (Puffer, 2002).

Table 3-1: Overview of compiled sampled and their locations

Country	Region	Location names	Location#	Position km	N. of analyses Th/Nb <0.15	N. of analyses Th/Nb ≥0.15	Reference
N	Møre og Romsdal	Lepsøy	1	18	18	1	(a)
N	Møre og Romsdal	Brattvåg, Sunnaland	2	22	4		(a)
N	Møre og Romsdal	Tennøy, Lauvøy and Skår	3	31	12	1	(a)
N	Møre og Romsdal	Otrøy, Midøy, Dryna	4	35	10	1	(a)
N	Møre og Romsdal	Dragneset, Øygardsneset	5	40	7		(a)
N	Trøndelag	Driva, Oppdal	6	91	14		(b)
N	Trøndelag	Oppdal	7	94	15		(a)
N	Møre og Romsdal	Åsbøen, Ura, Årnes	8	109	11		(a)
N	Møre og Romsdal	Vasslivatnet	9	149	4		(a)
N	Trøndelag	Orkanger	10	178	30		(a, b)
N	Trøndelag	Ystland, Geita, Kjøra	11	184	15		(a)
S	Jämtland	Sylarna	12	204	46		(b, c)
S	Jämtland	Lunndörs-, Anaris-, Ottfjällene	13	225	9		(d)
S	Jämtland	Lunndörs-, Anaris-, Ottfjällene	14	233	154		(b, e)
S	Jämtland	Alsen	15	280	12		(b)
N	Trøndelag	Leksdalsvann	16	290	14		(f)
N	Trøndelag	Leksdal	17	315	31		(b)
S	Jämtland	Ansætten	18	326	9		(b)
N	Trøndelag	Turtbakktjørna	19	339	6		(b)
N	Trøndelag	Snåsa-Lurudal	20	351	6		(b)
N	Trøndelag	Sørli	21	360	13	1	(g)
S	Jämtland	Strøms-Vattudal	22	396	6		(b)
S	Jämtland	Storsjauten	23	422	7		(b)

S	Jämtland	Borgahällen, Dabbsjön	24	444	10		(b)
S	Lappland	Kultsjøen	25	471	2		(b)
S	Lappland	Piesa	26	675	2		(b)
S	Lappland	Tsäkkok	27	709	11		(d, h)
S	Sarek National Park	Pårte, Sarek National Park	28	734	8	1	(d)
S	Lappland	Äpar Favorithällen, Sarek National Park	29	758	23		(i)
S	Lappland	Äpar, Sarektjåkka, Sarek National Park	29	758	9	4	(d)
S	Lappland	Kebnekaise	30	822	20	4	(d, j, k)
S	Lappland	Nissosnoukki, south of Tornetrask	31	867	2		(d)
S	Lappland	Váivvancohkka, north of Tornetrask	32	887	8	5	(d, l)
N	Troms, Indre	Rohkunborri, Jounnetcohkat, Kistufell	33	902	21	2	(d, m)
N	Troms, Indre	Njumis, Høgskardet	34	925	16	2	(d, m)
S	Lappland	Tjuotjmer	35	956	2	2	(d)
N	Troms	Corrovarre	36	1072	19		(d, n)
	Total				**606**	**24**	

References: (a) = Hollocher et al. (2007); (b) = Solyom et al. (1985); (c) = Pettersson (2003); (d) = this study; (e) = Solyom et al. (1979); (f) = Andreasson et al. (1979); (g) = Beckholmen and Roberts (1990); (h) = Kullerud et al. (1990); (i) = Svenningsen (1994); (j) = Kirsch and Svenningsen (2016); (k) = Baird et al. (2014); (l) = Kathol (1989); (m) = Stølen (1994); (n) = Roberts (1990).
Abbreviations: N = Norway; S = Sweden.

The older published geochemical data were mainly analyzed by X-ray fluorescence (XRF) and instrumental neutron activation, providing major element and some trace element compositions (Andréasson et al., 1979; Solyom et al., 1979; Kathol, 1989; Stølen, 1994; Svenningsen, 1994a; Beckholmen and Roberts, 1999; Pettersson, 2003). The more recent data sets include full trace elements by inductively coupled plasma mass spectrometry (ICP-MS; Baird et al., 2014; Hollocher et al., 2007; Kirsch

and Svenningsen, 2016; Svenningsen, 1994). Supporting information S5 lists the compiled data. The Sr isotope composition of plagioclase phenocrysts were measured in situ in nine samples by laserablation multicollector inductively coupled plasma mass spectrometry at Aarhus Geochemistry and Isotope Research Platform, Aarhus University. Numerous studies have recently published accurate andprecise plagioclase Sr data measured by laser-ablation multicollector inductively coupled plasma mass spectrometry (e.g. Ramos et al., 2004; Kimura et al., 2013; Wilson et al., 2017). Our analyses were done on ~1-cm-thick rock billets, with laser spot placement guided by micro-XRF petrography. The method employed is described in detail in supporting information S6 and summarized here: A 193-nm excimer laser (Resonetics RESOlution) was used to ablate 154-μm-diameter spots, with the ablated material carried in a He + Ar carrier gas to a Nu Plasma II multicollector inductively coupled plasma mass spectrometry.

Data were reduced with corrections for Kr, CaAr, and Rb isobaric interferences on the Sr isotopes. A rock glass bracketing standard (BCR-2) was used to correct the offset between Sr and Rb mass bias factors and Rb-Sr element fractionation (to ensure an accurate age correction). Interference-corrected $^{87}Sr/^{86}Sr$ ratios were normalized to an in-house bytownite standard. Measurements of an additional in-house standard (fused plagioclase) yielded $^{87}Sr/^{86}Sr = 0.704716 \pm 0.000071$ (2 standard deviation; n = 10), in agreement with a reference value of 0.704701 ± 0.000016 (based on solution multicollector inductively coupled plasma mass spectrometry measurements of four different fragments). The $^{87}Sr/^{86}Sr$ for rock standards with $^{87}Rb/^{86}Sr$ up to 0.066 were also reproduced accurately, and only analyses of plagioclase with $^{87}Rb/^{86}Sr < 0.066$ are reported here (4 of 81 analyses had $^{87}Rb/^{86}Sr > 0.066$). The Sr isotope data are reported in supporting information S7.

6. Results

6.1. Major and Trace Element Compositions

The new data set for the Scandinavian Dyke Complex defines a coherent suite of tholeiitic ferrobasalt with 5–11 wt% MgO, 44–53 wt% SiO_2, and 9–16 wt% FeO_{tot} (Fig. 3-3, supporting information S2). The TiO_2 (1.0–4.0 wt%) and Zr (72–350 ppm) increase, and Cr (684–68 ppm) decreases with decreasing MgO (Fig. 3-3), consistent with a control by fractional crystallization. The new data set is similar to the compiled data set also shown in Figure 3-3. In a multielement diagram, the incompatible trace element compositions of dykes from the northern segment form largely flat patterns from the least (right side) to the most (left side) incompatible elements (Fig. 3-4). The compositional variation is relatively high for K, U, Ba, and Rb; this can probably be ascribed to alteration and/or metamorphic effects. Although the rocks range from magmatic (dolerite) to metamorphic (garnet amphibolite; Fig. 3-2), there are no significant differences of the elements used in this contribution between the two rock types in the Sarek area where

they can be compared (online supporting information S8). The trace element patterns of the southern segment, in contrast, generally increase from right to left and also show increased variation for K, U, Ba, and Rb.

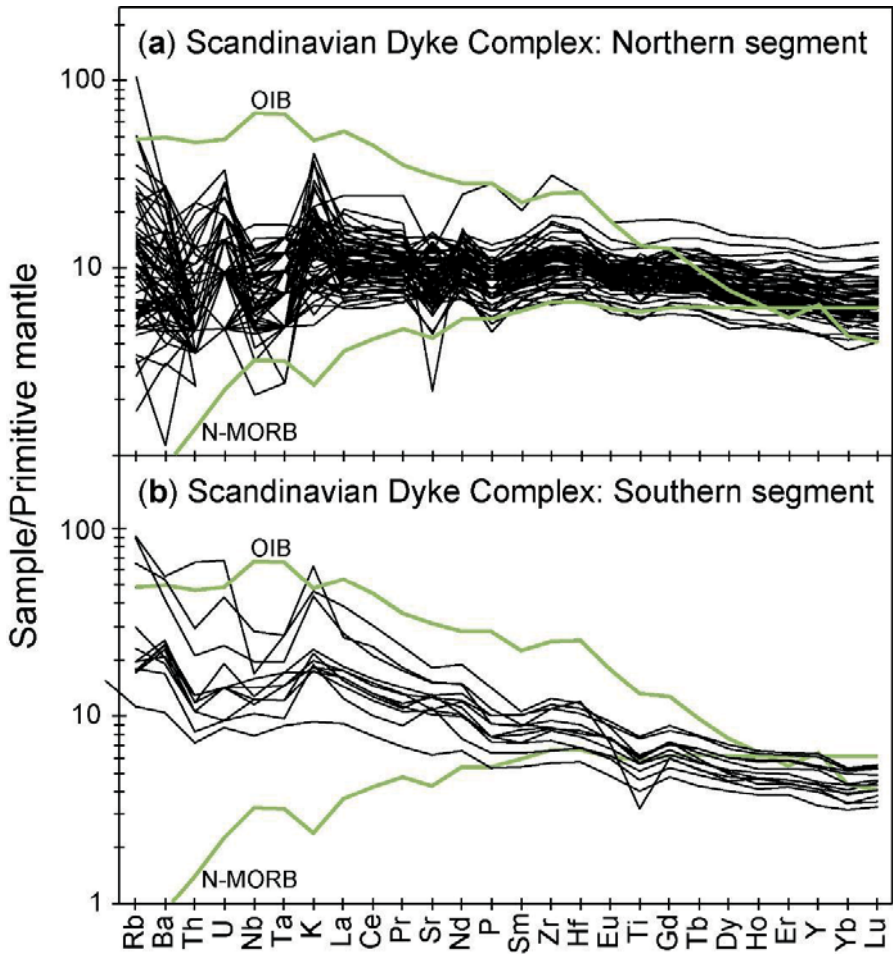

Multi-element diagram showing the new data of this study for samples of the northern segment (**a**) and of the southern segment (**b**) of the Scandinavian Dyke Complex. The elements are arranged with increasing incompatibility in mantle rocks from right to left and are normalized to primitive mantle (Sun and McDonough, 1989). Also shown are normal mid-ocean ridge basalt (N-MORB) and ocean island basalt (OIB) (Sun and McDonough, 1989).

6.2. Sr Isotope Composition

The Sr isotope composition in plagioclase phenocrysts from nine samples are shown in Figure 3-5. The southern (five samples) and northern (four samples) segments of the dyke complex define two fields with lower bounds for initial (615 Ma) $^{87}Sr/^{86}Sri$ of 0.7033 and 0.7025 (one point at 0.7024), respectively.

The scatter within each sample toward higher values is considerable. However, the plagioclase $^{87}Sr/^{86}Sri$ is not correlated with bulk rock Th/Nb.

7. Analyses of Geochemical Variations

7.1. Assessment of Crustal Contamination

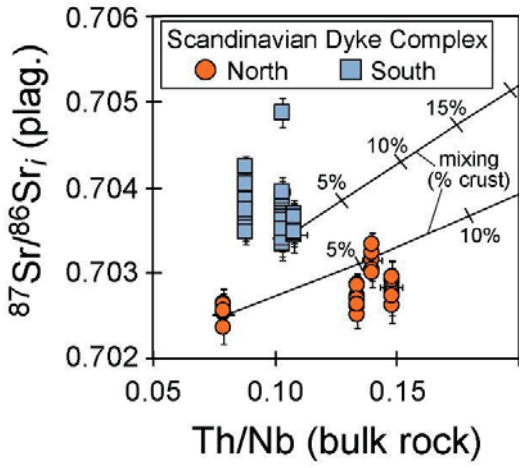

Figure 3-5: Initial (615 Ma) 87Sr/86Sri in plagioclase phenocrysts vs. whole rock Th/Nb in five dykes from the southern segment and four dykes in the northern segment of the Scandinavian Dyke Complex. Each data point represents a single laser ablation analysis. Methods and data are given in Supplementary files 6 and 7.

The present contribution focuses on mantle processes, and we have, therefore, first assessed the potential role of crustal contamination. High Th/Nb is a hallmark of continental crust (0.47; Albarède, 2003). This ratio is little affected by mantle melting and fractional crystallization as Nb and Th are almost equally incompatible. Moreover, Th and Nb are available in most of the sample sets compiled here. We have excluded samples (n = 24) with Th/Nb > 0.15, resulting in a final data set with 606 samples that will be used throughout this contribution (Tab. 3-1). The role of crustal contamination can also be assessed in a diagram of Th/Yb versus Nb/Yb that Pearce (2008) used to distinguish an array of melts formed from mantle sources in the oceans (far away from continental crust; Fig. 3-6a). In this diagram, the average compositions, calculated for the dykes in each area, the screened data set falls within the oceanic mantle melt array or straddles the upper bound. Also shown are the samples with Th/Nb > 0.15 and two mixing curves between MORBs and average continental crust indicating that most of these samples have assimilated 5% to 30% continental crust. This analysis demonstrates that the screened data set reflects melting of mantle sources akin to those of the ocean basins, although minor crustal contamination cannot be ruled out. Below, the Sr isotope data show contamination of some samples in the screened data set (<7% crust, section 7.3). Such crustal contamination will not change the results of the following analysis of mantle dynamics.

7.2. Lateral Geochmical zoning

The ΔNb value of basaltic rocks is a proxy for Nb enrichment of the mantle source. The ΔNb notation was defined for the present-day North Atlantic where Fitton et al. (1997) demonstrated that in a

log-log plot of Nb/Y versus Zr/Y, the basaltic rocks from Iceland defined a compositional field that was relatively enriched in Nb and separated from the compositions of normal MORB away from Iceland. They defined the ΔNb as

$$\Delta Nb = 1.74 + log\frac{Nb}{Y} - 1.92\frac{Zr}{Y} \quad (1)$$

This equation results in positive values for basalts that are geochemically enriched in Nb (*i.e.* similar to Iceland) and negative values for samples that are relatively depleted. Following Fitton et al. (1997), basalts with positive and negative ΔNb can be explained as originating from mantle sources enriched and depleted in Nb, respectively. The ΔNb notation is particularly useful in the present study for two reasons. First, it is based on trace elements that are relatively immobile (Pearce, 2008) and therefore are expected to be changed minimally during metamorphic reactions (supporting information S8). Second, the elements Nb, Zr, and Y are well determined by X-ray fluorescence and instrumental neutron activation methods and are therefore available in the older, published data sets.

Figure 3-7a shows the variation in ΔNb of the dykes along > 1,000 km of Scandinavian nappes and showing average values for our new data set and for the published data set (Tab. 3-1 and Fig. 3-1). In both data sets, the southern segment has positive ΔNb reaching values up to + 0.59 between 300 and 500 km; that is, Nb is enriched 5.9 times relative to ΔNb of zero for a given Zr/Y (Fitton et al., 1997). The northern segment (675–1,075 km) has lower ΔNb and shows a northward decreasing trend with negative values down to −0.23 (Fig. 3-7a).

Other trace elements such as the rare earth elements are only available in the present data set, and in the more recently published data sets (Baird et al., 2014; Hollocher et al., 2007; Kirsch and Svenningsen, 2016; Svenningsen, 1994). Figure 3-7b shows the variation in the slope of a light rare earth element (La) relative to a middle rare earth element (Sm) normalized to chondrite (La/SmN). The available La/SmN data also show pronounced lateral differences in both data sets from elevated values (1.35 to 2.10) in the southern segment to lower values in the northern segment (0.87–1.47). This is consistent with the trace element patterns shown in Figure 3-4. A positive correlation of La/SmN and ΔNb (Fig. 3-8) in both data sets confirms the lateral zoning in incompatible elements from enriched basaltic compositions in the southern segment to more depleted compositions in the northern segment.

7.3. Sr Isotopic Composition of the Mantle Sources

The reported Sr isotope composition in plagioclase phenocrysts shows the plagioclase $^{87}Sr/^{86}Sri$ is not correlated with bulk rock Th/Nb (Fig. 3-5). The generally higher $^{87}Sr/^{86}Sri$ of the southern segment

(lower bound of 0.7033), therefore, cannot be explained by a greater degree of crustal contamination than the basalts of the northern segment (lower bound of 0.7025). The scatter within segment is considerable but can partly be explained by up to 7% crustal contamination, as indicated by mixing lines between low $^{87}Sr/^{86}Sri$ basalt end members and continental crust (Fig. 3-5). We also note that crustal contamination is much more prevalent in the northern segment, for example, with a higher frequency of samples with Th/Nb > 0.15 relative to the southern segment (Tab. 3-1 and online supporting information S2 and S5). Nevertheless, plagioclases from three of the four samples from the north have $^{87}Sr/^{86}Sri$ that are indistinguishable within error and appear to have been minimally contaminated. Fluids related to Caledonian metamorphism and/or weathering may have disturbed the Rb-Sr systematics, although there is no indication of elemental disturbance (supporting information S8). Moreover, such effects are avoided by analyzing Sr isotopes in unaltered plagioclase phenocrysts, instead of bulk rocks. We therefore conclude that crustal contamination (< 7%) is recorded by some plagioclase phenocrysts, but the least radiogenic plagioclase grains show that the magmas and, therefore, the mantle source of the southern segment were enriched ($^{87}Sr/^{86}Sr_i$ ~0.7033) relative to the northern segment ($^{87}Sr/^{86}Sr_i$ ~0.7025). This is corroborated by bulk rock $^{87}Sr/^{86}Sr_i$ of 0.7028 ± 0.0002 reported for the Corrovarre dykes in the north (area 36, Fig. 3-1) and 0.7037 ± 0.0003 for the Ottfjället dykes in the south (location 14, Fig. 3-1; Zwaan and van Roermund, 1990; Bingen and Demaiffe, 1999).

8. Geochemical Modelling of Mantle Source and Temperature

To constrain the possible mantle melting dynamics, mantle potential temperature (T_P), and source lithologies that can explain the observed compositions of the Scandinavian Dyke Complex, we present the results of new mantle melting models. We apply both major and trace element modelling. In particular, we seek explanations for the described geochemical zoning in ΔNb, La/Sm, and $^{87}Sr/^{86}Sr$ from south to north of the magma-rich margin (Fig. 3-5 and 3-7).

8.1. Major element modelling

The major element compositions of primitive basalts can provide constraints on mantle potential temperature, T_P (e.g. Herzberg et al., 2007). Notably, such constraints are independent of those derived from the forward trace element modelling discussed below. Here we apply the thermobarometer of Lee et al. (2009) that, based on an extensive parameterization of experimental data, provides estimates for the temperature and pressure of final melt segregation from olivine + pyroxene-bearing mantle sources. This thermobarometer is based primarily on the inverse relationship between pressure and the melt SiO_2 content (Carmichael, 2004) and the positive correlation of temperature and melt MgO content (Lee and Chin, 2014).

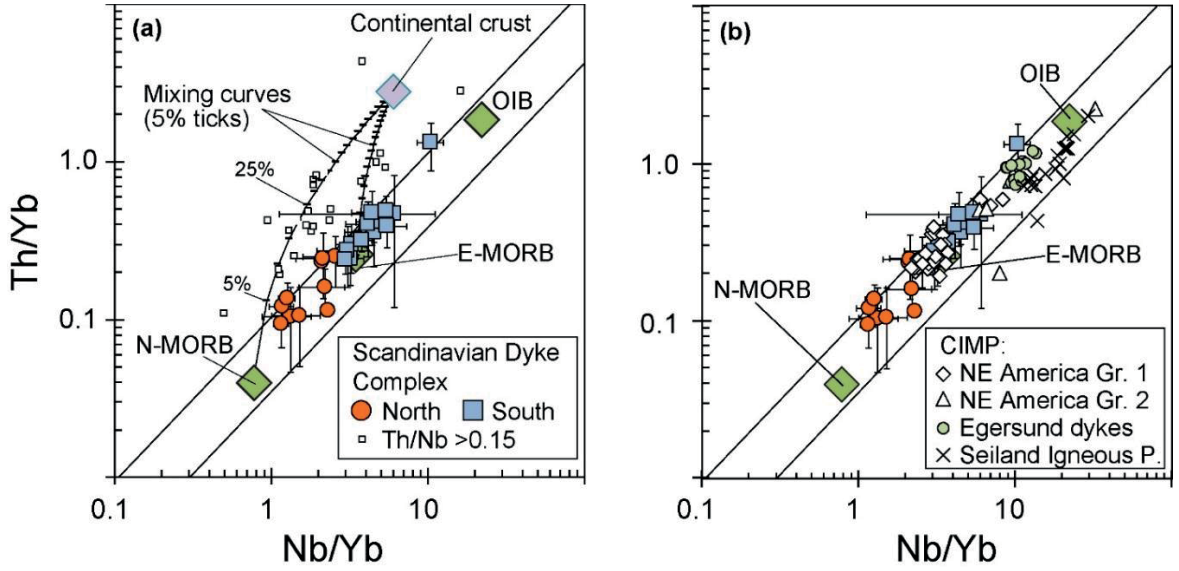

Figure 3-6: a) Th/Yb vs. Nb/Yb showing the average compositions for the 37 locations of the Scandinavian Dyke Complex (Fig. 3-1, Table 3-1); symbols are separated into southern and northern segments of the magma-rich margin. The average compositions are based on 606 samples screened for crustal contamination (Th/Nb < 0.15). The remaining 24 samples judged to be crustally contaminated (Th/Nb ≥ 0.15) are also plotted as individual points. The oceanic mantle array is from Pearce (2008) and the compositions of depleted mid-ocean ridge basalt (N-MORB), enriched mid-ocean ridge basalt (E-MORB), and ocean island basalt (OIB) are from Sun and McDonough (1989). Average continental crust is from Albarède (2003). The two lines with 5% tick marks illustrate mixing of continental crust with N-MORM and E-MORB. b) Th/Yb vs. Nb/Yb for other rocks of the Central Iapetus Magmatic Province (CIMP): NE American tholeiites (Group 1: Ernst and Buchan, 2010; Volkert et al. 2015); NE American Laurentian OIB (Group 2: Puffer, 2002); Egersund dykes (Bingen and Demaiffe, 1999); Seiland Igneous Province alkali-basalt dykes (Reginiussen et al., 1995).

Application of this thermobarometer to evolved basalts requires that the composition of the evolved melt is controlled by olivine fractionation alone. Thus, the program first estimates the primary melt composition by adding olivine until the melt is in equilibrium with a given mantle olivine composition, which we assume has an Mg#, that is, Mg / (Mg + Fe), of 0.91. The equilibrium temperature and pressure of this primary melt composition are subsequently constrained by the parameterization. Conveniently, both calculations are performed using the Excel spreadsheet provided by Lee et al. (2009). Following Lee et al. (2009), T_P is then calculated by (a) back-projecting the equilibrium temperature and pressure to the peridotite solidus along a melting path parameterized using the model of Katz et al. (2003) and (b) then finding T_P as the potential temperature of the mantle adiabat that intersects the solidus at this pressure and temperature.

Similar to Lee et al. (2009), we assume that only samples of the Scandinavian Dyke Complex with more than 8.5 wt% MgO can be assumed to be largely controlled by olivine fractionation. Due to the possible increase in SiO_2 of the magmas as a consequence of crustal assimilation, we only consider samples with Th/Nb < 0.15 as discussed above. Using these criteria, the major element composition of 39 samples was entered into the spreadsheet, and 32 of these yielded temperature and pressure estimates for final melt segregation in the mantle source. These temperatures range from 1,382 to 1,652 °C and the pressures from 1.3 to 5.0 GPa as shown in supporting information S13 The corresponding T_P range from 1,436 to 1,584 °C for the entire data set(online supporting information S13), and the kernel density distribution (n = 32) is shown in Figure 3-9 The samples that gave T_P estimates are distributed over the entire dyke swarm (12 locations in the southern segment and 2 locations in the northern segment; Tab. 3-1 and Fig. 3-1) and exhibit a Gaussian density distribution with a top at 1,498 °C, but with four outliers close to 1,580 °C. We conclude that the major element thermobarometer consistently yields mantle potential temperatures significantly above ambient mantle (ΔT_P of 100–250°C), with a maximum density just below 1,500°C (ΔT_P of 170°C). A significant difference between T_P of the southern and northern segments cannot be discerned.

8.2. Trace Element Modelling

We modeled the compositions of basaltic melts produced by melting dynamically upwelling mantle using the REEBOX PRO application (Brown and Lesher, 2016). This forward model calculates the composition of the incompatible lithophile trace elements in mantle melts using the latest thermodynamic and experimental constraints on melting reactions and mineral-melt partitioning coefficients and can simulate passive and active upwelling scenarios, melting of several potential mantle lithologies and allows for exploring variable T_P. The model assumes incremental batch (*i.e.* near-fractional) melting of the upwelling mantle. This is simulated in a stepwise fashion where the melting column is subdivided into a finite number of decompression steps between the solidus and the base of the non-melting lithosphere. Each small decompression step involves melting and instantaneous removal of the melt and recalculation of the trace element composition of the residual mantle. The instantaneous melt composition is calculated using the equation for nonmodal batch melting, and the composition of the residual mantle is calculated by mass balance (Brown and Lesher, 2016). In the next decompression step, the previous residual mantle parcel moves up to slightly lower pressure (simulating upwelling) and melts again, producing a slightly more depleted residual mantle and so forth. All instantaneous melts generated

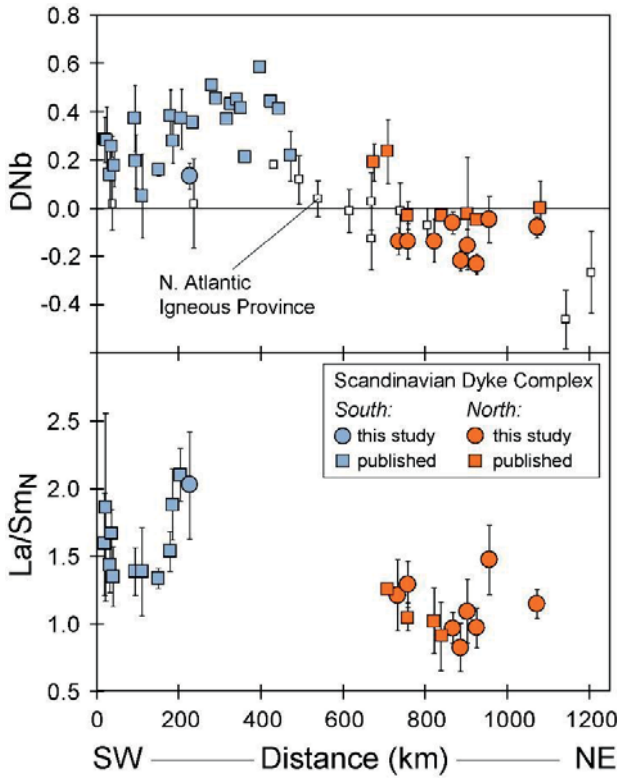

Fig. 3-7. SW to NE compositional variation in the Scandinavian Dyke Complex. (a) Nb (1 s.d. error bars) showing average values for our new dataset and for the published dataset for 36 locations (Fig. 3-1, Table 3-1). Also shown are lateral variations in Nb of the North Atlantic Igneous Province (NAIP) with radial distance from the assumed centre of the proto-Icelandic mantle plume (Fitton et al., 1997). To fit the scale used here, 350 km is subtracted from the published distances to the plume centre; (b) La/SmN for 22 locations where ICPMS data are available (Svenningsen, 1994; Hollocher et al., 2007; Baird et al., 2014; Kirsch and Svenningsen, 2016; this study).

within the melting region are pooled together to form an aggregate melt composition (e.g., equation 12 in Brown and Lesher, 2016). We assume the 2-D shape of the melting region is triangular (apex at the top) where melting takes place in upwelling mantle parcels but stops when convection turns to horizontal; it is therefore often referred to as the corner-flow model initially developed to simulate melting dynamics at mid-ocean spreading ridges (Plank and Langmuir, 1992) but appears applicable also to the formation of LIPs associated with continental rifting (Brown and Lesher, 2016). Melting begins at the solidus intersection with the mantle adiabat (specified by its T_P), and the maximum degree of melting (F_{max}) is obtained at the upper apex of the melting region. In the triangular melting region, the average degree of melting ($F_{average}$) for the pooled melt is given by equation 28 of Brown and Lesher (2016).

A key factor for the composition of melts produced by dynamically upwelling peridotite mantle is the transition from garnet to spinel stability. In REEBOX PRO, garnet is stable on the pyrolite peridotite solidus at pressures above 2.7 GPa, whereas spinel is stable below 3 GPa (Brown and Lesher, 2016), producing a 0.3-GPa transition where both phases exist. Garnet preferentially holds back the heaviest rare earth elements, and this effect is best monitored by the ratio of a middle rare earth element (Dy) to a heavy rare earth element (Yb) normalized to chondrite (Dy/Yb_N). A plot of Dy/Yb_N versus La/Sm_N (Fig. 3-10) therefore relates to the garnet effect on the y-axis and mantle source composition and degree of melting (Tegner et al., 1998b) on the x-axis, assuming a homogeneous peridotite source. The effects of fractional crystallization and crustal contamination are largely negligible in this diagram; both Dy/Yb_N and La/Sm_N are unrelated to a fractionation index such as

MgO (online supporting information S9) and to the Th/Nb proxy for crustal contamination (online supporting information S10).

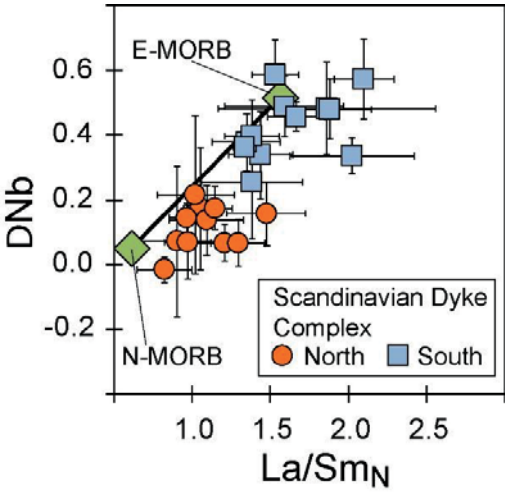

Figure 3-8. Average Nb vs La/SmN (1 s.d. error bars) for the Scandinavian Dyke Complex; symbols separated into southern and northern segments. Shown are 23 locations where ICPMS data are available (Svenningsen, 1994; Hollocher et al., 2007; Baird et al., 2014; Kirsch and Svenningsen, 2016; this study). Also shown are the compositions of N-MORB and E-MORB (Sun and McDonough, 1989)

The data for the southern and northern segments plot in two fields in Figure 3-10 with higher La/Sm_N (1.4–2.1) in the southern segment compared to the northern segment (0.9–1.5); both segments have about the same range in Dy/Yb_N (1.16–1.33). These values are compared to model results for melting-enriched mantle (primitive mantle; McDonough and Sun, 1995) at T_P from ambient mantle (1,330°C) to 1,630°C, that is, ΔT_P of 0 to 300°C (Fig. 3-10a). The result of increasing ΔT_P is increasing Dy/Yb_N values; this is the consequence of the garnet effect due to deeper intersection of the mantle solidus at higher T_P. The compositions of dykes in the southern segment are well explained by model melts of primitive mantle for average degrees of melting from 3% to 10% and ΔT_P ranging from 75 to 150°C; these values are similar to estimates for basalts formed in other LIPs (Tegner et al., 1998b; Herzberg and Gazel, 2009; Brown and Lesher, 2014). The more depleted compositions of the northern segment can only be fit by the model melts of primitive mantle at very high ΔT_P (> 200°C) and more than 12% average melting. In contrast, the dyke compositions of the northern segment are better explained by model melts assuming a depleted mantle source (depleted MORB mantle of Salters and Stracke, 2004; Fig. 3-10b). The data fall between model curves for ΔT_P ranging from 75 to 150°C, suggesting average degrees of melting from 3% to 6%. In theory, it is also possible to explain the more enriched compositions of the southern segment by melting depleted mantle at moderate ΔT_P (50–75°C), although this would require very low average degrees of melting (< 3%; Fig. 3-10b). Such low degrees of melting, however, are not likely to produce the tholeiitic major element compositions of the southern dykes (Fig. 3-3). Likewise, ΔNb and Sr isotopes (Fig. 3-3, 3-5, 3-7) are also best explained by a lateral change from an enriched mantle source in the south and a depleted mantle source in the north.

8.3. Summary of Geochemical Modelling

We conclude that the lateral compositional changes in the rare earth element compositions of the dyke complex (Fig. 3-4, 3-7, 3- 8 and 10) are best explained by melting mantle that was anomalously hot

relative to ambient mantle (ΔT_P of 75–150°C). Elevated T_P is independently confirmed by the major element modelling yielding ΔT_P of 100–250°C with no discernable difference between the southern and northern segments (Fig. 3-9). The rare earth element modelling shows the melting domain is best explained if it was zoned with enriched lithologies and compositions (primitive mantle) under the southern segment and depleted lithologies and compositions (depleted MORB mantle) under the northern segment. This interpretation is corroborated by the Sr isotope compositions (Fig. 3-5).

Mantle warming due to long-term thermal insulation by continental lithosphere can produce ΔT_P up to 100°C (Coltice et al., 2007; Herzberg and Gazel, 2009) and therefore does not provide a fulfilling explanation for the modeled temperatures. Moreover, the distinct compositional zoning in trace elements and Sr isotopes (Fig. 3-4, 3-5, 3-7 and 3-8) and the basalt compositions similar to the oceanic mantle array (Fig. 3-6) favor an explanation by upwelling of a zoned mantle plume akin to Iceland today and to the NAIP ca. 56 Myr ago (Fitton et al., 1997). Analogue and computational modelling supports the view that mantle plumes may be laterally zoned on a length scale of 1,000 km with a compositionally enriched central portion and a more depleted outer margin (Jones et al., 2016).

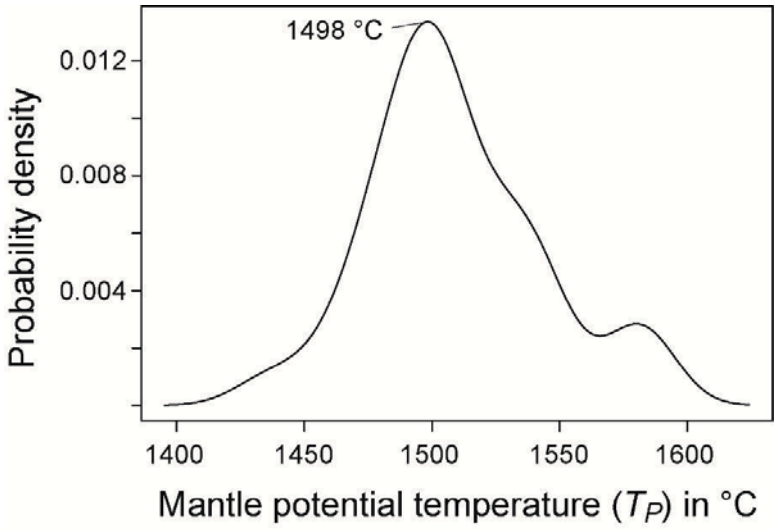

Figure 3-9. Gaussian kernel density distribution of mantle potential temperature (TP) calculated for samples of the Scandinavian Dyke Complex (n=32). The final equilibrium temperature and pressure of the magmas in the mantle were calculated using the major element thermobarometer of Lee et al. (2009) and converted to TP using the method described in the text. The TP of the entire dataset, covering 14 locations in both the southern and northern segments, exhibit a gaussian density distribution with a top at 1498 °C, but with four outliers close to 1580 °C The calculations were restricted to largely uncontaminated (Th/Nb < 0.15) and primitive samples that contained more than 8.5 wt% MgO. The data are listed in Supplementary file 13. The kernel density estimations follow the method discussed in Rudge (2008) and were calculated using the Free Statistics Software of Wessa (2015).

9. A 615 Ma Plate Reconstruction of Baltica and Laurentia

Two LLSVPs (Garnero et al., 2007) today exist at the core-mantle boundary beneath Africa (dubbed TUZO) and the Pacific (JASON). Using hybrid mantle frames (combination of moving hot spot and true polar wander (TPW)-corrected paleomagnetic frames), it has been argued that the LLSVPs have been stable for at least 300 Myr with deep plumes sourcing LIPs (Fig. 3-11a) and kimberlites mostly from their margins (Torsvik et al., 2014; Torsvik et al., 2016). That remarkable correlation between surface volcanism and deep mantle features potentially provides a novel and quantitative way to derive "absolute" plate motions in a mantle reference frame before Pangea. This approach assumes that TUZO and JASON have remained nearly stationary before Pangea time and that the origin of mantle plumes can be tied to their edges. These views are, however, far from being universally accepted and have generated debate in the geophysical literature. We will therefore briefly review some of the pros and cons for this assumption here.

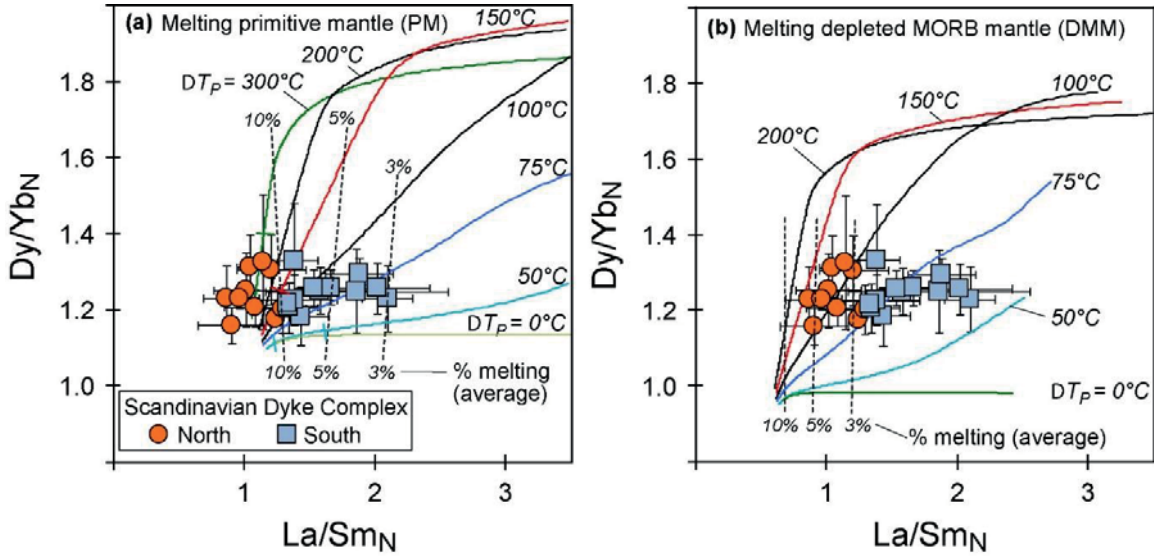

Figure 3-10. Dy/YbN vs. La/SmN of the Scandinavian Dyke Complex; symbols separated into southern and northern segments. (a) Forward model melts produced by melting primitive mantle (PM, McDonough and Sun, 1995) at mantle potential temperatures from 1330°C to 1630°C, i.e. up to 300°C above ambient mantle. (b) Forward model melts produced by melting depleted MORB mantle (DMM, Salters and Stracke, 2004) at the same mantle potential temperatures as in (a). Modelling based on REEBOX PRO (Brown and Lesher, 2016), see text.

9.1. Stability and PGZs of LLSVPs

That plumes mainly form at the margins of the LLSVPs and that they are approximately stable through time have wide implications and have promoted a number of numerical modelling experiments to reproduce and explain (or reject) these features. Among the most avid opponents are those who deny the very existence of mantle plumes, mantle modelers disagreeing with the interpretation of LLSVPs as mantle

structures with distinct chemical properties (e.g. Davies et al., 2015), and those suggesting that LLSVPs are highly mobile and simply shaped and destroyed by sinking slabs (e.g. Flament et al., 2017).

Numerical models of mantle convection have been used to investigate the stability of the LLSVPs, and they have shown that it is possible to maintain stability for hundreds of million years (Steinberger and Torsvik, 2012; Bower et al., 2013; Bull et al., 2014) and their continued existence for billions of years (Mulyukova et al., 2015). But incorporating paleogeographic constraints into mantle convection models (as, e.g., attempted by Flament et al., 2017) requires greatly improved plate tectonic models and numerical codes that incorporate the bridgmanite to post-bridgmanite transition in the lowermost mantle. This important phase transition causes an abrupt viscosity drop of three to four orders of magnitude (Ammann et al., 2010; Nakada and Karato, 2012). This weakens slab material, eases and disperses the lateral flow above the core-mantle boundary, and effectively stabilizes and strengthens the LLSVPs against lateral pushing forces (Li et al., 2014, 2015; Heyn et al., 2018).

Testing the stability of the LLSVPs in a robust manner is in fact very challenging. Their stability is observed from LIPs from the Indo-Atlantic realm (Fig. 3-11a) where it is possible to build an absolute mantle reference frame back to 320 Ma (Pangea assembly). The Indo-Atlantic realm includes the bulk of the Earth's continents and oceans that are generally characterized by passive margins (e.g., the Atlantic). Conversely, numerical models for subduction and mantle convection to test their stability are mostly derived from plate models for the Pacific-Panthalassic from where we have no means to develop an absolute plate motion reference frame before the Cretaceous; the Panthalassic (the Earth's subduction “factory”) is entirely synthesized before 150 Ma and comprised almost 50% of the Earth's surface.

Earth is a degree-2 planet with two antipodal thermochemical LLSVP piles, TUZO and JASON; modern-type plate tectonics has been operational since at least the Neoproterozoic - and why should Planet Earth be fundamentally different before and after Pangea? There is in fact no evidence for a radical change in the mantle structure associated with Pangea assembly and dispersal - only projected models: Zhong et al. (2007) argued from the outcome of a numerical model that Pangea formed above a major down-welling, and that following continental assembly, a sub-Pangea upwelling later developed as mantle return flow in response to circum-Pangea subduction. In such a model, TUZO should not have existed before Pangea, because convection would have been dominated by a degree-1 mode with only one upwelling above JASON. But during Pangea assembly, the mantle beneath it was littered with cold Rheic slabs, and it is difficult to foresee how that could have turned into an upwelling and the birth of TUZO within a few tens of million years. But perhaps more importantly, Pangea was not a static supercontinent overlying the same part of the mantle for long but drifted systematically northward over the mantle during its existence.

9.2. Paleogeographic Reconstruction of Baltica and Laurentia

Assuming that the TUZO and JASON LLSVPs have remained nearly stationary before Pangea time and that the origin of mantle plumes can be tied to their edges, it is possible to establish a geologically reasonable palaeogeographic model for the entire Phanerozoic (Torsvik et al., 2014). In this model the continents are positioned using the latitude from paleomagnetic data, whereas the longitude is defined in such a way that LIPs and kimberlites are positioned above the edges (PGZs) of TUZO and JASON at eruption times. We refer to this procedure as the PGZ reconstruction method, and here we use this method, which also include an iterative TPW correction, to calibrate longitude.

The supercontinent Rodinia, which probably existed in the Neoproterozoic from ca. 1,000 to 600 Ma, has been recognized by most paleogeographers (e.g. Li et al., 2008), but the details of its continental makeup are debated (Meert, 2014). Dispersals of both Pangea and Rodinia appear to have been contemporaneous with massive LIP volcanism, with Pangea located above TUZO from its assembly to dispersal, and Rodinia probably located above the antipodal JASON during the Neoproterozoic (e.g. Li and Zhong, 2009). Most paleogeographers show Laurentia located next to Baltica and Amazonia in Rodinia and the Late Precambrian breakup of Rodinia led to the opening of the Iapetus Ocean. With reliable paleomagnetic data from the 615 Ma Egersund dykes (Walderhaug et al., 2007) in southwest Norway, we can reconstruct those continents so that LIP-related volcanism and kimberlites plot nearly vertically above the eastern edge of JASON. In this reconstruction—using the PGZ reconstruction method—we moved the continents iteratively in longitude (based on the Egersund paleomagnetic data) and with TPW refinements until we achieved a reasonable fit between (i) an estimated LIP center to explain the formation of the Scandinavian Dyke Complex at a hyperextended margin offshore Baltica (Andersen et al., 2012), (ii) the 616 Ma Egersund dykes (Baltica), (iii) the 615 Ma Long Range dykes (Laurentia), and (iv) contemporaneous kimberlites in Laurentia (613 Ma) and Baltica (610 Ma; Fig. 3-1a). Laurentia, Amazonia, and Baltica are reconstructed to the central-eastern part of JASON, but Fig. 3-11b is a paleomagnetic reconstruction which places Baltica at latitudes between 45° and 75°S, and the JASON PGZ has been counterrotated 70° to account for TPW (see method in Torsvik et al., 2014).

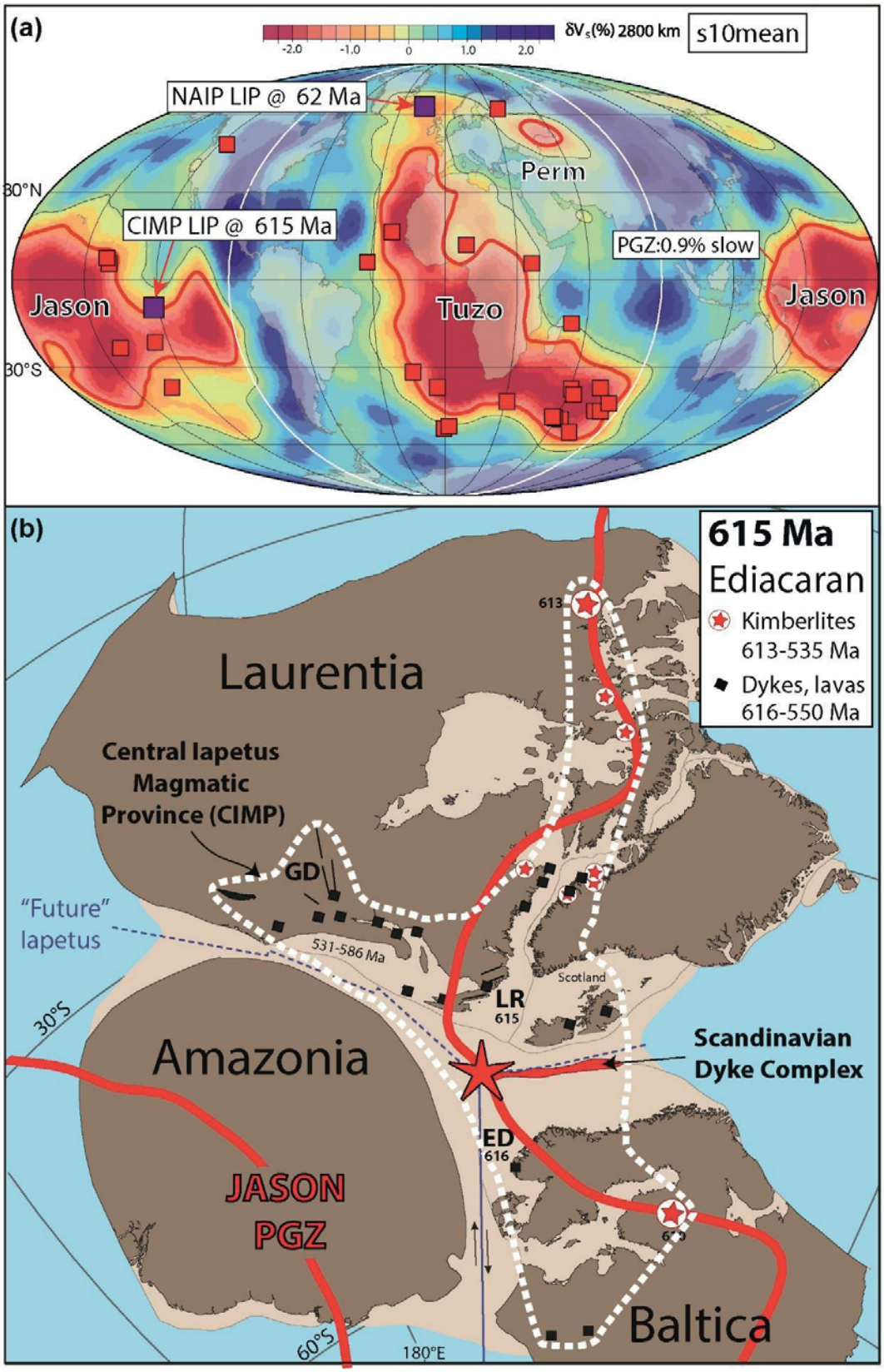
(a)
δVs(%) 2800 km
-2.0
-1.0
0
1.0
2.0
s10mean
NAIP LIP @ 62 Ma
Perm
30°N
CIMP LIP @ 615 Ma
PGZ:0.9% slow
Jason
Tuzo
Jason
30°S
(b)
615 Ma
Ediacaran
Kimberlites
613-535 Ma
Dykes, lavas
616-550 Ma
613
Laurentia
Central Iapetus
Magmatic
Province (CIMP)
GD
"Future"
Iapetus
531-586 Ma
Scotland
LR
615
30°S
Amazonia
Scandinavian
Dyke Complex
ED
616
JASON
PGZ
Baltica
60°S
180°E

Figure 3-11 (opposite page): (a) Reconstructed LIPs (15-297 Ma) draped on the s10mean tomography model where the Plume Generation Zone (PGZ) correspond to the 0.9% slow contour (updated from Doubrovine et al., 2016). Most LIPs overly the PGZs but the Columbia River Basalt is anomalous because it is above a region of faster-than-average anomalies. (b) Paleomagnetic reconstruction of East Rodinia at around 615 Ma using the PGZ reconstruction method calibrated in longitude by LIP related volcanism and kimberlites. The white dotted line indicates the extent of the Central Iapetus Magmatic Province (CIMP, black squares and lines are dykes as in Fig. 3-1a). Magmatism linked to the CIMP is well preserved in the Caledonian Särv, Seve and Corrovarre Nappes (central Scandinavia), which are characterized by the spectacular Scandinavian Dyke Complex. The dyke complex was emplaced into continental sediments along the nascent Iapetus margin tentatively located in the paleogeographic reconstruction. We have counter-rotated the JASON plume generation zones (thick red line) to account for TPW, so that one can examine how LIP related volcanism and kimberlites directly relate to the PGZs in the paleomagnetic frame. GD = Grenville Dyke Complex; LR = Long Range Dyke Complex; ED = Egersund Dyke Complex. Red star indicates the location of the suggested mantle plume.

10. Discussion

10.1. Origin of the CIMP

The groups 1 and 2 dyke swarms of CIMP in NE America (Laurentia; see section 2) have compositions very similar to the Scandinavian Dyke Complex (Fig. 3-3 and 3-6). Many group 1 dykes are intermediate between the compositions of the northern and southern segments in Scandinavia but extend to more enriched compositions similar to the southern segment (Fig. 3-6b; online supporting information S11 and S12). The sparsely available data for group 2 also overlaps compositionally with those of the southern segment in Scandinavia and extend to more enriched compositions similar to OIB (Fig. 3-6b). Similarly, the transitional to alkali basalt dykes of Egersund in SW Norway plot between enriched MORB and OIB (Bingen and Demaiffe, 1999), and the alkali basalt dykes of the Seiland Igneous Province (Reginiussen et al., 1995) are also close to OIB (Fig. 3-6b). The corollary of this is that similar magma types, all with Th/Yb and Nb/Yb ratios plotting within the oceanic mantle array, were emplaced as dyke complexes in NE Laurentia and SW Baltica, but at variable times. For example, the OIB-like Egersund dykes intruding in situ Proterozoic Baltican basement were an early phase (616 Ma), whereas similar OIB-like magmas of group 2 dykes of Laurentia and of the Seiland Igneous Province were younger (570–550 Ma). Similar magmas of group 1 dykes in Laurentia and the Scandinavian Dyke Complex were emplaced within the same time window from 615 to 590 Ma with most magmatic activity in Baltica between 607 and 595 Ma (Baird et al., 2014 Gee et al., 2016; Svenningsen, 2001); this is probably the most voluminous and intense CIMP event. The compositional variability, the prolonged basaltic magmatism (616–550 Ma), and the eruption over a vast area (> 9 million square kilometers, Fig. 3-1) are best explained by melting of multiple, diachronous mantle plume sources upwelling into rifting and thinning continental lithosphere. We surmise that the multiple basalt and kimberlite events of the CIMP (Ernst and Bell, 2010) are best explained by the

coincidence of CIMP and a mantle PGZ as depicted in Fig. 3-11. This interpretation corroborates many previous arguments for the involvement of mantle plumes across CIMP (e.g. Burke and Dewey, 1973; Seymour and Kumarapeli, 1995; Andréasson et al., 1998; Bingen and Demaiffe, 1999; Puffer, 2002; Hodych and Cox, 2007; Hollocher et al., 2007; Ernst and Bell, 2010; Larsen et al., 2018).

10.2. The North Atlantic Wilson Cycle: Two LIPs and Two Mantle Plumes?

A comparison of the two LIPs of the North Atlantic Wilson Cycles (NAIP and CIMP) shows that their basaltic magmas are remarkably similar in terms of major and trace element compositions (Fig. 3-3, 3-6 and 3-7). Moreover, the structure and magmatic construction (magma-rich margin) of the two continent-ocean transitions have been shown to be very similar offshore Norway today (NAIP) and in the Neoproterozoic (CIMP; Abdelmalak et al., 2015). Similar to our conclusions above, the NAIP has been explained by melting of enriched mantle plume material at elevated ΔT_P (90–210°C; Brown and Lesher, 2014; Herzberg and Gazel, 2009; Tegner et al., 1998b). Moreover, Fitton et al. (1997) showed lateral compositional zoning of NAIP magmas similar to the Scandinavian Dyke Complex (Fig. 3-7a) and explained this as the result of melting of a laterally zoned mantle plume composed in the interior of enriched but heterogeneous mantle surrounded by an outer sheath of more depleted mantle. Another similarity of the two LIPs is the close association with continental breakup. In the Scandinavian Dyke Complex, the Tsäkkok location in northern Sweden (#27, Tab. 3-1 and Fig. 3-1) includes pillow lavas (now eclogite) that according to Kullerud et al. (1990) formed within the incipient ocean floor at the thinned edge of Baltica. In NAIP, the first occurrence of oceanic-type low-Ti basalts in the East Greenland volcanic succession was explained as the development of the incipient ocean floor during the main flood basalt event (Tegner et al., 1998b). Following Buiter and Torsvik (2014), we therefore propose that the two opening phases of the North Atlantic Wilson Cycles both were associated with LIPs that originated from mantle plumes. The compositional similarity of CIMP and NAIP suggests that the compositions of the two mantle PGZs of JASON and TUZO (Fig. 3-11) may be very similar.

10.3. Can LIPs Be Used as Piercing Points for Plate Reconstructions?

The remarkable correlation of reconstructed LIPs (Fig. 3-11a) and kimberlites suggests long-term stability of TUZO and JASON LLSVPs, and there are therefore strong arguments for their quasi-stability through most of the Earth's history as discussed in section 9.1. Using the PGZ reconstruction method of surface-to-core-mantle boundary correlation to locate continents in longitude and an iterative approach for defining a paleomagnetic reference frame corrected for TPW, we have built an absolute plate reconstruction for East Rodinia in the Ediacaran (615 Ma). In this model, the LIP-related CIMP dyke swarms and lavas and the kimberlites are assumed sourced from the PGZ at the margin of JASON (Fig. 3-11b). Plume-derived magmatism is therefore used as piercing points for absolute mantle-frame plate reconstructions. The PGZ

reconstruction method is probably the only way forward to semi-quantitatively position continents in longitude before Pangea and has previously been used successfully to reconstruct the 510 Ma Kalkarindji LIP (Western Australia) to the northeastern margin of TUZO (Torsvik et al., 2014). But if TUZO and JASON were highly mobile, or if Earth alternated between degree-2 (two upwellings such as TUZO and JASON and two downwellings as today) and degree-1 modes (e.g., Zhong et al., 2007), then this method is invalidated, and we have no means for calibrating longitude using LIPs and kimberlites as piecing points to derive absolute reconstructions before Pangea.

11. Conclusions

A more than 1,000 km long magma-rich, pre-Caledonian rifted continental margin of Baltica formed during the Ediacaran. The ~616–590 Ma breakup magmatism following a long period (~200 Ma) of crustal extension and rifting of Rodinia includes prominent dyke complexes in NE America (Laurentia) and NW Europe (Baltica). The Scandinavian Dyke Complex of the magma-rich margin in Baltica is one of several magmatic complexes making up the huge CIMP, a LIP associated with the initiation of the Caledonian Wilson Cycle. Our compilation of new and published geochemical data from the Scandinavian Dyke Complex shows a pronounced lateral variation of ΔNb, La/Sm_N, and Sr isotopes from SW to NE along more than 1,000 km. Geochemical modelling shows this geochemical zoning is best explained by melting related to a broad mantle plume that had elevated potential temperatures (ΔT_P of 75–150°C based on rare earth elements and ΔT_P of 100–250°C based on major elements) and was enriched (primitive mantle) in the south and depleted (depleted MORB mantle) in the north. The origin of CIMP appears to have involved several mantle plumes. This is best explained if the segments of Rodinia that broke up in Baltica and Laurentia coincided with a mantle PGZ identified to be located along the margins of one of the two LLSVPs (JASON) in the deepest mantle. We therefore propose the Scandinavian Dyke Complex and other CIMP plumes may be used as piercing points for plate reconstruction, positioning Baltica and Laurentia above the eastern edge of JASON in the Ediacaran (635–544 Ma). The CIMP formed over a prolonged period between 616 and 550 Ma during the first known, Iapetus, opening stage of the North Atlantic Wilson Cycles. The NAIP was emplaced during the second opening phase, starting at around 62 Ma, and with seafloor spreading initiated at ca. 54 Ma. We therefore conclude that the known opening phases of the North Atlantic Wilson Cycles involved two LIPs and two mantle plumes.

Acknowledgments

Lara O'Dwyer Brown assisted with the compilation of geochemical data and drafting of figures. Svend Joensen assisted with Sr isotope measurements. The data are available as supporting information online. This research was funded by the Danish National Research Foundation Niels Bohr Professorship grant 26-123/8 and the Norwegian Research Council CoE-grant 223272 to CEED and to FRINAT Project 250327. The University of Padova, Italy, and a sabbatical stipend from Aarhus University Research Foundation to Tegner provided space and time to write this publication. This work benefitted from constructive and very useful journal reviews and editorial handling of Claudio Faccenna.

Chapter 4

A review and reinterpretation of the architecture of the South and South-Central Scandinavian Caledonides—A magma-poor to magma-rich transition and the significance of the reactivation of rift inherited structures

Johannes Jakob, Torgeir B. Andersen, Hans Jørgen Kjøll

This paper has been published in *Earth Science Reviews*

The electronic version of the paper is available online at: https://doi.org/10.1016/j.earscirev.2019.01.004

Abstract: Interpretations of the pre-Caledonian rifted margin of Baltica commonly reconstruct it as a simple, tapering, wedge-shaped continental margin dissected by half graben, with progressively more rift-related magmas towards the ocean-continent transition zone. It is also interpreted to have had that simple architecture along-strike the whole length of the margin. However, present-day rifted margins show a more complex architecture, dominated by different and partly diachronous segments both along and across strike. Here, we show that the composition and the architecture of the Baltican-derived nappes of the South and South Central Scandinavian Caledonides are to a large extend rift-inherited. Compositional variations of nappes in similar tectonostratigraphic positions can be ascribed to variations along-strike the rifted margin, including a magma-rich, a magma-rich to magma-poor transition zone, and a magma-poor segment of the margin. The architecture of the nappe stack that includes the Baltican-derived nappes was formed as a result of the reactivation of rift-inherited structures and the stacking of rift domains during the Caledonian Orogeny.

1. Introduction

The present architecture of the Scandinavian Caledonides is principally the result of the Silurian–Devonian Scandian continental collision of Baltica-Avalonia with Laurentia, the subsequent late- to post-orogenic extension, and deep erosion (e.g. Fossen, 2010; Corfu et al., 2014). During the Scandian collision and in parts during the early-Caledonian events affecting the distal margin of Baltica, the rifted continental margin of Baltica was deeply buried beneath Laurentia and a complex stack of nappes was thrust over great distances towards the south-east onto Baltica. The underlying autochthon comprises Archean to Paleoproterozoic basement in the north and Mesoproterozoic basement in the south that is covered by (par)autochthonous metasediments of Neoproterozoic to latest Silurian age. The nappe-stack comprises allochthons of Baltican, transitional oceanic-continental, oceanic, and Laurentian affinity.

The allochthons of Baltican affinity include Neoproterozoic pre- to post-rift successions as well as post-rift continental margin deposits of Cambrian to Silurian age and foreland basin sediments deposited in front of and incorporated into the advancing thrust sheets during the Scandian Orogeny (e.g. Nystuen et al., 2008). Baltican-derived basement and basement-cover nappes are commonly referred to as the Lower and Middle Allochthons and are interpreted to contain transgressive sequences deposited along the Iapetus margin of Baltica (Roberts and Gee, 1985; Stephens and Gee, 1989). Ophiolite/island arc assemblages and nappes of Laurentian affinity are commonly referred to as the Upper and Uppermost Allochthons, respectively.

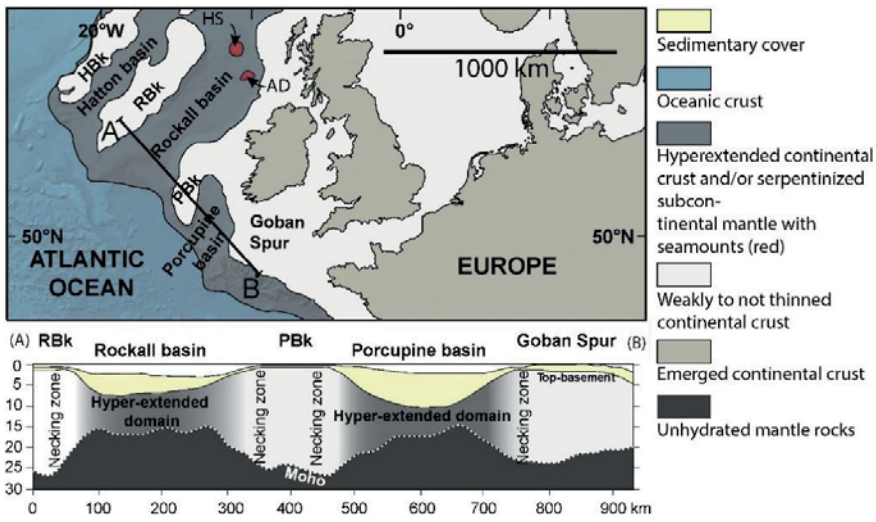

Figure 4-1: Map of the hyperextended domains of the southern North Atlantic. Figure redrawn after Mohn et al. (2014); map modified from Péron-Pinvidic and Manatschal (2010) and Lundin and Doré (2011); profile modified from Welford et al. (2012). Please note the presence of seamounts in the northern Rockall basin. HBk, Hatton Bank; RBk, Rockall Bank; PBk, Porcupine Bank; AD, Anton Dohrn Seamount; HS, Hebrides Seamount.

In the traditional tectonostratigraphic scheme, all units with ocean-floor-like lithologies are referred to as ophiolites or dismembered ophiolites and are interpreted to have initially formed in an ocean, outboard of all rocks with continental affinity (Roberts and Gee, 1985). The traditional interpretations assume that a mostly uniform and continuous tectonostratigraphy with the same palaeogeographic significance can be traced along the entire length of the Scandinavian Caledonides (e.g. Gee et al., 2016). However, present-day understanding of continental margins and their remnants within mountain belts is that rifted margins have a more complex architecture, dominated by different and partly diachronous segments both along and across strike. Such segmentations may include very different fault geometries and structural styles, producing major variations in width and length of basins and highs as well as more fundamental and larger-scale variations with magma-poor and magma-rich segments (e.g. Mohn et al., 2010; Péron-Pinvidic and Manatschal, 2010).

On a regional scale, passive margins may also be decorated with relatively narrow failed-rift basins that separate thicker and variably sized continental slivers or blocks from the adjacent continent (e.g. Péron-Pinvidic and Manatschal, 2010; Chenin et al., 2017). Such basins may be floored by stretched to hyperextended/hyper-thinned continental crust, transitional crust or embryonic oceanic crust. The Orphan, Porcupine and Rockall basins off-shore Newfoundland and the British and Irish Isles as well as the Norway Basin adjacent to the Jan Mayen continental ridge and the margin of Norway, are good present-day examples (Peron-Pinvidic et al., 2012; Kimbell et al., 2017). Within the thinned crust, guyots may also be present, e.g. the Anton Dohrn and Hebrides seamounts or the Rosemary bank in the northern continuation of the Rockall trough (Fig. 4-1). These seamounts are attributed to episodic magmatic pulses of the Iceland plume during opening of the North Atlantic (O'Connor et al., 2000). Another modern-day analogue of an across-strike, complexly structured, rifted margin is provided by the Red Sea detachment systems in Eritrea (Talbot and Ghebreab, 1997). Later inversion and incorporation of such complexly configured passive margins into a mountain belt, as discussed by Beltrando et al. (2014), results in a tectonostratigraphy with laterally changing nappe characteristics that may include previous extensional slivers of continental basement associated with hyperextended deep basins, sediments with or without spreading-related magmatism, and in several cases also exhumed hydrated/carbonated mantle peridotites (e.g. Müntener et al., 2009). A structural succession with such characteristics does not easily comply with the traditional, belt-long, tectonostratigraphic correlations and the traditional nomenclature used in the Scandinavian Caledonides.

Here, we describe and discuss a re-interpretation of the tectonostratigraphy of the South and South-Central Scandinavian Caledonides. A key area for the understanding of the architecture and re-

interpretation of the tectonostratigraphy is where the southern magma-poor segment (Andersen et al., 2012; Jakob et al., 2017; Jakob et al., 2018) faces the northern magma-rich segment (e.g. Andréasson, 1994; Kjøll et al., 2019a; Tegner et al., 2019). We suggest that lithostratigraphic units, previously assigned to the Upper Allochthon and hence of suspect to outboard status have typical characteristics of magma-poor and magma-rich continental margins and ocean-continent transitions (OCT). In the Caledonides, these rocks are, however, variably overprinted by orogenic deformation and metamorphism (e.g. Jakob et al., 2018, Kjøll et al., 2019a). Nevertheless, many of their lithological characteristics are well-enough preserved to be compared with present-day passive margins and examples of fossil OCT zones in other mountain belts, for example the Alps and the Pyrenees (e.g. Lagabrielle et al., 2010; Beltrando et al., 2014).

We show that a gradual transition from the magma-rich to the magma-poor segment was related to the formation of a large Jotun-type basement microcontinent/continental sliver and its termination in the Gudbrandsdalen area in central-south Norway. Furthermore, we also suggest that the nappes of Baltican affinity can be divided into rift domains that are well-established from present-day rifted margins, i.e. a proximal/necking domain, an extended domain; a distal/outer domain, and a microcontinent.

2. Tectonostratigraphic units in the South and South-Central Caledonides

2.1. The South Scandinavian Caledonides

2.1.1. Neoproterozoic syn-rift basins with little to no syn-rift magmatic rocks

In southern Norway (Fig. 4-2), Late Proterozoic to Lower Palaeozoic continentally derived deposits locally lie unconformable on Baltican basement or on allochthonous crystalline rocks (Bingen et al., 2011). These include the Osen-Røa, Kvitvola, Synnfjell, Valdres NCs (Nystuen, 1983; Nickelsen et al., 1985). The Late Proterozoic successions are interpreted to represent proximal pre- and syn-rift sediments, which vary from fluvial to marine deposits (Nickelsen et al., 1985; Nystuen et al., 2008). Marinoan (*c.* 630 Ma) and/or the younger Gaskiers glaciogenic deposits (*c.* 580 Ma) are present in several of these units (e.g. Nystuen et al., 2008; Lamminen et al., 2015). In some cases, the Neoproterozoic sediments are stratigraphically overlain by Cambrian to Lower Ordovician post-rift black-shale and carbonate successions, which in turn, are locally overlain by Lower to Middle Ordovician turbidites that grade from distal at the base to proximal at the top (e.g. Nickelsen et al., 1985; Owen and Bockelie, 1990; Greiling and Garfunkel, 2007).

In other areas, mostly in south-western Norway, the fossiliferous Cambrian–Ordovician overlies a glacially striated basement floor in Hardangervidda (Fig. 4-2) and are in turn overthrust by mica schists (Holmasjø Formation) of unknown age (see Gabrielsen et al., 2015). With the exception of the ~616 Ma

Egersund mafic dykes, minor volcanics and dykes in the Hedmark basin and a horizon of basaltic volcanics on Hardangervidda (Andresen and Gabrielsen, 1979; Nystuen, 1987; Bingen et al., 1998) mafic magmatic rocks are absent in the Baltican basement and the Neoproterozoic–Ordovician succession in the foreland area of South-Scandinavia.

2.1.2. The Lower Bergsdalen Nappe

The Lower Bergsdalen Nappe includes crystalline basement and Proterozoic metasediments, which are associated with metamorphosed basic to intermediate plutons and volcanics (Kvale, 1945; Fossen, 1993). Interleaved with the coarse-grained metasediments and magmatic rocks are phyllites and mica schists Kvale (1945). The metasediments are mainly coarse-grained meta-arkoses and quartzites. Some of the granites in the crystalline sheets were dated by the Rb-Sr whole-rock method at 1274–953 Ma (Pringle et al., 1975; Gray, 1978). Kvale (1945) interpreted the quartzites to be the oldest rocks of the Lower Bergsdalen Nappe because mafic and felsic magmas intrude into the metasediments. Consequently, the quartzites were interpreted to be pre-Sveconorwegian in age (> 1274 Ma).

The Lower Bergsdalen Nappe is positioned structurally above the Western Gneiss Region (WGR), a thin discontinuous cover of mica schists (Wennberg et al., 1998) and allochthonous metasediments, which are possibly equivalent to the Synnfjell NC (Fig. 4-4). It is structurally overlain by a unit of metasediments that contain a number of detrital and solitary metaperidotite bodies (see section 2.1.3). The Lower Bergsdalen Nappe can be traced around the core of the Bjørnafjorden Antiform (Fig. 4-2), as originally defined by Kvale (1945).

2.1.3. Metaperidotite-bearing metasedimentary complexes

Between the Bergen Arcs and Lom (Fig. 4-2) a prominent metasediment-dominated complex, which contains numerous mantle-derived metaperidotite lenses (< 2 km long) and local clastic serpentinites, including detrital breccias, conglomerates, and sandstones has been mapped (Andersen et al., 2012). The metasedimentary matrix is dominated by originally fine-grained sediments, now mica-schist and phyllite. Because of its mixed character, this unit has been non-genetically referred to as a mélange by Andersen et al., (2012) and Jakob et al., (2017; 2018). However, to avoid confusion with other metaperidotite-bearing mélanges, such as those that have been formed at the plate interface in subduction zones and because of its resemblance with reworked OCT assemblages in other mountain belts (Andersen et al., 2012; Jakob et al., 2017; Beltrando et al., 2014), we refer to this unit as an OCT assemblage.

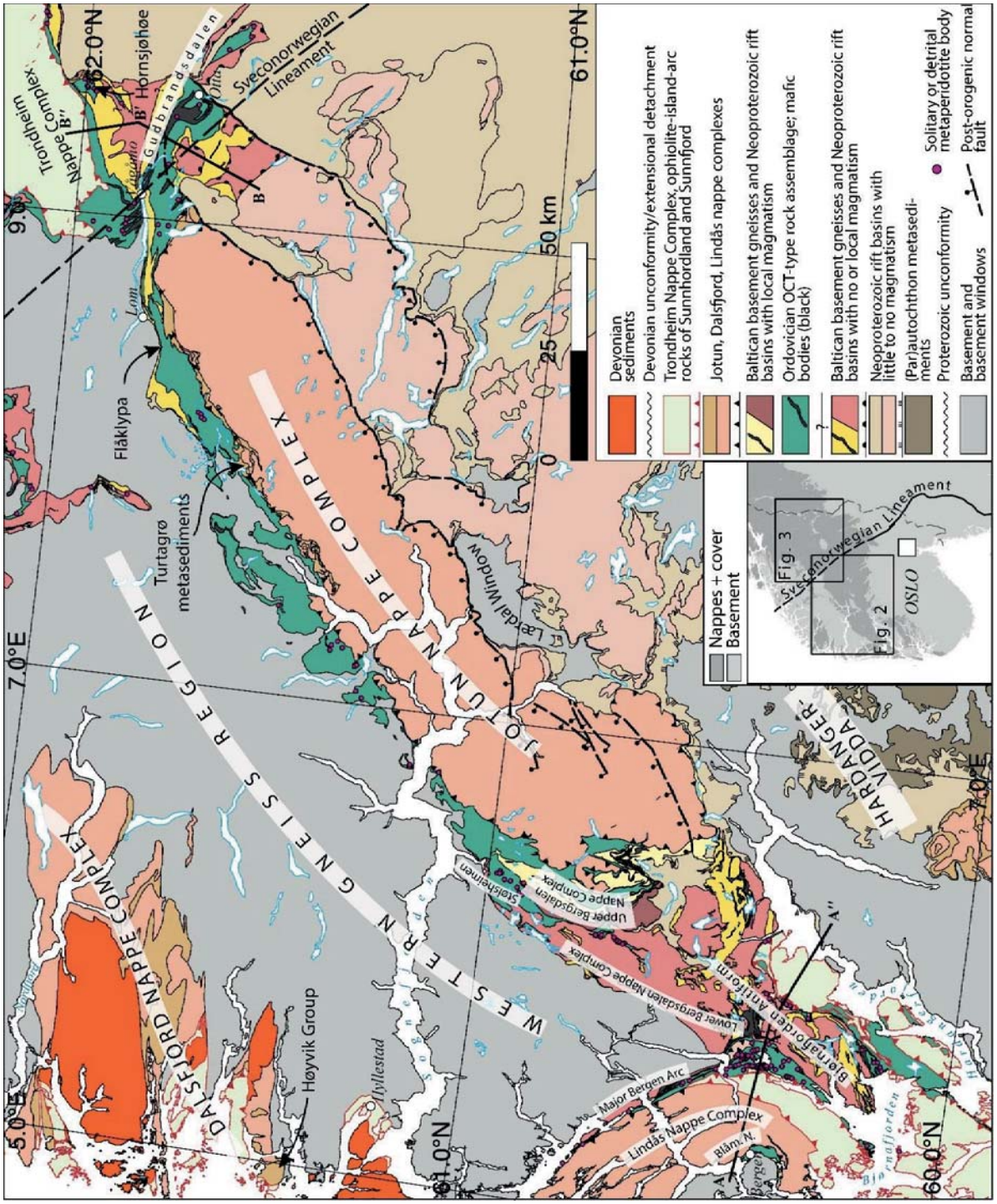

Figure 4-2: Tectonostratigraphic map of the South Caledonides between Bergen and Gudbrandsdalen showing the first-order thrust of the main tectonic units. Cross section shown in Figure 4-5.

The OCT assemblage structurally overlies the WGR and Lower Bergsdalen NC. From the Major Bergen Arc and around the Bjørnafjorden Antiform, it can be traced below both the allochthonous crystalline rocks of the Lindås nappe (section 2.1.5), the Upper Bergsdalen NC (section 2.1.4), as well as the main ophiolite/island-arc nappe complexes of the Iapetus (section 2.1.6). From Stølsheimen across Sognefjorden, NE-wards to Lom (Fig. 4-2), the same OCT unit has been mapped continuously below the western flank of the Jotun NC.

The mostly pelitic metasediments also contain lenses of meta-conglomerate and meta-sandstone as well as thin calcareous horizons, up to 40 km long and thin (<1 km) discontinuous sheets of Proterozoic gneisses, minor gabbro and granodiorite of Late Cambrian to early Middle Ordovician age (487 to 471 Ma) and lenses of undated mafic rocks in the SW (Jakob et al., 2018). Conglomerates and sandstones with a continental source (quartzite, vein quartz, granite clasts, one dated at 1033 Ma) indicate a Baltican-affine source (Andersen et al., 2012). Detrital zircons show that sedimentation continued at least into the Middle Ordovician (468 Ma) (Slama and Pedersen, 2015).

Late Scandian (~427 to 415 Ma) syn-orogenic granitoids intrude both the metasediments of the Major Bergen Arc, including the OCT assemblage, as well as the Jotun and Lindås NCs in western Norway (Austrheim, 1990; Jakob et al., 2018; Wennberg et al., 2001; Lundmark and Corfu, 2007). The mafic and granitoid intrusives, which occur near the southern termination of the Jotun NC, in the Major Bergen Arc, and at Stølsheimen are unknown between Stølsheimen and Lom (Fig. 4-2).

The entire OCT assemblage experienced upper greenschist to amphibolite facies metamorphism during the Scandian Orogeny after ~430 Ma (Jakob et al., 2017; 2018). Because of its characteristic lithological assemblage that resembles those of inverted magma-poor hyperextended margins in other orogens (e.g. Beltrando et al., 2014), the OCT assemblage is interpreted to have formed by pre-Scandian hyperextension and exhumation of subcontinental mantle or by the reworking of a magma-poor hyperextended rifted margin in the Ordovician (Andersen et al., 2012; Jakob et al., 2018).

2.1.4 The Upper Bergsdalen and Blåmannen nappes

The Upper Bergsdalen NC represents a second sequence of allochthonous Baltican basement gneisses and metamorphosed continental margin sequences that are intercalated with Lower Palaeozoic phyllites and mica schists; similar to the Lower Bergsdalen Nappe (Kvale, 1945). The southern part of the Upper Bergsdalen NC is structurally overlain by the Jotun NC (section 2.1.5), whereas south of Sognefjorden, the rocks of the Upper Bergsdalen NC trail out into the mica schists of the OCT assemblage (Fig. 4-2). The metaperidotites of the OCT assemblage, however, consistently occur structurally below the Upper Bergsdalen NC. The lower thrust sheets of the Upper Bergsdalen NC are dominated by crystalline

gneisses whereas the upper thrust sheets are mostly composed of metasediments that are locally associated with mafic igneous rocks.

A meta-rhyolite of the Upper Bergsdalen NC was dated at 1219 ±111 Ma (Rb-Sr whole rock analysis, Gray, 1978). The magmatic history of the Upper Bergsdalen Nappe is apparently similar to that of the Lower Bergsdalen Nappe. However, a number of undated mafic sheets and dykes cutting metasediments occur in both of the Bergsdalen nappes, and their complete Proterozoic and younger (?) intrusive history is not yet known. The Blåmannen Nappe in the minor Bergen Arc is another sliver of basement-cover rocks that structurally overlies the OCT assemblage. It consists of allochthonous crystalline basement that is unconformably overlain by a sedimentary sequence, including a tillite, that is suggested to have been deposited in the Proterozoic (Fossen, 1988; Fossen and Dunlap, 1998).

2.1.5 The Jotun, Dalsfjord and Lindås nappe complexes

The Jotun, Dalsfjord and Lindås NCs are large nappes of crystalline basement of Baltican affinity (Fig. 4-2), some of which are associated with or partly unconformably overlain by Neoproterozoic continental margin sequences, including the Turtagrø metasediments on the western flank of the Jotun NC and the Høyvik Group in the Dalsfjord NC (Heim et al., 1977; Nickelsen et al., 1985; Andersen et al., 1998). The crystalline rocks of these NCs are Mesoproterozoic in age and are dominantly anorthosite-mangerite-charnockite-granite (AMCG) magmatic rocks, which experienced high-grade metamorphism during the Sveconorwegian orogeny (e.g. Austrheim, 1987; Corfu and Emmet, 1992; Bingen et al., 2001; Corfu and Andersen, 2002; Lundmark and Corfu, 2007, 2008).

Unlike the continental metasediments in the Osen-Røa, Kvitvola, Synnfjell and Valdres nappes, the Høyvik Group contains a mid-ocean ridge-type mafic dyke-swarm and minor pillow-basalts at high stratigraphic levels (Andersen et al., 1998). The Høyvik Group and the dykes were deformed and metamorphosed before the deposition of the Middle Silurian (Wenlock) Herland Group (Andersen et al., 1998). $^{40}Ar/^{39}Ar$ cooling ages of phengitic mica in the Høyvik metasediments show that the deformation occurred before 447–449 Ma (Andersen et al., 1998; Eide et al., 1999). The Herland Group metasandstones and metaconglomerates are unconformably overlain by the Sunnfjord obduction mélange and the ~443 Ma Solund-Stavfjord Ophiolite Complex (Dunning and Pedersen, 1988; Andersen et al., 1990a; Furnes et al., 1990). The Herland Group deposition and transgression, and the deposition of the Sunnfjord mélange is interpreted to herald the obduction and emplacement of the Solund-Stavfjord ophiolite (Andersen et al., 1990b; Skjerlie and Furnes, 1990).

The Lindås NC is another AMCG basement nappe of Baltican affinity, which is structurally positioned above the OCT assemblage (Fig. 4-2). The composition and age of the Lindås NC is similar to

those of the Dalsfjord NCs. The north-western trailing end of the Lindås NC contains ~430 Ma eclogites (Austrheim, 1990; Glodny et al., 2008) indicating an early Scandian deep burial and metamorphism of the Lindås NC. Unlike the Dalsfjord NCs, the Lindås NC contains minor Late Scandian (430–418 Ma) syn-orogenic granitoids (Austrheim, 1990; Wennberg et al., 1998; Kühn et al., 2002).

The Jotun NC is a large sheet of crystalline mostly AMCG rocks that is similar to those discussed-above. On its western flank, the Jotun NC includes highly strained metasediments, which are referred to as the Turtagrø metasediments. The Turtagrø metasediments are similar to the sparagmites of the Valdres NC and are apparently also free of syn-rift magmatic rocks (Koestler, 1983). Locally, there are abundant Late Scandian syn-orogenic granitoid dykes (~427 Ma Årdal Dyke Complex) intruding the Jotun NC (Lundmark and Corfu, 2007).

In this study, we treat the Jotun, Dalsfjord and Lindås NCs as a large composite unit due to their similar AMCG-lithologies, geochronological fingerprints, and tectonostratigraphic position structurally above the OCT assemblage and below the outboard nappes of Iapetus and Laurentian origin.

2.1.6 Ophiolites and magmatic arc rocks of western Norway

The structurally highest Scandian thrust nappes of the SW Caledonides consist of a complex assemblage of ophiolite-island-arc and magmatic intrusive complexes (e.g. Andersen and Andresen, 1994). In the Major Bergen Arc the ~489 Ma Gullfjellet ophiolite (Dunning and Pedersen, 1988) was emplaced above the Lindås NC, as well as the OCT assemblages (Fig. 4-2). The ophiolite/island-arc complexes occur again structurally above the Baltican-affine continental rocks between Hyllestad and Nordfjord, and structurally above OCT assemblages near the north-eastern termination of the Jotun NCs (see section 2.2.4). The Dalsfjord NC and its sedimentary cover is structurally overlain by the ~443 Ma Solund-Stavfjord ophiolite, which was constructed on the remnants of early Ordovician ophiolite/island-arc in a back-arc basin setting (Furnes et al., 1990). The Late Cambrian to Early Ordovician ophiolite island-arc complexes in the SW Caledonides are interpreted to have originated along the Laurentian margin of the Iapetus. They record a protracted history of subduction, arc-continent collision, volcanism and sedimentation, as well as Early-Caledonian metamorphism and deformation prior to Scandian thrusting of the nappes onto Baltica (Andersen and Andresen, 1994; Furnes et al., 2012).

2.2. The South-Central Caledonides

2.2.1 Autochthon and Neoproterozoic syn-rift sediments with little to no syn-rift magmatic rocks

In the South-Central Caledonides (Fig. 4-3) the basement and minor (par)autochthonous metasediments are exposed in a series of tectonic windows, including the WGR, the Atnsjøen Window and

the core of the Skardøra Antiform (e.g. Sjöström, 1983; Nystuen, 1987). The structurally lowest nappes are the Osen-Røa and Kvitvola nappes (Fig. 4-4), which preserve continental margin sequences that contain little to no syn-rift igneous rocks (see also section 2.1.1). A few isolated minor occurrences of tholeiitic basalt can be found stratigraphically overlying quartzites of the Osen-Røa NC (Nystuen, 1987). Towards the north-east into Sweden, these (par)autochthonous and allochthonous continental margin successions can be correlated with the Dividal Group and the Risbäck NC (Törnebohm, 1896; Føyn and Glaessner, 1979; Gee et al., 1985)

2.2.2 Sheets of crystalline basement gneisses

Structurally above the proximal syn-rift to post-rift sediments of the Osen-Røa and Kvitvola NCs is a series of crystalline basement gneisses that can be traced from Norway across the Skardøra Antiform into Sweden (Fig. 4-3). In Sweden, east of the Skardøra Antiform (Fig. 4-3), the gneisses are referred to as the Tännäs Augen Gneiss. The Tännäs Augen Gneiss is Mesoproterozoic in age (~1685–1610 Ma; Claesson, 1980) and is locally mylonitised along tectonic contacts at its base and top. These gneisses are apparently without Ediacaran syn-rift intrusives.

West of the Skardøra Antiform, the gneisses can be traced as a thin band, at a consistent tectonostratigraphic level, along-strike into the Gudbrandsdalen Antiform (Fig. 4-3). Here, the gneisses are referred to as the Høvringen Gneiss Complex, Rudihø Crystalline Complex and Mukampen Suite (Strand, 1951; Lamminen et al., 2011; Heim and Corfu, 2017; Gjelsvik, 1946). The allochthonous gneisses of the Rudihø and the Mukampen Suite are 1700–1200Ma and experienced high-grade metamorphism associated with some magmatism at 920 to 900 Ma (Lamminen et al., 2011; Heim and Corfu, 2017). A late tonalitic dyke cutting the Mukampen Suite was dated at ~430 Ma (Heim and Corfu, 2017). Similar to the Tännäs Augen Gneiss east of the Skardøra Antiform, no Ediacaran syn-rift intrusives have been reported from these gneisses. Thus, the gneisses at Høvringen, Rudihø and Mukampen are similar in age, composition and metamorphic history to the Tännäs Augen Gneiss and some of the large crystalline nappes of the South Norwegian Caledonides.

2.2.3 Neoproterozoic syn-rift sediment basins with syn-rift magmatic rocks

Structurally above the sheets of Baltican basement gneisses are Neoproterozoic metasedimentary complexes in the Särv and Seve NCs, a well as in the Hummelfjell and Heidal Groups (Fig 4-3). The Särv and the structurally overlying Seve NCs comprise Neoproterozoic pre- to syn-rift continental margin sediments that contain a large volume of rift-related mafic dykes and local volcanics (Solyom et al., 1979; Hollocher et al., 2012; Kumpulainen et al., 2016; Tegner et al., 2019). The Särv and Seve metasediments experienced greenschist facies Scandian metamorphism in the east (Särv) (Gilotti and Kumpulainen, 1986)

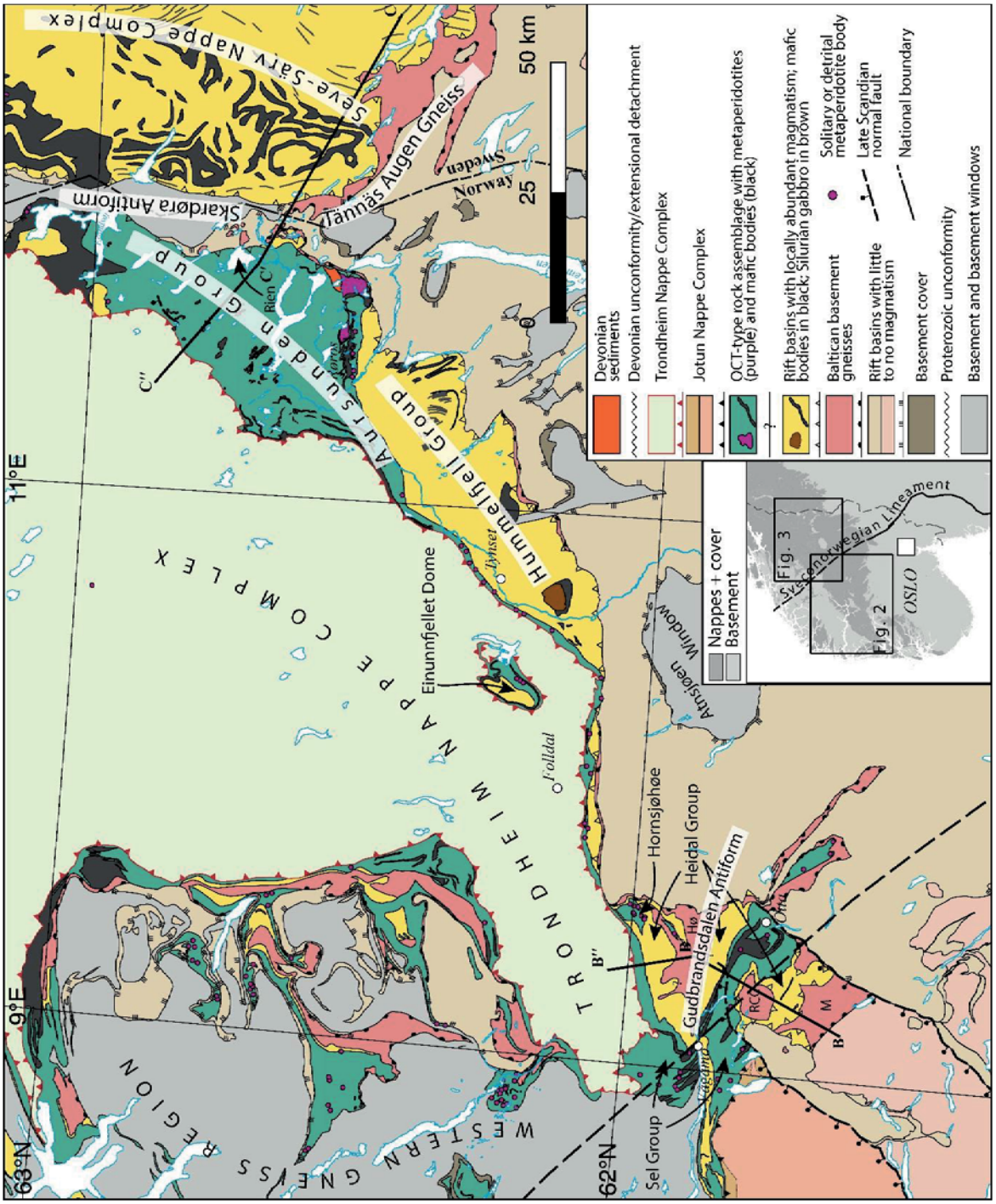

Figure 4-3: Tectonostratigraphic map of the South-Central Caledonides between Gudbrandsdalen and the Skardøra Antiform showing the first-order tectonic units of the Scandian Orogen. Cross section shown in Fig. 4-5.

and an increase in Scandian metamorphism towards the west (Seve). Regionally, the Seve NC experienced diachronous amphibolite to eclogite (ultra-)high-pressure (UHP) metamorphism in the Early (~482 Ma) to Late Ordovician (~445 Ma) (Root and Corfu, 2011; Majka et al., 2014; Klonowska et al., 2017).

The mafic dyke swarms and plutons in the Särv and Seve NCs including the ~596 Ma Ottfjället Dykes are interpreted to represent Iapetus break-up magmatism (e.g. Andréasson, 1994; Kumpulainen et al., 2016; Tegner et al., 2019). Regional studies of the Seve NC in Central and North Sweden show that pre-Caledonian continental margin-type metasediments in most parts are densely intruded by pre-Caledonian, Ediacaran mafic dyke swarms. These complexes are interpreted to represent the magma-rich segment of the Baltican rifted margin (e.g. Andreasson, 1994; Svenningsen, 2001; Tegner et al., 2019). The regional geochemistry of the ~1000 km long Scandinavian Dyke Swarm indicate that formation of the melts was related to a large igneous province (LIP) formed by a mantle plume associated with the Central Iapetus Magmatic Province (Tegner et al., 2019). The Seve NC also contains a number of solitary metaperidotite bodies and detrital serpentinites (e.g. Stigh, 1979) and the Ediacaran OCT is considered to be represented by the upper sections of the Seve NC (e.g. Andréasson et al., 1992; Svenningsen, 2001; Kjøll et al., 2019a).

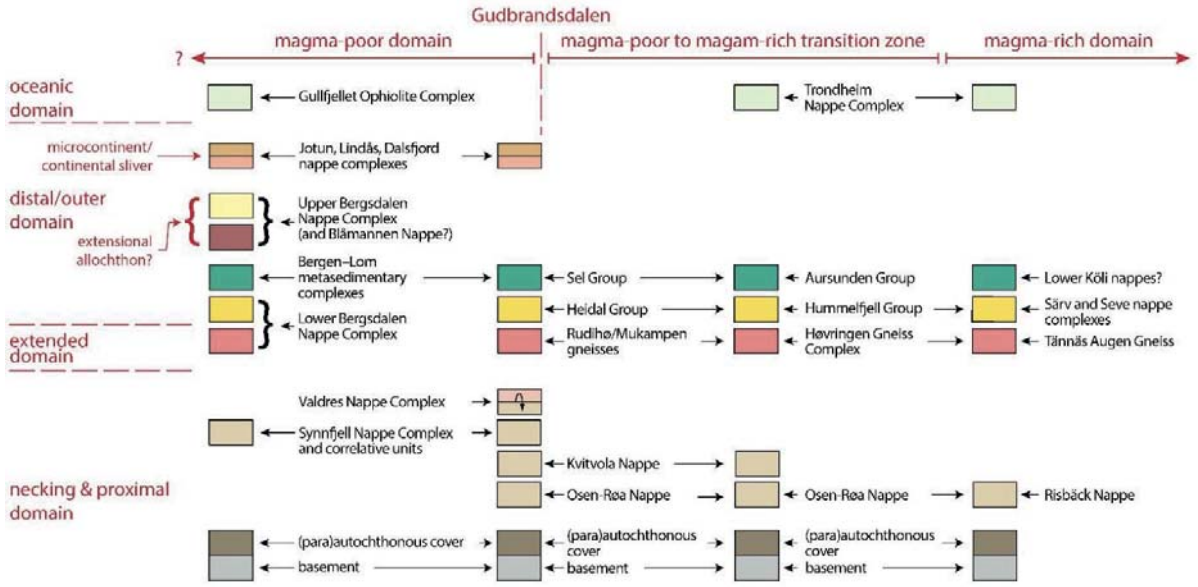

Figure 4-4: Tectonostratigraphic correlations between the South and South-Central Caledonides. Interpretation of the main tectonic units with respect to rift-inheritances in red

The Särv and Seve NCs can be correlated with the Hummelfjell and Heidal Groups in Norway (Fig. 4-3, 4-4) (Gjelsvik, 1945; Rui and Bakke, 1975; Nilsen, 1988). The Hummelfjell and Heidal metasediments

are mostly composed of Neoproterozoic quartzites and meta-arkoses that locally grade upwards into metapelites, and experienced similar metamorphic conditions as the adjacent Seve NC in Sweden (Törnebohm, 1896; Holmsen, 1943; Nilsen and Wolff, 1989).

The metasediments of the Hummelfjell Group contain a number of undated mafic intrusives and volcanics, which traditionally have been correlated with the rift-related igneous rocks in the Särv and Seve NCs (Tørnebohm, 1896; Holmsen, 1943). The number and volume of mafic igneous rocks within these Neoproterozoic successions decrease in south-westerly direction from the Särv and Seve NCs towards the Heidal Group. However, some mafic intrusives are reported from the upper sections of the Heidal Group (Gjelsvik, 1946; Strand, 1951). Gjelsvik (1946) also reported granitoid dykes cutting the mafic intrusives within the Heidal Group. However, none of these rocks have yet been dated.

2.2.4 Metaperidotite-bearing metasedimentary complexes

Between Vågåmo and the Skardøra Antiform (Fig. 4-3), metaperidotite-bearing metasediments structurally above the Heidal and Hummelfjell groups are referred to as the Sel Group (Bøe et al., 1993; Sturt et al., 1995; Nilsson et al., 1997) and Aursunden Group (Nilsen, 1988; Nilsen and Wolff, 1989). A lithological assemblage similar to those of the Sel and Aursunden groups also occurs in the Einunnfjellet Dome area (Fig. 4-3) overlying Neoproterozoic quartzites correlated with the Hummelfjell Group (Nilsen and Wolff, 1989; (McClellan, 1994; McClellan, 2004).

The mica schist matrix of the metaperidotite-bearing complexes between Vågåmo and the Skardøra Antiform are similar to the OCT assemblages further southwest, and contain both solitary and detrital metaperidotites, siliciclastic metaconglomerates and metasandstones as well as layers and lenses of turbidite-deposits. A major difference to the OCT assemblages between Stølsheimen and Lom is that the metaperidotite-bearing complexes between Vågåmo and the Skardøra Antiform also contain a large number of metamorphosed mafic bodies of unknown age. South of lake Rien (Fig. 4-3), an undeformed quartz diorite pluton intrudes schists of the Aursunden Group and contains xenoliths of the surrounding schists. Similar to some of the Late Scandian granitoids in the Major Bergen Arc (Jakob et al., 2018) the granitoid at Rien contains euhedral magmatic epidote indicating emplacement of the granitoid at pressures above 4 kbar (Naney, 1983; Zen and Hammarstrom, 1984; Schmidt and Poli, 2004).

The Sel Group in the Gudbrandsdalen Antiform (Sturt and Ramsay, 1997, 1999) contains numerous discontinuous lenses of monomict detrital serpentinites. Near Otta, one locality also hosts an island-type Dapingian–Darriwilian fauna (Bruton and Harper, 1981; Harper et al., 2008), which shows that sedimentation at this stratigraphic level took place in the Early–Middle Ordovician. The Aursunden Group is also suggested to be of Cambrian–Ordovician age (Nilsen and Wolff, 1989). Both the Sel and the

Aursunden Group are considered to have been deposited on the uppermost metasediments of the Heidal Group as well as on sheets of mafic crystalline rocks at the base of the Ordovician metasedimentary complexes, which, in turn are supposed to have tectonic contacts with the Heidal and Hummelfjell Groups below (e.g. Bøe et al., 1993; Nilsson et al., 1997; Sturt and Ramsay, 1999; Sturt et al., 1991). Apparent depositional contacts between the metaperidotite-bearing complexes and the units structurally below are exposed, e.g., at Vågåmo and Hornsjøhøe (Fig. 4-3).

2.2.5 The Trondheim Nappe Complex

The rocks of the Trondheim NC are dominated by three separate tectonic units, i.e. the Støren, Gula and Meråker nappes, all of which are composed of oceanic, ophiolite and island-arc assemblages (Guezou, 1978; Wolff, 1979; Gee and Sturt, 1985; Nilsen et al., 2003; Nilsen et al., 2007; Slagstad et al., 2014) (Fig. 4-3). All units of the Trondheim NC are intruded by ~440–430 Ma bimodal plutons (Dunning and Grenne, 2000 Nilsen et al., 2003, 2007). The Silurian plutons also intrude and are associated with older Cambrian–Ordovician ophiolite/arc rocks, e.g. in the Trondheim area or near Folldal, and with low-grade sediments containing Laurentian fossils as well as a Middle Silurian trondhjemite pluton, which contains inherited zircons of Archean age (Burton and Bockelie, 1980; Nilsen et al., 2003; 2007; Slagstad et al., 2014). Thus, the plutonic history of the Trondheim NC is similar to that of the ophiolite/island-arc complexes in the SW Caledonides (section 2.1.6).

The Gula nappes were commonly believed to be of Baltican origin. However, the assumption of a Baltican origin of the Gula nappes was founded on Tremadocian graptolites and similarities in trace element geochemistry of black shales from the Gula nappes and the Cambrian (par)autochthon of Baltica (e.g Gee, 1981). The *Rhapdinopora flabelliformis sociale* fossils in the so-called Dictyonema shales of the Gula nappes have also been described from the Tremadoc in Argentina, China, Belgium, and Newfoundland and are considered to be near cosmopolitan (e.g. Wang and Servais, 2015). Similarly, the high contents of V, Mo and U in black shales from the Gula nappes and the (para)autochthonous Cambrian–Ordovician of Baltica are rather indicators for the depositional environment than of provenance. Because of the lack of evidence for unequivocal Baltican origin and the common intrusive history in all nappes of the Trondheim NC as well as the faunal indications for a Laurentian affinity in the western Trondheim NC, we consider the entire Trondheim NC to be exotic with respect to Baltica.

Sturt et al. (1995) followed by Nilsson et al. (1997) suggested that the Sel and Aursunden groups are also unconformable on the Gula nappes. However, an unconformity below the Ordovician metasediments and on top of the Heidal and Hummelfjell groups, as well as their continuation into the Särv and Seve nappes, would stich the continental margin successions together with the oceanic assemblages of the Trondheim NC nappes as early as the Early–Middle Ordovician. The presence of such a terrane-link

would require moving the Neoproterozoic metasediments of the Heidal and Hummelfjell Groups and as well the Ediacaran sediments of the Särv and Seve nappes structurally below the Trondheim NC before the deposition of the Sel and Aursunden groups. Moreover, the Laurentian, Baltican and Celtic faunas were highly diverse at the time of the deposition of the OCT assemblages in the Early-Middle Ordovician and did not unify before the Wenlock (Harper et al., 2009; Torsvik and Cocks, 2017). We therefore consider it to be highly unlikely, and not demonstrated that the Sel and Aursunden Groups are unconformable on the rocks of the Trondheim NC in the Early-Middle Ordovician.

3 Discussion

3.1 The Jotun Microcontinent

Because the Jotun as well as the Dalsfjord and Lindås NCs display similar AMGC lithologies and geochronological histories as the Baltican craton, (Bingen et al., 2001; Corfu and Andersen, 2002; Lundmark and Corfu, 2007, 2008; Corfu et al., 2014; Roffeis and Corfu, 2014; Corfu and Andersen, 2015) these nappes are all considered to have a Baltican ancestry. However, because the Jotun and Lindås NCs structurally overlie the OCT assemblage, in theory, they could have been detached from the Baltican plate in the Ediacaran and moved independently throughout the Cambrian–Ordovician, or they may even be exotic with respect to Baltica and originate, e.g., from Gondwana or Laurentia. Unfortunately, there are no palaeomagnetic or other constraints on the Cambrian–Ordovician latitudinal position of these units and no fossils have been described from the metasediments associated with the crystalline rocks of the Jotun, Dalsfjord or Lindås NCs. Therefore, their plate tectonic history remains partly speculative and can only be inferred based on the lithological/geochronological dataset, its tectonic relationships with the other nappes and the lithostratigraphic correlations along the mountain belt.

An outboard origin of the large crystalline nappes of Southern Scandinavia would require that these rocks were near the leading edge of the upper plate during the Cambrian–Silurian, either near the Laurentian margin or the peri-Gondwanan terranes, see e.g. Domeier (2015) for a review of the closure of the Iapetus. However, the lack of magmatic arc rocks in the crystalline basement nappes of Southern Norway and the occurrence of Late Ordovician to early Silurian metamorphic rocks including eclogites in the Dalsfjord and Lindås NCs suggest that these NCs were part of the lower plate, i.e. Baltica, during the closure of the Iapetus.

Similar problems arise if we consider a scenario where these large basement nappes rifted off Baltica in the Ediacaran and subsequently moved independently of Baltica for ~200 million years, until the Scandian Orogeny, just to be juxtaposed with each other and Baltica after the continental collision in the

Silurian. In this context it is important to consider that the Iapetus did not close by simple orthogonal convergence, but involved large-scale clockwise and counter-clockwise rotations of Baltica as well as major changes in plate-motion directions throughout the Cambrian to Silurian (Torsvik and Cocks, 2005; Cocks and Torsvik, 2011; Domeier, 2015).

The radiometric ages of magmatic and metamorphic minerals from the crystalline nappes are similar to those of the Baltican autochthonous basement and are of Gothian age (1.7–1.6 Ga). The Gothian autochthonous domains closest to the crystalline nappes lie partly to the NE of the present-day position of the crystalline nappes. A SE directed emplacement of these NCs agrees with the Scandian kinematics (e.g. Fossen, 1992) and may indicate that the Baltican craton continued to the NW beyond the present-day North-Atlantic continental margin. Such a pre-Caledonian continuation of Baltica has previously been suggested by, e.g., (Lamminen et al., 2011; Lamminen et al., 2015) but is inherently difficult to test due to pervasive overprint by Caledonian Orogeny and the limits of the present-day continental margin.

Although a direct causal relationship is difficult to demonstrate, the NE termination of the Jotun NC near Vågåmo (Fig. 4-2, 4-3) correlates remarkably well with a major NW-SE trending change in the Baltican basement structure, which coincides with a Sveconorwegian lineament across southern Scandinavia (Olesen et al., 2010; Frasetto and Thybo, 2013; Kolstrup and Maupin, 2013). Whereas the outboard Caledonian nappes continue across this boundary, the transition from a magma-rich to a magma-poor domain also coincides with this lineament. We suggest that the magma-rich to magma-poor as well as the termination of the very large Baltican basement NCs both represent primary features of the pre-Caledonian margin of Baltica that most likely were inherited from the Middle Proterozoic structure of Baltica, which has been surprisingly little discussed in the large-scale architecture of the Scandinavian Caledonides.

By using the OCT assemblage as a reference level in the tectonostratigraphy, a first order architecture of the Pre-Caledonian margin of Baltica can be deduced by “unstacking” the nappes. Orthogneisses and metasediments of the Jotun NC structurally overlie the OCT assemblage on the western side of the Jotun NC. The OCT assemblage can be traced into the Gudbrandsdalen area where it structurally overlies the Heidal Group and sheets of basement gneisses (Fig. 4-3 and 4-4), which, in turn, structurally overly the proximal rift-basins, including the Osen-Røa, Kvitvola, Synnfjell and Valdres NCs. Therefore, before the inversion of the Caledonian margin of Baltican, a basin, which was floored by transitional crust (the OCT assemblage), separated the proximal basins and thinned continental crust to the SE from the rocks of the Jotun NC.

Whereas, the Neoproterozoic metasediments of the proximal basins structurally below the Jotun NC contain no syn-rift igneous rocks, the rocks of the Høyvik Group and the orthogneisses of the Dalsfjord NC contain mafic dykes and pillow basalts (Andersen et al., 1990, 1998; Corfu and Andersen, 2002). We suggest that the dyke swarm in the Høyvik Group and other correlative units of the Dalsfjord NC indicate that these rocks represent the ocean facing NW (present-day coordinates) magma-rich rifted segment of a crystalline block(s) outboard of the OCT assemblage. The distal position with respect to Baltica is also indicated by the Middle Ordovician deformation and metamorphism which affected the Dalsfjord-Høyvik basement-cover pair before ~449 Ma (Andersen et al., 1998), whereas the proximal part of the rifted margin in the south apparently was little affected by this event.

With regard to the points discussed above, we support the model that interprets the large crystalline basement nappes of South Norway as a former microcontinent. Although, separated from the main Baltica continent by hyperextension and formation of the magma-poor OCT-unit, it still formed part of the Baltican lithospheric plate in the period between the Ediacaran and the Silurian. An outboard palaeoposition of these continental blocks was already suggested by Andersen et al. (1991, 2012) and Jakob et al. (2018), who interpreted these continental units as part of a microcontinent or continental sliver, referred to as the Jotun Microcontinent (Andersen et al., 1991). We suggest that the microcontinent included the Dalsfjord, Lindås, and Jotun NCs, if not all the large AMCG–nappe complexes in Southern Norway.

3.2 The magma-rich to magma-poor transition zone

Almost all the Neoproterozoic sedimentary sequences that are structurally above the sheets of allochthonous Baltican basement, including the Lower Bergsdalen NC, Tännäs, Høvringen, Rudihø and Mukampen gneisses, contain mafic igneous rocks. Because, these metasediments are interpreted to represent Meso–Neoproterozoic pre- to syn-rift sediments that were deposited on the thinned Baltican craton, the mafic (and minor felsic) intrusions within these sedimentary sequences must be younger. The rocks of the Heidal Group, Hummelfjell Group, as well as the Särv and Seve nappes can be correlated by their petrology, depositional age, and tectonostratigraphic position. Several of them contains diamictites interpreted as tillites and some also contain newly discovered stomatolites (Kjøll et al.; 2019a). Therefore, we follow the classical interpretations of Tørnebohm (1896) and Holmsen (1943), that the mafic intrusives in the Neoproterozoic sequences of the Hummelfjell Group can be correlated with those in the Särv and Seve NCs, which were emplaced by LIP–magmatism (Tegner et al. in press) at ~608–596 Ma (see section 2.2.3 and Fig. 4-4).

The regional correlation of these units results in a relatively simple tectonostratigraphy for the South-Central Caledonides (Fig. 4-4), i.e. from base to top: 1) basement with cover (also in windows); 2) Neoproterozoic metasediments mostly without mafic igneous rocks; 3) a level of thin allochthonous basement gneisses; 4) Neoproterozoic metasediments with mafic igneous rocks; 5) Cambro-Ordovician metasedimentary complexes with abundant meta-peridotite bodies; and 6) the outboard ophiolite/island-arc complexes, including the Trondheim NC.

Although masked by some additional complexities, this simple tectonostratigraphy of the South-Central Caledonides can also be recognised in the South Caledonides. The structural position of the Upper Bergsdalen NC between the Jotun NC (above) and the metaperidotite-bearing metasediments (below), suggests that it originated outboard of the transitional crust basin. Because the Upper Bergsdalen NC trails out into the Ordovician OCT assemblage near Sognefjorden (Fig. 4-2), it apparently was also separated from the Jotun Microcontinent; at least during the shortening of the margin but perhaps since the Ediacaran. Because of the presence of a mafic dyke swarm in the Høyvik Group of the Dalsfjord NC and a lack of mafic intrusions in the units structurally below the Jotun NC and in the metasediments of the Blåmannen Nappe, we suggest that the magma-rich margin of Baltica was diverted to the outboard side of the Jotun Microcontinent. Because of the similarities of the Neoproterozoic succession, it is possible that mafic dykes in the quartzites of the Lower and Upper Bergsdalen NCs may also have been emplaced during the Ediacaran; although this remains to be substantiated by radiometric dating.

As discussed above, the rift-inherited domains of the Pre-Caledonian margin along strike of the orogen include a magma-rich part preserved in the Särv and Seve NCs a magma-poor part that is presently structurally below the remnants of the Jotun Microcontinent (Fig. 4-4). The Neoproterozoic continental margin successions between the magma-rich part in the north-east and the magma-poor part in the south-west are characterised by a south-westerly decrease in the abundance of syn-rift mafic plutons and volcanics. We interpret this progressive reduction of mafic igneous rocks in the Hummelfjell and Heidal groups to represent a magma-rich to magma-poor transition zone that stretches for about 200 km from the Särv (Tossåsfjället basin) and Seve NCs to the north-eastern termination of the Jotun NC (Heidal Group). It is also noteworthy that the transition also coincides with the pre-rift Sveconorwegian lineament parallel to Gudbrandsdalen (see above; inset map in Fig. 4-2 and Fig. 4-6). The radiometric evidence as well as the pre-deformation and metamorphic relative ages of the mafic intrusives within the Seve and Särv NC, which correlates with the Hummelfjell Group, demonstrate that the magma-poor to magma-rich transition zone is a primary rift-inherited feature of the Central Caledonides and Ediacaran in age.

3.3 Correlation of Ordovician sequences in the South-Central Caledonides

The correlation of the tectonic units in the South and South-Central Caledonides presented above is further corroborated by the continuity of the peridotite-bearing OCT assemblages from the Bergen Arcs to the Skardøra Antiform (Figs. 4-2, 4-3, 4-4). The cross sections A to C (Fig. 4-2, 4-3, 4-5) demonstrate the consistent organisation of the nappe complexes (see section 3.2). However, a complexity is added by the presence of the Jotun Microcontinent and the Bergsdalen NCs in the SW. The Neoproterozoic successions are not present between Stølsheimen and Lom. It is likely that these units were excised by the post-orogenic extension during exhumation of the WGR (e.g. Andersen et al., 1991; Fossen, 2010).

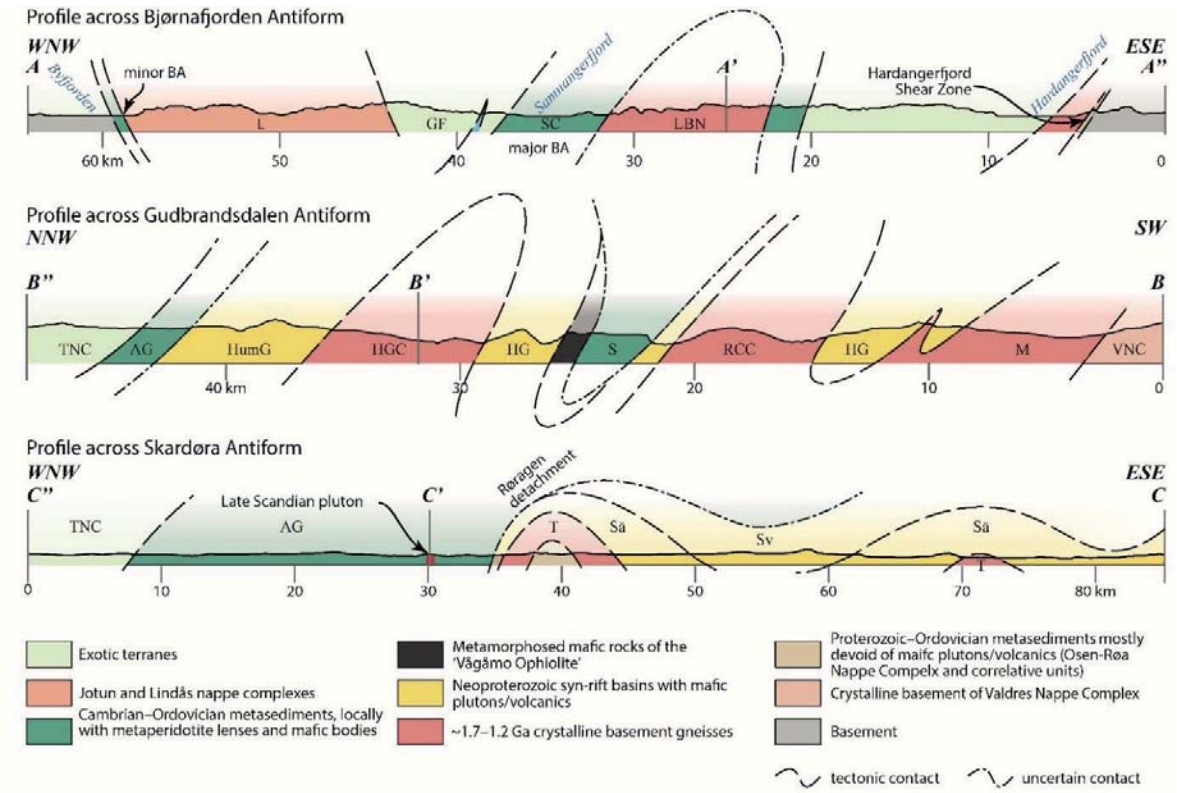

Figure 4-5: Simplified cross sections across the OCT-type assemblages in South and Central Norway illustrating the tectonostratigraphic consistency of the units (Fig. 4-2, 4-3). No vertical exaggeration. Note that original thrust-related orientations have been rotated during extensional tectonics and that, therefore, a precise reconstruction of fold geometries is difficult. AG–Aursunden Group; BA–Bergen Arc; LBNC–Lower Bergsdalen Nappe Complex; GF–Gullfjellet Complex; HC–Heidal Complex; HGC–Høvringen Gneiss Complex; HumG–Hummelfjell Complex; JNC–Jotun Nappe Complex; L–Lindås Nappe Complex; M–Mukampen Suite; RCC–Rudihø Crystalline Complex; S–Sel Group metasediments; SC–Samnanger Complex; Sv–Seve Nappe Complex; Sä–Särv Nappe Complex; T–Tännäs Augen Gneiss; TNC–Trondheim Nappe Complex; VNC–Valdres Nappe Complex

However, the Cambrian to Ordovician metaperidotite-bearing OCT metasediments can be traced almost seamlessly between Bergen and the Skardøra Antiform. These Cambrian–Ordovician units can be correlated by the litho- and tectonostratigraphy and also a continuous metamorphic signature as well as their depositional age across the Gudbrandsdalen Antiform.

3.3.1 Early–Middle Ordovician reworking of an older rifted margin vs. an Ordovician extensional formation of the Ordovician units

Whereas the depositional and magmatic history of the Neoproterozoic metasedimentary complexes is relatively well-constrained, the origin and significance of the Cambro–Ordovician OCT assemblages is more uncertain due to the paucity of datable rocks in this unit. For the origin of the OCT assemblages three key characteristics must be addressed: (1) the resemblance with other OCT assemblages; (2) the duration of deposition of the matrix sediments into the Middle Ordovician (~470 Ma; Slama and Pedersen, 2015) and (3) the intrusion of minor mafic to granitoid plutons dated at 487–471 Ma (Jakob et al., 2017b). Two scenarios for the formation of the metaperidotite-bearing metasedimentary units might be proposed: (1) The OCT assemblage was formed by reworking of an older Ediacaran basin and OCT zone in the Late Cambrian to Middle-Ordovician; or (2) it was formed by thinning of the crust in the Late Cambrian to Middle Ordovician, which was accompanied or followed by minor intrusions.

In the first scenario, the reworking of an older OCT zone assemblages may have been linked to compression along the Baltican margin in the Late Cambrian to Middle Ordovician. The reworking of transitional crust inboard of the Jotun Microcontinent was accompanied by the emplacement of minor mafic to felsic igneous rocks into older sediments at 487, 476 and 471 Ma (Jakob et al, 2018) and continued sedimentation with detrital zircons as young as 468 Ma into the Dapingian–Darriwilian (Burton and Harper, 1981; Slama and Pedersen, 2015). Resetting of zircons at 482 Ma in the Øygarden basement window (Fig. 4-2) west of the Lindås NC (Wiest et al., 2018) may also be linked to this event.

Because, there is no radiometric evidence for Pre-Scandian penetrative deformation and metamorphism in the Baltican autochthon of South Norway except at Øygarden (Wiest et al., 2018), the Early-Caledonian reworking likely involved only the outermost part of the Baltica margin, including nappes that comprise the OCT in the magma-rich part of the margin, e.g. the Seve NC, and along the western margin (Høyvik-Dalsfjord segment) of the Jotun Microcontinent.

Other indications for compression, uplift and erosion along the Baltican margin in the Early Ordovician are provided by 482 Ma eclogites in the northernmost Seve NC (Root and Corfu, 2012), the occurrences of turbidites that overly and are intercalated with Early–Middle Ordovician metapelites, which also include the Cr- and Ni-rich Elnes Formation in the Oslo region (Bjørlykke and Englund, 1979; Bruton

et al., 2010) the Föllinge Formation in Sweden (Greiling and Garfunkel, 2007) and Cambrian–Ordovician successions of the proximal basins (Nickelsen et al., 1985). Moreover, from the Gudbrandsdalen area towards the north-east (Fig. 4-3), the OCT assemblage contains an increasing number of mafic bodies. Thus, the Ordovician units may reflect the increase of mafic igneous rocks of the underlying Neoproterozoic successions (section 3.2) and may further support the notion that the metasedimentary complexes between Gudbrandsdalen and the Skardøra Antiform represent the remnants of the reworked outermost rifted margin of Baltica. However, except for one 618 Ma garnet (Cutts and Smit, 2018) no Ediacaran crystallisation ages have been reported from the OCT assemblage.

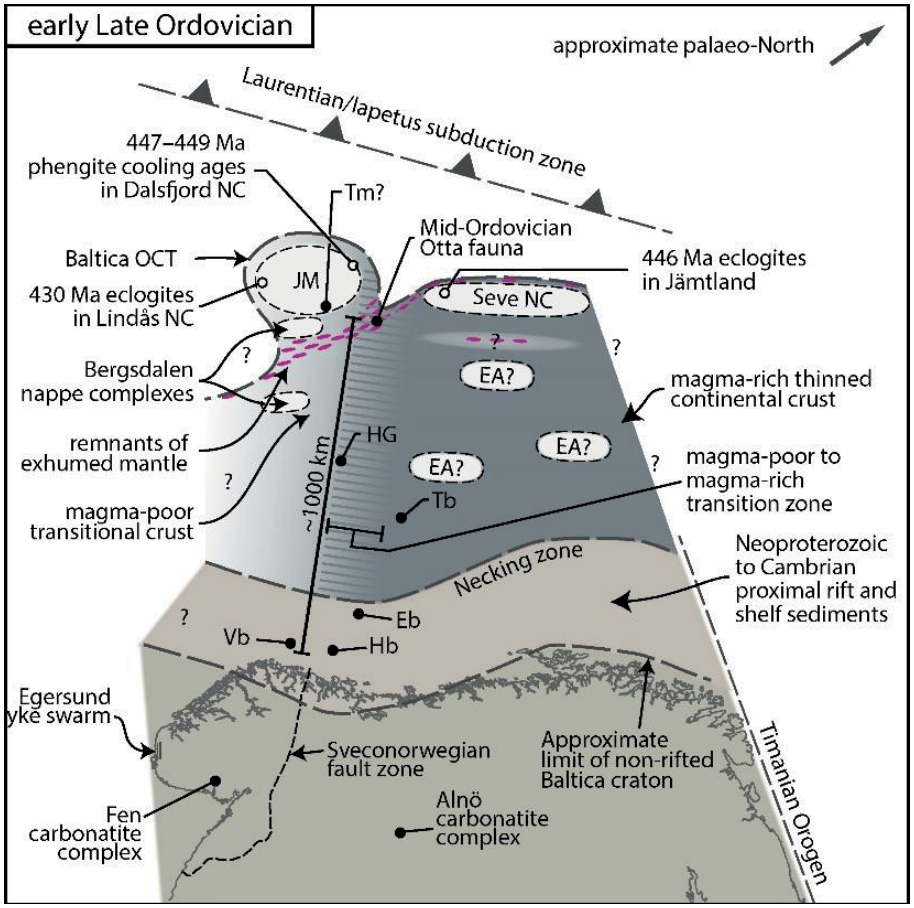

Figure 4-6: Cartoon representation of the architecture of the rifted margin of Baltica in the early Late Ordovician before onset of prolonged Scandian inversion. Figure redrawn from Jakob et al. (2017b); Nystuen et al. (2008). Purple ellipses represent mantle exposed at the sea floor. The island type Otta fauna is placed ~1000 km away from the Baltic craton margin. The size of the Jotun Microcontinent is approximately 200x300 km. Black circles indicate the palaeoposition of thrust nappes. Open circles indicate the palaeoposition of tectonic units and geological events at some time after onset of earliest Scandian inversion of the margin. EA, extensional allochthon; Eb, Engerdalen basin; HG, Heidal Group; Hb, Hedmark basin; JM, Jotun Microcontinent; NC, nappe complex; Tb, Tossåsfjället basin; Tm, Turtagrø metasediments; Vb, Valdres

The closure of the OCT basin inboard of the Jotun Microcontinent and the reworking of the OCT assemblage, is comparable with the closure of narrow oceanic basins in the Alpine Tethys realm as described by Chenin et al. (2017). The difference in style of the pre-Scandian deformation and metamorphism in the South and the Central Caledonides may be directly linked to the presence of the large, strong and mostly intact Mesoproterozoic continental crust of the Jotun Microcontinent, which thwarted pre-Scandian deep burial and deformation compared to deep burial and high-pressure metamorphism of rocks in the Seve NC and along the westernmost Dalsfjord-Høyvik area.

However, except for the 618 Ma garnet, no other rocks in the OCT assemblages yielded Ediacaran ages that could be linked to the opening of the Iapetus whereas Lower Ordovician ages abound. And, because, the minimum age of some of the peridotite-bearing metasediments pre-date a minor 487 ±2 Ma gabbro in the Bergen Arcs (Jakob et al., 2018), these assemblages may have formed during a second phase of rifting in the Cambrian to Middle Ordovician (≥487–468 Ma). A modern-day analogue for this scenario could be the Tyrrhenian basin, that opened in the Pliocene–Quaternary during a phase of hyperextension and rifting after initial phase of opening of the Sardinia Province Basin in the Oligocene–Miocene. (e.g. Prada et al., 2016; Savelli and Ligi, 2017). However, the Tyrrhenian opened in an upper plate, back-arc setting, for which there is little evidence in the Caledonides. None of the Baltican nappes are associated with an arc of that age and the (HPLT) metamorphism in the Høyvik-Dalsfjord and Seve NC rather indicate a lower plate configuration for the distal margin of Baltica.

The OCT assemblage may also have formed by thinning of a forearc basin and subsequent obduction of the Ordovician units onto the Ediacaran sequences. Forearc extension has been suggested for the highly dismembered south Tibetan ophiolites (Maffione et al., 2015). However, because of the lack of evidence for an (intraoceanic) arc along the Baltican margin of that time, the Baltican affinity of discontinuous slivers of crystalline gneisses within the OCT assemblage metasediments (Jakob et al. 2018) and the structural position of the large crystalline NCs, it is difficult to explain the formation of the OCT assemblages in a forearc setting.

As an alternative to an upper plate configuration of Baltica, the OCT assemblage may have been formed with Baltica being the lower plate. On these terms the second stage of rifting and thinning may also have been related to the subduction of the northern part of the Baltica margin at about 482 Ma and may be comparable with the opening of the South China Sea (e.g. Morley, 2002; Clift et al., 2008; Bai et al., 2015; Larsen et al., 2018a).

3.4 Early Scandian shortening of a wide Baltica rifted margin

The main large-scale nappe translation onto Baltica took place during the final continent-continent collision, and the penetrative deformation and (U)HP metamorphism of the Baltican basement occurred in the Late Silurian to Early Devonian, as demonstrated by the continuous SE-NW metamorphic gradient along the floor thrust and into the WGR (e.g. Hacker et al., 2010 ;Jakob et al., 2018; Fauconnier et al., 2014). The outermost parts of the Baltican margin, however, may have experienced shortening as early as ~450 Ma (see above). In figure 4-6 and 4-7 the palaeogeographic position of the basin with the OCT assemblage is constrained by the island-type Otta fauna, for which we estimate a minimum distance to the Baltican craton of about 1000 km, a distance great enough for the Otta fauna not to mix with the Baltican (or Laurentian) cratonic faunas. The Jotun Microcontinent is estimated to have had a minimum size of about 200x300 km based on the present extent of the Jotun, Lindås and Dalsfjord NCs. Thus, the distance between the outboard margin of the Jotun Microcontinent and the cratonic margin of Baltica was in the order of 1200 km.

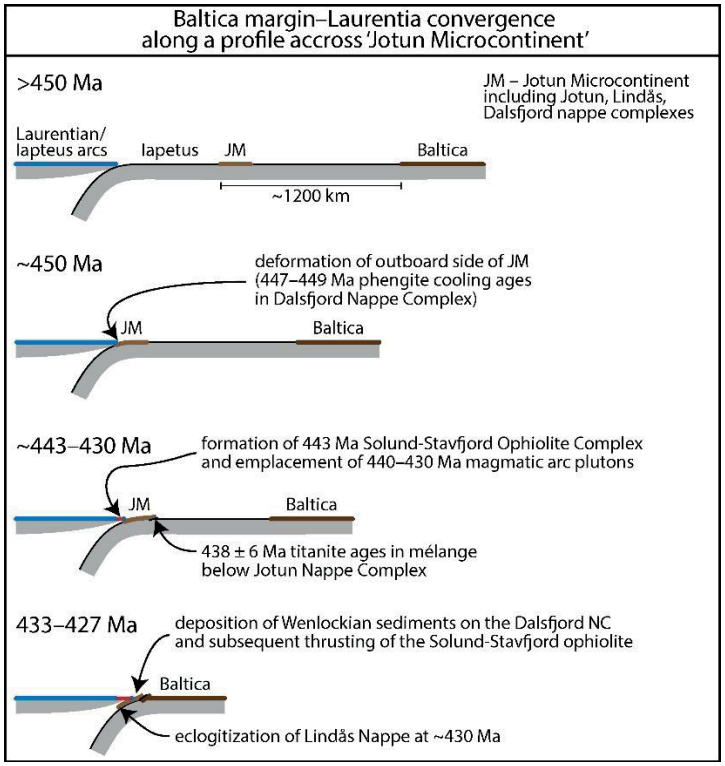

Figure 4-7: Cartoon representation of Iapetus closure and the prolonged inversion of the very wide Baltica rifted margin before the Scandian collision after 430Ma.

Palaeo-plate tectonic models for the closure of the Iapetus Ocean (e.g. Domeier, 2015) indicate that a far outboard Jotun Microcontinent inboard of a seaway as well as hyperextended to rifted segments would have been in contact with the Laurentian cratonic margin at ~450 Ma. The arrival of the Jotun Microcontinent at the Iapetan/Laurentian subduction zone is constrained by the deformation of the Høyvik-Dalsfjord and Seve NC at ~450 Ma as well as by the eclogitisation of the Lindås NC at ~430 Ma. The age constraints for the Scandian deformation are based on the obduction and thrusting of the ~443 Ma Solund-Stavfjord back-arc ophiolite onto the fossil-bearing Wenlockian (433–427 Ma) Herland Group (see summary in

Fig. 4-7). The shortening of the thinned margin was completed at the time the two necking domains of the Laurentian and Baltican continents collided, which coincided with the cessation of subduction-related magmatism, the earliest subduction of the WGR and the emplacement of syn-collisional granitoids in Baltican and Laurentian nappes, including the 430–415 Ma granitoids in the Norwegian allochthons (described-above) and 435–415 Ma granitoids on Greenland and Svalbard (Kalsbeek et al., 2008; Gasser, 2014).

The shortening of ~1200 km of the Baltican margin between ~450 and 435 Ma would have required convergence rates between the Laurentian and Baltican cratons of about 8 cm/yr, which is well within the limits of those of published plate tectonic models (Torsvik et al., 1996; Torsvik and Cocks, 2005; Domeier, 2015). Crustal thickening with maximum burial of the WGR and the thrusting onto the foreland, however, continued into the Lower Devonian.

The eclogites (446 Ma) in mafic dyke swarms hosted by the continental sediments of the Seve NC in Jämtland, Sweden, indicate that this part of the Seve NC was in a similar outboard position (≥1200 km) as the Jotun Microcontinent (Fig. 4-4). The even older HP metamorphic ages in the Seve NC further north (~480 to 460 Ma; Root and Corfu, 2012; Klonowska et al., 2017) may indicate that the onset of deformation along of the Baltican margin was oblique and diachronous, and that the northern part of the Baltican margin was affected before the segments in the south. However, Early–Middle Ordovician faunas of Laurentia, Baltica and at Otta are distinct and the Iapetus probably was at its widest at this time (Torsvik and Cocks, 2017). Therefore, alternative to an Early-Middle Ordovician incipient oblique closure of the Iapetus, the outermost Baltica margin may have experienced a collision (arc-continent?) in the late Cambrian–early Middle Ordovician. However, direct evidence for an arc arriving at the pre-Caledonian Baltica margin at that time is lacking.

3.5 Rift-inheritances in the South and Central Caledonides

3.5.1 Rift-inherited domains across-strike in the Scandinavian Caledonides

It is commonly suggested that rift-inherited structures in continental margins are reactivated during collision and have paramount influence on the architecture in mountain belts (Mohn et al., 2012; Vitale Brovarone et al., 2013; Mohn et al., 2014; Epin et al., 2017). It is therefore, important to identify possible rift-inherited structures in the Caledonides and to include those into the tectonic evolution of the orogen.

The rift-inherited magma-rich and magma-poor segments are linked by a strike-parallel transition zone of approximately 200 km width (section 3.2). Rift inheritance is also seen in transverse sections of the mountain belt. The consistency of the tectonostratigraphy and the characteristic lithological assemblages within the main tectonic units play a key-role in this interpretation (Fig. 4-4, 4-5, 4-6). In particular, the

sediment-hosted metaperidotite-bearing assemblages represent a ‘marker horizon’ that links the South-West with the Central Caledonides. This OCT zone-remnants are at a consistent structural level and allow for a re-interpretation of the across-strike architecture of the mountain belt. The traditional use of Lower, Middle and Upper Allochthon is inadequate as previously outlined by Corfu et al. (2014), because, the tectonostratigraphy is inherited from the highly irregular rifted margin and is not a result of shortening of a continuous and uniform rifted margin. Therefore, the nappe stack is better described in terms of rift-domains defined by comparison with present-day margins, including the proximal and necking domains and as well as hyperextended and distal domains, with or without major magmatic components (e.g. Peron-Pinvidic et al., 2013).

The proximal/necking domain of the Scandinavian Caledonides includes the (par)autochthonous and allochthonous Neoproterozoic successions that contain little to no syn-rift magmatism, e.g. the Osen-Røa, Synnfjell, Dividal and Risbäck NCs (see also Fig. 4-4). These proximal rift basins record a dominantly siliciclastic input until the occurrence of minor mafic plutons and volcanics (Nystuen, 1983; Nystuen et al., 2008; Lamminen 2011). After the early rift-phase and minor mafic magmatism, the sediment system changes from siliciclastic dominated to carbonate and carbonate-shale dominated (e.g. the Biri Formation). Similar carbonate and carbonate-shale successions are also reported from the rift basins of eastern Laurentia (e.g. Nystuen et al., 2008), which indicate a comprehensive rift-wide change of the system.

Relative changes in sea level move the sedimentary depo-centres either continent-ward or ocean-ward during transgression or regression events, respectively. However, changes in the tectonic activity comprehensively changes the sediment influx into the rift system (e.g. Mohn et al., 2010). For example, the cessation of tectonic activity in proximal rifted-margin basins is believed to coincide with and to be linked to the development of so-called thinning faults due to localization of extension in the future necking and distal domains and the onset of lithospheric break up (Mohn et al., 2010; Mohn et al., 2011). Therefore, the contemporaneous occurrence of carbonate and shale formations, immediately after a phase of minor mafic magmatism, that seal the previously deposited, siliciclastic, main-rift sequences in many proximal rift basins along the Baltican and Laurentian margins, may indicate the cessation of tectonic activity within these proximal basins. We suggest that the proximal basins record an early rift-phase of initial distributed extension until the localization of extension in the future necking and distal domains and that the localization of extension was broadly contemporaneous with the syn-rift magmatism.

With the exception of the nappes comprised of continental metasediments structurally below the Jotun NC, the proximal basins are consistently overthrust by a series of thin crystalline basement nappes with Baltican affinity (Lower Bergsdalen Nappe, Tännäs, Høvringen, Rudihø and Mukampen gneisses). A simple restoration of these nappes require that these gneisses originally were positioned outboard of the

proximal domain of the margin. Moreover, their consistent structural position indicates that they represent a regional structural element in the continental margin rather than local imbrications. In present-day passive margins, the hyperextended domain (if identified) is positioned between the necking domain and the zone of exhumed mantle in magma-poor margins, or inboard the zone of main syn-rift magmatism in magma-rich margins (e.g. Péron-Pinvidic et al., 2013; Abdelmalak et al., 2017). Because there is little evidence for Ediacaran magmatism reported from these basement nappes, and because of their structural position between the proximal basins and the Neoproterozoic successions, in which syn-rift igneous rocks abound, we suggest that these gneisses represent rift-inherited thinned continental crust (≤10 km), that were outboard of the necking domain after rifted margin formation.

In the magma-poor to magma-rich transition zone and the magma-rich segment of the margin, these gneisses are overlain by Neoproterozoic successions containing abundant syn-rift magmatic rocks, which we interpret as the distal domain of the rifted margin. In the magma-poor segment of the margin the distal domain is characterised by metaperidotite bearing units that are dominantly composed of fine grained metasediments but also include coarser grained metasediments and slivers of continental crust (extensional allochthones). In the South Caledonides, those distal domain assemblages are structurally overlain by the Jotun microcontinent (Fig. 4-3, 4-4, 4-5, 4-6).

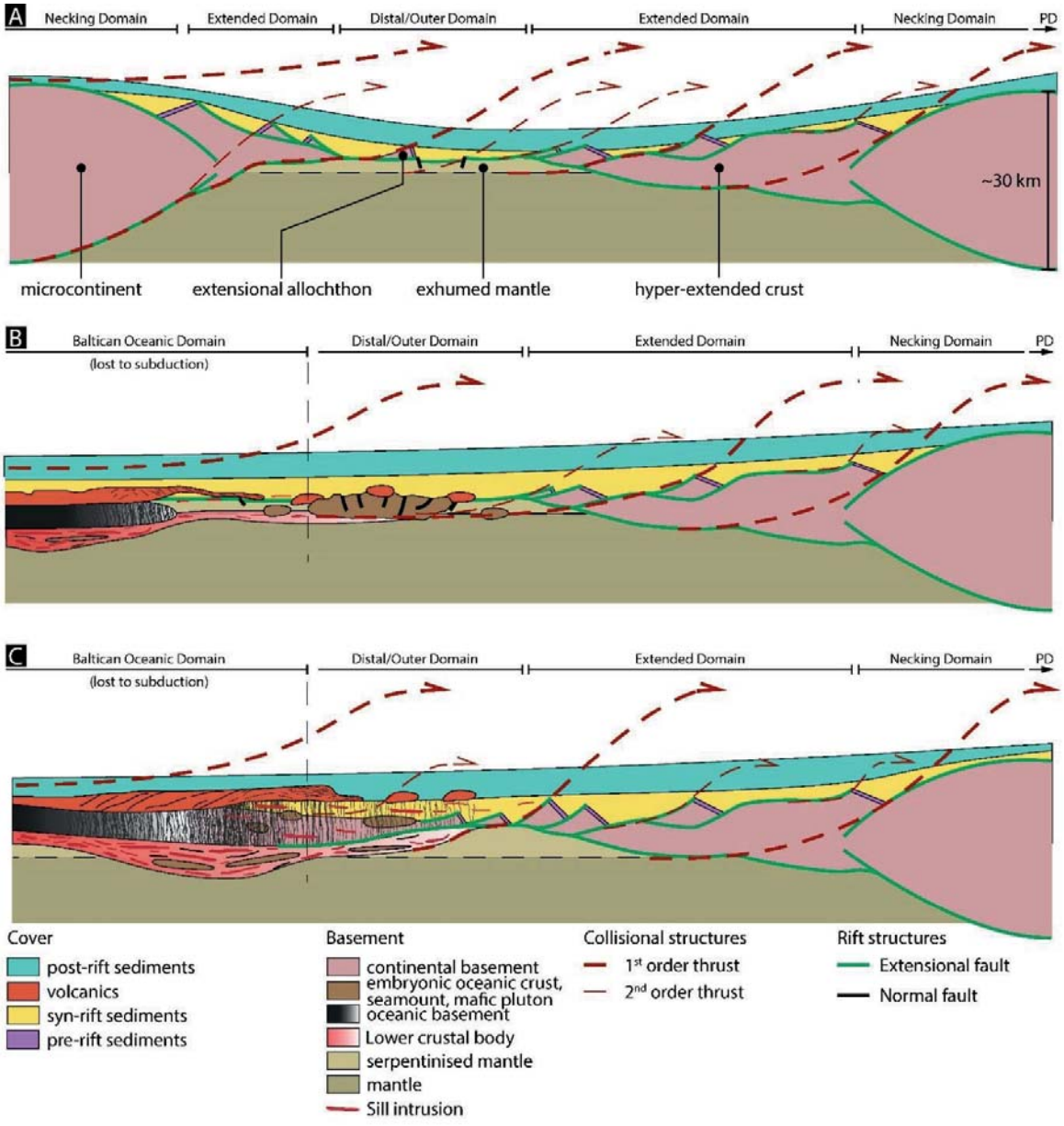

Figure 4-8: A) Conceptual collisional reactivation of rift inherited structures of three rift segments along strike the rifted margin. A) Closure in of a hyperextended thinned magma-poor narrow oceanic basin and between thinned continental crust of the cratonic rifted margin and a microcontinent. Figure redrawn from (Baird et al., 2014; Bernard Bingen et al., 1998; Svenningsen, 2001). (Figure redrawn from Epin et al., 2018). PD—–Proximal Domain. B) Conceptual collisional reactivation of rift inherited structures in section across a magma-poor to magma-rich transition zone. C) Conceptual collisional reactivation of rift

3.5.2 The importance of the rift-inherited margin architecture during the Scandian orogeny

By comparing our observations from the Caledonides with studies in the Alps, we find that structures inherited from the rifted margins were reactivated and developed as major 1st order thrusts systems during the orogenic shortening of the Baltica margin (e.g. Jakob et al., 2018; Manatschal, 2004; Mohn et al., 2011, 2014; Epin et al., 2017) (Fig. 4-8). An imbrication of the rift domains was likely accommodated by smaller 2nd order thrusts exploiting discontinuities within the units, e.g. changes in rheology or along rift-inherited faults. The thrusting during the main orogenic events which probably were separated in time (Ordovician and Silurian to Devonian) was apparently in sequence, because, the stacking-order of Baltican nappes reflects cross-sections of the pre-Caledonian margin. Therefore, for simplicity, the shortening of the Baltica margin is in the following depicted as a single phase of shortening, neglecting possible pre-Scandian tectonism and metamorphism of the outermost margin.

In the Caledonides, nappes that contain the outermost margin of Baltica including the OCT, the extensional basement allochthons, exhumed meta-peridotites, probably also embryonic oceanic crust (or seamounts) at Vågåmo and Røros, as well as other dismembered ophiolites were emplaced onto the Neoproterozoic successions that host the rift-related mafic dyke swarms. Consecutively, the assemblages of the magma-rich and the magma-rich to magma-poor transition zone were thrust over thinned continental crust of the distal domain. The nappes of the distal domain were, in turn, thrust over the Neoproterozoic successions of the proximal/necking domain by a thrust system, which may represent the reactivated thinning faults of the necking domain. Internal imbrication of the individual domains was accommodated by sub-sets of thrust with smaller offsets.

4 Summary and Conclusions

New data and field observations as well as re-interpretations based on a modern understanding of present-day continental margins, put new constraints on the evolution and architecture of the pre-Caledonian margin of Baltica. We suggest that the major differences along strike in the mountain belt originated by the highly irregular and discontinuous template related to the formation of the pre-Caledonian margin of Baltica. The most important change occurred where the large (>200 x 300 km) Jotun Microcontinent rifted away from Baltica in the Neoproterozoic. The NE-termination of the microcontinent may have been inherited from a Middle Proterozoic basement structure, because, the termination of the crystalline nappes correlates with the trace of the Sveconorwegian lineament across southern Scandinavia (Figs 4-1 and 4-7). This structure appears to be a fundamental lithospheric lineament in Scandinavia as seen by the change from shallow to deeper MOHO from SW to NE as well as magnetic anomaly studies

(Kolstrup and Maupin, 2013; Frasetto and Thybo, 2013; Olesen et al., 2010). This pre-Caledonian lineament also coincides with the magma-poor to magma-rich segmentation along the continental margin as described-above. We suggest that large-scale discontinuities in the Sveconorwegian basement across south Scandinavia were important structural elements both during the construction of the pre-Caledonian margin of Baltica as well as during the Caledonian plate-convergence and Scandian collision.

This study shows that the present-day tectonostratigraphy of the South and South-Central Caledonides was formed by the orogenic shortening of a highly irregular, Ediacaran, pre-Caledonian, rifted margin of Baltica. The nappe stack from its base to the top reflects a cross section from proximal to distal rift domains. A summary of observations and interpretations presented above include:

- After the post-Sveconorwegian assembly of Rodinia, followed a long (~200 Ma) period of attempted continental rifting, widespread stretching of the shield area and deposition of thick sedimentary successions through the Cryogenic and into the Ediacaran as described by Nystuen et al. (2008).
- The continental break-up and the eventual formation of the pre-Caledonian continental margin of Baltica may have been associated with the arrival of a mantle plume and widespread plume-magmatism at ~615–595 Ma (e.g. Bingen et al., 1998; Svenningsen, 2001; Baird et al., 2014; Tegner et al., 2019; Kjøll et al., 2019a).
- Most of the pre-Caledonian margin of Baltica facing the Iapetus Ocean, including the less-well preserved westernmost margin of the Jotun Microcontinent was apparently magma-rich. However, inboard of the Jotun Microcontinent opened a magma-poor basin and seaway that was floored by hyperextended to transitional crust (Andersen et al., 2012; Jakob et al., 2018). Rift-related mafic igneous rocks have not been identified in this basin or in the adjacent autochthon of Baltica except for the mafic ~615 Ma dyke swarm in the Egersund area (Bingen et al., 1998).
- The along-strike transition from the magma-rich to the magma-poor part took place over an approximately 200 km long orogen-parallel zone between Røros and Vågåmo. This magma-rich to magma-poor transition zone is preserved in the Neoproterozoic successions of the Hummelfjell and Heidal Groups, which represent a continuation of the Särv and Seve NCs into Norway. Additional elements of the magma-rich to magma-poor transition are the incipient formation of oceanic crust in the OCT zone, which locally may be preserved between Vågåmo and Røros as well as in the continuation of OCT assemblage into Sweden (Nilsson and Roberts, 2014).
- A poorly-understood early subduction and shortening of the outermost Baltica margin may have occurred already during latest Cambrian to the Middle Ordovician and affected mainly the Seve NC. This pre-Scandian event may have been associated with or coincident with the reworking of the older hyperextended margin or a second phase of extension in the South Caledonides.

- Major shortening of the Baltican margin started at about 450 Ma when the outermost parts of the very wide (≥1200 km) Baltican rifted margin entered subduction zone(s) in front of Laurentia.
- Deformation in the proximal/necking domains as well as the large-scale nappe translation over the Baltican craton, Scandian metamorphism and associated granite magmatism took place during the Scandian Orogeny (continent–continent collision) in the late Silurian (after ~430 Ma) into the Early Devonian.
- The across-strike architecture of the nappe stack can be attributed to the stacking of rift domains. In the Central Caledonides, the stacked rift domains, from top to base, include the distal margin with the fossil OCT and break-up magmatism, remnants of the hyperextended domain and proximal rift basins. In the South Caledonides, the nappe stack also includes the Jotun Microcontinent thrust over the remnants of a failed rift hyperextended basin, floored by transitional crust. In the NE it is transitional into magma-poor to magma-rich transition zone and overlies the proximal Neoproterozoic basins. In SW the Upper and Lower Bergsdalen NCs, near the southern termination of the Jotun Microcontinent, were originally outboard and inboard of the hyperextended basin, respectively, and all units were thrust over the proximal basins. All of the rift-inherited tectonic units are structurally overlain by the outboard nappes with origins in the Iapetus and Laurentia.

Acknowledgements

We thank Geoffroy Mohn for fruitful discussions during field trips in the Scandinavian Caledonides as well as the Alps. Johan Petter Nystuen is thanked for many discussions regarding the pre-Caledonian Margin of Baltica. Comments by reviewers Håkon Fossen, Trond Slagstad and Othmar Müntener improved greatly the manuscript. The Centre for Earth Evolution and Dynamics is funded by CoE-Grant 223272 from the Research Council of Norway and this research is funded by is funded by Grant 250327/F20 from the Research Council of Norway to the project “Hyperextension in magma-poor and magma-rich domains along the pre-Caledonian passive margin of Baltica”.

Epilogue

This thesis presents field observations from a suite of rift-related rocks preserved in the Scandinavian Caledonides. The rocks formed in the Late Neoproterozoic when Baltica and Laurentia rifted apart with the help of a mantle plume. The study area comprises a thick sedimentary succession of rift-related rocks that show the transition from an incipient sag-basin into a proper rift-basin. The succession also includes a glaciogenic diamictite unit, correlated with the Marinoan glaciation. The entire sequence was buried to 8-14 km depth when it was cut by a plume-related mafic dyke swarm, which caused local contact metamorphic partial melting and an upward migration of the brittle-ductile transition. The magma influx rate was greater than the tectonic stretching rate and this caused the entire crust to be inflated by mafic magma and cause local vertical thickening in the rift zone.

Due to the dense nature of such areas, as they are mainly comprised of mafic rocks, they are rarely exposed at the surface. The rocks studied herein were thrusted onto Baltica during the Caledonian Orogeny and were not lost to subduction. Locally, the rocks have escaped most penetrative Caledonian strain and reside within kilometer scale boudins. This has provided the unique opportunity to study the deep parts of a magma-rich rifted margin, which is generally poorly known due to challenges related to sub-basalt seismic imaging. The observations and analytical results presented here therefore shed light on processes that are otherwise hidden or camouflaged in seismic noise. Furthermore, it also allows to study details on the meter- to micro-scale adding important knowledge on the ambient conditions during continental rifting in a magma-rich tectonic setting.

Appendices

Appendix 1

Methods

1. Field work

Part of this field work has been conducted in remote, mountainous areas where proper planning is key to obtaining good results. The primary transportation methods have been by helicopter and on foot. National parks in Norway and Sweden have an intricate application system for landing and sampling permits, which altogether have taken several weeks to complete. Some of the field work was also carried out on foot, with helicopter drop-off and pick-up, spending several nights camping with colleagues or alone.

A total of four field seasons from 2015 to 2018 have been conducted for this thesis, in the areas indicated in figure 0-12. These field trips have included lithological and structural mapping as well as sampling for geochemistry, geochronology and thin section petrography. A total of 435 samples has been collected for petrography and geochemical analyses on the SEM, EMPA or whole rock analyses.

2. Photogrammetry

An integral part of this thesis has been to take large overview photographs of mountain cliffs which expose the dyke swarm (Kjøll et al., 2019a; 2019b; Chapter 1 and 2 this thesis). These models were acquired using two methods: 1) DSLR camera with an attached GPS and 2) DJI Phantom 4 drone with camera and GPS sensor. The georeferenced pictures were then processed using Adobe Lightroom to highlight contrasts and colors before further processing and building of a 3D model was conducted using Agisoft PhotoScan Professional. The 3D model was then exported as an .obj which can be read by the open source software Lime, developed by the Basin Research Group at the University of Bergen (Buckley et al., 2019). This software allows direct measurements of lines and planes using two and three reference points, respectively.

3. U-Pb Chemical Abrasion Isotope Dilution Thermal Ionization Mass Spectrometry (CA-ID-TIMS)

Cleaned rock samples were crushed prior to heavy mineral separation using magnetic properties and density (DIM; 3.1 g/cm^3). Zircons were selected by hand under the binocular microscope based on color, clarity, crystal shape and internal structures. The zircons were then chemically annealed for 72 hours at 900°C. After the annealing, the zircons were chemically abraded in HF at *c*. 180°C to remove any crystal

domains containing extensive radiation damage and thus subjected to Pb-loss. Different durations of the chemical abrasion were chosen on the basis of the zircon appearance, if strongly metamict, the chemical abrasion only lasted for 3 hours, if clear with no visible defects 15 to 20 hours were chosen. The picked zircons were then photographed and washed in the ultrasonic with HNO_3, water and acetone to remove contaminants. After weighing the zircons were loaded into Teflon bombs with a ^{205}Pb-^{202}Pb-^{235}U spike, HF- and HNO_3 and dissolved at about 200°C for 5 days. In order to remove cations that may inhibit ionization, the zircon solutions were passed through anion-exchange resin in micro-columns (Krogh, 1973). The wash was kept for Lu/Hf analysis. The Pb and U sample, together with a silica gel, was then loaded onto a degassed Re-filament and measured in a Finnigan MAT 262 mass spectrometer at the University of Oslo. The blank composition at the University of Oslo TIMS lab is $^{206}PB/^{204}Pb$ = 18.59 ±91%, $^{207}Pb/^{204}Pb$ = 15.57 ± 0.32% and $^{208}Pb/^{204}Pb$ = 37.52 ± 0.74% (errors are 1σ). Data reduction was done using Tripoli (Bowring et al., 2011) and ages were calculated using excel macros (Schmitz and Schoene, 2007). Concordia diagrams were generated using Isoplot (Ludwig, 1992). A $^{238}U/^{235}U$ of 137.88 was used for the age calculations.

4. U-Pb Laser-Ablation Inductively Coupled Plasma Mass Spectrometry (LA-ICP-MS)

The samples that were collected for detrital zircon analyses were washed and cleaned in the ultrasonic bath for 10 minutes to remove all residue form the surface, before they were crushed in two stages: 1) Jaw crusher, 2) Retsch mill. The crushed rock was then panned, and zircons were handpicked and randomly sampled for analyses. The sampled zircons were cast in epoxy resin, polished and imaged by cathodoluminescence (CL) or UVD using a JEOL JSM 6460LV scanning electron microscope at the University of Oslo. U–Pb analyses were carried using a Nu Plasma HR multi-collector mass spectrometer with a NewWave LUV 213 Nd-YAG and a Cetac LSX-213 G2+ laser microprobe at the Department of Geosciences, University of Oslo. The analytical protocols of Andersen et al. (2009) and Rosa et al. (2008) were followed for U–Pb. A beam diameter of 50 μm and a pulse frequency of 10 Hz were used during acquisition. Data reduction was done using a excel spreadsheet program for U–Pb, U–Pb ages were calculated using the decay constants of Steiger and Jäger (1977). Discordance percentages were calculated as described in Kristoffersen et al. (2013). Ages are given as ^{206}Pb–^{238}U and only ages that are less than 10% discordant are used for the age probability plots. Zircons from GJ-1 (Belousova et al., 2005), 91500 (Wiedenbeck et al., 1995) and A382 (Huhma et al., 2012) were used as standards to calibrate the data. The open source software “detzrcr”, written for “R” was used to plot the data (Andersen et al., 2018).

5. Jadeite-in-clinopyroxene geothermobarometry

Well-preserved and alteration free clinopyroxene crystals were chosen from carbon-coated thin sections and 2-5 EMPA measurements were conducted for each chosen crystal. Individual analyses were coupled with the "liquid" composition, assumed to be similar to the whole rock composition of the chilled margins of the dikes as the rocks in question show no evidence for glass and the chilled margins presumably quenched against the host-rock, not allowing for any differentiation to occur. The excel spreadsheet provided in the supplementary material of Neave and Putirka (2017) was utilized for the calculations. Four filters proposed by Neave and Putirka (2017) were applied considering 6 oxygen a.p.f.u: 1) stoichiometry, excluding all stoichiometric values > 4.02 and < 3.99; 2) minimum value of 0.01 for the jadeite component; 3) minimum value of 0.11 for Al and 4) equilibrium with the proposed liquid composition. The latter was constrained from whole-rock compositions where chilled margins were preserved. A one standard deviation test was applied to each sample to exclude outliers.

6. Ti-in-Bt geothermometry

For temperature calculations Titanium-in-Biotite geothermometry, developed by Engel and Engel (1960) and refined by Henry et al. (2005), was conducted on carbon-coated, polished thin sections. The biotites varied in size from *c.* 100μm to 1mm and occur with a seemingly random orientation within compositional bands that define the bedding, together with dendritic and poikilitic garnets. Within these bands, biotite is the dominant mineral. Other minerals found include quartz, plagioclase, orthoclase and muscovite with accessory minerals dominated by zircon, apatite and tourmaline. Only samples with homogenous signature when viewed with BSE were used in the calculations. The calculation utilizes Mg/(Mg+Fe) and Ti (a.p.f.u) normalized considering 22 oxygen atoms. Outliers from each thin section were excluded by subjecting the data to 2σ test. An average from each area was calculated from all the analyses that fell within the 2σ brackets.

7. Theriak Domino

Samples of meta-sediments, collected in the field at various distances from the dikes, were cut in such a way that the mineralogy could be considered homogenous, i.e. zones of similar composition was collected and crushed into fine powder. Major, minor and trace element composition were measured using XRD at Bureau Veritas Commodities Canada Ltd.

The chemical input for Theriak Domino (de Capitani and Petrakakis, 2010) data was calculated from the oxide whole rock weight percent composition and reduced into the chemical system KNCFMASH. The rock was fluid saturated at the time of dike emplacement. Garnet isopleths and pseudosections were calculated using Theriak-Domino and put together using adobe illustrator.

Appendix 2

Detrital zircon data

HJK_1032

69.763786N, 21.680540E

Sample/ spot #	[U] ppm	Conc% Central	Ages $^{207}Pb/^{206}Pb$	±σ	$^{207}Pb/^{235}U$	±σ	$^{206}Pb/^{238}U$	±σ
1032r-47	103	-9.8	1709	19	1625	17	1561	26
1032r-59	440	-9.7	1322	16	1247	13	1205	18
1032r-85	90	-9.7	1709	21	1625	11	1561	10
1032r-7	748	-9.4	1626	15	1546	13	1489	20
1032r-68	165	-9.3	1031	18	969	12	942	15
1032r-9r	292	-9.2	1680	14	1601	14	1542	20
1032r-23	215	-9	1600	14	1525	13	1471	18
1032r-64	1133	-9	1612	22	1537	18	1483	25
1032r-83	206	-9	1504	20	1431	11	1382	10
1032r-40	63	-8.9	1514	22	1442	20	1393	29
1032r-62	117	-8.9	1691	17	1615	17	1557	25
1032r-43	2950	-8.7	1126	14	1065	11	1035	14
1032r-12	410	-8.6	1646	14	1573	13	1519	20
1032r-13	154	-8.6	1255	13	1191	10	1156	14
1032r-41	367	-8.4	1517	15	1448	13	1402	18
1032r-72	250	-8.2	1668	20	1599	10	1547	9
1032r-112	148	-8.2	1646	21	1577	11	1525	10
1032r-3	516	-8	1188	13	1131	10	1101	13
1032r-84	468	-8	1397	19	1334	9	1296	8
1032r-101	215	-8	1622	20	1555	11	1506	10
1032r-18	360	-7.9	1498	14	1434	12	1392	17
1032r-70	91	-7.6	1518	18	1456	16	1414	23
1032r-106	138	-7.6	1668	21	1604	11	1556	11
1032r-6	422	-7.5	1674	14	1611	14	1563	21
1032r-25	334	-7.5	1637	15	1574	13	1528	19
1032r-107	82	-7.5	1495	20	1435	10	1395	9
1032r-22	316	-7.4	1594	14	1532	13	1488	18
1032r-77	157	-7.3	1168	18	1115	8	1089	7
1032r-108	212	-7.3	1639	20	1577	11	1532	10
1032r-20c	979	-7.2	1603	14	1542	13	1499	19
1032r-10	736	-7.1	1393	13	1338	12	1304	16
1032r-103	146	-7.1	1624	21	1565	11	1522	10
1032r-110	150	-7.1	1614	20	1555	11	1511	10
1032r-4	294	-7	1154	14	1104	10	1079	13

1032r-17	1458	-6.9	1599	14	1542	13	1501	19
1032r-26	408	-6.9	1666	15	1607	13	1563	20
1032r-96	415	-6.9	1993	22	1931	13	1874	14
1032r-30	109	-6.8	966	16	922	9	904	11
1032r-42	111	-6.8	1501	16	1446	13	1409	18
1032r-35	232	-6.6	1693	14	1637	13	1594	20
1032r-102	703	-6.5	1726	20	1670	11	1626	10
1032r-9c	434	-6.4	1678	15	1623	14	1582	21
1032r-48	217	-6.4	1619	16	1566	15	1527	23
1032r-86	356	-6.3	1683	20	1630	11	1589	9
1032r-28	1317	-6.2	1453	14	1403	12	1371	17
1032r-55	129	-6.2	1708	17	1655	16	1614	25
1032r-57	224	-6.2	1686	17	1634	16	1594	25
1032r-91	497	-6.2	1691	21	1639	11	1598	10
1032r-116	484	-6.2	1657	22	1605	11	1566	10
1032r-34	952	-6.1	1429	13	1381	12	1350	17
1032r-73	478	-6	1688	20	1638	11	1599	9
1032r-109	205	-6	1623	20	1574	11	1537	11
1032r-113	649	-6	1549	21	1500	11	1465	10
1032r-97	311	-5.9	1509	20	1462	10	1430	8
1032r-78	363	-5.8	1744	20	1695	11	1655	11
1032r-2	333	-5.7	1621	14	1573	13	1538	20
1032r-27	634	-5.6	1618	15	1572	13	1538	20
1032r-29	478	-5.6	1092	14	1054	10	1035	12
1032r-105	463	-5.6	1501	20	1456	10	1425	9
1032r-33	357	-5.3	952	14	918	9	904	10
1032r-45	147	-5.3	1651	16	1607	15	1573	23
1032r-79	524	-5.3	1503	20	1461	10	1432	9
1032r-24	569	-5.2	1529	14	1487	12	1458	18
1032r-63	999	-5.2	998	16	964	11	950	14
1032r-69	995	-4.3	1468	17	1434	15	1411	23
1032r-61	850	-3.9	1163	16	1136	12	1121	16
1032r-32	987	-3.7	1501	14	1472	12	1452	18
1032r-94	123	-3.7	1271	21	1244	9	1228	8
1032r-58	804	-3.6	1539	16	1510	15	1489	23
1032r-71	181	-3.6	1152	19	1127	8	1114	6
1032r-65	522	-3.5	1260	17	1234	14	1220	19
1032r-100	325	-3.4	1131	20	1108	8	1096	7
1032r-93	437	-3.3	1650	21	1622	11	1602	10
1032r-31	239	-3	933	15	915	9	907	10
1032r-49	760	-2.6	1545	16	1524	16	1509	24
1032r-80	282	-2.4	1642	21	1622	11	1607	11
1032r-56	514	-2.3	949	16	935	10	929	13

1032r-21	1706	-1.8	999	13	987	9	982	12
1032r-1	156	-1.6	904	14	895	8	891	10
1032r-44	88	-1.4	1274	16	1263	13	1257	18
1032r-19	110	-1.3	921	16	912	9	909	11
1032r-50	756	-1.3	1146	16	1136	12	1132	16
1032r-87	1625	-1.2	1224	19	1215	9	1210	9
1032r-37	315	-0.9	1671	15	1664	14	1658	23
1032r-36	346	-0.5	1149	14	1145	10	1143	13
1032r-92	332	-0.1	1040	20	1039	8	1039	6
1032r-51	141	1.5	1459	17	1471	15	1479	23
1032r-111	482	2.2	1569	21	1586	11	1599	12
1032r-95	261	3.4	1659	20	1686	11	1708	12
1032r-104	176	7.6	1543	21	1602	13	1646	16
1032r-98	741	8.2	1601	21	1665	12	1716	15
1032r-53	804	.	1224	15	1224	13	1224	18

HJK_1042

63.072082N / 13.126549E

			Ages					
Sample/ spot #	**[U] ppm**	**Conc% Central**	**$^{207}Pb/^{206}Pb$**	**±σ**	**$^{207}Pb/^{235}U$**	**±σ**	**$^{206}Pb/^{238}U$**	**±σ**
1042-01	50	-4.2	1145	17	1116	8	1101	8
1042-02	107	-5.2	1567	15	1525	9	1495	11
1042-03	506	-5.8	1686	15	1637	10	1600	12
1042-04	351	-6.8	1843	16	1783	11	1733	14
1042-05	358	-5.4	1150	15	1112	7	1092	7
1042-06r	462	-9.4	1244	14	1174	7	1137	8
1042-07c	485	-8.1	1493	14	1428	9	1384	10
1042-08	1982	-5.4	1128	14	1091	7	1072	8
1042-09	91	-7.8	1506	16	1443	9	1400	11
1042-10c	84	-6.1	1689	16	1638	10	1598	12
1042-10r	285	-5.6	1691	15	1643	10	1606	12
1042-11	486	-4	972	15	947	6	936	6
1042-12	385	-3.4	1143	15	1120	7	1108	7
1042-13c	183	-6.4	1661	16	1607	10	1566	12
1042-13r	113	-7.4	1663	16	1601	10	1554	12
1042-14	275	-5.8	1645	15	1597	10	1561	12
1042-15	471	-4.4	1155	14	1124	7	1108	8
1042-16	272	-3.5	1154	15	1129	7	1116	7
1042-17	151	-8	1145	15	1089	7	1061	8
1042-18	431	-4.4	1592	15	1556	9	1530	11

1042-19	166	-5.9	1143	15	1102	7	1081	7
1042-20	288	-4.3	1136	14	1106	7	1091	8
1042-22	153	-6.4	1590	15	1538	10	1500	12
1042-23	163	-4.2	1505	15	1471	9	1448	11
1042-24	580	3.7	936	14	959	7	969	7
1042-25	307	-7.5	1452	14	1392	9	1353	10
1042-25c	389	-4.4	1476	14	1441	10	1418	12
1042-25r	527	-1.5	1468	15	1456	9	1448	11
1042-26	668	-2.6	1488	15	1468	9	1454	10
1042-27	41	-6.6	1645	16	1589	10	1548	13
1042-28	294	-5.1	1128	14	1093	7	1075	7
1042-29	97	-5.7	1649	15	1602	10	1566	13
1042-30	495	-5.5	1467	15	1423	9	1394	10
1042-31	229	-5.2	1245	15	1207	8	1186	9
1042-32	372	-4.2	1658	15	1623	10	1596	13
1042-33	50	-7	1551	16	1494	10	1454	11
1042-34	180	-5.2	1480	15	1439	9	1411	11
1042-35	64	-8	1613	16	1546	10	1497	12
1042-36	258	-4.2	1540	16	1506	9	1483	11
1042-37	810	-4.1	978	15	952	6	941	6
1042-38	193	-7	1548	15	1491	9	1451	11
1042-39	104	-6.4	1607	15	1554	10	1516	12
1042-40	175	-5.8	1247	15	1204	8	1181	8
1042-41	369	-7.1	1678	15	1618	10	1573	13
1042-42	390	-6.5	1651	15	1596	10	1555	12
1042-43r	158	-6.1	1648	15	1597	10	1558	13
1042-44	568	-5.9	1478	15	1431	9	1400	10
1042-45	525	-8.5	1668	15	1596	11	1542	14
1042-46	133	-6.5	972	16	930	7	913	7
1042-47	486	-0.1	1107	15	1106	7	1106	7
1042-48	334	-6.1	1253	15	1208	8	1183	8
1042-49	453	-0.4	1474	15	1471	9	1469	11
1042-51	91	-3.8	946	15	922	7	912	7
1042-52	103	-6.7	1608	15	1552	10	1512	12
1042-53	525	-5.2	1547	15	1505	10	1475	12
1042-54	828	-3.7	1330	16	1302	9	1285	10
1042-55	290	-1.8	1495	15	1481	10	1471	12
1042-57	996	-2	1330	15	1315	8	1306	10
1042-59	134	-5.8	1597	16	1549	10	1514	12
1042-61	442	-7.2	1570	15	1511	10	1469	12
1042-62	367	-9.6	1154	15	1086	7	1052	8
1042-63	163	-6.1	1154	16	1111	8	1089	8
1042-64r	364	-6.2	1624	15	1573	10	1535	12

1042-66	239	-7.3	1506	15	1447	9	1408	11
1042-67	453	-4.5	1136	15	1105	8	1090	8
1042-68	281	-6.5	1685	16	1630	10	1588	12
1042-69	919	-5.9	1258	15	1214	8	1190	9
1042-70	233	-6.1	1516	15	1466	9	1432	11
1042-71	587	-8.4	1217	17	1156	8	1123	8
1042-72	49	-7.4	953	17	906	8	887	8
1042-73	833	-6.2	1580	16	1529	11	1493	16
1042-74	148	-6.8	1689	16	1631	10	1586	13
1042-75	73	-6.5	1268	16	1220	9	1193	10
1042-76	389	-4.8	1255	15	1221	8	1201	9
1042-77	439	-7	1748	16	1688	11	1641	15
1042-80	979	-5.1	1543	12	1502	9	1473	12
1042-85	292	-4.1	1600	13	1567	8	1542	11
1042-86	144	-7.2	946	13	901	6	883	7
1042-88	348	-7.9	1677	13	1610	10	1559	15
1042-91	887	-2.4	1160	11	1144	7	1135	9
1042-92	139	-7.2	1680	13	1619	9	1573	12
1042-93	61	-7.9	1139	13	1084	8	1057	10
1042-94	161	-9.3	1684	12	1604	10	1544	14
1042-95	222	-6.9	1201	12	1151	7	1125	7
1042-96	118	-6.2	1538	13	1488	9	1452	12
1042-97	228	-8.1	1583	12	1515	8	1468	11
1042-98	370	-3.8	1543	12	1513	10	1491	15
1042-100	200	-9.6	1523	12	1444	9	1391	12
1042-101	179	-7	1543	13	1487	10	1447	15
1042-104	305	-6.4	1693	13	1638	9	1596	12
1042-105	185	-7.8	1618	13	1553	9	1505	11
1042-106	351	-5.8	1261	12	1218	8	1194	9
1042-107	180	-8.6	1536	12	1466	9	1418	12
1042-109	467	-3.8	1533	12	1502	9	1481	12
1042-110	232	-7.6	1658	13	1593	9	1545	12
1042-111	381	-9.7	1661	13	1578	11	1517	15
1042-112	599	-6.7	1665	13	1608	9	1565	12
1042-113	324	-7.4	1660	13	1597	11	1550	17
1042-114	152	-4.4	1588	13	1552	9	1526	12
1042-115	449	-1.3	1109	12	1100	7	1096	8
1042-116	277	-2.8	1470	12	1448	8	1433	10
1042-117	631	-2.6	1617	12	1596	9	1579	13
1042-118	383	-3.8	1623	12	1591	9	1568	13
1042-119	349	-4.5	1008	12	979	6	966	7
1042-120	224	-1.7	915	13	905	6	900	7
1042-123	96	-7.4	1578	13	1517	10	1474	13

1042-124	907	-4.4	986	12	958	6	946	7
1042-126	143	-6.9	1546	13	1490	9	1451	12
1042-127	57	-6.4	1546	13	1494	9	1457	12
1042-128	497	-9.6	1288	12	1215	8	1175	9
1042-129	108	-6.5	1147	13	1101	7	1079	8
1042-130	305	-7.1	1478	13	1421	9	1383	12
1042-131	87	-7.9	1544	13	1479	9	1434	12
1042-132	403	-5.4	1568	12	1524	9	1492	12
1042-133	389	-9	1495	12	1422	9	1374	11
1042-135	79	-5.3	935	14	902	7	888	7
1042-137	511	-7.7	1559	13	1495	9	1451	12
1042-138	169	-6.4	1280	13	1232	8	1205	9
1042-139	203	-6.6	1145	13	1099	7	1075	8
1042-140	179	-8.9	1181	13	1116	7	1084	9
1042-142	196	-6.4	1140	12	1095	7	1072	9
1042-144	115	-7.6	1656	13	1592	10	1544	13
1042-145	141	-7.6	1615	12	1552	9	1506	13
1042-146	413	-8.8	1609	13	1535	10	1482	14

HJK_1049

62.983933N / 12.971567E

			Ages					
Sample/ spot #	**[U] ppm**	**Conc% Central**	**^{207}Pb/ ^{206}Pb**	**±σ**	**^{207}Pb/ ^{235}U**	**±σ**	**^{206}Pb/ ^{238}U**	**±σ**
1049-21	1096	-9.7	1432	40	1354	24	1306	27
1049-15c	673	-8.8	1453	35	1383	20	1338	23
1049-11	93	-8.1	1030	34	977	16	953	16
1049-19	692	-7.6	1560	38	1497	24	1454	28
1049-2	493	-6.9	1043	29	997	12	976	12
1049-27c	465	-6.8	977	12	934	15	915	21
1049-26-1	218	-6.7	1367	13	1315	20	1284	30
1049-14	291	-6.5	1631	36	1577	22	1537	26
1049-15r	281	-5.6	1494	35	1449	22	1419	26
1049-9	1458	-5.1	1004	34	971	15	957	15
1049-10c	939	-5.1	1289	34	1251	18	1229	21
1049-7	575	-4.1	1243	29	1214	15	1197	16
1049-5	1786	-3.4	975	29	953	13	944	13
1049-29	1708	-3.3	945	12	924	16	915	21
1049-17	77	-3	933	40	915	17	908	17
1049-23	1395	-2.8	1126	11	1107	17	1097	24

1049-8	69	-2	1139	33	1125	16	1118	18
1049-16c	95	-1.5	1068	36	1058	18	1053	19
1049-16r	200	-0.7	890	39	886	17	884	18
1049-22r	880	-0.4	866	42	864	18	863	18
1049-22c	359	3	1001	41	1020	19	1028	20
1049-27r	413	0	996	12	996	17	996	24

HJK_1001

69.835019N / 21.643498E

			Ages					
Sample/ spot #	**[U] ppm**	**Conc% Central**	**$^{207}Pb/^{206}Pb$**	**±σ**	**$^{207}Pb/^{235}U$**	**±σ**	**$^{206}Pb/^{238}U$**	**±σ**
1001-01c	43	-5.8	1342	11	1298	9	1271	13
1001-01r	174	-2.5	1339	9	1320	9	1309	13
1001-03	77	-2.8	992	10	974	8	966	11
1001-04	104	-2.8	1033	10	1014	7	1006	10
1001-05	268	-3.7	1092	9	1067	8	1055	10
1001-06	153	-7.9	1112	9	1057	8	1031	10
1001-07	1297	-1	1314	9	1307	9	1302	13
1001-08	325	-6.4	1223	10	1176	9	1151	12
1001-09	305	-4.4	978	10	950	7	938	9
1001-10	251	-6.2	1303	10	1256	9	1229	12
1001-11	387	-1.2	1040	9	1032	7	1028	10
1001-12	262	-4.2	1077	9	1049	8	1036	10
1001-13	113	-3.4	1399	9	1373	9	1357	14
1001-14	525	-3.8	1352	9	1323	9	1305	13
1001-15	274	-8	1113	10	1057	8	1031	11
1001-16	162	-5.8	1160	9	1119	8	1098	11
1001-17	229	-0.6	1064	9	1060	10	1059	13
1001-20	667	-0.8	1493	11	1486	12	1482	18
1001-21	430	-5.9	1675	7	1625	9	1587	14
1001-21-2	419	-5	1705	7	1664	9	1630	14
1001-23	110	-7.7	1069	8	1016	6	992	8
1001-24	710	-3.5	1480	7	1452	8	1434	12
1001-25c	81	-8.1	1505	8	1439	8	1395	12
1001-25r	210	-7.7	1455	8	1394	9	1354	14
1001-26-1	152	-5.8	1037	8	998	6	981	8
1001-26-2	125	-4.7	1027	8	996	6	982	8
1001-27c	289	-3	1289	7	1267	7	1254	10
1001-27r	370	2	1307	7	1322	8	1331	12

1001-28	103	-7.9	1067	9	1014	6	989	8
1001-29c	137	-5.7	1038	8	1001	6	984	8
1001-29r	110	-5.1	1030	8	996	6	981	8
1001-31	297	.	1129	7	1129	7	1129	9
1001-32	473	-8.7	1331	6	1265	7	1226	11
1001-33	79	-8.7	1098	8	1038	6	1009	8
1001-34	108	-6.4	1393	7	1343	8	1312	11
1001-35	102	-1.1	1056	8	1049	6	1045	8
1001-36	76	-6.2	990	9	950	6	932	7
1001-37	100	-5.8	1092	9	1053	7	1034	9
1001-38	269	-6.2	1479	7	1430	8	1397	12
1001-39	104	-6.3	1374	7	1325	7	1295	11
1001-40	48	-6	983	10	944	6	928	7
1001-41	381	-5.8	1837	7	1786	9	1743	16
1001-42c	316	-3.8	1068	7	1042	6	1030	8
1001-43	74	-6.7	1016	10	972	6	953	8
1001-44	57	-8.3	985	10	932	6	909	7
1001-46c	197	-5.2	1597	7	1554	9	1523	14
1001-46r	212	-5.8	1606	7	1558	9	1523	14
1001-47c	351	-6.3	1351	7	1303	8	1273	11
1001-48	327	-7.1	1646	7	1587	9	1542	14
1001-50	341	2.7	720	8	734	7	739	8
1001-50-2	82	3.5	759	15	777	18	784	23
1001-51	143	-3.1	1038	9	1017	7	1008	9
1001-53	234	-8.5	1594	8	1523	8	1473	13
1001-54c	248	-7.1	1353	7	1298	7	1266	11
1001-54r	270	-5	1348	7	1309	7	1286	11
1001-56	153	-8.5	1401	9	1334	10	1293	15
1001-57	187	-6.3	1511	7	1460	8	1426	12
1001-58	142	-5.6	1329	7	1287	7	1262	11
1001-59c	224	-8.5	1407	7	1340	8	1299	11
1001-59r	513	-8.9	1157	8	1093	7	1061	10
1001-60	422	-5.2	1011	7	977	6	962	8
1001-61	128	-7.8	1560	8	1496	9	1452	13
1001-62	280	-6.5	1155	7	1109	7	1086	9
1001-63	210	-4	1020	8	994	6	982	8
1001-64	448	-4.3	1337	7	1304	8	1284	12
1001-65	367	-3.1	1026	7	1006	6	997	8
1001-66	140	-7	969	9	925	7	906	9
1001-67	217	-3.4	1036	7	1013	6	1003	8
1001-68	191	-6.2	1188	7	1143	7	1120	10
1001-71	116	-2.5	1038	10	1021	8	1013	10
1001-72	359	-9.6	1596	7	1516	9	1459	14

1001-73	87	-7.1	1038	9	991	6	970	8
1001-77	390	-4.6	1488	7	1452	9	1427	13
1001-78	225	-6	1659	8	1609	9	1570	15
1001-79	226	-5.5	1019	8	983	6	967	8
1001-80	133	-9.5	946	12	886	8	862	10
1001-81-1	193	-7.8	1145	8	1091	7	1063	10
1001-81-2	110	-6.2	1189	9	1145	7	1122	10
1001-87-1	455	-8	1287	13	1227	12	1193	16
1001-88	174	-9.7	1035	13	969	10	941	12
1001-83	598	-9.6	1590	13	1510	14	1453	21
1001-90	103	-6.1	1172	14	1129	11	1106	15
1001-91	479	-4.9	1064	13	1031	11	1016	14
1001-92	398	-8.7	1591	14	1518	14	1467	21
1001-93	371	-6.3	1072	13	1029	12	1009	16
1001-93-2	342	-4.4	1136	13	1106	11	1091	15
1001-94-1	397	-2.1	1475	15	1459	15	1448	23
1001-95	253	-6.4	1039	13	996	10	977	13
1001-98	359	-7.9	2024	14	1953	17	1886	28
1001-99	104	-7.9	1136	14	1080	11	1053	14
1001-100	12	-4.6	1600	19	1563	23	1535	36
1001-101	313	-5.2	1243	14	1205	11	1184	15
1001-102	103	-6.7	1090	15	1044	10	1022	13
1001-106	174	-7	1200	14	1149	12	1123	17
1001-107	111	-4.9	1081	13	1047	11	1031	14
1001-109	229	-2.8	1554	13	1531	13	1515	21
1001-111	309	-8.3	1195	13	1134	11	1103	15
1001-112	84	-7.4	879	16	835	10	818	12
1001-114	252	-9.9	1610	13	1527	13	1467	20
1001-115	107	-4.9	1505	14	1466	13	1439	20
1001-117	271	-3.1	1010	14	990	10	981	13
1001-118	219	-0.8	1038	14	1033	11	1030	14
1001-119	280	-5	1110	13	1075	10	1059	14
1001-120	57	-4.3	1238	15	1207	12	1190	16
1001-122	161	-7.1	1436	15	1381	13	1345	18
1001-123	248	-1.6	1048	14	1037	10	1032	13
1001-124	174	.	1042	15	1042	10	1042	13
1001-125	501	-2.6	1252	13	1233	11	1222	16
1001-126	32	-1.5	1134	12	1124	7	1119	9
1001-127	379	0.1	1327	9	1328	6	1329	8
1001-128c	1007	3.4	1255	8	1280	6	1294	8
1001-129	386	-3.9	1207	8	1179	5	1164	7
1001-130	128	-9.6	1299	9	1226	6	1185	8
1001-131	117	-4.1	1284	9	1253	6	1235	8

1001-132	323	-6.2	1459	8	1411	6	1378	8
1001-133	312	-3.6	1421	8	1393	6	1374	9
1001-134	36	-8.2	1464	11	1398	11	1355	17
1001-135	37	-4.8	1389	11	1353	7	1330	10
1001-136	55	-4.4	958	12	931	5	919	6
1001-137	508	-3.8	1281	7	1253	5	1236	7
1001-139c	366	-5.9	1605	8	1557	7	1521	10
1001-139r	98	-5.8	1597	9	1549	8	1515	11
1001-140	495	-4.1	1150	8	1122	6	1107	7
1001-141	297	-4.5	1273	8	1240	6	1221	7
1001-143	301	-7.9	1153	8	1097	5	1069	7
1001-144	1400	0.9	1006	8	1012	5	1014	7
1001-145	172	-3.8	1060	9	1035	5	1023	6
1001-147	34	-6.7	1039	12	995	6	975	7
1001-148	545	-4.3	1515	8	1481	7	1457	10
1001-149	282	-0.6	1024	8	1020	5	1019	6
1001-150	271	-2.9	1027	8	1008	5	999	6
1001-151	100	-5.8	1242	10	1200	6	1176	8
1001-152	127	-7.9	1078	10	1024	5	999	6
1001-153	622	-3.9	1464	8	1433	7	1413	10
1001-154	232	-4.1	1039	8	1012	5	999	6
1001-156	389	4.8	1034	8	1064	6	1080	7
1001-158	158	-4.4	1486	8	1450	7	1427	9
1001-159	47	-5.4	974	12	940	5	926	5
1001-160	48	4.5	1226	11	1258	8	1276	11
1001-161	210	-5.2	1646	8	1604	8	1571	11
1001-162	704	-3.5	1467	8	1439	7	1420	9
1001-163	119	-8.3	1737	9	1666	7	1609	10
1001-164	552	-2.9	1315	8	1293	6	1280	8
1001-165	231	-5.9	1163	8	1121	6	1100	7
1001-166	198	-5.3	1075	9	1039	5	1022	7
1001-167	58	-5.2	1080	10	1044	6	1027	7
1001-169	69	-7.2	988	10	941	5	921	6
1001-171	748	-4.6	1618	8	1580	7	1552	11
1001-174	147	-7.4	1118	9	1067	6	1042	7
1001-175	12	-7.6	959	19	911	9	891	9

HJK_3077

67.48712N, 17.46725E

Sample/ spot #	[U] ppm	Conc% Central	Ages $^{207}Pb/^{206}Pb$	±σ	$^{207}Pb/^{235}U$	±σ	$^{206}Pb/^{238}U$	±σ
3077-01	116	-13.6	1467	24	1355	17	1286	22
3077-02	132	-0.6	1377	22	1373	14	1370	17
3077-03	171	-2.9	1483	23	1460	15	1444	18
3077-02r	606	5.7	1078	22	1116	12	1135	14
3077-04	28	1.3	1093	24	1101	12	1105	14
3077-05c	30	-1.3	1030	25	1021	12	1017	13
3077-05r	188	1.9	1040	23	1052	12	1058	13
3077-06r	66	-19.3	1317	39	1163	18	1082	17
3077-06c	16	-33.6	1449	38	1149	17	998	13
3077-06c2	16	-12.6	1031	27	946	12	910	12
3077-07r	31	-60.3	1176	40	634	13	493	8
3077-08	188	-10.2	933	25	869	12	844	13
3077-09	67	-6.2	1259	24	1214	14	1188	16
3077-10c	90	-4.5	1474	24	1438	16	1414	22
3077-10r	238	0	1440	24	1440	16	1440	21
3077-11c	83	-34.1	1562	137	1245	60	1070	29
3077-11r	174	-4.4	1125	14	1095	19	1080	27
3077-13	161	-14.3	1336	15	1224	20	1162	29
3077-14	75	-5.9	1378	15	1332	22	1304	34
3077-15	417	-6.8	1133	14	1085	19	1062	27
3077-16	167	-8.1	1225	14	1166	20	1134	29
3077-17	13	-66.9	3051	93	2024	68	1176	52
3077-18	241	-1.1	1102	14	1094	19	1090	28
3077-18r	52	-51.3	1370	32	884	20	703	19
3077-19c	478	-0.1	1171	14	1170	20	1170	30
3077-20c	164	-11.2	1460	15	1369	23	1311	35
3077-20r	54	-7	1397	16	1342	24	1308	36
3077-21	341	-12.8	1166	33	1073	22	1028	27
3077-22	202	-9.7	1704	14	1620	27	1557	45
3077-23c	185	-9.3	1639	13	1560	31	1503	51
3077-23r	139	-27.3	1545	13	1301	26	1159	37
3077-24	137	-3.1	1889	13	1861	37	1837	69
3077-25r	54	-15.7	1389	20	1262	26	1189	37
3077-25c	99	-20.5	991	14	852	19	800	24
3077-26r	160	-4.9	1601	13	1560	31	1531	52
3077-26c	156	-6.7	1575	13	1520	30	1481	49
3077-27r	352	1.4	1454	12	1466	29	1473	49
3077-27c	177	-1.3	1473	12	1463	29	1456	48

3077-27r2	93	-11	1164	13	1085	22	1045	31
3077-27c2	42	-22.2	1278	16	1103	23	1016	30
3077-28	404	4.7	1238	11	1271	25	1291	40
3077-29	1006	8.5	1156	11	1213	25	1245	40
3077-30r	86	-0.2	953	13	952	20	951	28
3077-30c	70	-24	1154	22	974	21	896	26
3077-31c	65	-1.6	1269	13	1257	25	1250	39
3077-32c	96	-4.1	1346	12	1315	26	1296	40
3077-32r	115	-0.1	1312	12	1311	26	1311	41
3077-33	57	-11.3	1062	14	985	21	951	28
3077-34c	38	-27.5	1639	24	1386	27	1227	38
3077-34r	40	-20.5	1257	14	1098	22	1019	31
3077-35c	312	-8.7	1573	12	1501	28	1451	46
3077-35r	135	-17.1	1542	12	1396	26	1303	40
3077-36c	217	2.9	1238	17	1259	21	1271	32
3077-36r	178	-0.2	1223	17	1222	20	1222	30
3077-37	92	-12.9	1226	20	1129	19	1080	26
3077-38	264	-12.7	1860	18	1746	28	1652	46
3077-39c	42	-11.7	1003	20	926	17	894	22
3077-39r	43	-5.7	1104	18	1066	19	1047	26
3077-40c	45	-37.4	1951	81	1560	43	1288	36
3077-40r	77	-0.7	1219	18	1214	22	1211	32
3077-41	767	2.3	1380	16	1398	25	1409	40
3077-42c	35	-32.8	1551	34	1250	25	1082	28
3077-42r	76	-37.7	1658	73	1291	37	1082	29
3077-43	25	-54.5	3052	187	2311	136	1568	134
3077-44	264	1.2	1085	18	1093	21	1097	30
3077-45	154	-1.9	1719	17	1703	30	1691	53
3077-46c	238	-31	1729	136	1432	66	1240	39
3077-46c2	105	1.9	1166	18	1179	23	1186	34
3077-46r	196	-27.7	1355	24	1123	23	1007	30
3077-47	109	-4.8	1091	8	1059	17	1043	25
3077-48	37	-37.4	1361	19	1033	19	885	23
3077-49	34	-28.7	1456	20	1206	20	1072	27
3077-50	143	-6.8	1743	9	1684	25	1638	44
3077-51c	502	1.4	1237	7	1247	21	1253	33
3077-51r	349	-22.6	1556	10	1358	23	1236	33
3077-52r	43	-27.8	935	15	750	16	689	20
3077-53	11	-47	1783	73	1284	39	1007	31
3077-54c	72	0.3	1078	10	1080	21	1081	31
3077-54r	112	-31.9	1075	40	838	27	751	30
3077-55	465	-14.1	1552	38	1432	48	1354	72
3077-58	40	-33.3	1529	48	1225	38	1060	45

3077-57	173	-17.2	1125	36	1001	31	945	39
3077-58r	26	-28.9	971	41	772	24	705	26
3077-59	26	-48.7	1597	81	1102	40	869	34
3077-60	114	-30.2	1528	40	1257	36	1104	46
3077-61	204	-25.3	1523	36	1301	37	1170	50
3077-62	29	-18.9	1399	37	1244	36	1156	49
3077-63	51	-25.6	1450	39	1230	36	1109	46
3077-64	38	-20.1	1282	38	1124	33	1044	43
3077-65	35	-37.5	1266	41	950	29	820	32
3077-66c	48	-39.9	1348	41	995	30	843	33
3077-67	85	2.2	1011	18	1024	12	1031	16
3077-66r	17	-70.2	1623	167	789	50	527	11
3077-68	129	2.4	1475	17	1493	16	1506	25
3077-67r	166	2.9	999	17	1018	12	1026	16
3077-69	68	-29.8	1316	24	1069	14	951	14
3077-70	726	-7.7	942	17	894	11	875	13
3077-71	327	3	1091	16	1110	12	1120	17
3077-72c	213	-11.1	1592	18	1498	16	1433	23
3077-72r	42	-10.4	1570	27	1483	24	1423	35
3077-73	44	-2.7	1529	18	1508	16	1492	24
3077-74c	36	-1.7	1589	18	1576	16	1565	25
3077-74r	24	-14.8	1358	20	1240	15	1174	19
3077-75c	35	-41.2	1381	25	1010	13	848	13
3077-75r	396	1.6	1024	17	1034	12	1039	16
3077-76c	65	-6.1	1364	18	1316	14	1288	20
3077-76r	95	-3.2	1315	17	1291	14	1276	19
3077-77	92	-2.9	1593	18	1570	16	1552	24
3077-78	279	-1.7	1526	18	1513	16	1503	23
3077-79	308	2.9	1124	17	1143	13	1154	17
3077-80	163	-1.6	1761	18	1748	17	1736	27
3077-81	87	-14.6	1212	19	1102	13	1048	15
3077-82	100	-23.9	1467	29	1263	17	1146	18
3077-83	119	-5.3	1444	17	1402	15	1375	21
3077-84	18	-8.7	1068	20	1009	12	982	14
3077-85c	14	-18.6	1278	23	1133	15	1058	18
3077-85r	255	-8.8	1108	23	1047	14	1018	17
3077-86	98	-7.5	1743	25	1678	30	1626	49
3077-87	88	-42.5	1799	195	1358	84	1096	36
3077-88	375	-16.5	1242	84	1116	35	1053	28
3077-89	62	-1.3	1353	24	1343	23	1337	35
3077-90	42	-13.5	1139	32	1042	20	996	25
3077-90r	262	-7.2	1078	23	1028	19	1005	25
3077-91	52	-12.2	1697	24	1592	25	1513	38

3077-92	115	-8.3	1092	24	1035	18	1008	23
3077-93	153	-20.9	1186	25	1028	18	955	22
3077-94	26	-40.5	1556	43	1167	24	969	23
3077-95	28	-3.6	1462	28	1434	22	1415	32
3077-96c	136	0	697	27	698	13	698	15
3077-97r	27	-8.1	1076	29	1021	19	995	22
3077-97c	58	0.4	990	29	993	18	994	22
3077-99	92	-17.7	1189	31	1057	22	995	28
3077-100	56	-24.8	1232	38	1038	19	948	19
3077-101	100	-43.4	1508	44	1093	22	897	18
3077-102c	174	-9.3	1176	35	1109	20	1075	23
3077-102r	252	-21.7	1315	51	1141	25	1052	22
3077-103	107	-14.1	1671	37	1548	27	1460	35
3077-104	67	-15.8	1352	37	1226	23	1156	26
3077-105	99	-14.3	1084	37	984	19	940	21
3077-106	62	-13.6	1388	37	1280	24	1216	28
3077-108	162	-0.6	1346	18	1342	17	1339	26
3077-109	165	4.9	919	17	948	13	961	17
3077-110	78	-10.5	1316	19	1236	17	1191	24
3077-111	396	5.3	1036	17	1069	15	1086	20
3077-112	20	-6.4	1647	20	1594	21	1554	32
3077-113	223	2.6	1398	18	1417	19	1431	29
3077-114	123	-3.3	2671	23	2639	34	2598	71
3077-115	86	-4.4	1013	19	984	14	971	18
3077-116c	89	-6.1	1086	20	1045	15	1025	20
3077-116r	92	-7.1	1058	20	1010	15	988	20

A-15-S-39a and b

68.390199N, 19.215219E

			Ages					
Sample/ spot #	**[U] ppm**	**Conc% Central**	**$^{207}Pb/^{206}Pb$**	**±σ**	**$^{207}Pb/^{235}U$**	**±σ**	**$^{206}Pb/^{238}U$**	**±σ**
A39a-01c	354	-0.5	1678	17	1673	25	1670	42
A39a-01r	939	-2.9	1489	17	1466	24	1450	39
A39a-02	207	-3.9	1301	17	1272	20	1255	30
A39a-03	98	-1.3	1349	17	1339	20	1332	30
A39a-04c	319	-9.4	1457	17	1381	20	1333	31
A39a-04r	965	0.5	1162	17	1165	18	1166	26
A39a-05	409	1.5	1587	17	1600	23	1609	38
A39a-06	190	-4.5	1543	17	1507	22	1481	34

A39a-07	46	-6.8	1067	18	1021	17	1000	22
A39a-08	164	0.6	1702	17	1707	24	1711	40
A39a-09	141	-1.9	1567	17	1551	23	1540	37
A39a-10	67	-23.5	2040	18	1809	25	1615	40
A39a-11	90	-4.1	1030	17	1003	15	991	21
A39a-12c	274	-2.9	1600	17	1577	23	1560	37
A39a-12r	240	-8.3	1521	17	1453	20	1407	31
A39a-13	239	4.9	1334	16	1370	19	1393	30
A39a-14	243	0	2647	19	2647	33	2648	72
A39a-14r	333	-3.1	2581	19	2552	33	2516	68
A39a-15	112	3.4	1512	16	1538	22	1557	37
A39a-24	52	5.3	1514	18	1555	36	1585	62
A39a-25	171	-10.2	1363	17	1283	14	1236	18
A39a-26	101	-13.9	2393	20	2257	20	2110	32
A39a-27	54	-15.2	1247	18	1132	16	1073	21
A39a-28	161	-2.5	1585	17	1565	16	1550	24
A39a-29	96	-6.7	1400	18	1348	12	1315	16
A39a-30	152	-7.2	3213	28	3141	26	3030	49
A39a-31	102	-4	1225	19	1196	11	1180	13
A39a-32	263	-9.3	2691	23	2600	21	2483	36
A39a-33	294	-4	1679	18	1645	14	1619	20
A39a-34	435	-4.9	1619	16	1578	12	1548	17
A39a-35	218	-9.7	1222	16	1151	9	1113	11
A39a-36	958	-3.8	1295	16	1266	10	1250	13
A39a-37	291	-5.8	1443	15	1398	11	1368	14
A39a-38c	209	-4.6	1070	16	1039	9	1025	11
A39a-38r	110	-4.1	1070	16	1043	9	1030	11
A39a-39	560	-4.8	1816	17	1775	13	1740	18
A39a-40c	125	-11.5	1344	17	1254	12	1202	14
A39a-40r	672	-1.2	1448	16	1439	11	1433	15
A39a-41r	168	-4.9	1373	18	1336	19	1313	29
A39a-41c	907	-12.7	1253	17	1157	17	1107	24
A39a-42	421	-5.8	1601	17	1553	22	1518	35
A39a-43	964	-1.2	1179	17	1171	17	1167	25
A39a-44	443	0.8	1028	17	1034	16	1036	22
A39a-45	37	-8.1	1111	22	1055	18	1028	23
A39a-46	165	-3.9	1789	18	1756	24	1728	41
A39a-47	888	-4.6	1451	17	1415	21	1392	32
A39a-48	184	-5.5	1754	18	1707	24	1670	40
A39a-49	409	-13.7	1535	18	1420	21	1344	30
A39a-50	1114	1.6	1452	17	1464	23	1473	36
A39a-51	315	-1.5	1079	18	1069	16	1064	23
A39a-52	829	3.2	1361	18	1385	21	1401	32

A39a-53	209	-3.4	1342	18	1316	19	1300	29
A39a-54	343	-3.7	1650	18	1619	23	1596	38
A39a-55c	148	-10.1	1145	15	1074	14	1039	20
A39a-55r	104	-3.3	1080	15	1058	14	1047	20
A39a-56	212	-15.7	1401	16	1274	17	1200	24
A39a-57	152	-9.3	1071	15	1008	16	979	21
A39a-58	200	-1.9	1746	15	1730	22	1717	38
A39a-59	185	-12.2	1498	16	1397	20	1333	30
A39a-60	306	-2.1	1628	15	1610	21	1597	35
A39a-61	231	-2	1387	15	1371	19	1362	29
A39a-62	187	-2.7	2106	16	2082	26	2057	49
A39a-63	73	-5.3	1232	16	1194	18	1173	27
A39a-64	783	2	1548	15	1564	23	1575	38
A39a-65	492	2.1	1207	15	1222	19	1230	28
A39a-66	226	-6.2	1386	15	1338	21	1308	32
A39a-67	334	0.1	1075	15	1076	18	1077	26
A39a-68	286	2.9	1643	15	1667	25	1685	44
A39a-86	170	-16.7	1882	27	1728	22	1604	30
A39a-87	296	1	1666	9	1674	18	1681	31
A39a-88r	355	1.4	1075	9	1084	13	1089	18
A39a-88c	577	-14	1305	10	1197	15	1137	22
A39a-89	321	-1.8	1027	11	1015	12	1009	17
A39a-90	291	-9.9	1369	37	1292	23	1246	27
A39a-91	228	-7.8	1317	10	1258	14	1224	21
A39a-92	425	-0.7	1318	9	1313	15	1309	23
A39a-93	255	-15.6	2696	12	2537	26	2343	52
A39a-94	100	-1.5	1063	11	1053	13	1049	18
A39a-95	1128	2.8	1207	9	1226	14	1237	22
A39a-96	385	3.2	1680	9	1705	19	1726	33
A39a-97c	265	5.7	1065	9	1102	13	1121	19
A39a-97r	461	3.2	1027	9	1047	13	1057	19
A39a-98c	77	-2.7	1031	12	1013	12	1005	17
A39a-98r	77	-9.9	1062	16	995	13	964	17
A39a-99	370	1.7	1444	9	1457	16	1466	27
A39a-100	130	-5	1071	14	1038	13	1022	17
A39a-101	77	-0.4	1848	10	1844	20	1841	36
A39a-102	216	-1.2	1228	10	1219	14	1214	21
A39a-103	337	-0.6	1622	10	1617	18	1613	30
A39a-104	336	1.5	1737	10	1749	19	1759	34
A39a-105	601	-1.5	1385	9	1374	16	1367	25
A39a-106	317	1.9	999	10	1011	12	1017	17
A39a-107	430	0.3	1125	10	1127	14	1128	20
A39a-108	78	-0.5	1017	12	1013	12	1012	17

A39a-109	175	-1.5	1602	9	1590	17	1581	29
A39a-110	645	-4.3	1408	10	1375	16	1353	25
A39a-111	324	-11.6	1488	10	1394	16	1332	24
A39a-112	342	1.5	1673	9	1685	18	1695	32
A39a-113	46	-22.1	1087	13	927	13	862	16
A39a-114	218	-7	1755	10	1695	18	1647	31
A39a-115	512	-0.4	1274	10	1271	15	1269	23
A39a-116c	321	-20.4	993	10	855	12	803	15
A39a-116r	880	-0.7	1007	9	1003	14	1001	20
A39a-117	549	2.7	1471	9	1492	17	1506	28
A39a-118	146	-1.3	2821	12	2808	29	2791	66
A39a-119	554	3.4	1038	9	1060	13	1070	19
A39a-121r	86	-5.6	1080	10	1042	13	1024	19
A39a-121c	155	-4.3	1079	10	1051	13	1037	18
A39a-122	129	-8	1102	11	1047	13	1020	18
A39a-123	344	-11.1	1471	10	1381	16	1324	24
A39a-124	173	-3.4	1784	10	1755	19	1731	33
A39a-126	154	0.3	1641	10	1643	18	1645	32
A39a-127	347	-3.3	1173	11	1150	14	1138	20
A39a-128	240	-3.6	1294	10	1268	15	1252	23
A39a-129	132	-1	1140	10	1133	14	1130	20
A39a-130	175	-0.1	1024	11	1023	13	1023	18
A39a-131c	52	-3.1	1646	11	1620	19	1600	32
A39a-131r	663	0.7	1625	10	1631	19	1636	32
A39a-132	74	-11.8	1218	13	1130	14	1085	20
A39a-133	194	0.9	1011	11	1017	13	1020	19
A39a-134	497	-1.4	2632	12	2619	28	2601	61
A39a-135	108	-3.4	1057	11	1034	13	1023	19
A39a-136	686	3.4	1673	10	1701	19	1723	34
A39a-137	312	-5.2	1414	10	1373	17	1348	26
A39a-138	85	-6.8	2087	12	2025	22	1965	40
A39a-139	126	-0.1	1434	11	1434	17	1434	27
A39a-140	329	2.2	1067	11	1082	14	1089	21
A39b-08	136	-1.3	2742	16	2730	29	2713	64
A39b-07	26	-1.9	1129	17	1116	15	1110	21
A39b-06	275	5.8	1285	13	1326	16	1352	26
A39b-05	84	-4.2	1064	14	1036	14	1023	19
A39b-04r	167	-5	1638	12	1596	18	1564	29
A39b-04c	266	-0.1	1644	12	1643	18	1642	31
A39b-03	490	-2.4	1018	12	1003	12	995	16
A39b-02	291	0.7	1055	12	1059	13	1061	18
A39b-01r	120	0.1	1643	13	1645	18	1646	31
A39b-01c	146	-2.4	1646	13	1627	20	1612	33

A39b-15	202	-1.1	1609	12	1600	18	1593	30
A39b-14	461	2.4	1188	13	1205	14	1215	20
A39b-13	172	-13.4	1519	14	1407	16	1334	24
A39b-12	399	-16.6	1342	13	1210	16	1138	22
A39b-11r	235	-3.8	1648	13	1617	20	1592	33
A39b-11c	422	-4.1	1651	13	1617	22	1591	38
A39b-10	271	-5	1205	12	1169	16	1150	24
A39b-09	584	2.5	1032	12	1048	13	1056	18

HJK_1091

68.738904N, 19.462460E

			Ages					
Sample/ spot #	**[U] ppm**	**Conc% Central**	**$^{207}Pb/^{206}Pb$**	**±σ**	**$^{207}Pb/^{235}U$**	**±σ**	**$^{206}Pb/^{238}U$**	**±σ**
1091-02	155	1.1	1127	13	1134	15	1138	22
1091-01	210	-6.7	1065	13	1019	16	998	22
1091-04	109	-2.3	1748	13	1729	21	1713	37
1091-05	137	-0.5	1625	13	1621	21	1618	35
1091-06	242	-0.5	1312	13	1308	18	1306	27
1091-07	107	-9.2	1534	13	1458	18	1407	28
1091-08	182	0.6	1138	13	1142	15	1145	21
1091-09	116	-2.5	1512	13	1492	18	1478	29
1091-10	633	-3.6	915	13	893	14	884	19
1091-11	152	6.2	1246	14	1289	16	1315	25
1091-12	112	7.6	1126	13	1177	16	1205	24
1091-13	293	0.7	1153	13	1157	14	1160	21
1091-14	185	-21.7	2652	16	2424	25	2163	46
1091-15c	181	-2.9	1022	13	1002	13	994	18
1091-15r	72	-0.7	1045	14	1041	14	1038	19
1091-16	118	1.4	1076	15	1085	15	1090	22
1091-17	22	-3.7	1026	20	1002	16	991	21
1091-18	187	-1.7	1351	13	1339	17	1331	27
1091-19	115	-31.3	2283	16	1950	27	1652	44
1091-20	47	-0.3	1008	15	1006	14	1005	20
1091-21	176	-0.8	1043	13	1038	14	1035	20
1091-22	19	-3.9	1150	22	1123	17	1109	23
1091-23	110	13.7	1080	13	1167	22	1215	35
1091-24	91	-3.7	1127	16	1102	17	1089	24
1091-25	416	-13.8	740	14	664	13	642	16
1091-25-2	379	-15.7	780	14	691	12	664	15

1091-26	72	6.6	1036	14	1078	19	1098	28
1091-27	292	-19.6	1250	14	1098	17	1023	23
1091-28	387	3.9	977	13	1001	20	1012	28
1091-29	349	-17.7	1533	14	1382	19	1287	28
1091-30	227	7.8	1816	14	1880	26	1938	50
1091-31	38	10.1	952	16	1012	17	1041	25
1091-32	49	-7.5	851	23	807	13	791	15
1091-33	109	-5.2	1573	14	1531	18	1501	29
1091-34	335	1.2	1074	14	1082	14	1086	20
1091-35	175	-13.7	1762	14	1640	21	1546	33
1091-36	217	11.9	1411	14	1498	23	1560	39
1091-37	199	-10.1	1606	13	1521	18	1460	28
1091-38	364	0.7	1230	13	1235	16	1238	24
1091-39-2	68	-6.6	1417	15	1365	17	1332	25
1091-40	416	2.9	1114	14	1134	15	1144	21

P-15-S-7

67.213676N, 17.622968E

Sample/ spot #	[U] ppm	Conc% Central	Ages $^{207}Pb/^{206}Pb$	±σ	$^{207}Pb/^{235}U$	±σ	$^{206}Pb/^{238}U$	±σ
P7-01	72	-34.7	1229	18	946	13	829	15
P7-02	183	-6.4	1061	14	1018	13	999	18
P7-01-2	191	-33.4	1375	44	1086	21	948	20
P7-03	101	-3.5	1015	15	992	13	982	18
P7-04-1	169	-10.1	1496	15	1413	17	1359	25
P7-04-2	719	1.2	1025	14	1033	14	1037	19
P7-05	152	-5	1774	15	1731	20	1696	33
P7-06	188	-3.6	915	15	893	12	885	16
P7-07	91	-2.8	1036	15	1018	14	1009	18
P7-08r	635	-3.4	1067	13	1044	14	1033	19
P7-08c	405	0.7	1159	13	1164	15	1166	22
P7-14	158	-12.3	1443	14	1344	9	1282	12
P7-16	39	-13.5	1142	13	1045	8	999	9
P7-18	181	-1.8	1338	8	1324	8	1315	12
P7-23	69	-0.4	1061	11	1059	8	1057	11
P7-09c	451	-9.7	1252	8	1180	8	1141	11
P7-09r	261	-39.8	1401	14	1042	11	880	13
P7-10	206	3.2	1500	8	1524	10	1542	16
P7-10r	583	-1.6	1525	9	1512	11	1503	18
P7-11	120	-20.4	1248	13	1090	8	1012	10

P7-12r	424	-25	1645	11	1418	12	1272	16
P7-13	233	-2.7	1378	8	1358	9	1345	13
P7-15	101	-36.3	1554	24	1215	12	1033	9
P7-17	96	-3.1	1355	8	1332	8	1317	12
P7-19c	63	-4.3	1967	9	1929	12	1894	20
P7-19r	156	-41.9	1671	18	1252	21	1023	25
P7-20	130	-13.4	1133	15	1037	8	993	9
P7-21	111	-24	1220	13	1034	9	948	11
P7-22	86	-1.6	1016	10	1005	7	1001	9
P7-24	607	-15.4	1651	48	1518	62	1424	94
P7-24r	183	-25.8	1186	33	987	13	900	9
P7-25	103	-15.6	1372	9	1247	9	1176	12
P7-26	115	-19.4	1242	21	1092	10	1019	9
P7-27	234	-2.9	1035	8	1016	7	1008	10
P7-28	85	-71.5	2742	127	1626	68	908	26
P7-28-2	87	-12.3	985	14	905	8	872	10
P7-29c	369	0.4	1073	8	1075	8	1077	12
P7-29r	711	-8.7	1156	9	1094	9	1063	13
P7-30	457	1.5	1153	8	1163	8	1168	12
P7-31	298	-13.8	1096	12	1000	8	956	9
P7-31-2	455	2.3	1033	8	1048	7	1055	10
P7-32	63	-3.7	1157	10	1132	8	1118	11
P7-33	115	-1.7	1320	9	1307	8	1299	12
P7-34	169	-6.8	1326	11	1274	9	1244	12
P7-35	151	-5.5	1582	8	1537	9	1504	15
P7-36	104	-2.3	1067	9	1052	7	1044	10
P7-37	69	-1.5	1053	10	1043	7	1038	9
P7-38	153	-16.4	1710	9	1564	10	1459	15
P7-39c	186	-13.2	1470	16	1362	11	1294	13
P7-39r	31	-5	1355	10	1317	10	1294	14
P7-40	439	1	1364	8	1372	9	1377	13
P7-41	347	-25.5	1418	10	1201	8	1084	11
P7-42	208	0.4	1623	9	1627	10	1629	16
P7-43	37	-18	1159	12	1026	8	964	10
P7-45	297	-8.6	1439	11	1371	9	1327	13
P7-46	167	0.3	1058	9	1060	7	1061	10
P7-47	53	-43.3	1722	48	1279	22	1032	12
P7-48	109	-5.1	1586	9	1544	10	1513	16
P7-49	535	-9.8	1600	9	1517	10	1459	15
P7-50	240	-2	1605	8	1589	10	1577	16
P7-51	225	-36.2	1144	26	859	10	752	8
P7-52c	201	-19	1267	14	1119	9	1044	10
P7-52r	294	-56.1	2213	116	1515	57	1067	25

P7-53	654	0.4	1520	8	1524	10	1526	16
P7-54	101	-1.2	1022	10	1014	7	1011	10
P7-55	112	-6.7	1446	9	1393	9	1359	13
P7-56	232	-2.4	1401	8	1383	9	1371	14
P7-57	251	-6.1	1399	9	1351	9	1321	13
P7-58	129	-2.2	1014	9	1000	7	994	9
P7-59	102	-2.2	1073	9	1059	8	1052	11
P7-60	221	-37	1259	33	949	13	821	8
P7-61	250	-2.9	1240	9	1219	8	1208	12
P7-62	116	-2.8	1020	10	1002	7	993	9
P7-63	129	-2.5	1053	10	1036	8	1028	10
P7-64	178	-50.9	1665	35	1129	15	872	8
P7-64r	411	-11.6	1106	9	1025	8	988	10
P7-65	431	-1	1057	8	1051	7	1048	10
P7-66	65	-52.2	1851	55	1267	23	952	10
P7-67	126	-15.2	1602	10	1471	10	1382	15
P7-68	238	-1.7	1619	9	1604	10	1594	16
P7-69	586	-5.2	1368	12	1329	10	1304	13
P7-70	135	-5.5	1217	12	1177	9	1156	12
P7-71	419	-8	2557	11	2479	17	2386	35
P7-72c	766	-3.9	1436	9	1406	10	1386	15
P7-72r	130	-2.5	1465	9	1445	10	1432	15
P7-73	29	-3.9	1079	13	1053	9	1040	11
P7-74	129	-13.3	1000	11	911	8	875	9
P7-75c	153	-11.2	2421	11	2313	15	2192	27
P7-75r	178	-62.6	1227	51	640	14	486	6
P7-76	466	0	1361	9	1361	10	1361	15
P7-77	270	-1.9	1370	9	1355	9	1346	14
P7-78	187	-2	1362	9	1346	9	1337	14
P7-79	189	-2	1058	9	1045	8	1039	10
P7-80	145	-2.4	1046	9	1031	8	1023	10
P7-81	240	-22.9	1280	10	1098	9	1009	11
P7-82	149	-3.2	1366	9	1342	9	1327	14
P7-83	151	-13	2637	11	2507	16	2349	31
P7-84	290	-3.2	1697	12	1671	12	1650	19
P7-85	28	-19.2	1056	15	921	9	866	11
P7-86	24	-9.5	1123	60	1057	22	1025	11
P7-87	158	-1.4	1026	10	1017	8	1013	11
P7-88	219	-54.3	1878	18	1257	11	926	10
P7-89	62	-6.3	916	12	878	8	862	9
P7-90	108	-3.3	1057	10	1036	8	1025	11
P7-91	439	-31.9	1709	10	1404	10	1211	13
P7-92	62	-43.4	987	22	668	8	578	6

P7-93	61	-5.7	1025	11	988	8	971	10
P7-94	63	-4.7	1012	12	982	8	968	10
P7-95	36	-6	1150	12	1108	9	1086	11
P7-96	78	-2.6	1167	10	1149	9	1139	12
P7-97	422	-2.1	1083	9	1069	8	1062	11
P7-98	332	-3.2	1501	9	1475	10	1457	16
P7-99	102	-5.4	1253	9	1213	9	1191	12
P7-100	510	-2.5	1364	9	1345	9	1334	14
P7-101	198	-4.2	1651	9	1616	11	1589	17
P7-102	131	-17.2	1559	11	1412	11	1316	15
P7-103	219	-4.2	1000	10	973	8	961	10
P7-104	135	-12.8	1734	14	1621	12	1536	17
P7-105	145	-33.8	1596	93	1280	39	1100	13
P7-106	64	-8.2	1157	10	1099	8	1070	11
P7-107	183	-27.4	2182	54	1901	30	1654	20
P7-108	64	-5	1025	12	992	8	977	10
P7-109	145	-4.6	1374	10	1338	10	1316	15
P7-110	123	-5.4	1304	10	1264	9	1240	13
P7-111	376	-12	1624	17	1521	11	1449	14
P7-112	314	-1.9	1061	16	1048	8	1042	9
P7-113c	432	-31.1	2007	129	1690	71	1446	59
P7-113r	475	-6.3	1338	16	1290	11	1261	15
P7-114	58	-5.7	1005	17	968	8	951	9
P7-115	108	-2.2	1007	17	993	8	987	8
P7-116	130	-42.8	1429	33	1032	14	855	8
P7-117	135	-31.9	1353	34	1081	14	952	8
P7-118	52	-30.5	1119	25	887	10	797	8
P7-119	172	-8.9	1247	15	1181	9	1145	10
P7-120	101	-13.2	1005	17	918	8	882	8
P7-121	188	-1.5	1069	16	1059	8	1054	9
P7-122	811	-9.6	1357	16	1282	10	1238	12
P7-123	129	-4.5	1493	16	1457	11	1432	13
P7-124	343	-12.4	1825	17	1714	12	1625	16
P7-125	205	-36.3	1518	58	1183	24	1008	13
P7-126	128	-3.7	1680	17	1649	12	1625	16
P7-127	222	-46.3	1630	26	1161	12	926	9
P7-128	373	-31.7	1430	19	1152	10	1010	9
P7-129	101	-11.4	2585	25	2472	21	2337	32

HJK_2102

68.404485N, 19.248038E

Sample/ spot #	[U] ppm	Conc% Central	Ages $^{207}Pb/^{206}Pb$	±σ	$^{207}Pb/^{235}U$	±σ	$^{206}Pb/^{238}U$	±σ
2102-01	43	-5.9	1042	13	1003	17	985	24
2102-02	88	-4.6	1389	9	1353	21	1331	33
2102-03	31	-6.1	1297	13	1251	20	1224	30
2102-04	146	-8.9	1616	9	1541	23	1487	38
2102-05	286	1.5	1448	8	1459	22	1467	37
2102-06	33	-2.1	1071	13	1057	18	1050	25
2102-07	23	-23.4	1629	212	1419	91	1284	33
2102-08c	125	0.3	1160	9	1162	19	1163	28
2102-08r	116	0.8	1034	10	1039	17	1041	25
2102-09	128	2.3	1241	8	1257	20	1266	31
2102-10	392	14.8	1045	8	1137	19	1186	30
2102-100	214	-0.1	1003	35	1002	13	1002	8
2102-101c	47	-6	1120	37	1078	14	1057	10
2102-102	225	-7.6	1031	37	981	13	959	8
2102-103	251	1.8	985	36	996	13	1001	9
2102-104	105	-1.7	1032	37	1022	13	1017	8
2102-105	227	-4.2	1210	36	1180	15	1164	10
2102-106	117	-5	1619	38	1578	18	1548	14
2102-107	334	-1.2	1340	36	1331	16	1325	11
2102-108	279	-5.5	1336	36	1294	16	1269	10
2102-109	77	-6.7	1587	38	1531	18	1491	13
2102-11	61	-0.6	1071	13	1067	18	1065	26
2102-110	890	-16.2	1131	36	1014	14	960	9
2102-111	480	1.5	1009	36	1018	13	1023	8
2102-112	651	0.2	1097	37	1098	14	1099	9
2102-12	77	1.9	1485	9	1500	23	1510	39
2102-13	83	3.2	1033	9	1053	18	1063	26
2102-14	241	4.2	1041	8	1068	18	1081	26
2102-15	104	1.1	1613	9	1622	25	1629	43
2102-16	525	-0.9	1402	25	1395	27	1391	41
2102-17	213	-0.5	1647	26	1643	31	1640	51
2102-18	367	-0.4	1269	25	1266	25	1265	37
2102-19	372	0.8	1500	26	1507	29	1512	47
2102-20	89	-3.3	1089	28	1067	23	1056	30
2102-21	202	-0.3	1037	26	1035	22	1034	30
2102-22	304	-3.5	1502	27	1474	29	1455	45
2102-23	289	-0.8	1035	27	1030	22	1027	30
2102-24	137	-2.9	1091	28	1071	23	1062	31

2102-25	129	-1.7	1483	28	1470	29	1460	46
2102-26	99	-3.2	1035	28	1014	22	1004	30
2102-27	380	-0.6	1075	26	1070	23	1068	32
2102-32	287	-1.2	1631	17	1621	14	1613	22
2102-33	150	-3.4	1069	17	1047	10	1036	12
2102-34	1430	2.1	989	16	1002	12	1008	17
2102-35	138	-16.8	1155	20	1032	11	975	12
2102-36	78	-3.9	1325	18	1296	12	1278	16
2102-37	313	-12.2	1658	173	1552	75	1476	20
2102-38	291	-2.7	1251	17	1232	13	1221	17
2102-39	283	0.4	1086	17	1089	11	1091	13
2102-40	155	-7.2	2719	22	2648	23	2557	43
2102-41	231	-2.9	1630	18	1606	14	1588	21
2102-42	97	-1.6	1062	18	1051	11	1046	13
2102-43	432	-0.3	1014	17	1012	11	1011	15
2102-44	193	-4.3	1344	18	1311	12	1291	16
2102-45	527	-3.2	928	18	908	10	900	12
2102-46	95	-20.8	1025	19	881	9	825	10
2102-47	158	-0.3	1098	17	1096	11	1095	14
2102-48	194	-1.4	1489	18	1477	14	1469	20
2102-49	190	-8.2	1105	17	1048	10	1021	12
2102-50	400	-6.9	1606	28	1549	17	1507	20
2102-51	575	-15	973	16	874	12	836	15
2102-52	112	-1	1189	20	1182	12	1178	14
2102-53	865	-3.7	1126	24	1100	13	1087	15
2102-54	412	-1.7	1070	16	1059	11	1054	13
2102-55	219	0	1073	18	1073	11	1073	13
2102-56	145	-0.2	1055	17	1053	11	1053	14
2102-57	14	-19.3	1249	40	1100	18	1026	16
2102-58	122	-26	1968	19	1712	16	1510	22
2102-59	276	-2.8	1488	18	1467	14	1452	19
2102-60	241	-0.9	1073	17	1067	10	1064	13
2102-61	330	-7.7	1045	19	993	10	969	11
2102-62	206	-4.3	1479	19	1445	14	1422	18
2102-63	1043	-3	1617	19	1592	16	1574	22
2102-64	230	0.1	1026	20	1027	11	1027	12
2102-65	807	-45.1	1831	32	1351	31	1069	36
2102-66	829	-2.2	1628	20	1610	15	1596	21
2102-67	97	-4.3	1162	21	1132	12	1116	14
2102-68	1141	-0.2	1291	20	1289	13	1288	18
2102-69	155	-4.5	1232	21	1199	12	1181	15
2102-70	133	-5.3	1593	20	1550	15	1518	20
2102-71	129	-6.9	1300	21	1248	13	1218	15

2102-72	212	2.6	948	21	964	11	971	12
2102-73	292	-1.5	1589	21	1577	15	1569	21
2102-74	495	0.2	1352	20	1354	14	1354	18
2102-75	145	-7.3	1096	21	1046	12	1022	13
2102-76	266	0.4	1043	21	1046	11	1047	13
2102-77	116	-3.8	1379	21	1350	14	1332	18
2102-78	435	1.3	1373	20	1382	14	1389	18
2102-79	203	-1.6	1373	21	1361	14	1353	18
2102-80	720	1.9	1429	22	1443	15	1453	21
2102-81	193	-2.3	1097	21	1081	12	1073	14
2102-82	302	-1.7	1332	21	1319	14	1311	18
2102-83	1382	-27.9	1496	24	1251	21	1113	26
2102-84	620	-1.1	1226	21	1218	14	1214	18
2102-85	732	-3.2	1608	20	1582	16	1563	23
2102-86	161	-7.1	1553	21	1495	15	1454	20
2102-87	156	1.8	1302	21	1314	14	1322	17
2102-88	268	-11.4	1062	21	984	11	950	13
2102-89	221	-3.9	1155	22	1128	12	1114	14
2102-90	220	-5.4	1279	21	1239	13	1216	16
2102-91	433	-2.8	1631	37	1608	18	1590	14
2102-92	801	0.8	1472	36	1478	17	1483	12
2102-93c	58	-4	1190	34	1162	15	1146	10
2102-93r	364	-17.4	852	41	746	11	712	6
2102-94	271	1.3	1252	34	1261	15	1267	10
2102-95	208	-1.4	1310	34	1300	16	1293	12
2102-96	69	-5.1	986	35	954	13	940	8
2102-97	960	-10.2	1423	36	1341	17	1291	15
2102-98	181	0.6	955	35	959	12	961	7
2102-99c	219	-4.9	1578	36	1538	18	1510	13
2102-99r	160	-3.5	1603	36	1574	18	1553	13
2102b-01	235	-3.1	1348	18	1325	13	1310	17
2102b-02	491	-14.6	1753	18	1624	15	1526	21
2102b-03	105	-6.6	1102	19	1056	11	1034	14
2102b-04	108	-3.7	1060	19	1035	11	1023	12
2102b-05	209	0.9	1071	18	1078	11	1081	13
2102b-06	332	-6.5	1571	18	1517	15	1479	22
2102b-07	94	-7.1	1584	21	1525	16	1483	22
2102b-08	217	0.8	1322	17	1328	13	1332	17
2102b-09	384	0.8	1437	17	1443	14	1447	20
2102b-10	341	-0.7	1618	17	1613	15	1608	23
2102b-100	348	-1.1	1475	19	1466	14	1460	19
2102b-101	253	-2.3	1392	19	1375	13	1364	17
2102b-102	434	-2	1178	20	1164	12	1157	15

2102b-11	68	-2.2	1069	18	1055	11	1048	13
2102b-12	380	0.2	1130	17	1132	12	1132	15
2102b-13	212	-0.4	1601	17	1597	15	1594	22
2102b-14	159	-1.9	1094	18	1081	11	1075	14
2102b-15	220	-7.6	1468	17	1407	13	1367	18
2102b-16	174	-3.6	1669	18	1639	17	1615	27
2102b-17	61	-5.9	1068	22	1029	12	1010	14
2102b-18	436	-25.4	2396	21	2130	19	1866	27
2102b-19	114	-4.2	1619	17	1585	15	1559	22
2102b-20	151	-1.8	1608	13	1593	13	1583	20
2102b-21	46	-6.1	1167	14	1124	11	1102	15
2102b-22	155	-9.3	1415	13	1341	12	1296	17
2102b-23	832	-5.7	1744	12	1696	16	1657	27
2102b-24	459	-5.2	1419	12	1378	12	1351	17
2102b-25	579	-2.1	1101	12	1087	10	1079	13
2102b-26	37	-6.1	1039	17	998	11	980	14
2102b-27	247	-4.6	1035	13	1005	9	991	12
2102b-28	144	-4.8	1037	13	1005	9	991	12
2102b-29	253	-4.9	1659	13	1618	14	1587	21
2102b-30	87	-5.6	1056	15	1019	10	1002	12
2102b-31	176	-5.8	1621	13	1573	14	1537	21
2102b-32	425	-8.5	1645	13	1573	14	1520	22
2102b-33	49	-4.4	1118	14	1088	11	1073	14
2102b-34	75	-11	2692	16	2583	21	2445	40
2102b-35	220	-5.6	1636	12	1589	13	1554	20
2102b-36	98	-5.1	1401	13	1361	12	1336	17
2102b-37	766	-7.9	1093	13	1039	12	1013	17
2102b-38	721	-2.6	1079	12	1062	12	1054	16
2102b-39	121	-9.9	2524	16	2427	19	2314	37
2102b-40	40	-8	1609	14	1542	14	1494	20
2102b-41	147	-1.6	1091	14	1080	10	1075	13
2102b-42	532	-2.9	1382	13	1360	13	1346	19
2102b-43	157	-4.9	1647	13	1606	13	1574	21
2102b-44	122	-5.9	1335	14	1290	11	1263	16
2102b-45c	119	-6	1560	14	1510	14	1475	20
2102b-45r	107	-5	1566	13	1525	13	1496	19
2102b-46	482	-9.4	1299	13	1228	13	1187	18
2102b-47	229	-6.8	1598	14	1542	15	1501	23
2102b-48	185	-10.6	1686	14	1594	13	1526	20
2102b-49	312	-11.9	2686	16	2567	20	2420	39
2102b-50	81	-5.9	1357	15	1312	12	1285	17
2102b-51	192	-5	1675	14	1633	14	1600	21
2102b-52	294	-12.4	1620	13	1514	14	1439	20

2102b-53	271	-3.2	1611	13	1585	14	1566	21
2102b-54	87	-5.9	1064	14	1024	10	1006	13
2102b-55	43	-7.3	1288	15	1234	12	1203	16
2102b-56	199	-4.2	1438	13	1405	13	1383	19
2102b-57	84	-6.4	1065	14	1021	10	1001	13
2102b-58	132	-6.4	1734	14	1679	14	1636	22
2102b-59	559	1.2	1178	13	1186	12	1191	16
2102b-60	426	1.2	1755	13	1765	15	1773	25
2102b-61	250	-1.3	1335	19	1326	12	1320	16
2102b-62	178	-8.2	1493	19	1426	13	1382	18
2102b-63	164	-4.2	1742	19	1706	15	1677	22
2102b-64	52	-6	1332	19	1287	12	1259	15
2102b-65	85	-5.7	1640	20	1593	14	1557	20
2102b-66	162	-11.3	992	19	918	11	888	13
2102b-67	159	-2.9	1344	19	1322	13	1309	17
2102b-68	70	-10.6	1365	35	1282	17	1233	15
2102b-69	284	-1	1016	19	1010	10	1006	11
2102b-70	203	-3.6	1203	18	1178	11	1164	14
2102b-71	438	-0.6	1657	20	1652	15	1648	21
2102b-72	170	-1.1	998	18	991	10	988	11
2102b-73	108	-11.3	1622	19	1526	14	1457	18
2102b-75	279	-1.6	1596	19	1582	14	1573	20
2102b-76	36	-1.2	993	23	986	11	982	12
2102b-77	223	-11.7	1361	18	1270	12	1216	15
2102b-78	97	-2.4	1273	18	1256	12	1245	15
2102b-79	140	-0.3	1601	19	1599	14	1597	20
2102b-80	406	2	1056	19	1069	11	1076	13
2102b-81	120	-2.6	1769	20	1746	16	1728	23
2102b-82	292	-10.1	1756	20	1668	15	1599	21
2102b-83	36	-6.6	1568	21	1514	15	1476	20
2102b-84	166	-4.2	1224	21	1194	12	1177	14
2102b-85	401	4.7	1052	19	1083	11	1098	13
2102b-86	367	1.4	1194	19	1204	12	1209	15
2102b-87	25	-9.2	1599	23	1523	16	1468	21
2102b-88	154	0.7	1009	20	1013	10	1015	12
2102b-89	608	1.2	972	19	980	11	983	14
2102b-90	140	-2.9	1613	19	1589	15	1571	20
2102b-91	410	-17.3	1391	20	1251	12	1171	14
2102b-92	167	-37.5	1438	58	1099	23	936	11
2102b-93	242	-25.5	2031	22	1779	16	1571	20
2102b-94	137	-5.8	1355	20	1310	13	1283	16
2102b-95	377	-0.6	1123	20	1118	11	1116	13
2102b-96	285	-2.7	1375	20	1354	13	1341	17

2102b-97	57	-6.7	1352	21	1301	13	1270	16
2102b-98	80	-5.5	1062	21	1025	11	1008	12
2102b-99	77	-4.5	1303	21	1270	13	1250	16

Appendix 3

Akkajaure gneiss

Sample/ spot #	[U] ppm	Ratios $^{207}Pb/^{206}Pb$	±2σ	$^{207}Pb/^{235}U$	±2σ	$^{206}Pb/^{238}U$	±2σ	ρ	Conc% Central
HJK_2026 67.43663N / 17.797396E									
2026-01r	366	0.105	0.001	3.660	0.036	0.254	0.002	0.851	-16.4
2026-01c	207	0.105	0.001	3.734	0.034	0.257	0.002	0.826	-16.1
2026-03	316	0.105	0.001	3.637	0.033	0.252	0.002	0.823	-17.2
2026-03_02	406	0.105	0.001	3.837	0.034	0.265	0.002	0.812	-13.2
2026-04	235	0.105	0.001	3.573	0.032	0.246	0.002	0.814	-19.3
2026-06	299	0.107	0.001	4.248	0.041	0.288	0.002	0.836	-7.9
2026-07c	179	0.104	0.001	3.852	0.036	0.268	0.002	0.835	-11.3
2026-08	239	0.107	0.001	4.073	0.042	0.276	0.002	0.861	-11.7
2026-09c	255	0.105	0.001	3.836	0.037	0.266	0.002	0.848	-12.6
2026-10	108	0.104	0.001	3.548	0.035	0.247	0.002	0.829	-17.9
2026-11	87	0.106	0.001	4.039	0.041	0.277	0.002	0.828	-10.1
2026-13	432	0.105	0.001	3.884	0.045	0.267	0.003	0.889	-12.7
2026-14c	584	0.107	0.001	3.880	0.040	0.263	0.002	0.857	-15.3
2026-15	89	0.103	0.001	3.342	0.045	0.236	0.003	0.904	-20.2
2026-17	268	0.102	0.001	3.402	0.031	0.241	0.002	0.817	-18.4
2026-17r	173	0.103	0.001	3.554	0.035	0.249	0.002	0.843	-16.7
2026-18	185	0.102	0.001	3.285	0.031	0.233	0.002	0.820	-20.9
2026-19	369	0.107	0.001	4.299	0.048	0.291	0.003	0.887	-6.9
2026-20	321	0.102	0.001	3.422	0.030	0.243	0.002	0.816	-17.3
2026-21c	140	0.108	0.001	4.478	0.045	0.300	0.002	0.827	-5.1
2026-22	113	0.099	0.001	3.144	0.058	0.230	0.004	0.919	-19.2
2026-23	404	0.104	0.001	3.796	0.038	0.265	0.002	0.858	-12
2026-24r	79	0.105	0.001	3.849	0.043	0.265	0.003	0.866	-13.6
2026-24c	196	0.103	0.001	3.501	0.033	0.247	0.002	0.828	-17.1
2026-25-1	238	0.101	0.001	3.142	0.029	0.227	0.002	0.822	-21.6
2026-25-2	386	0.105	0.001	3.878	0.036	0.268	0.002	0.814	-11.8
2026-26	340	0.104	0.001	3.699	0.034	0.258	0.002	0.824	-14.2
2026-05	128	0.112	0.001	4.997	0.097	0.324	0.005	0.811	-1.6

References

Á Horni, J., Hopper, J. R., Blischke, A., Geisler, W. H., Stewart, M., McDermott, K., Judge, M., Erlendsson, Ö., and Árting, U., 2017, Regional distribution of volcanism within the North Atlantic Igneous Province: Geological Society, London, Special Publications, v. 447, no. 1, p. 105.

Abdelmalak, M. M., Andersen, T. B., Planke, S., Faleide, J. I., Corfu, F., Tegner, C., Shephard, G. E., Zastrozhnov, D., and Myklebust, R., 2015, The ocean-continent transition in the mid-Norwegian margin: Insight from seismic data and an onshore Caledonian field analogue: Geology, v. 43, no. 11, p. 1011-1014.

Abdelmalak, M. M., Faleide, J. I., Planke, S., Gernigon, L., Zastrozhnov, D., Shephard, G. E., and Myklebust, R., 2017, The T‐Reflection and the Deep Crustal Structure of the Vøring Margin, Offshore mid‐Norway: Tectonics, v. 36, no. 11, p. 2497-2523.

Abdelmalak, M. M., Mourgues, R., Galland, O., and Bureau, D., 2012, Fracture mode analysis and related surface deformation during dyke intrusion: Results from 2D experimental modelling: Earth and Planetary Science Letters, v. 359, p. 93-105.

Abdelmalak, M. M., Planke, S., Faleide, J., Jerram, D. A., Zastrozhnov, D., Eide, S., and Myklebust, R., 2016, The development of volcanic sequences at rifted margins: New insights from the structure and morphology of the Vøring Escarpment, mid‐Norwegian Margin: Journal of Geophysical Research: Solid Earth, v. 121, no. 7, p. 5212-5236.

Ágústsdóttir, T., Woods, J., Greenfield, T., Green, R. G., White, R. S., Winder, T., Brandsdóttir, B., Steinthórsson, S., and Soosalu, H., 2016, Strike‐slip faulting during the 2014 Bárðarbunga‐Holuhraun dike intrusion, central Iceland: Geophysical Research Letters, v. 43, no. 4, p. 1495-1503.

Airaghi, L., Lanari, P., de Sigoyer, J., and Guillot, S., 2017, Microstructural vs compositional preservation and pseudomorphic replacement of muscovite in deformed metapelites from the Longmen Shan (Sichuan, China): Lithos, v. 282-283, p. 262-280.

Albarède, F., 2003, Geochemistry: An Introduction, Cambridge, Cambridge University Press.

Albrecht, L. G., 2000, Early structural and metamorphic evolution of the Scandinavian Caledonides: a study of the eclogite-bearing Seve Nappe Complex at the Arctic Circle, Sweden [Ph.D.: Lund University.

Allen, P. A., and Allen, J. R., 2013, Basin analysis: Principles and application to petroleum play assessment, John Wiley & Sons.

Allen, P. A., Bowring, S., Leather, J., Brasier, M., Cozzi, A., Grotzinger, J. P., McCarron, G., and Amthor, J. E., Chronology of Neoproterozoic glaciations: new insights from Oman, *in* Proceedings The 16th International Sedimenetological Congress, Abstract Volume, Johannesburg, South Africa2002, p. 7-8.

Allken, V., Huismans, R. S., and Thieulot, C., 2012, Factors controlling the mode of rift interaction in brittle-ductile coupled systems: A 3D numerical study: Geochem. Geophys. Geosyst., v. 13, p. Q05010.

Ammann, M. W., Brodholt, J. P., Wookey, J., and Dobson, D. P., 2010, First-principles constraints on diffusion in lower-mantle minerals and a weak D′′ layer: Nature, v. 465, p. 462.

Andersen, T., Andersson, U. B., Graham, S., Åberg, G., and Simonsen, S. L., 2009, Granitic magmatism by melting of juvenile continental crust: new constraints on the source of Palaeoproterozoic granitoids in Fennoscandia from Hf isotopes in zircon: Journal of the Geological Society, v. 166, no. 2, p. 233.

Andersen, T., Kristoffersen, M., and Elburg, M. A., 2016, How far can we trust provenance and crustal evolution information from detrital zircons? A South African case study: Gondwana Research, v. 34, p. 129-148.
-, 2018, Visualizing, interpreting and comparing detrital zircon age and Hf isotope data in basin analysis – a graphical approach: Basin Research, v. 30, no. 1, p. 132-147.
Andersen, T., Skjerlie, K., and Furnes, H., 1990a, The Sunnfjord Melange, evidence of Silurian ophiolite accretion in the west Norwegian Caledonides: Journal of the Geological Society, v. 147, no. 1, p. 59-68.
Andersen, T. B., 1998, Extensional tectonics in the Caledonides of southern Norway, an overview: Tectonophysics, v. 285, no. 3-4, p. 333-351.
Andersen, T. B., and Andresen, A., 1994, Stratigraphy, tectonostratigraphy and the accretion of outboard terranes in the Caledonides of Sunnhordland, W. Norway: Tectonophysics, v. 231, no. 1-3, p. 71-84.
Andersen, T. B., Berry, H. N., Lux, D. R., and Andresen, A., 1998, The tectonic significance of pre-Scandian 40Ar/39Ar phengite cooling ages in the Caledonides of western Norway: Journal of the Geological Society, v. 155, no. 2, p. 297-309.
Andersen, T. B., Corfu, F., Labrousse, L., and Osmundsen, P.-T., 2012, Evidence for hyperextension along the pre-Caledonian margin of Baltica: Journal of the Geological Society, v. 169, no. 5, p. 601-612.
Andersen, T. B., and Jamtveit, B., 1990, Uplift of deep crust during orogenic extensional collapse: A model based on field studies in the Sogn ‐ Sunnfjord Region of western Norway: Tectonics, v. 9, no. 5, p. 1097-1111.
Andersen, T. B., Jamtveit, B., Dewey, J., and Swensson, E., 1991, Subduction and eduction of continental crust: major mechanism during continent-continent collision and orogenic extensional collapse, a model based on the south Caledonides: Terra Nova, v. 3, p. 303-310.
Andersen, T. B., Skjerlie, K. P., and Furnes, H., 1990b, The Sunnfjord Melange, evidence of Silurian ophiolite accretion in the West Norwegian Caledonides: Journal of the Geological Society, v. 147, no. 1, p. 59.
Anderson, E. M., 1905, The dynamics of faulting: Transactions of the Edinburgh Geological Society, v. 8, no. 3, p. 387-402.
Anderson, E. M., 1936, The dynamics of the formation of cone sheets, ring dykes and cauldron subsidences: Proceedings of the Royal Society of Edimburgh, v. 56, p. 128-163.
Andréasson, P.-G., 1986, The Sarektjåkkå Nappe, Seve terranes of the northern Swedish Caledonides: GFF, v. 108, no. 3, p. 263-266.
Andréasson, P.-G., Allen, A., Aurell, O., Boman, D., Ekestubbe, J., Goerke, U., Lundgren, A., Nilsson, P., and Sandelin, S., 2018, Seve terranes of the Kebnekaise Mts., Swedish Caledonides, and their amalgamation, accretion and affinity: GFF, p. 1-28.
Andréasson, P.-G., Svenningsen, O., Johansson, I., Solyom, Z., and Xiaodan, T., 1992, Mafic dyke swarms of the Baltica-Iapetus transition, Seve Nappe Complex of the Sarek Mts., Swedish Caledonides: GFF, v. 114, no. 1, p. 31-45.
Andréasson, P.-G., Svenningsen, O. M., and Albrecht, L., 1998, Dawn of Phanerozoic orogeny in the North Atlantic tract; evidence from the Seve-Kalak Superterrane, Scandinavian Caledonides: GFF, v. 120, no. 2, p. 159-172.
Andréasson, P., 1994, The Baltoscandian margin in Neoproterozoic-early Palaeozoic times. Some constraints on terrane derivation and accretion in the Arctic Scandinavian Caledonides: Tectonophysics, v. 231, no. 1, p. 1-32.
Andréasson, P., Solyom, Z., and Roberts, D., 1979, Petrochemistry and tectonic significance of basic and alkaline-ultrabasic dykes in the Leksdal Nappe, Northern Trondheim Region, Norway: Norges geologiske undersøkelse, v. 348, p. 47-72.
Andresen, A., and Gabrielsen, R., 1979, Major element chemistry of metavolcanic rocks and tectonic setting of the Precambrian Dyrskard Gro up, Hardangervidda, south Norway: Nor. Geol. Tidsskr.

Andresen, A., and Steltenpohl, M. G., 1994, Evidence for ophiolite obduction, terrane accretion and polyorogenic evolution of the north Scandinavian Caledonides: Tectonophysics, v. 231, no. 1, p. 59-70.
Armitage, J. J., Henstock, T. J., Minshull, T. A., and Hopper, J. R., 2009, Lithospheric controls on melt production during continental breakup at slow rates of extension: Application to the North Atlantic: Geochemistry, Geophysics, Geosystems, v. 10, no. 6.
Austrheim, H., 1987, Eclogitization of lower crustal granulites by fluid migration through shear zones: Earth and Planetary Science Letters, v. 81, no. 2-3, p. 221-232.
Austrheim, H., 1990, Fluid Induced Processes in the Lower Crust as Evidenced by Caledonian Eclogitization of Precambrian Granulites, Bergen Arcs, Western-Norway: University of Oslo.
Bai, Y., Wu, S., Liu, Z., Müller, R. D., Williams, S. E., Zahirovic, S., and Dong, D., 2015, Full-fit reconstruction of the South China Sea conjugate margins: Tectonophysics, v. 661, p. 121-135.
Baird, G. B., Figg, S. A., and Chamberlain, K. R., 2014, Intrusive age and geochemistry of the Kebne Dyke Complex in the Seve Nappe Complex, Kebnekaise Massif, arctic Sweden Caledonides: GFF, v. 136, no. 4, p. 556-570.
Barnes, C., Majka, J., Schneider, D., Walczak, K., Bukała, M., Kośmińska, K., Tokarski, T., and Karlsson, A., 2018, High-spatial resolution dating of monazite and zircon reveals the timing of subduction–exhumation of the Vaimok Lens in the Seve Nappe Complex (Scandinavian Caledonides): Contributions to Mineralogy and Petrology, v. 174, no. 1, p. 5.
Bastow, I. D., Booth, A. D., Corti, G., Keir, D., Magee, C., Jackson, C. A. L., Warren, J., Wilkinson, J., and Lascialfari, M., 2018, The Development of Late‐Stage Continental Breakup: Seismic Reflection and Borehole Evidence from the Danakil Depression, Ethiopia: Tectonics, v. 37, no. 9, p. 2848-2862.
Bastow, I. D., and Keir, D., 2011, The protracted development of the continent–ocean transition in Afar: Nature Geoscience, v. 4, no. 4, p. 248.
Bastow, I. D., Keir, D., and Daly, E., 2011, The Ethiopia Afar Geoscientific Lithospheric Experiment (EAGLE): Probing the transition from continental rifting to incipient seafloor spreading: Volcanism and evolution of the African lithosphere, v. 478, p. 1-26.
Be'eri-Shlevin, Y., Gee, D., Claesson, S., Ladenberger, A., Majka, J., Kirkland, C., Robinson, P., and Frei, D., 2011, Provenance of Neoproterozoic sediments in the Särv nappes (Middle Allochthon) of the Scandinavian Caledonides: LA-ICP-MS and SIMS U–Pb dating of detrital zircons: Precambrian Research, v. 187, no. 1-2, p. 181-200.
Beckholmen, M., and Roberts, D., 1999, Mafic dykes in the Leksdal Nappe at Sorli, Central Norwegian Caledonides: geochemistry and palaeotectonic implications: NGU Bulletin, v. 435, p. 59-67.
Belousova, E. A., Griffin, W. L., and O'Reilly, S. Y., 2005, Zircon Crystal Morphology, Trace Element Signatures and Hf Isotope Composition as a Tool for Petrogenetic Modelling: Examples From Eastern Australian Granitoids: Journal of Petrology, v. 47, no. 2, p. 329-353.
Beltrando, M., Manatschal, G., Mohn, G., Dal Piaz, G. V., Brovarone, A. V., and Masini, E., 2014, Recognizing remnants of magma-poor rifted margins in high-pressure orogenic belts: The Alpine case study: Earth-Science Reviews, v. 131, p. 88-115.
Beltrando, M., Stockli, D. F., Decarlis, A., and Manatschal, G., 2015, A crustal‐scale view at rift localization along the fossil Adriatic margin of the Alpine Tethys preserved in NW Italy: Tectonics, v. 34, no. 9, p. 1927-1951.
Bender, H., Ring, U., Almqvist, B. S. G., Grasemann, B., and Stephens, M. B., 2018, Metamorphic Zonation by Out-of-Sequence Thrusting at Back-Stepping Subduction Zones: Sequential Accretion of the Caledonian Internides, Central Sweden: Tectonics, v. 37, no. 10, p. 3545-3576.
Bertelsen, H. S., Rogers, B. D., Galland, O., Dumazer, G., and Abbana Bennani, A., 2018, Laboratory modelling of coeval brittle and ductile deformation during magma emplacement into viscoelastic rocks: Frontiers in Earth Science, v. 6.

Bertrand-sarfati, J., and Siedlecka, A., 1980, Columnar stromatolites of the terminal Precambrian Porsanger Dolomite and Grasdal Formation of Finnmark, north Norway: Norsk Geologisk Tidsskrift, v. 60, no. 1, p. 1-27.
Bialas, R. W., Buck, W. R., and Qin, R., 2010, How much magma is required to rift a continent?: Earth and Planetary Science Letters, v. 292, no. 1-2, p. 68-78.
Biari, Y., Klingelhoefer, F., Sahabi, M., Funck, T., Benabdellouahed, M., Schnabel, M., Reichert, C., Gutscher, M.-A., Bronner, A., and Austin, J. A., 2017, Opening of the central Atlantic Ocean: Implications for geometric rifting and asymmetric initial seafloor spreading after continental breakup: Tectonics, v. 36, no. 6, p. 1129-1150.
Bingen, B., Belousova, E. A., and Griffin, W. L., 2011, Neoproterozoic recycling of the Sveconorwegian orogenic belt: Detrital-zircon data from the Sparagmite basins in the Scandinavian Caledonides: Precambrian Research, v. 189, no. 3-4, p. 347-367.
Bingen, B., Birkeland, A., Nordgulen, O., and Sigmond, E. M. O., 2001, Correlation of supracrustal sequences and origin of terranes in the Sveconorwegian orogen of SW Scandinavia: SIMS data on zircon in clastic metasediments: Precambrian Research, v. 108, no. 3-4, p. 293-318.
Bingen, B., Davis, W. J., Hamilton, M. A., Engvik, A. K., Stein, H. J., Skar, O., and Nordgulen, O., 2008, Geochronology of high-grade metamorphism in the Sveconorwegian belt, S. Norway: U-Pb, Th-Pb and Re-Os data: Norwegian Journal of Geology, v. 88, no. 1, p. 13-42.
Bingen, B., and Demaiffe, D., 1999, Geochemical signature of the Egersund basaltic dyke swarm, SW Norway, in the context of late-Neoproterozoic opening of the Iapetus Ocean: Norsk Geologisk Tidsskrift, v. 79, no. 2, p. 69-86.
Bingen, B., Demaiffe, D., and Breemen, O. V., 1998, The 616 Ma old Egersund basaltic dike swarm, SW Norway, and late Neoproterozoic opening of the Iapetus Ocean: The Journal of Geology, v. 106, no. 5, p. 565-574.
Bingen, B., Griffin, W. L., Torsvik, T. H., and Saeed, A., 2005, Timing of Late Neoproterozoic glaciation on Baltica constrained by detrital zircon geochronology in the Hedmark Group, south-east Norway: Terra Nova, v. 17, no. 3, p. 250-258.
Bingen, B., and Solli, A., 2009, Geochronology of magmatism in the Caledonian and Sveconorwegian belts of Baltica: synopsis for detrital zircon provenance studies: Norwegian Journal of Geology, v. 89, no. 4, p. 267-290.
Bjorklund, L., 1990, Geology of the Akkajaure-Tysfjord-Lofoten Traverse, N. Scandinavian Caledonides: University of Technology and University of Göteborg.
Björklund, L., 1985, The Middle and Lower Allochthons in the Akkajaure-Tysfjord Area, northern Scandinavian Caledonides: The Caledonide Orogen—Scandinavia and Related Areas, p. 515-528.
Bjørlykke, K., and Englund, J. O., 1979, Geochemical response to upper precambrian rift basin sedimentation and lower paleozoic epicontinental sedimentation in South Norway: Cemical Geology, v. 27.
Blaich, O. A., Faleide, J. I., and Tsikalas, F., 2011, Crustal breakup and continent‐ocean transition at South Atlantic conjugate margins: Journal of Geophysical Research: Solid Earth, v. 116, no. B1.
Boillot, G., Grimaud, S., Mauffret, A., Mougenot, D., Kornprobst, J., Mergoil-Daniel, J., and Torrent, G., 1980, Ocean-continent boundary off the Iberian margin: a serpentinite diapir west of the Galicia Bank: Earth and Planetary Science Letters, v. 48, no. 1, p. 23-34.
Bower, D. J., Gurnis, M., and Seton, M., 2013, Lower mantle structure from paleogeographically constrained dynamic Earth models: Geochemistry, Geophysics, Geosystems, v. 14, no. 1, p. 44-63.
Bowring, J. F., McLean, N. M., and Bowring, S., 2011, Engineering cyber infrastructure for U‐Pb geochronology: Tripoli and U‐Pb_Redux: Geochemistry, Geophysics, Geosystems, v. 12, no. 6.
Bowring, S., Myrow, P., Landing, E., Ramezani, J., and Grotzinger, J., Geochronological constraints on terminal Neoproterozoic events and the rise of Metazoan, *in* Proceedings EGS-AGU-EUG Joint Assembly2003.

Brown, E. L., and Lesher, C. E., 2014, North Atlantic magmatism controlled by temperature, mantle composition and buoyancy: Nature Geoscience, v. 7, p. 820.
Brown, E. L., and Lesher, C. E., 2016, REEBOX PRO: A forward model simulating melting of thermally and lithologically variable upwelling mantle: Geochemistry, Geophysics, Geosystems, v. 17, no. 10, p. 3929-3968.
Brun, J. P., and Beslier, M. O., 1996, Mantle exhumation at passive margins: Earth and Planetary Science Letters, v. 142, no. 1, p. 161-173.
Brune, S., 2016, Rifts and rifted margins: A review of geodynamic processes and natural hazards: Plate Boundaries and Natural Hazards, v. 219, p. 13.
Brune, S., Heine, C., Pérez-Gussinyé, M., and Sobolev, S. V., 2014, Rift migration explains continental margin asymmetry and crustal hyper-extension: Nature Communications, v. 5.
Bruton, D. L., Gabrielsen, R. H., and Larsen, B. T., 2010, The Caledonides of the Oslo Region, Norway – stratigraphy and structural elements: Norwegian Journal of Geology, v. 90.
Bryan, S. E., and Ernst, R. E., 2008, Revised definition of Large Igneous Provinces (LIPs): Earth-Science Reviews, v. 86, no. 1, p. 175-202.
Buck, W. R., and Karner, G., 2004, Consequences of asthenospheric variability on continental rifting: Rheology and deformation of the lithosphere at continental margins, v. 62, p. 1-30.
Buckley, S. J., Ringdal, K., Naumann, N., Dolva, B., Kurz, T. H., Howell, J. A., and Dewez, T. J. B., 2019, LIME: Software for 3-D visualization, interpretation, and communication of virtual geoscience models: Geosphere, v. 15, no. 1, p. 222-235.
Buiter, S. J., and Torsvik, T. H., 2014, A review of Wilson Cycle plate margins: A role for mantle plumes in continental break-up along sutures?: Gondwana Research, v. 26, no. 2, p. 627-653.
Bull, A. L., Domeier, M., and Torsvik, T. H., 2014, The effect of plate motion history on the longevity of deep mantle heterogeneities: Earth and Planetary Science Letters, v. 401, p. 172-182.
Burchardt, S., Troll, V. R., Mathieu, L., Emeleus, H. C., and Donaldson, C. H., 2013, Ardnamurchan 3D cone-sheet architecture explained by a single elongate magma chamber: Sci. Rep., v. 3.
Burke, K., and Dewey, J. F., 1973, Plume-Generated Triple Junctions: Key Indicators in Applying Plate Tectonics to Old Rocks: The Journal of Geology, v. 81, no. 4, p. 406-433.
Burke, K., Steinberger, B., Torsvik, T. H., and Smethurst, M. A., 2008, Plume generation zones at the margins of large low shear velocity provinces on the core–mantle boundary: Earth and Planetary Science Letters, v. 265, no. 1, p. 49-60.
Burton, D. L., and Bockelie, J. F., 1980, Geology and Paleontology of the Hølonda area, Western Norway—A Fragment of North America? The Caledonides in the USA. D. R. Wones: Virginia Polytechnic Institute and State University, Department of Geological Science, Blacksburg.
Burton, D. L., and Harper, D. A. T., 1981, Brachiopods and trilobites of the early Ordovician serpentine Otta Conglomerate, south central Norway: Norwegian Journal of Geology.
Bøe, R., Sturt, B. A., and Ramsay, D. M., 1993, The conglomerates of the Sel Group, Otta-Vaga area, Central Norway: an example of a terrane-linking succession: NGU Bulletin, v. 425.
Campbell, I. H., 2007, Testing the plume theory: Chemical Geology, v. 241, no. 3, p. 153-176.
Carmichael, I. S. E., 2004, The activity of silica, water, and the equilibration of intermediate and silicic magmas: American Mineralogist, v. 89, no. 10, p. 1438-1446.
Cashman, P. H., 1989, Geometry and kinematics of extensional deformation along the northern edge of the Rombak Window, Nordland, North Norway: NGU Bulletin, v. 415, p. 71-85.
Cawood, P. A., and Hawkesworth, C. J., 2015, Temporal relations between mineral deposits and global tectonic cycles: Geological Society, London, Special Publications, v. 393, no. 1, p. 9-21.
Cawood, P. A., McCausland, P. J., and Dunning, G. R., 2001, Opening Iapetus: constraints from the Laurentian margin in Newfoundland: Geological Society of America Bulletin, v. 113, no. 4, p. 443-453.
Cawood, P. A., Strachan, R. A., Pisarevsky, S. A., Gladkochub, D. P., and Murphy, J. B., 2016, Linking collisional and accretionary orogens during Rodinia assembly and breakup: Implications for models of supercontinent cycles: Earth and Planetary Science Letters, v. 449, p. 118-126.

Chenin, P., Manatschal, G., Picazo, S., Müntener, O., Karner, G., Johnson, C., and Ulrich, M., 2017, Influence of the architecture of magma-poor hyperextended rifted margins on orogens produced by the closure of narrow versus wide oceans: Geosphere, v. 13, no. 2, p. 559-576.
Chew, D. M., and van Staal, C. R., 2014, The ocean–continent transition zones along the Appalachian–Caledonian margin of Laurentia: examples of large-scale hyperextension during the opening of the Iapetus Ocean: Geoscience Canada, v. 41, no. 2, p. 165-185.
Christiansson, P., Faleide, J., and Berge, A., 2000, Crustal structure in the northern North Sea: an integrated geophysical study: Geological Society, London, Special Publications, v. 167, no. 1, p. 15-40.
Claesson, S., 1980, A Rb-Sr isotope study of granitoids and related mylonites in the Tännäs Augen Gneiss Nappe, southern Swedish Caledonides: GFF, v. 102, no. 4, p. 403-420.
Clemens, J. D., and Holness, M. B., 2000, Textural evolution and partial melting of arkose in a contact aureole: a case study and implications: Visual Geosciences, v. 5, no. 4, p. 1-14.
Clerc, C., Jolivet, L., and Ringenbach, J.-C., 2015, Ductile extensional shear zones in the lower crust of a passive margin: Earth and Planetary Science Letters, v. 431, p. 1-7.
Clerc, C., and Lagabrielle, Y., 2014, Thermal control on the modes of crustal thinning leading to mantle exhumation: Insights from the Cretaceous Pyrenean hot paleomargins: Tectonics, v. 33, no. 7, p. 1340-1359.
Clerc, C., Ringenbach, J.-C., Jolivet, L., and Ballard, J.-F., 2018, Rifted margins: Ductile deformation, boudinage, continentward-dipping normal faults and the role of the weak lower crust: Gondwana Research, v. 53, p. 20-40.
Clift, P., Lee, G. H., Anh Duc, N., Barchausen, U., Van Long, H., and Zhen, S., 2008, Seismic reflection evidence for a dangerous grounds miniplate: no extrusion origin for the South China Sea: Tectonics, v. 27.
Cocks, L. R. M., and Torsvik, T. H., 2011, The Palaeozoic geography of Laurentia and western Laurussia: A stable craton with mobile margins: Earth-Science Reviews, v. 106.
Coltice, N., Phillips, B. R., Bertrand, H., Ricard, Y., and Rey, P., 2007, Global warming of the mantle at the origin of flood basalts over supercontinents: Geology, v. 35, no. 5, p. 391-394.
Contrucci, I., Klingelhöfer, F., Perrot, J., Bartolome, R., Gutscher, M.-A., Sahabi, M., Malod, J., and Rehault, J.-P., 2004, The crustal structure of the NW Moroccan continental margin from wide-angle and reflection seismic data: Geophysical Journal International, v. 159, no. 1, p. 117-128.
Corfu, F., 2004, U–Pb age, setting and tectonic significance of the anorthosite–mangerite–charnockite–granite suite, Lofoten–Vesterålen, Norway: Journal of Petrology, v. 45, no. 9, p. 1799-1819.
Corfu, F., and Andersen, T. B., 2002, U–Pb ages of the Dalsfjord Complex, SW Norway, and their bearing on the correlation of allochthonous crystalline segments of the Scandinavian Caledonides: International Journal of Earth Sciences, v. 91, no. 6, p. 955-963.
Corfu, F., and Andersen, T. B., 2015, Proterozoic magmatism in the southern scandinavian caledonides, with special reference to the occurrences in the Eikefjord Nappe: GFF.
Corfu, F., and Emmet, T., 1992, U-Pb age of the Leirungsmyran gabbroic complex, Jorun Nappe, southern Norway: Norwegian Journal of Geology, v. 72, p. 369-374.
Corfu, F., Gasser, D., and Chew, D. M., 2014, New Perspectives on the Caledonides of Scandinavia and Related Areas, Geological Society of London.
Corfu, F., Gerber, M., Andersen, T. B., Torsvik, T. H., and Ashwal, L. D., 2011, Age and significance of Grenvillian and Silurian orogenic events in the Finnmarkian Caledonides, northern Norway: Canadian Journal of Earth Science, v. 48, p. 419-440.
Corfu, F., Roberts, R. J., Torsvik, T., Ashwal, L. D., and Ramsay, D. M., 2007, Peri-Gondwanan elements in the Caledonian nappes of Finnmark, Northern Norway: Implications for the Paleogeographic framework of the Scandinavian Caledonides: American Journal of Science, v. 307, p. 434-458.
Courtillot, V., Jaupart, C., Manighetti, I., Tapponnier, P., and Besse, J., 1999, On causal links between flood basalts and continental breakup: Earth and Planetary Science Letters, v. 166, no. 3, p. 177-195.

Cutts, J. A., and Smit, M. A., 2018, Rates of deep continental burial from Lu-Hf garnet chronology and Zr-in-rutile thermometry on (ultra)high-pressure rocks: Tectonics, v. 37.
Dallmeyer, R., Andréasson, P., and Svenningsen, O., 1991, Initial tectonothermal evolution within the Scandinavian Caledonide accretionary prism: constraints from 40Ar/39Ar mineral ages within the Seve Nappe Complex, Sarek Mountains, Sweden: Journal of Metamorphic Geology, v. 9, no. 2, p. 203-218.
Daniels, K. A., Bastow, I., Keir, D., Sparks, R., and Menand, T., 2014, Thermal models of dyke intrusion during development of continent–ocean transition: Earth and Planetary Science Letters, v. 385, p. 145-153.
Davies, D. R., Goes, S., and Sambridge, M., 2015, On the relationship between volcanic hotspot locations, the reconstructed eruption sites of large igneous provinces and deep mantle seismic structure: Earth and Planetary Science Letters, v. 411, p. 121-130.
de Capitani, C., and Petrakakis, K., 2010, The computation of equilibrium assemblage diagrams with Theriak/Domino software: American Mineralogist, v. 95, no. 7, p. 1006-1016.
Dempster, T., Rogers, G., Tanner, P., Bluck, B., Muir, R., Redwood, S., Ireland, T., and Paterson, B., 2002, Timing of deposition, orogenesis and glaciation within the Dalradian rocks of Scotland: constraints from U–Pb zircon ages: Journal of the Geological Society, v. 159, no. 1, p. 83-94.
Dewey, J. F., 1988, Extensional collapse of orogens: Tectonics, v. 7, no. 6, p. 1123-1139.
Dewey, J. F., and Burke, K., 1974, Hot Spots and Continental Break-up: Implications for Collisional Orogeny: Geology, v. 2, no. 2, p. 57-60.
Dietrich, V., 1970, Die Stratigraphie der Platta-Decke: Fazielle Zusammenhänge zwischen Oberpenninikum und Unterostalpin, Geologisches Institut der Eidg. Technischen Hochschule und der Universität.
Direen, N. G., and Crawford, A. J., 2003, Fossil seaward-dipping reflector sequences preserved in southeastern Australia: a 600 Ma volcanic passive margin in eastern Gondwanaland: Journal of the Geological Society, v. 160, no. 6, p. 985-990.
Domeier, M., 2015, A plate tectonic scenario for the Iapetus and Rheic oceans: Gondwana Research.
Dunning, G. R., and Grenne, T., 2000, U-Pb age dating and paleotectonic significance of trondhjemite from the type locality in the Central Norwegian Caledonides: NGU Bulletin, no. 437.
Dunning, G. R., and Pedersen, R. B., 1988, U/Pb ages of ophiolites and arc-related plutons of the Norwegian Caledonides: implications for the development of Iapetus: Contributions to Mineralogy and Petrology, v. 98, no. 1, p. 13-23.
Duretz, T., Petri, B., Mohn, G., Schmalholz, S. M., Schenker, F. L., and Müntener, O., 2016, The importance of structural softening for the evolution and architecture of passive margins: Scientific Reports, v. 6, p. 38704.
Eide, E. A., Osmundsen, P. T., Meyer, G. B., Kendrick, M. A., and Corfu, F., 2002, The Nesna Shear Zone, north-central Norway: an 40 Ar/39 Ar record of Early Devonian-Early Carboniferous ductile extension and unroofing: Norwegian Journal of Geology/Norsk Geologisk Forening, v. 82, no. 4.
Eide, E. A., Torsvik, T. H., Andersen, T. B., and Arnaud, N. O., 1999, Early Carboniferous unroofing in western Norway: A tale of alkali feldspar thermochronology: The Journal of Geology, v. 107, no. 3, p. 353-374.
Eldholm, O., 1991, Magmatic tectonic evolution of a volcanic rifted margin: Marine Geology, v. 102, no. 1-4, p. 43-61.
Eldholm, O., and Grue, K., 1994, North Atlantic volcanic margins: dimensions and production rates: Journal of Geophysical Research: Solid Earth, v. 99, no. B2, p. 2955-2968.
Engel, A. J., and Engel, C. G., 1960, Progressive metamorphism and granitization of the major paragneiss, northwest Adirondack mountains, New York part II: Mineralogy: Geological Society of America Bulletin, v. 71, no. 1, p. 1-58.
Engi, M., Lanari, P., and Kohn, M. J., 2017, Significant Ages—An Introduction to Petrochronology: Reviews in Mineralogy and Geochemistry, v. 83, no. 1, p. 1-12.

Epin, M.-E., Manatschal, G., and Amann, M., 2017, Defining diagnostic criteria to describe the role of rift inheritance in collisional orogens: the case of the Err-Platta nappes (Switzerland): Swiss Journal of Geosciences, v. 110, no. 2, p. 419-438.
Ernst, R. E., and Bell, K., 2010, Large igneous provinces (LIPs) and carbonatites: Mineralogy and Petrology, v. 98, no. 1-4, p. 55-76.
Escartín, J., Hirth, G., and Evans, B., 2001, Strength of slightly serpentinized peridotites: Implications for the tectonics of oceanic lithosphere: Geology, v. 29, no. 11, p. 1023-1026.
Eyles, N., and Januszczak, N., 2004, 'Zipper-rift': a tectonic model for Neoproterozoic glaciations during the breakup of Rodinia after 750 Ma: Earth-Science Reviews, v. 65, no. 1-2, p. 1-73.
Faleide, J. I., Tsikalas, F., Breivik, A. J., Mjelde, R., Ritzmann, O., Engen, O., Wilson, J., and Eldholm, O., 2008, Structure and evolution of the continental margin off Norway and the Barents Sea: Episodes, v. 31, no. 1, p. 82-91.
Fauconnier, J., Labrousse, L., Andersen, T. B., Beyssac, O., Duprat-Oualid, S., and Yamato, P., 2014, Thermal structure of a major crustal shear zone, the basal thrust in the Scandinavian Caledonides: Earth and Planetary Science Letters, v. 385, p. 162-171.
Fettes, D. J., Macdonald, R., Fitton, J. G., Stephenson, D., and Cooper, M. R., 2011, Geochemical evolution of Dalradian metavolcanic rocks: implications for the break-up of the Rodinia supercontinent: Journal of the Geological Society, v. 168, no. 5, p. 1133.
Fichter, L. S., 1999, The Wilson Cycle, Volume 2019.
Fitton, J. G., Saunders, A. D., Norry, M. J., Hardarson, B. S., and Taylor, R. N., 1997, Thermal and chemical structure of the Iceland plume: Earth and Planetary Science Letters, v. 153, no. 3, p. 197-208.
Flament, N., Williams, S., Müller, R. D., Gurnis, M., and Bower, D. J., 2017, Origin and evolution of the deep thermochemical structure beneath Eurasia: Nature Communications, v. 8, p. 14164.
Forsyth, D., and Uyeda, S., 1975, On the Relative Importance of the Driving Forces of Plate Motion: Geophysical Journal International, v. 43, no. 1, p. 163-200.
Fossen, H., 1988, The Ulriken gneiss complex and the Rundemanen Formation: a basement-cover relationship in the Bergen Arcs, West Norway: Norges geologiske undersøkelse Bulletin, v. 412, p. 67-86.
-, 1993, Structural evolution of the Bergsdalen Nappes, southwest Norway: Norges geologiske undersøkelse Bulletin, v. 424, p. 23-50.
-, 2010, Structural geology, Cambridge University Press.
Fossen, H., and Dunlap, W. J., 1998, Timing and kinematics of Caledonian thrusting and extensional collapse, southern Norway: evidence from 40 Ar/39 Ar thermochronology: Journal of structural geology, v. 20, no. 6, p. 765-781.
Fossen, H., Khani, H. F., Faleide, J. I., Ksienzyk, A. K., and Dunlap, W. J., 2017, Post-Caledonian extension in the West Norway–northern North Sea region: the role of structural inheritance: Geological Society, London, Special Publications, v. 439, no. 1, p. 465.
Franke, D., 2013, Rifting, lithosphere breakup and volcanism: comparison of magma-poor and volcanic rifted margins: Marine and Petroleum geology, v. 43, p. 63-87.
Frasetto, A., and Thybo, H., 2013, Receiver function analysis of the crust and upper mantle in fennoscandia – isostatic implications: Earth and Planetary Science Letters, v. 381.
French, S. W., and Romanowicz, B., 2015, Broad plumes rooted at the base of the Earth's mantle beneath major hotspots: Nature, v. 525, p. 95.
Furnes, H., Dilek, Y., and Pedersen, R. B., 2012, Structure, geochemistry, and tectonic evolution of trench-distal backarc oceanic crust in the western Norwegian Caledonides, Solund-Stavfjord ophiolite (Norway): Bulletin, v. 124, no. 7-8, p. 1027-1047.
Furnes, H., Skjerlie, K., Pedersen, R., Andersen, T., Stillman, C. J., Suthren, R., Tysseland, M., and Garmann, L., 1990, The Solund–Stavfjord Ophiolite Complex and associated rocks, west Norwegian Caledonides: geology, geochemistry and tectonic environment: Geological Magazine, v. 127, no. 3, p. 209-224.

Gabrielsen, R. H., Nystuen, J. P., Jarsve, E. M., and Lundmark, A. M., 2015, The Sub-Cambrian Peneplain in southern Norway: its geological significance and its implications for post-Caledonian faulting, uplift and denudation: Journal of the Geological Society, v. 172, no. 6, p. 777-791.
Galerne, C. Y., Galland, O., Neumann, E.-R., and Planke, S., 2011, 3D relationships between sills and their feeders: evidence from the Golden Valley Sill Complex (Karoo Basin) and experimental modelling: Journal of Volcanology and Geothermal Research, v. 202, no. 3-4, p. 189-199.
Galerne, C. Y., Neumann, E.-R., and Planke, S., 2008, Emplacement mechanisms of sill complexes: Information from the geochemical architecture of the Golden Valley Sill Complex, South Africa: Journal of Volcanology and Geothermal Research, v. 177, no. 2, p. 425-440.
Galland, O., Burchardt, S., Hallot, E., Mourgues, R., and Bulois, C., 2014, Dynamics of dikes versus cone sheets in volcanic systems: Journal of Geophysical Research: Solid Earth, v. 119, no. 8, p. 6178-6192.
Garnero, E. J., Lay, T., and McNamara, A., 2007, Implications of lower-mantle structural heterogeneity for the existence and nature of whole-mantle plumes: Special Papers-Geological Society of America, v. 430, p. 79.
Gasser, D., 2014, The Caledonides of Greenland, Svalbard and other Arctic areas: status of research and open questions: Geological Society, London, Special Publications, v. 390, no. 1, p. 93-129.
Gasser, D., Jeřábek, P., Faber, C., Stünitz, H., Menegon, L., Corfu, F., Erambert, M., and Whitehouse, M., 2015, Behaviour of geochronometers and timing of metamorphic reactions during deformation at lower crustal conditions: phase equilibrium modelling and U–Pb dating of zircon, monazite, rutile and titanite from the Kalak Nappe Complex, northern Norway: Journal of Metamorphic Geology, v. 33, no. 5, p. 513-534.
Gee, D. G., 1975, A tectonic model for the central part of the Scandinavian Caledonides: American Journal of Science, v. 275, p. 468-515.
Gee, D. G., 1981, The Dictyonema-bearing phyllites at Nordaunevoll, eastern Trondelag, Norway: Norwegian Journal of Geology, v. 61.
Gee, D. G., Andréasson, P.-G., Li, Y., and Krill, A., 2016, Baltoscandian margin, Sveconorwegian crust lost by subduction during Caledonian collisional orogeny: GFF, p. 1-16.
Gee, D. G., Janák, M., Majka, J., Robinson, P., and van Roermund, H., 2013, Subduction along and within the Baltoscandian margin during closing of the Iapetus Ocean and Baltica-Laurentia collision: Lithosphere, v. 5, no. 2, p. 169-178.
Gee, D. G., Ladenberger, A., Dahlqvist, P., Majka, J., Be'eri-Shlevin, Y., Frei, D., and Thomsen, T., 2014, The Baltoscandian margin detrital zircon signatures of the central Scandes: Geological Society, London, Special Publications, v. 390, no. 1, p. 131-155.
Gee, D. G., and Sturt, B., 1985, The Caledonide orogen: Scandinavia and related areas, Wiley.
Geoffroy, L., 2001, The structure of volcanic margins: some problematics from the North-Atlantic/Labrador–Baffin system: Marine and Petroleum Geology, v. 18, no. 4, p. 463-469.
-, 2005, Volcanic passive margins: Comptes Rendus Geoscience, v. 337, no. 16, p. 1395-1408.
Geoffroy, L., Burov, E. B., and Werner, P., 2015, Volcanic passive margins: another way to break up continents: Scientific Reports, v. 5, p. 14828.
Gernigon, L., Franke, D., Geoffroy, L., Schiffer, C., Foulger, G. R., and Stoker, M., 2019, Crustal fragmentation, magmatism, and the diachronous opening of the Norwegian-Greenland Sea: Earth-Science Reviews.
Gernigon, L., Lucazeau, F., Brigaud, F., Ringenbach, J.-C., Planke, S., and Le Gall, B., 2006, A moderate melting model for the Vøring margin (Norway) based on structural observations and a thermo-kinematical modelling: Implication for the meaning of the lower crustal bodies: Tectonophysics, v. 412, no. 3, p. 255-278.
Gernigon, L., Ringenbach, J.-C., Planke, S., and Le Gall, B., 2004, Deep structures and breakup along volcanic rifted margins: insights from integrated studies along the outer Vøring Basin (Norway): Marine and Petroleum Geology, v. 21, no. 3, p. 363-372.

Gillard, M., Sauter, D., Tugend, J., Tomasi, S., Epin, M.-E., and Manatschal, G., 2017, Birth of an oceanic spreading center at a magma-poor rift system: Scientific Reports, v. 7, no. 1, p. 15072.
Gilotti, J. A., and Kumpulainen, R. A., 1986, Strain softening induced ductile flow in the Särv thrust sheet, Scandinavian Caledonides: Journal of Structural Geology, v. 8, no. 3, p. 441-455.
Gjelsvik, T., 1945, Anorthosittkolpekset i Heidal: Norwegian Journal of Geology, v. 26, p. 58.
Gladczenko, T. P., Skogseid, J., and Eldhom, O., 1998, Namibia volcanic margin: Marine Geophysical Researches, v. 20, no. 4, p. 313-341.
Glodny, J., Kühn, A., and Austrheim, H., 2008, Geochronology of fluid-induced eclogite and amphibolite facies metamorphic reactions in a subduction–collision system, Bergen Arcs, Norway: Contributions to Mineralogy and Petrology, v. 156, no. 1, p. 27-48.
Gouiza, M., and Paton, D. A., 2019, The role of inherited lithospheric heterogeneities in defining the crustal architecture of rifted margins and the magmatic budget during continental breakup: Geochemistry, Geophysics, Geosystems.
Gray, J. W., 1978, Structural history and Rb-Sr geochronology of Eksingedalen, west Norway: University of Aberdeen.
Greiling, R. O., and Garfunkel, Z., 2007, An Early Ordovician (Finnmarkian?) foreland basin and related lithospheric flexure in the Scandinavian Caledonides: American Journal of Science, v. 307, no. 2, p. 527-553.
Guezou, J.-C., 1978, Geology and structure of the Dombås-Lesja Area, Southern Trondheim Region, South-central Norway: NGU Bulletin, no. 340.
Hacker, B. R., Andersen, T. B., Johnston, S., Kylander-Clark, A. R., Peterman, E. M., Walsh, E. O., and Young, D., 2010, High-temperature deformation during continental-margin subduction & exhumation: The ultrahigh-pressure Western Gneiss Region of Norway: Tectonophysics, v. 480, no. 1, p. 149-171.
Halliday, A., Graham, C., Aftalion, M., and Dymoke, P., 1989, Short paper: the depositional age of the Dalradian Supergroup: U-Pb and Sm-Nd isotopic studies of the Tayvallich Volcanics, Scotland: Journal of the Geological Society, v. 146, no. 1, p. 3-6.
Halls, H. C., and Fahrig, W. F., 1987, Mafic dyke swarms, Geological Association of Canada Special Paper, Volume 34: Toronto, Canada, p. 503.
Halverson, G. P., Hoffman, P. F., Schrag, D. P., Maloof, A. C., and Rice, A. H. N., 2005, Toward a Neoproterozoic composite carbon-isotope record: Geological Society of America Bulletin, v. 117, no. 9-10, p. 1181-1207.
Halverson, G. P., Maloof, A. C., and Hoffman, P. F., 2004, The Marinoan glaciation (Neoproterozoic) in northeast Svalbard: Basin Research, v. 16, no. 3, p. 297-324.
Harper, D. A. T., Owen, A. W., and Bruton, D. L., 2009, Ordovician life around the Celtic fringes: diversifications, extinctions and migrations of brachiopod and trilobite faunas at middle latitudes: Geological Society, London, Special Publications, v. 325, no. 1, p. 157-170.
Heim, M., and Corfu, F., 2017, Heidal revisited-new light on critical elements in the allochthon of the classical Otta region (South Norway): EGU Gen. Assem., v. 2017.
Heim, M., Schärer, U., and Milnes, A. G., 1977, The nappe complex in the Tyin-Bygdin-Vang region, central southern Norway: Norsk Geologisk Tidsskrift, v. 57, p. 171-178.
Heimdal, T. H., Callegaro, S., Svensen, H. H., Jones, M. T., Pereira, E., and Planke, S., 2019, Evidence for magma–evaporite interactions during the emplacement of the Central Atlantic Magmatic Province (CAMP) in Brazil: Earth and Planetary Science Letters, v. 506, p. 476-492.
Heimdal, T. H., Svensen, H. H., Ramezani, J., Iyer, K., Pereira, E., Rodrigues, R., Jones, M. T., and Callegaro, S., 2018, Large-scale sill emplacement in Brazil as a trigger for the end-Triassic crisis: Scientific Reports, v. 8, no. 1, p. 141.
Henry, D. J., Guidotti, C. V., and Thomson, J. A., 2005, The Ti-saturation surface for low-to-medium pressure metapelitic biotites: implications for geothermometry and Ti-substitution mechanisms: American Mineralogist, v. 90, no. 2-3, p. 316-328.

Herzberg, C., Asimow, P. D., Arndt, N., Niu, Y., Lesher, C. M., Fitton, J. G., Cheadle, M. J., and Saunders, A. D., 2007, Temperatures in ambient mantle and plumes: Constraints from basalts, picrites, and komatiites: Geochemistry, Geophysics, Geosystems, v. 8, no. 2.
Herzberg, C., and Gazel, E., 2009, Petrological evidence for secular cooling in mantle plumes: Nature, v. 458, p. 619.
Heyn, B. H., Conrad, C. P., and Trønnes, R. G., 2018, Stabilizing Effect of Compositional Viscosity Contrasts on Thermochemical Piles: Geophysical Research Letters, v. 45, no. 15, p. 7523-7532.
Hill, R. I., 1991, Starting plumes and continental break-up: Earth and Planetary Science Letters, v. 104, no. 2, p. 398-416.
Hodych, J. P., and Cox, R. A., 2007, Ediacaran U–Pb zircon dates for the Lac Matapédia and Mt. St.-Anselme basalts of the Quebec Appalachians: support for a long-lived mantle plume during the rifting phase of Iapetus opening: Canadian Journal of Earth Sciences, v. 44, no. 4, p. 565-581.
Hoffman, P. F., Kaufman, A. J., Halverson, G. P., and Schrag, D. P., 1998, A Neoproterozoic snowball earth: science, v. 281, no. 5381, p. 1342-1346.
Hoffman, P. F., and Schrag, D. P., 2002, The snowball Earth hypothesis: testing the limits of global change: Terra nova, v. 14, no. 3, p. 129-155.
Hoffmann, K.-H., Condon, D., Bowring, S., and Crowley, J., 2004, U-Pb zircon date from the Neoproterozoic Ghaub Formation, Namibia: constraints on Marinoan glaciation: Geology, v. 32, no. 9, p. 817-820.
Holbrook, W. S., Larsen, H. C., Korenaga, J., Dahl-Jensen, T., Reid, I. D., Kelemen, P. B., Hopper, J. R., Kent, G. M., Lizarralde, D., Bernstein, S., and Detrick, R. S., 2001, Mantle thermal structure and active upwelling during continental breakup in the North Atlantic: Earth and Planetary Science Letters, v. 190, no. 3, p. 251-266.
Hollocher, K., Robinson, P., Walsh, E., and Roberts, D., 2012, Geochemistry of amphibolite-facies volcanics and gabbros of the Støren Nappe in extensions west and southwest of Trondheim, western gneiss region, Norway: A key to correlations and paleotectonic settings: American Journal of Science, v. 312, no. 4, p. 357-416.
Hollocher, K., Robinson, P., Walsh, E., and Terry, M. P., 2007, The Neoproterozoic Ottfjället dike swarm of the middle allochthon, traced geochemically into the Scandian hinterland, Western Gneiss Region, Norway: American Journal of Science, v. 307, no. 6, p. 901-953.
Holmsen, P., 1943, Geologiske og petrografiske undersøkelser i området Tynset-Femunden: NGU Bulletin, v. 158.
Holtedahl, O., 1922, A tillite-like conglomerate in the Eocambrian Sparagmite of southern Norway: American Journal of Science, no. 20, p. 165-173.
Huhma, H., Mänttäri, I., Peltonen, P., Kontinenz, A., Halkoaho, T., Hanski, E., Hokkanen, T., Hölttä, P., Juopperi, H., Konnunaho, J., Lahaye, Y., Luukkonen, E., Pietikäinen, K., Pulkkinen, A., Sorjonen-Ward, P., Vaasjoki, M., and Whitehouse, M., 2012, The age of the Archaean greenstone belts in Finland, Special Paper of the Geological Survey of Finland, Volume 2012, p. 74-175.
Huismans, R., and Beaumont, C., 2011, Depth-dependent extension, two-stage breakup and cratonic underplating at rifted margins: Nature, v. 473, p. 74.
Huismans, R. S., and Beaumont, C., 2014, Rifted continental margins: The case for depth-dependent extension: Earth and Planetary Science Letters, v. 407, p. 148-162.
Hyde, W. T., Crowley, T. J., Baum, S. K., and Peltier, W. R., 2000, Neoproterozoic 'snowball Earth' simulations with a coupled climate/ice-sheet model: Nature, v. 405, no. 6785, p. 425-429.
Iyer, K., Schmid, D. W., Planke, S., and Millett, J., 2017, Modelling hydrothermal venting in volcanic sedimentary basins: Impact on hydrocarbon maturation and paleoclimate: Earth and Planetary Science Letters, v. 467, p. 30-42.
Jakob, J., Alsaif, M., Corfu, F., and Andersen, T. B., 2017, Age and origin of thin discontinuous gneiss sheets in the distal domain of the magma-poor hyperextended pre-Caledonian margin of Baltica, southern Norway: Journal of the Geological Society, v. 174, no. 3, p. 557-571.

Jakob, J., Andersen, T. B., and Kjøll, H. J., 2019, A review and reinterpretation of the architecture of the South and South-Central Scandinavian Caledonides—A magma-poor to magma-rich transition and the significance of the reactivation of rift inherited structures: Earth-Science Reviews, v. 197, p. 513-528.
Jakob, J., Boulvais, P., and Andersen, T. B., 2018, Oxygen and carbon isotope compositions of carbonates in a prominent lithologically mixed unit in the central South Norwegian Caledonides: International Journal of Earth Sciences, v. 107, no. 4, p. 1445-1463.
Jamtveit, B., Svensen, H., Podladchikov, Y. Y., and Planke, S., 2004, Hydrothermal vent complexes associated with sill intrusions in sedimentary basins: Physical Geology of High-Level Magmatic Systems. Geological Society, London, Special Publications, v. 234, p. 233-241.
Janák, M., van Roermund, H., Majka, J., and Gee, D., 2013, UHP metamorphism recorded by kyanite-bearing eclogite in the Seve Nappe Complex of northern Jämtland, Swedish Caledonides: Gondwana Research, v. 23, no. 3, p. 865-879.
Johannes, W., 1984, Beginning of melting in the granite system Qz-Or-Ab-An-H 2 O: Contributions to Mineralogy and Petrology, v. 86, no. 3, p. 264-273.
Jones, T. D., Davies, D. R., Campbell, I. H., Wilson, C. R., and Kramer, S. C., 2016, Do mantle plumes preserve the heterogeneous structure of their deep-mantle source?: Earth and Planetary Science Letters, v. 434, p. 10-17.
Kalsbeek, F., Higgins, A. K., Jepsen, H. F., and al., e., 2008, Granites and granites in the East Greenland Caledonides, The Geological Society of America, Memoir.
Kamo, S. L., and Gower, C. F., 1994, Note: U-Pb baddeleyite dating clarifies age of characteristic paleomagnetic remanence of Long Range dykes, southeastern Labrador.
Kamo, S. L., Gower, C. F., and Krogh, T. E., 1989, Birthdate for the lapetus Ocean? A precise U-Pb zircon and baddeleyite age for the Long Range dikes, southeast Labrador: Geology, v. 17, no. 7, p. 602-605.
Kamo, S. L., Krogh, T. E., and Kumarapeli, P. S., 1995, Age of the Grenville dyke swarm, Ontario–Quebec: implications for the timing of lapetan rifting: Canadian Journal of Earth Sciences, v. 32, no. 3, p. 273-280.
Karson, J. A., and Brooks, C. K., 1999, Structural and magmatic segmentation of the Tertiary East Greenland volcanic rifted margin: Geological Society, London, Special Publications, v. 164, no. 1, p. 313-338.
Kathol, B., 1989, Evolution of the rifted and subducted late proterozoic to early Paleozoic Baltoscandian margin in the Torneträsk section, northern Swedish Caledonides: Stockholm Contributions in Geology, v. 42, no. 1, p. 83.
Katz, R. F., Spiegelman, M., and Langmuir, C. H., 2003, A new parameterization of hydrous mantle melting: Geochemistry, Geophysics, Geosystems, v. 4, no. 9.
Kavanagh, J. L., 2018, Mechanisms of Magma Transport in the Upper Crust—Dyking, Volcanic and Igneous Plumbing Systems, Elsevier, p. 55-88.
Keir, D., Bastow, I. D., Pagli, C., and Chambers, E. L., 2013, The development of extension and magmatism in the Red Sea rift of Afar: Tectonophysics, v. 607, p. 98-114.
Keir, D., Pagli, C., Bastow, I. D., and Ayele, A., 2011, The magma-assisted removal of Arabia in Afar: Evidence from dike injection in the Ethiopian rift captured using InSAR and seismicity: Tectonics, v. 30, no. 2.
Kelemen, P. B., and Holbrook, W. S., 1995, Origin of thick, high‐velocity igneous crust along the US East Coast Margin: Journal of Geophysical Research: Solid Earth, v. 100, no. B6, p. 10077-10094.
Keller, T., May, D. A., and Kaus, B. J., 2013, Numerical modelling of magma dynamics coupled to tectonic deformation of lithosphere and crust: Geophysical Journal International, v. 195, no. 3, p. 1406-1442.
Kendall, B., Creaser, R. A., and Selby, D., 2006, Re-Os geochronology of postglacial black shales in Australia: Constraints on the timing of “Sturtian” glaciation: Geology, v. 34, no. 9, p. 729-732.

Kimbell, G. S., Stewart, M. A., Gradmann, S., Shannon, P. M., Funck, T., Haase, C., Stoker, M. S., and Hopper, J. R., 2017, Controls on the location of compressional deformation on the NW European margin: Geological Society, London, Special Publications, v. 447, no. 1, p. 249.
Kimura, J.-I., Takahashi, T., and Chang, Q., 2013, A new analytical bias correction for in situ Sr isotope analysis of plagioclase crystals using laser-ablation multiple-collector inductively coupled plasma mass spectrometry: Journal of Analytical Atomic Spectrometry, v. 28, no. 6, p. 945-957.
Kirkland, C. L., Bingen, B., Whitehouse, M., Beyer, E., and Griffin, W., 2011, Neoproterozoic palaeogeography in the North Atlantic Region: inferences from the Akkajaure and Seve Nappes of the Scandinavian Caledonides: Precambrian Research, v. 186, no. 1, p. 127-146.
Kirkland, C. L., Daly, J. S., Eide, E. A., and Whitehouse, M. J., 2007, Tectonic evolution of the Arctic Norwegian Caledonides from a texturally- and structurally-constrained multi-isotopic (Ar-Ar, Rb-Sr, Sm-Nd, U-Pb) study: American Journal of Science, v. 307, no. 2, p. 459-526.
Kirsch, M., and Svenningsen, O. M., 2015, Root zone of a continental rift: the Neoproterozoic Kebnekaise Intrusive Complex, northern Swedish Caledonides: GFF, p. 1-23.
Kirschvink, J. L., 1992, Late Proterozoic low-latitude global glaciation: the snowball Earth.
Kjøll, H. J., Andersen, T. B., Corfu, F., Labrousse, L., Tegner, C., Abdelmalak, M. M., and Planke, S., 2019a, Timing of break-up and thermal evolution of a pre-Caledonian Neoproterozoic exhumed magma-rich rifted margin: Tectonics.
Kjøll, H. J., Galland, O., Labrousse, L., and Andersen, T. B., 2019b, Emplacement mechanisms of a dyke swarm across the Brittle-Ductile transition and the geodynamic implications for magma-rich margins: Earth and Planetary Science Letters.
Klausen, M. B., 2006, Similar dyke thickness variation across three volcanic rifts in the North Atlantic region: Implications for intrusion mechanisms: Lithos, v. 92, no. 1, p. 137-153.
Klausen, M. B., and Larsen, H. C., 2002, East Greenland coast-parallel dike swarm and its role in continental breakup: Special paper-Geological Society of America, no. 362, p. 133-158.
Klonowska, I., Janák, M., Majka, J., Petrík, I., Froitzheim, N., Gee, D. G., and Sasinková, V., 2017, Microdiamond on Åreskutan confirms regional UHP metamorphism in the Seve Nappe Complex of the Scandinavian Caledonides: Journal of Metamorphic Geology, v. 35, no. 5, p. 541-564.
Koehl, J.-B. P., Bergh, S. G., and Wemmer, K., 2018, Neoproterozoic and post-Caledonian exhumation and shallow faulting in NW Finnmark from K‐Ar dating and p/ T analysis of fault rocks: Solid Earth, v. 9, no. 4, p. 923-951.
Koestler, A., 1983, Zentral Komplex und NW-Randzone der Jotundecke West-Jotunheimen, Südnorwegen: Strukturgeologie und Geochronologie: ETH Zurich.
Kolstrup, M. L., and Maupin, V., 2013, A Proterozoic boundary in southern Norway revealed by joint-inversion of P-receiver functions and surface waves: Precambrian Research, v. 238.
Kristoffersen, M., Andersen, T., and Andresen, A., 2013, U–Pb age and Lu–Hf signatures of detrital zircon from Palaeozoic sandstones in the Oslo Rift, Norway: Geological Magazine, v. 151, no. 5, p. 816-829.
Kristoffersen, M., Andersen, T., Elburg, M. A., and Watkeys, M. K., 2016, Detrital zircon in a supercontinental setting: locally derived and far-transported components in the Ordovician Natal Group, South Africa: Journal of the Geological Society, v. 173, no. 1, p. 203-215.
Krogh, T., 1973, A low-contamination method for hydrothermal decomposition of zircon and extraction of U and Pb for isotopic age determinations: Geochimica et Cosmochimica Acta, v. 37, no. 3, p. 485-494.
Krumbholz, M., Hieronymus, C. F., Burchardt, S., Troll, V. R., Tanner, D. C., and Friese, N., 2014, Weibull-distributed dyke thickness reflects probabilistic character of host-rock strength: Nature communications, v. 5, p. 3272.
Kullerud, K., Stephens, M., and Zachrisson, E., 1990, Pillow lavas as protoliths for eclogites: evidence from a late Precambrian-Cambrian continental margin, Seve Nappes, Scandinavian Caledonides: Contributions to Mineralogy and Petrology, v. 105, no. 1, p. 1-10.

Kumpulainen, R. A., 1980, Upper Proterozoic stratigraphy and depositional environments of the Tossåsfjället Group, Särv Nappe, southern Swedish Caledonides: GFF, v. 102, no. 4, p. 531-550.
Kumpulainen, R. A., 2011, Chapter 61 The Neoproterozoic glaciogenic Lillfjället Formation, southern Swedish Caledonides: Geological Society, London, Memoirs, v. 36, no. 1, p. 629.
Kumpulainen, R. A., and Greiling, R. O., 2011, Chapter 60 Evidence for late Neoproterozoic glaciation in the central Scandinavian Caledonides: Geological Society, London, Memoirs, v. 36, no. 1, p. 623.
Kumpulainen, R. A., Hamilton, M. A., Söderlund, U., and Nystuen, J. P., 2016, A new U-Pb baddeleyite age for the Ottfjället dolerite dyke swarm in the Scandinavian Caledonides - a minimum age for late Neoproterozoic glaciation in Baltica, Nordic Geologic Winter Meeting: Helsinki.
Kumpulainen, R. A., and Nystuen, J. P., 1985, Late Proterozoic basin evolution and sedimentation in the westernmost part of Baltoscandia: The Caledonide Orogen—Scandinavia and Related Areas, v. 1, p. 213-245.
Kvale, A., 1945, Petrologic and structural studies in the Bergsdalen quadrangle, Western Norway, Part 1, Petrography: Bergens Museums Årbok, v. 1.
Kühn, A., Glodny, J., Austrheim, H., and Råheim, A., 2002, The Caledonian tectono-metamorphic evolution of the Lindås Nappe: Constraints from U-Pb, Sm-Nd and Rb-Sr ages of granitoid dykes: Norwegian Journal of Geology/Norsk Geologisk Forening, v. 82, no. 1.
Kühn, D., and Dahm, T., 2008, Numerical modelling of dyke interaction and its influence on oceanic crust formation: Tectonophysics, v. 447, no. 1-4, p. 53-65.
Labails, C., Olivet, J.-L., Aslanian, D., and Roest, W. R., 2010, An alternative early opening scenario for the Central Atlantic Ocean: Earth and Planetary Science Letters, v. 297, no. 3, p. 355-368.
Labrousse, L., Hetényi, G., Raimbourg, H., Jolivet, L., and Andersen, T. B., 2010, Initiation of crustal-scale thrusts triggered by metamorphic reactions at depth: Insights from a comparison between the Himalayas and Scandinavian Caledonides: Tectonics, v. 29, no. 5.
Labrousse, L., Huet, B., Le Pourhiet, L., Jolivet, L., and Burov, E., 2016, Rheological implications of extensional detachments: Mediterranean and numerical insights: Earth-Science Reviews, v. 161, p. 233-258.
Ladenberger, A., Be, eri-Shlevin, Y., Claesson, S., Gee, D. G., Majka, J., and Romanova, I. V., 2014, Tectonometamorphic evolution of the Åreskutan Nappe – Caledonian history revealed by SIMS U–Pb zircon geochronology: Geological Society, London, Special Publications, v. 390, no. 1, p. 337.
Lagabrielle, Y., Labaume, P., and de Saint Blanquat, M., 2010, Mantle exhumation, crustal denudation, and gravity tectonics during Cretaceous rifting in the Pyrenean realm (SW Europe): Insights from the geological setting of the lherzolite bodies: Tectonics, v. 29, no. 4.
Lamminen, J., Andersen, T., and Nystuen, J. P., 2011, Zircon U-Pb ages and Lu-Hf isotopes from basement rocks associated with Neoproterozoic sedimentary successions in the Sparagmite Region and adjacent areas, South Norway: the crustal architecture of western Baltica: Norwegian Journal of Geology, v. 91, p. 35-55.
Lamminen, J., Andersen, T., and Nystuen, J. P., 2015, Provenance and rift basin architecture of the Neoproterozoic Hedmark Basin, South Norway inferred from U–Pb ages and Lu–Hf isotopes of conglomerate clasts and detrital zircons: Geological Magazine, v. 152, no. 1, p. 80-105.
Larsen, H. C., Mohn, G., Nirrengarten, M., Sun, Z., Stock, J., Jian, Z., Klaus, A., Alvarez-Zarikian, C., Boaga, J., and Bowden, S., 2018a, Rapid transition from continental breakup to igneous oceanic crust in the South China Sea: Nature Geoscience, p. 1.
Larsen, R. B., Grant, T., Sørensen, B. E., Tegner, C., McEnroe, S., Pastore, Z., Fichler, C., Nikolaisen, E., Grannes, K. R., Church, N., ter Maat, G. W., and Michels, A., 2018b, Portrait of a giant deep-seated magmatic conduit system: The Seiland Igneous Province: Lithos, v. 296-299, p. 600-622.
Lavier, L. L., and Manatschal, G., 2006, A mechanism to thin the continental lithosphere at magma-poor margins: Nature, v. 440, no. 7082, p. 324.

Le Heron, D. P., Hogan, K. A., Phillips, E. R., Huuse, M., Busfield, M. E., and Graham, A. G. C., 2019, An introduction to glaciated margins: the sedimentary and geophysical archive: Geological Society, London, Special Publications, v. 475, no. 1, p. 1-8.
Lee, C.-T. A., and Chin, E. J., 2014, Calculating melting temperatures and pressures of peridotite protoliths: Implications for the origin of cratonic mantle: Earth and Planetary Science Letters, v. 403, p. 273-286.
Lee, C.-T. A., Luffi, P., Plank, T., Dalton, H., and Leeman, W. P., 2009, Constraints on the depths and temperatures of basaltic magma generation on Earth and other terrestrial planets using new thermobarometers for mafic magmas: Earth and Planetary Science Letters, v. 279, no. 1, p. 20-33.
Legrand, D., Calahorrano, A., Guillier, B., Rivera, L., Ruiz, M., Villagomez, D., and Yepes, H., 2002, Stress tensor analysis of the 1998-1999 tectonic swarm of northern Quito related to the volcanic swarm of Guagua Pichincha volcano, Ecuador: Tectonophysics, v. 344, no. 1-2, p. 15-36.
Levell, B., Argent, J., Doré, A., and Fraser, S., Passive margins: overview, *in* Proceedings Geological Society, London, Petroleum Geology Conference series2010, Volume 7, Geological Society of London, p. 823-830.
Li, Y., Deschamps, F., and Tackley, P. J., 2014, Effects of low-viscosity post-perovskite on the stability and structure of primordial reservoirs in the lower mantle: Geophysical Research Letters, v. 41, no. 20, p. 7089-7097.
-, 2015, Effects of the post-perovskite phase transition properties on the stability and structure of primordial reservoirs in the lower mantle of the Earth: Earth and Planetary Science Letters, v. 432, p. 1-12.
Li, Z.-X., Bogdanova, S., Collins, A., Davidson, A., De Waele, B., Ernst, R., Fitzsimons, I., Fuck, R., Gladkochub, D., and Jacobs, J., 2008, Assembly, configuration, and break-up history of Rodinia: a synthesis: Precambrian research, v. 160, no. 1, p. 179-210.
Li, Z.-X., and Zhong, S., 2009, Supercontinent–superplume coupling, true polar wander and plume mobility: Plate dominance in whole-mantle tectonics: Physics of the Earth and Planetary Interiors, v. 176, no. 3, p. 143-156.
Lindahl, I., Stevens, B. P., and Zwaan, K. B., 2005, The geology of the Vaddas area, Troms: a key to our understanding of the Upper Allochthon in the Caledonides of northern Norway: Norges Geologiske Undersøkelse, v. 445, no. 5.
Ludwig, R. K., 1992, ISOPLOT a plotting and regression program for radiogenic-isotope data, version 2.57: US Geol. Surv., Open File Rept., v. 40.
Lundin, E. R., and Doré, A. G., 2011, Hyperextension, serpentinization, and weakening: A new paradigm for rifted margin compressional deformation: Geology, v. 39, no. 4, p. 347-350.
Lundmark, A., and Corfu, F., 2007, Age and origin of the Ardal dike complex, SW Norway: False isochrons, incomplete mixing, and the origin of Caledonian granites in basement nappes: Tectonics, v. 26.
-, 2008, Late-orogenic Sveconorwegian massif anorthosite in the Jotun Nappe Complex, SW Norway, and causes of repeated AMCG magmatism along the Baltoscandian margin: Contributions to Mineralogy and Petrology, v. 155, no. 2, p. 147-163.
Maccaferri, F., Rivalta, E., Keir, D., and Acocella, V., 2014, Off-rift volcanism in rift zones determined by crustal unloading: Nature Geoscience, v. 7, no. 4, p. 297.
Maffione, M., van Hinsbergen, D. J. J., Koornneef, L. M. T., Huang, W., Guilmette, C., Hodges, K., Borneman, N., Ding, L., and Kapp, P., 2015, Forearc hyperextension dismembered the south Tibetan ophiolites: Geology, v. 43, no. 6, p. 475-478.
Magee, C., Muirhead, J. D., Karvelas, A., Holford, S. P., Jackson, C. A. L., Bastow, I. D., Schofield, N., Stevenson, C. T. E., McLean, C., McCarthy, W., and Shtukert, O., 2016, Lateral magma flow in mafic sill complexes: Geosphere, v. 12, no. 3, p. 809-841.
Maijer, C., and Verschure, R., 1998, Petrology and isotope geology of the Hunnedalen monzonoritic dyke swarm, SW Norway: a possible late expression of Egersund anorthosite magmatism: Norges geologiske undersøkelse Bulletin, v. 434, p. 83-107.

Majka, J., Rosén, Å., Janák, M., Froitzheim, N., Klonowska, I., Manecki, M., Sasinková, V., and Yoshida, K., 2014, Microdiamond discovered in the Seve Nappe (Scandinavian Caledonides) and its exhumation by the "vacuum-cleaner" mechanism: Geology, v. 42, no. 12, p. 1107-1110.
Manatschal, G., 2004, New models for evolution of magma-poor rifted margins based on a review of data and concepts from West Iberia and the Alps: International Journal of Earth Sciences, v. 93, no. 3, p. 432-466.
Manatschal, G., Froitzheim, N., Rubenach, M., and Turrin, B. D., 2001, The role of detachment faulting in the formation of an ocean-continent transition: insights from the Iberia Abyssal Plain: Geological Society, London, Special Publications, v. 187, no. 1, p. 405.
Manatschal, G., and Müntener, O., 2009, A type sequence across an ancient magma-poor ocean–continent transition: the example of the western Alpine Tethys ophiolites: Tectonophysics, v. 473, no. 1, p. 4-19.
Manatschal, G., and Nievergelt, P., 1997, A continent-ocean transition recorded in the Err and Platta nappes (Eastern Switzerland): Eclogae Geologicae Helvetiae, v. 90, no. 1, p. 3-28.
Marzoli, A., Renne, P. R., Piccirillo, E. M., Ernesto, M., Bellieni, G., and Min, A. D., 1999, Extensive 200-Million-Year-Old Continental Flood Basalts of the Central Atlantic Magmatic Province: Science, v. 284, no. 5414, p. 616.
McClellan, E. A., 1994, Contact relationships in the southeastern Trondheim Nappe complex, central-southern Norway: Implications for early Paleozoic tectonism in the Scandinavian Caledonides: Tectonophysics, v. 231, no. 1, p. 85-111.
McClellan, E. A., 2004, Metamorphic conditions across the Seve-Köli Nappe boundary, southeastern Trondheim region, Norwegian Caledonides: Comparison of garnet-biotite thermometry and amphibole chemistry: Norwegian Journal of Geology, v. 54.
McDermott, C., Lonergan, L., Collier, J. S., McDermott, K. G., and Bellingham, P., 2018, Characterization of Seaward-Dipping Reflectors Along the South American Atlantic Margin and Implications for Continental Breakup: Tectonics, v. 37, no. 9, p. 3303-3327.
McDermott, K., and Reston, T., 2015, To see, or not to see? Rifted margin extension: Geology, v. 43, no. 11, p. 967-970.
McDonough, W. F., and Sun, S. s., 1995, The composition of the Earth: Chemical Geology, v. 120, no. 3, p. 223-253.
Meert, J. G., 2014, Strange attractors, spiritual interlopers and lonely wanderers: The search for pre-Pangean supercontinents: Geoscience Frontiers, v. 5, no. 2, p. 155-166.
Menzies, M. A., Klemperer, S. L., Ebinger, C. J., and Baker, J., 2002, Characteristics of volcanic rifted margins, *in* Menzies, M. A., Klemperer, S. L., Ebinger, C. J., and Baker, J., eds., Volcanic Rifted Margins, Volume 362, Geological Society of America.
Merdith, A. S., Collins, A. S., Williams, S. E., Pisarevsky, S., Foden, J. D., Archibald, D. B., Blades, M. L., Alessio, B. L., Armistead, S., Plavsa, D., Clark, C., and Müller, R. D., 2017, A full-plate global reconstruction of the Neoproterozoic: Gondwana Research, v. 50, p. 84-134.
Meyer, R., Hertogen, J., Pedersen, R. B., Viereck-Götte, L., and Abratis, M., 2009, Interaction of mantle derived melts with crust during the emplacement of the Vøring Plateau, NE Atlantic: Marine Geology, v. 261, no. 1, p. 3-16.
Mjelde, R., Digranes, P., Van Schaack, M., Shimamura, H., Shiobara, H., Kodaira, S., Naess, O., Sørenes, N., and Vågnes, E., 2001, Crustal structure of the outer Vøring Plateau, offshore Norway, from ocean bottom seismic and gravity data: Journal of Geophysical Research: Solid Earth, v. 106, no. B4, p. 6769-6791.
Mjelde, R., Raum, T., Digranes, P., Shimamura, H., Shiobara, H., and Kodaira, S., 2003, Vp/Vs ratio along the Vøring Margin, NE Atlantic, derived from OBS data: implications on lithology and stress field: Tectonophysics, v. 369, no. 3, p. 175-197.
Mohn, G., Manatschal, G., Beltrando, M., and Haupert, I., 2014, The role of rift‐inherited hyper‐extension in Alpine‐type orogens: Terra Nova, v. 26, no. 5, p. 347-353.

Mohn, G., Manatschal, G., Beltrando, M., Masini, E., and Kusznir, N., 2012, Necking of continental crust in magma‐poor rifted margins: Evidence from the fossil Alpine Tethys margins: Tectonics, v. 31, no. 1.
Mohn, G., Manatschal, G., Masini, E., and Müntener, O., 2011, Rift-related inheritance in orogens: a case study from the Austroalpine nappes in Central Alps (SE-Switzerland and N-Italy): International Journal of Earth Sciences, v. 100, no. 5, p. 937-961.
Mohn, G., Manatschal, G., Müntener, O., Beltrando, M., and Masini, E., 2010, Unravelling the interaction between tectonic and sedimentary processes during lithospheric thinning in the Alpine Tethys margins: International Journal of Earth Sciences, v. 99, no. 1, p. 75-101.
Moreira, M., Breddam, K., Curtice, J., and Kurz, M. D., 2001, Solar neon in the Icelandic mantle: new evidence for an undegassed lower mantle: Earth and Planetary Science Letters, v. 185, no. 1, p. 15-23.
Morgan, W. J., 1971, Convection Plumes in the Lower Mantle: Nature, v. 230, no. 5288, p. 42-43.
Morley, C. K., 2002, A tectonic model for the Tertiary evolution of strike–slip faults and rift basins in SE Asia: Tectonophysics, v. 347, no. 4, p. 189-215.
Mulyukova, E., Steinberger, B., Dabrowski, M., and Sobolev, S. V., 2015, Survival of LLSVPs for billions of years in a vigorously convecting mantle: Replenishment and destruction of chemical anomaly: Journal of Geophysical Research: Solid Earth, v. 120, no. 5, p. 3824-3847.
Murthy, G., Gower, C., Tubrett, M., and Pätzold, R., 1992, Paleomagnetism of Eocambrian Long Range dykes and Double Mer Formation from Labrador, Canada: Canadian Journal of Earth Sciences, v. 29, no. 6, p. 1224-1234.
Mutter, J. C., Buck, W. R., and Zehnder, C. M., 1988, Convective partial melting: 1. A model for the formation of thick basaltic sequences during the initiation of spreading: Journal of Geophysical Research: Solid Earth, v. 93, no. B2, p. 1031-1048.
Mutter, J. C., Talwani, M., and Stoffa, P. L., 1982, Origin of seaward-dipping reflectors in oceanic crust off the Norwegian margin by “subaerial sea-floor spreading”: Geology, v. 10, no. 7, p. 353-357.
Müntener, O., Manatschal, G., Desmurs, L., and Pettke, T., 2009, Plagioclase Peridotites in Ocean–Continent Transitions: Refertilized Mantle Domains Generated by Melt Stagnation in the Shallow Mantle Lithosphere: Journal of Petrology, v. 51, no. 1-2, p. 255-294.
Nakada, M., and Karato, S.-i., 2012, Low viscosity of the bottom of the Earth’s mantle inferred from the analysis of Chandler wobble and tidal deformation: Physics of the Earth and Planetary Interiors, v. 192-193, p. 68-80.
Nakamura, K., 1977, Volcanoes as possible indicators of tectonic stress orientation—principle and proposal: Journal of Volcanology and Geothermal Research, v. 2, no. 1, p. 1-16.
Naliboff, J., and Buiter, S. J. H., 2015, Rift reactivation and migration during multiphase extension: Earth and Planetary Science Letters, v. 421, p. 58-67.
Naney, M. T., 1983, Phase equilibria of rock-forming ferromagnesian silicates in granitic systems: Amercan Journal of Science, v. 283.
Neave, D. A., and Putirka, K. D., 2017, A new clinopyroxene-liquid barometer, and implications for magma storage pressures under Icelandic rift zones: American Mineralogist, v. 102, no. 4, p. 777-794.
Nickelsen, R., Hossack, J., Garton, M., and Repetsky, J., 1985, Late Precambrian to Ordovician stratigraphy and correlation in the Valdres and Synnfjell thrust sheets of the Valdres area, southern Norwegian Caledonides; with some comments on sedimentation: The Caledonide Orogen—Scandinavia and Related Areas. Wiley and Sons, Chichester, p. 369-378.
Nielsen, C., and Thybo, H., 2009, Lower crustal intrusions beneath the southern Baikal Rift Zone: evidence from full-waveform modelling of wide-angle seismic data: Tectonophysics, v. 470, no. 3-4, p. 298-318.
Nilsen, O., 1988, The Tectonostratigraphic setting of Stratabound Sulphide Deposits in the southern Trondheim Region, Central Norwegian Caledonides: NGU Bulletin, v. 412.

Nilsen, O., Corfu, F., and Roberts, R. J., 2007, Silurian gabbro-diorite-trondhjemite plutons in the Trondheim Nappe complex, Caledonides, Norway: petrology and U-Pb geochronology: Norwegian Journal of Geology, no. 87.
Nilsen, O., Sundvoll, B., Roberts, D., and Corfu, F., 2003, U-Pb Geochronology and Geochemistry of Trondhjemites and a Norite Pluton from the SW Trondheim Region, Central Norwegian Caledonides: NGU Bulletin, v. 441
Nilsen, O., and Wolff, F. C., 1989, Geolgisk Kart Over Norge, Berggrunnskart Roros & Sveg.
Nilsson, L. P., and Roberts, D., 2014, A trail of ophiolitic debris and its detritus along the Trøndelag-Jämtland border correllations and palaeoge: NGU Bulletin, v. 453.
Nilsson, L. P., Sturt, B. A., and Ramsay, D. M., 1997, Ophiolitic ultramafites in the Folldal-Røros tract, and their Cr-(PGE) mineralisation: NGU Bulletin, v. 433.
Nystuen, J. P., 1969, On the paragenesis of chert and carbonate minerals in chert-bearing magnesitic dolomite from the Kvitvola Nappe, southern Norway: Nor. Geol. Unders, v. 258, p. 66-78.
-, 1976, Late Precambrian Moelv tillite deposited on a discontinuity surface associated with a fossil ice wedge, Rendalen, southern Norway: Norsk Geol. Tidsskr, v. 56, p. 29-50.
-, 1980, Stratigraphy of the Upper Proterozoic Engerdalen Group, Kvitvola Nappe, southeastern Scandinavian Caledonides: Geologiska Föreningen i Stockholm Förhandlingar, v. 102, no. 4, p. 551-560.
-, 1983, Nappe and thrust structures in the Sparagmite Region, southern Norway: Norges geologiske undersøkelse, v. 380, p. 67-83.
-, 1987, Synthesis of the tectonic and sedimentological evolution of the late Proterozoic-early Cambrian Hedmark Basin, the Caledonian Thrust Belt, southern Norway: Norsk geologisk tidsskrift, v. 67, no. 4, p. 395-418.
Nystuen, J. P., Andresen, A., Kumpulainen, R. A., and Siedlecka, A., 2008, Neoproterozoic basin evolution in Fennoscandia, East Greenland and Svalbard: Episodes, v. 31, no. 1, p. 35-43.
Nystuen, J. P., Kumpulainen, R. A., Söderlund, U., and Hamilton, M. A., 2016, The Varangerian/Marinoan glaciation in Scandinavia - new age constraints, Nordic Geological Winter Meeting: Helsinki.
Nystuen, J. P., and Lamminen, J. T., 2011, Chapter 59 Neoproterozoic glaciation of South Norway: from continental interior to rift and pericratonic basins in western Baltica: Geological Society, London, Memoirs, v. 36, no. 1, p. 613.
O'Connor, J. M., Stoffers, P., Wijbrans, J. R., Shannon, P. M., and Morrissey, T., 2000, Evidence from episodic seamount volcanism for pulsing of the Iceland plume in the past 70 Myr: Nature, v. 408, no. 6815, p. 954-958.
Olesen, O., Gellein, J., Gernigon, L., Kihle, O., J., K., Lauritsen, T., Mogaard, J. O., and R., M., 2010, Magnetic Anomaly Map, Norway and Adjacent Areas.
Oriolo, S., Wemmer, K., Oyhantçabal, P., Fossen, H., Schulz, B., and Siegesmund, S., 2018, Geochronology of shear zones – A review: Earth-Science Reviews, v. 185, p. 665-683.
Osmundsen, P. T., Péron-Pinvidic, G., Ebbing, J., Erratt, D., Fjellanger, E., Bergslien, D., and Syvertsen, S. E., 2016, Extension, hyperextension and mantle exhumation offshore Norway: a discussion based on 6 crustal transects: Norwegian Journal of Geology, v. 96, p. 343-372.
Owen, A. W., and Bockelie, J. F., 1990, The Ordovician successions of the Oslo region, Norway, NGU Trondheim.
Pasquare, F., and Tibaldi, A., 2007, Structure of a sheet-laccolith system revealing the interplay between tectonic and magma stresses at Stardalur Volcano, Iceland: Journal of Volcanology and Geothermal Research, v. 161, no. 1-2, p. 131-150.
Paulsson, O., and Andreasson, P.-G., 2002, Attempted break-up of Rodinia at 850 Ma: geochronological evidence from the Seve–Kalak Superterrane, Scandinavian Caledonides: Journal of the Geological Society, v. 159, no. 6, p. 751-761.
Pearce, J. A., 2008, Geochemical fingerprinting of oceanic basalts with applications to ophiolite classification and the search for Archean oceanic crust: Lithos, v. 100, no. 1, p. 14-48.

Pease, V., Daly, J., Elming, S.-Å., Kumpulainen, R., Moczydlowska, M., Puchkov, V., Roberts, D., Saintot, A., and Stephenson, R., 2008, Baltica in the Cryogenian, 850–630 Ma: Precambrian Research, v. 160, no. 1-2, p. 46-65.
Peron-Pinvidic, G., Gernigon, L., Gaina, C., and Ball, P., 2012, Insights from the Jan Mayen system in the Norwegian–Greenland sea—I. Mapping of a microcontinent: Geophysical Journal International, v. 191, no. 2, p. 385-412.
Péron-Pinvidic, G., and Manatschal, G., 2009, The final rifting evolution at deep magma-poor passive margins from Iberia-Newfoundland: a new point of view: International Journal of Earth Sciences, v. 98, no. 7, p. 1581-1597.
-, 2010, From microcontinents to extensional allochthons: witnesses of how continents rift and break apart?: Petroleum Geoscience, v. 16, no. 3, p. 189-197.
Péron-Pinvidic, G., Manatschal, G., Minshull, T. A., and Sawyer, D. S., 2007, Tectonosedimentary evolution of the deep Iberia‐Newfoundland margins: Evidence for a complex breakup history: Tectonics, v. 26, no. 2.
Peron-Pinvidic, G., Manatschal, G., and Osmundsen, P. T., 2013, Structural comparison of archetypal Atlantic rifted margins: A review of observations and concepts: Marine and Petroleum Geology, v. 43, p. 21-47.
Péron-Pinvidic, G., Manatschal, G., and Osmundsen, P. T., 2013, Structural comparison of archetypal Atlantic rifted margins: A review of observations and concepts: Marine and Petroleum Geology, v. 43, p. 21-47.
Petri, B., Duretz, T., Mohn, G., Schmalholz, S. M., Karner, G. D., and Müntener, O., 2019, Thinning mechanisms of heterogeneous continental lithosphere: Earth and Planetary Science Letters, v. 512, p. 147-162.
Pettersson, A., 2003, Jämförande litologisk och geokemisk studie av Sevens amfibolitkomplex i Sylarna och Kebnekaise: Examensarbeten i geologi vid Lunds universitet.
Pharaoh, T., 1985, The stratigraphy and sedimentology of autochthonous metasediments in the Repparfjord-Komagfjord Tectonic Window, west Finnmark, *in* Gee, D. G., and Sturt, B. A., eds., The Caledonide Orogen - Scandinavia and Related Areas, John Wiley & Sons Ltd, p. 347-372.
Pik, R., Marty, B., Carignan, J., Yirgu, G., and Ayalew, T., 2008, Timing of East African Rift development in southern Ethiopia: Implication for mantle plume activity and evolution of topography: Geology, v. 36, no. 2, p. 167-170.
Plank, T., and Langmuir, C. H., 1992, Effects of the melting regime on the composition of the oceanic crust: Journal of Geophysical Research: Solid Earth, v. 97, no. B13, p. 19749-19770.
Planke, S., and Alvestad, E., Seismic volcanostratigraphy of the extrusive breakup complexes in the northeast Atlantic: Implications from ODP/DSDP drilling, *in* Proceedings Proceedings of the Ocean Drilling Program, Scientific Results1999, Volume 163, p. 3-16.
Planke, S., and Eldholm, O., 1994, Seismic response and construction of seaward dipping wedges of flood basalts: Vøring volcanic margin: Journal of Geophysical Research: Solid Earth, v. 99, no. B5, p. 9263-9278.
Planke, S., Symonds, P. A., Alvestad, E., and Skogseid, J., 2000, Seismic volcanostratigraphy of large‐volume basaltic extrusive complexes on rifted margins: Journal of Geophysical Research: Solid Earth, v. 105, no. B8, p. 19335-19351.
Plink-Björklund, P., Björklund, L., and Loorents, K.-J., 2005, Sedimentary documentation of the break-up of Rodinia, Offerdal Nappe, Swedish Caledonides: Precambrian Research, v. 136, no. 1, p. 1-26.
Prada, M., Ranero, C. R., Sallarès, V., Zitellini, N., and Grevemeyer, I., 2016, Mantle exhumation and sequence of magmatic events in the Magnaghi–Vavilov Basin (Central Tyrrhenian, Italy): New constraints from geological and geophysical observations: Tectonophysics, v. 689, p. 133-142.
Pringle, I. R., Kvale, A., and Anonsen, L. B., 1975, The age of the Hernes granite, Lower Bergsdalen Nappe, western Norway: Norwegian Journal of Geology, v. 55, p. 191-195.

Pu, J. P., Bowring, S. A., Ramezani, J., Myrow, P., Raub, T. D., Landing, E., Mills, A., Hodgin, E., and Macdonald, F. A., 2016, Dodging snowballs: Geochronology of the Gaskiers glaciation and the first appearance of the Ediacaran biota: Geology, v. 44, no. 11, p. 955-958.
Puffer, J. H., 2002, A late Neoproterozoic eastern Laurentian superplume: Location, size, chemical composition, and environmental impact: American Journal of Science, v. 302, no. 1, p. 1-27.
Putirka, K. D., 2008, Thermometers and barometers for volcanic systems: Reviews in Mineralogy and Geochemistry, v. 69, no. 1, p. 61-120.
Ramos, F. C., Wolff, J. A., and Tollstrup, D. L., 2004, Measuring 87Sr/86Sr variations in minerals and groundmass from basalts using LA-MC-ICPMS: Chemical Geology, v. 211, no. 1, p. 135-158.
Reginiussen, H., Ravna, E. J. K., and Berglund, K., 1995, Mafic dykes from Øksfjord, Seiland Igneous Province, northern Norway: geochemistry and palaeotectonic significance: Geological Magazine, v. 132, no. 6, p. 667-681.
Rehnström, E. F., and Corfu, F., 2004, Palaeoproterozoic U–Pb ages of autochthonous and allochthonous granites from the northern Swedish Caledonides—regional and palaeogeographic implications: Precambrian Research, v. 132, no. 4, p. 363-378.
Rehnström, E. F., Corfu, F., and Torsvik, T. H., 2002, Evidence of a Late Precambrian (637 Ma) deformational event in the Caledonides of northern Sweden: The Journal of geology, v. 110, no. 5, p. 591-601.
Ren, S., Skogseid, J., and Eldholm, O., 1998, Late Cretaceous-Paleocene extension on the Vøring volcanic margin: Marine Geophysical Researches, v. 20, no. 4, p. 343-369.
Reusch, H., 1891, Det Nordlige Norges geologi. Med bidrag af Dahll T., Corneliussen OA, med profiler og Dahll's Geologisk Kart over det nordlige Norge'(1: 1,000,000): Nor. Geol. Unders., v. 3.
Rice, A. H. N., Edwards, M. B., Hansen, T. A., Arnaud, E., and Halverson, G. P., 2011, Glaciogenic rocks of the Neoproterozoic Smalfjord and Mortensnes formations, Vestertana Group, E. Finnmark, Norway: Geological Society, London, Memoirs, v. 36, no. 1, p. 593-602.
Rivalta, E., Taisne, B., Bunger, A. P., and Katz, R. F., 2015, A review of mechanical models of dike propagation: Schools of thought, results and future directions: Tectonophysics, v. 638, p. 1-42.
Roberts, D., 1990, Geochemistry of mafic dykes in the Corrovarre nappe, Troms, North Norway: Nor. geol. unders, v. 419, p. 45-54.
Roberts, D., and Gee, D. G., 1985, An introduction to the structure of the Scandinavian Caledonides: The Caledonide orogen–Scandinavia and related areas, v. 1, p. 55-68.
Roberts, R. J., Corfu, F., Torsvik, T., Ashwal, L. D., and Ramsay, D. M., 2006, Short-lived mafic magmatism at 560-570 Ma in the northern Norwegian Caledonides: U-Pb zircon age from the Seiland Igneous Province: Geological Magazine, v. 143, p. 887-903.
Roberts, R. J., Corfu, F., Torsvik, T., Hetherington, C. J., and Ashwal, L. D., 2010, Age of alkaline rocks in the Seiland Igneous Province, Northern Norway: Journal of the Geological Society, v. 167, p. 71-81.
Roca, E., Muñoz, J. A., Ferrer, O., and Ellouz, N., 2011, The role of the Bay of Biscay Mesozoic extensional structure in the configuration of the Pyrenean orogen: Constraints from the MARCONI deep seismic reflection survey: Tectonics, v. 30, no. 2.
Roffeis, C., and Corfu, F., 2014, Caledonian nappes of southern Norway and their correlation with Sveconorwegian basement domains: The Geological Society of London, v. 390.
Root, D., and Corfu, F., 2012, U–Pb geochronology of two discrete Ordovician high-pressure metamorphic events in the Seve Nappe Complex, Scandinavian Caledonides: Contributions to Mineralogy and Petrology, v. 163, no. 5, p. 769-788.
Rosa, D. R. N., Finch, A. A., Andersen, T., and Inverno, C. M. C., 2008, U–Pb geochronology and Hf isotope ratios of magmatic zircons from the Iberian Pyrite Belt: Mineralogy and Petrology, v. 95, no. 1, p. 47.
Rubin, A. M., 1992, Dike-induced faulting and graben subsidence in volcanic rift zones: Journal of Geophysical Research: Solid Earth, v. 97, no. B2, p. 1839-1858.

Rubin, A. M., 1993, Dikes vs. diapirs in viscoelastic rock: Earth and Planetary Science Letters, v. 119, no. 4, p. 641-659.
Rui, I. J., and Bakke, I., 1975, Stratabound sulphide mineralization in the Kjøli Area, Røros district, Norwegian Caledonides: Norwegian Journal of Geology, v. 55.
Saffman, P. G., and Taylor, G., 1958, The Penetration of a Fluid into a Porous Medium or Hele-Shaw Cell Containing a More Viscous Liquid: Proceedings of the Royal Society of London. Series A. Mathematical and Physical Sciences, v. 245, no. 1242, p. 312-329.
Salazar-Mora, C. A., Huismans, R. S., Fossen, H., and Egydio-Silva, M., 2018, The Wilson Cycle and Effects of Tectonic Structural Inheritance on Rifted Passive Margin Formation: Tectonics, v. 37, no. 9, p. 3085-3101.
Salters, V. J. M., and Stracke, A., 2004, Composition of the depleted mantle: Geochemistry, Geophysics, Geosystems, v. 5, no. 5.
Sassier, C., Leloup, P.-H., Rubatto, D., Galland, O., Yue, Y., and Lin, D., 2009, Direct measurement of strain rates in ductile shear zones: A new method based on syntectonic dikes: Journal of Geophysical Research: Solid Earth, v. 114, no. B1.
Satkoski, A. M., Hietpas, J., Samson, S. D., and Wilkinson, B. H., 2013, Likeness among detrital zircon populations—An approach to the comparison of age frequency data in time and space: GSA Bulletin, v. 125, no. 11-12, p. 1783-1799.
Savelli, C., and Ligi, M., 2017, An updated reconstruction of basaltic crust emplacement in Tyrrhenian sea, Italy: Scientific Reports, v. 7, no. 1, p. 18024.
Schaltegger, U., Desmurs, L., Manatschal, G., Müntener, O., Meier, M., Frank, M., and Bernoulli, D., 2002, The transition from rifting to sea-floor spreading within a magma-poor rifted margin: field and isotopic constraints: Terra Nova, v. 14, no. 3, p. 156-162.
Schmidt, M. W., and Poli, S., 2004, Magmatic Epidote: Reviews in Mineralogy and Geochemistry, v. 56, no. 1, p. 399-430.
Schmitz, M. D., and Schoene, B., 2007, Derivation of isotope ratios, errors, and error correlations for U‐Pb geochronology using 205Pb‐235U‐(233U)‐spiked isotope dilution thermal ionization mass spectrometric data: Geochemistry, Geophysics, Geosystems, v. 8, no. 8.
Schofield, N., Alsop, I., Warren, J., Underhill, J. R., Lehné, R., Beer, W., and Lukas, V., 2014, Mobilizing salt: Magma-salt interactions: Geology, v. 42, no. 7, p. 599-602.
Seymour, K. S., and Stephen Kumarapeli, P., 1995, Geochemistry of the Grenville Dyke Swarm: role of plume-source mantle in magma genesis: Contributions to Mineralogy and Petrology, v. 120, no. 1, p. 29-41.
Shumlyanskyy, L., Nosova, A., Billström, K., Söderlund, U., Andréasson, P.-G., and Kuzmenkova, O., 2016, The U–Pb zircon and baddeleyite ages of the Neoproterozoic Volyn Large Igneous Province: implication for the age of the magmatism and the nature of a crustal contaminant: GFF, v. 138, no. 1, p. 17-30.
Siedlecka, A., Roberts, D., Nystuen, J., and Olovyanishnikov, V., 2004, Northeastern and northwestern margins of Baltica in Neoproterozoic time: evidence from the Timanian and Caledonian Orogens: Geological Society, London, Memoirs, v. 30, no. 1, p. 169-190.
Sjöström, H., 1983, The Seve—Köli Nappe Complex of the Handöl—Storlien—Essandsjøen area, Scandinavian Caledonides: Geologiska Föreningen i Stockholm Förhandlingar, v. 105, no. 2, p. 93-117.
Skjerlie, K., and Furnes, H., 1990, Evidence for a fossil transform fault in the Solund‐Stavfjord ophiolite complex: West Norwegian Caledonides: Tectonics, v. 9, no. 6, p. 1631-1648.
Skogseid, J., 1994, Dimensions of the Late Cretaceous-Paleocene Northeast Atlantic rift derived from Cenozoic subsidence: Tectonophysics, v. 240, no. 1, p. 225-247.
Skogseid, J., Pedersen, T., Eldholm, O., and Larsen, B. T., 1992, Tectonism and magmatism during NE Atlantic continental break-up: the Vøring Margin: Geological Society, London, Special Publications, v. 68, no. 1, p. 305-320.

Slagstad, T., Pin, C., Roberts, D., Kirkland, C. L., Grenne, T., Dunning, G., Sauer, S., and Andersen, T., 2014, Tectonomagmatic evolution of the Early Ordovician suprasubduction-zone ophiolites of the Trondheim Region, Mid-Norwegian Caledonides: Geological Society, London, Special Publications, v. 390, no. 1, p. 541-561.
Slagstad, T., Roberts, N. M. W., and Kulakov, E., 2017, Linking orogenesis across a supercontinent; the Grenvillian and Sveconorwegian margins on Rodinia: Gondwana Research, v. 44, p. 109-115.
Slama, J., and Pedersen, R. B., 2015, Zircon provenance of SW Caledonian phyllites reveals a distant Timanian sediment source: Journal of the Geological Society, v. 172, no. 4, p. 465-478.
Smith, D. C., 1984, Coesite in clinopyroxene in the Caledonides and its implications for geodynamics: Nature, v. 310, no. 5979, p. 641.
Solyom, Z., Andréasson, P.-G., and Johansson, I., 1979, Geochemistry of amphibolites from Mt. Sylarna, Central Scandinavian Caledonides: Geologiska Föreningen i Stockholm Förhandlingar, v. 101, no. 1, p. 17-25.
Solyom, Z., Andréasson, P. G., and Johansson, I., 1985, Petrochemistry of late Proterozoic rift volcanism in Scandinavia II: The Särv dolerites (SD)—volcanism in the constructive arms of Iapetus.: Lund Publications in Geology, no. 35, p. 1-44.
Spacapan, J. B., Galland, O., Leanza, H. A., and Planke, S., 2017, Igneous sill and finger emplacement mechanism in shale-dominated formations: a field study at Cuesta del Chihuido, Neuquén Basin, Argentina: Journal of the Geological Society, v. 174, no. 3, p. 422-433.
Stab, M., Bellahsen, N., Pik, R., Quidelleur, X., Ayalew, D., and Leroy, S., 2016, Modes of rifting in magma‐rich settings: tectono‐magmatic evolution of Central Afar: Tectonics, v. 35, no. 1, p. 2-38.
Steiger, R. H., and Jäger, E., 1977, Subcommission on geochronology: Convention on the use of decay constants in geo- and cosmochronology: Earth and Planetary Science Letters, v. 36, no. 3, p. 359-362.
Steinberger, B., Bredow, E., Lebedev, S., Schaeffer, A., and Torsvik, T. H., 2019, Widespread volcanism in the Greenland–North Atlantic region explained by the Iceland plume: Nature Geoscience, v. 12, no. 1, p. 61.
Steinberger, B., and Torsvik, T. H., 2012, A geodynamic model of plumes from the margins of Large Low Shear Velocity Provinces: Geochemistry, Geophysics, Geosystems, v. 13, no. 1.
Stephens, M. B., and Gee, D. G., 1989, Terranes and polyphase accretionary history in the Scandinavian Caledonides: Geological Society of America Special Papers, v. 230, p. 17-30.
Stigh, J., 1979, Ultramafites and detrital serpentinites in the central and southern parts of the Caledonian allochthon in Scandinavia: University of Gothenburg.
Storey, B. C., 1995, The role of mantle plumes in continental breakup: case histories from Gondwanaland: Nature, v. 377, no. 6547, p. 301-308.
Storey, M., Duncan, R. A., and Tegner, C., 2007, Timing and duration of volcanism in the North Atlantic Igneous Province: Implications for geodynamics and links to the Iceland hotspot: Chemical Geology, v. 241, no. 3, p. 264-281.
Strand, T., 1951, The Sel and Vågå map areas: geology and petrology of a part of the Caledonides of central southern Norway, I kommisjon hos Aschehoug, v. 178.
Stratford, W., and Thybo, H., 2011, Crustal structure and composition of the Oslo Graben, Norway: Earth and Planetary Science Letters, v. 304, no. 3-4, p. 431-442.
Sturt, B. A., Bøe, R., Ramsay, D. M., and Bjerkgård, T., 1995, Stratigraphy of the Otta-Vågå tract and regional stratigraphic implications: NGU Bulletin, v. 427.
Sturt, B. A., and Ramsay, D. M., 1997, The Gudbrandsdalen Antiform – A major Late Caledonian structure: NGU Bulletin, v. 433.
-, 1999, Early Ordovician terrane-linkages between oceanic and continental terranes in the central Scandinavian Caledonides: Terra Nova, v. 11.

Sturt, B. A., Ramsay, D. M., and Neuman, R. B., 1991, The Otta Conglomerate, the Vågåmo Ophiolite – Further indications of early Ordovician Orogenesis in the Scandinavian Caledonides: Norwegian Journal of Geology, v. 71.
Stølen, L. K., 1994, The rift-related mafic dyke complex of the Rohkunborri Nappe, Indre Troms, northern Norwegian Caledonides: Nor. Geol. Tidsskr, v. 74, p. 35-47.
Svenningsen, O. M., 1994a, The Baltica–Iapetus passive margin dyke complex in the Sarektjåkkå Nappe, northern Swedish Caledonides: Geological Journal, v. 29, no. 4, p. 323-354.
-, 1994b, Tectonic significance of the meta-evaporitic magnesite and scapolite deposits in the Seve Nappes, Sarek Mts., Swedish Caledonides: Tectonophysics, v. 231, no. 1, p. 33-44.
-, 1995, Extensional deformation along the Late Precambrian-Cambrian Baltoscandian passive margin: the Sarektjåkkå Nappe, Swedish Caledonides: Geologische Rundschau, v. 84, no. 3, p. 649-664.
Svenningsen, O. M., 2000, Thermal history of thrust sheets in an orogenic wedge: 40Ar/39Ar data from the polymetamorphic Seve Nappe Complex, northern Swedish Caledonides: Geological Magazine, v. 137, no. 4, p. 437-446.
Svenningsen, O. M., 2001, Onset of seafloor spreading in the Iapetus Ocean at 608 Ma: precise age of the Sarek Dyke Swarm, northern Swedish Caledonides: Precambrian Research, v. 110, no. 1, p. 241-254.
Svensen, H., Corfu, F., Polteau, S., Hammer, Ø., and Planke, S., 2012, Rapid magma emplacement in the Karoo large igneous province: Earth and Planetary Science Letters, v. 325, p. 1-9.
Svensen, H., Jamtveit, B., Planke, S., and Chevallier, L., 2006, Structure and evolution of hydrothermal vent complexes in the Karoo Basin, South Africa: Journal of the Geological Society, v. 163, no. 4, p. 671-682.
Svensen, H., Planke, S., Malthe-Sørenssen, A., Jamtveit, B., Myklebust, R., Eidem, T. R., and Rey, S. S., 2004, Release of methane from a volcanic basin as a mechanism for initial Eocene global warming: Nature, v. 429, no. 6991, p. 542.
Sønderholm, M., Frederiksen, K. S., Smith, M. P., and Tirsgaard, H., 2008, Neoproterozoic sedimentary basins with glacigenic deposits of the East Greenland Caledonides: The Greenland Caledonides–Evolution of the Northeast Margin of Laurentia. The Greenland Caledonides. In: Mem. Geol. Soc. Amer, v. 202, p. 99-136.
Talbot, C. J., and Ghebreab, W., 1997, Red Sea detachment and basement core complexes in Eritrea: Geology, v. 25, no. 7, p. 655-658.
Tegner, C., Andersen, T. B., Kjøll, H. J., Brown, E. L., Hagen-Peter, G., Corfu, F., Planke, S., and Torsvik, T., 2019, A mantle Plume origin for the Scandinavian Dyke Complex: a "piercing point" for the 615 Ma plate reconstruction of Baltica?: Geochemistry, Geophysics, Geosystems, v. 20, no. 2, p. 1075-1094.
Tegner, C., Duncan, R., Bernstein, S., Brooks, C., Bird, D., and Storey, M., 1998a, 40 Ar 39 Ar geochronology of Tertiary mafic intrusions along the East Greenland rifted margin: Relation to flood basalts and the Iceland hotspot track: Earth and Planetary Science Letters, v. 156, no. 1, p. 75-88.
Tegner, C., Lesher, C. E., Larsen, L. M., and Watt, W. S., 1998b, Evidence from the rare-earth-element record of mantle melting for cooling of the Tertiary Iceland plume: Nature, v. 395, no. 6702, p. 591-594.
Tetreault, J., and Buiter, S., 2018, The influence of extension rate and crustal rheology on the evolution of passive margins from rifting to break-up: Tectonophysics, v. 746, p. 155-172.
Theissen-Krah, S., Zastrozhnov, D., Abdelmalak, M., Schmid, D., Faleide, J., and Gernigon, L., 2017, Tectonic evolution and extension at the Møre Margin–Offshore mid-Norway: Tectonophysics, v. 721, p. 227-238.
Thybo, H., Maguire, P., Birt, C., and Perchuć, E., 2000, Seismic reflectivity and magmatic underplating beneath the Kenya Rift: Geophysical Research Letters, v. 27, no. 17, p. 2745-2748.
Thybo, H., and Nielsen, C. A., 2009, Magma-compensated crustal thinning in continental rift zones: Nature, v. 457, no. 7231, p. 873.

Torgersen, E., Viola, G., Zwingmann, H., and Harris, C., 2014, Structural and temporal evolution of a reactivated brittle–ductile fault–Part II: Timing of fault initiation and reactivation by K–Ar dating of synkinematic illite/muscovite: Earth and Planetary Science Letters, p. 221-233.
Torsvik, T. H., Burke, K., Steinberger, B., Webb, S. J., and Ashwal, L. D., 2010, Diamonds sampled by plumes from the core-mantle boundary: Nature, v. 466, no. 7304, p. 352-355.
Torsvik, T. H., and Cocks, L. R. M., 2005, Norway in space and time: a centennial cavalcade: Norwegian Journal of Geology, v. 85, no. 1-2, p. 73-86.
Torsvik, T. H., and Cocks, L. R. M., 2013, Gondwana from top to base in space and time: Gondwana Research, v. 24, no. 3, p. 999-1030.
Torsvik, T. H., and Cocks, L. R. M., 2017, Silurian: Earth History and Palaeogeography.
Torsvik, T. H., Smethurst, M., Meert, J. G., Van der Voo, R., McKerrow, W., Brasier, M., Sturt, B., and Walderhaug, H., 1996, Continental break-up and collision in the Neoproterozoic and Palaeozoic—a tale of Baltica and Laurentia: Earth-Science Reviews, v. 40, no. 3, p. 229-258.
Torsvik, T. H., Smethurst, M. A., Burke, K., and Steinberger, B., 2006, Large igneous provinces generated from the margins of the large low-velocity provinces in the deep mantle: Geophysical Journal International, v. 167, no. 3, p. 1447-1460.
Torsvik, T. H., Steinberger, B., Ashwal, L. D., Doubrovine, P. V., and Trønnes, R. G., 2016, Earth evolution and dynamics—a tribute to Kevin Burke: Canadian Journal of Earth Sciences, v. 53, no. 11, p. 1073-1087.
Torsvik, T. H., van der Voo, R., Doubrovine, P. V., Burke, K., Steinberger, B., Ashwal, L. D., Trønnes, R. G., Webb, S. J., and Bull, A. L., 2014, Deep mantle structure as a reference frame for movements in and on the Earth: Proceedings of the National Academy of Sciences, v. 111, no. 24, p. 8735.
Tucholke, B. E., Sawyer, D. S., and Sibuet, J. C., 2007, Breakup of the Newfoundland–Iberia rift: Geological Society, London, Special Publications, v. 282, no. 1, p. 9.
Tugend, J., Gillard, M., Manatschal, G., Nirrengarten, M., Harkin, C., Epin, M.-E., Sauter, D., Autin, J., Kusznir, N., and McDermott, K., 2018, Reappraisal of the magma-rich versus magma-poor rifted margin archetypes: Geological Society, London, Special Publications, v. 476.
Törnebohm, 1896, Grunddagen af det centrala Scandinaviens bergbyggnad (mit einem Résumé in deutscher Sprache) Kongl: Svenska vetenskaps-akademiens handlingar, v. 28, p. 210.
van Wijk, J., Koning, D., Axen, G., Coblentz, D., Gragg, E., and Sion, B., 2018, Tectonic subsidence, geoid analysis, and the Miocene-Pliocene unconformity in the Rio Grande rift, southwestern United States: Implications for mantle upwelling as a driving force for rift opening: Geosphere, v. 14, no. 2, p. 684-709.
Vidal, G., 1976, Late Precambrian microfossils from the Visingso Beds in southern Sweden, Universitetsforlaget.
Vitale Brovarone, A., Beyssac, O., Malavieille, J., Molli, G., Beltrando, M., and Compagnoni, R., 2013, Stacking and metamorphism of continuous segments of subducted lithosphere in a high-pressure wedge: The example of Alpine Corsica (France): Earth-Science Reviews, v. 116, p. 35-56.
Walderhaug, H. J., Torsvik, T. H., Eide, E. A., Sundvoll, B., and Bingen, B., 1999, Geochronology and palaeomagnetism of the Hunnedalen dykes, SW Norway: implications for the Sveconorwegian apparent polar wander loop: Earth and Planetary Science Letters, v. 169, no. 1-2, p. 71-83.
Walderhaug, H. J., Torsvik, T. H., and Halvorsen, E., 2007, The Egersund dykes (SW Norway): a robust Early Ediacaran (Vendian) palaeomagnetic pole from Baltica: Geophysical Journal International, v. 168, no. 3, p. 935-948.
Wang, W., and Servais, T., 2015, A re-investigation of the Rhabdinopora flabelliformis fauna from the early Tremadocian 'Dictyonema Shale' in Belgium: Geologica Belgica, v. 18.
Weinberg, R. F., and Regenauer-Lieb, K., 2010, Ductile fractures and magma migration from source: Geology, v. 38, no. 4, p. 363-366.

Wennberg, O. P., Milnes, A. G., and Winsvold, I., 1998, The northern Bergen Are Shear Zone an oblique-lateral ramp In the Devonian extensional detachment system of western Norway: Norsk Geologisk Tidsskrift.
Wennberg, O. P., Skjerlie, K. P., and Dilek, Y., 2001, Field relationships and geochemistry of the Ostereide Dykes, Western Norway: implications for Caledonian tectonometamorphic evolution: Norwegian Journal of Geology/Norsk Geologisk Forening, v. 81, no. 4.
White, L. T., and Ireland, T. R., 2012, High-uranium matrix effect in zircon and its implications for SHRIMP U–Pb age determinations: Chemical Geology, v. 306, p. 78-91.
White, R., and McCausland, W. A., 2016, Volcano-tectonic earthquakes: A new tool for estimating intrusive volumes and forecasting eruptions: Journal of Volcanology and Geothermal Research, v. 309, p. 139-155.
White, R., and McKenzie, D., 1989, Magmatism at rift zones: the generation of volcanic continental margins and flood basalts: Journal of Geophysical Research: Solid Earth (1978–2012), v. 94, no. B6, p. 7685-7729.
White, R., Smith, L., Roberts, A., Christie, P., Kusznir, N., Roberts, A., Healy, D., Spitzer, R., Chappell, A., and Eccles, J., 2008, Lower-crustal intrusion on the North Atlantic continental margin: Nature, v. 452, no. 7186, p. 460-464.
White, R. S., Drew, J., Martens, H. R., Key, J., Soosalu, H., and Jakobsdóttir, S. S., 2011, Dynamics of dyke intrusion in the mid-crust of Iceland: Earth and Planetary Science Letters, v. 304, no. 3-4, p. 300-312.
White, R. S., Spence, G. D., Fowler, S. R., McKenzie, D. P., Westbrook, G. K., and Bowen, A. N., 1987, Magmatism at rifted continental margins: Nature, v. 330, no. 6147, p. 439.
White, S., Bretan, P., and Rutter, E., 1986, Fault-zone reactivation: kinematics and mechanisms: Philosophical Transactions of the Royal Society of London. Series A, Mathematical and Physical Sciences, v. 317, no. 1539, p. 81-97.
Whitmarsh, R., Manatschal, G., and Minshull, T., 2001, Evolution of magma-poor continental margins from rifting to seafloor spreading: Nature, v. 413, no. 6852, p. 150-154.
Whitney, D. L., and Evans, B. W., 2010, Abbreviations for names of rock-forming minerals: American mineralogist, v. 95, no. 1, p. 185-187.
Wiedenbeck, M., AlléLLÉ, P., Corfu, F., Griffin, W. L., Meier, M., Oberli, F., Quadt, A. V., Roddick, J. C., and Spiegel, W., 1995, Three natural zircon standards for U-Th-Pb, Lu-Hf, trace element and REE analyses: Geostandards Newsletter, v. 19, no. 1, p. 1-23.
Wiest, J. D., Jacobs, J., Ksienzyk, A. K., and Fossen, H., 2018, Sveconorwegian vs. Caledonian orogenesis in the eastern Øygarden Complex, SW Norway – geochronology, structural constraints and tectonic implications: Precambrian Research, v. 305, p. 1-18.
Wilson, A. H., Zeh, A., and Gerdes, A., 2017, In Situ Sr isotopes in Plagioclase and Trace Element Systematics in the Lowest Part of the Eastern Bushveld Complex: Dynamic Processes in an Evolving Magma Chamber: Journal of Petrology, v. 58, no. 2, p. 327-360.
Wilson, J. T., 1966, Did the Atlantic Close and then Re-Open?: Nature, v. 211, p. 676-681.
Wolff, F. C., 1979, Beskrivelse til de berggrunnsgeologiske kart Trondheim og Østersund 1:250 000 (med fargetrykt kart): NGU Bulletin, no. 353.
Zastrozhnov, D., Gernigon, L., Gogin, I., Abdelmalak, M., Planke, S., Faleide, J., Eide, S., and Myklebust, R., 2018, Cretaceous‐Paleocene Evolution and Crustal Structure of the Northern Vøring Margin (Offshore Mid‐Norway): Results from Integrated Geological and Geophysical Study: Tectonics, v. 37, no. 2, p. 497-528.
Zen, E.-A., and Hammarstrom, J. M., 1984, Magmatic epidote and its petrologic significance: Geology, v. 12.
Zhong, S., Zhang, N., Li, Z.-X., and Roberts, J. H., 2007, Supercontinent cycles, true polar wander, and very long-wavelength mantle convection: Earth and Planetary Science Letters, v. 261, no. 3, p. 551-564.

Ziegler, P. A., 1992, Plate tectonics, plate moving mechanisms and rifting: Tectonophysics, v. 215, no. 1, p. 9-34.
Ziegler, P. A., and Cloetingh, S., 2004, Dynamic processes controlling evolution of rifted basins: Earth-Science Reviews, v. 64, no. 1, p. 1-50.
Zwaan, B. K., and van Roermund, H. L., 1990, A rift-related mafic dyke swarm in the Corrovarre Nappe of the Caledonian Middle Allochthon, Troms, North Norway, and its tectonometamorphic evolution: Norges geologiske undersøkelse Bulletin, v. 419, p. 25-44.
Zwaan, K., Cramer, J., and Ryghaug, P., 1975, Prospekteringskartlegging i Kvænangen, Troms fylke: Unpubl. NGU-rapp, no. 1118/1, p. 76.